Role of HIV-1 Gag protein multimerization in the generation of nanodomains in lipid membranes

Naresh Yandrapalli

THÈSE

Pour obtenir le grade de

Docteur

Délivré par l'Université de Montpellier

Préparée au sein de l'école doctorale no. 168 CBS2
Sciences Chimiques et Biologiques por la Santé

Et de l'unité de recherche CPBS – CNRS FRE 3689

Spécialité : Molecular Biophysics

Présentée par Naresh Yandrapalli

Role of HIV-1 Gag protein multimerization in the generation of nanodomains in lipid membranes

Soutenue le 21st November, 2016devant le jury composé de

Dr. Parmeggiani Andrea, Professor, UM	Président du jury
Dr. Patricia Bassereau, DR1, Institut Curie	Rapporteur
Dr. Agnes Girard-Egrot, Professor,Université de Lyon	Rapporteur
Dr. Michel Franco, DR, IPMC	Examinateur
Dr. Catherine Picart, Professor, Grenoble-INP	Jury Invité
Dr. Delphine Muriaux, DR2, CPBS	Jury Invité
Dr. Cyril Favard	Directeur de these

Dedicated

to

"*everyone and everything that inspired me*"

Acknowledgements

These last few years at CPBS were quite eventful and left me many reasons to be thankful for. I would like to express my sincere gratitude to everyone who has contributed to this work in one way or another.

First and foremost, I would like to thank my supervisor, Dr. Cyril Favard, for providing me with an opportunity to join his laboratory as well as sharing his broad experience and knowledge. Your guidance and scientific knowledge were vital for this work. The inspiring, thriving scientific environment you have created is exceptional and I have really enjoyed being part of it. Thank YOU for being patient and supportive at the bleakest of times. Your professionalism, energy and incredible capacity to supervise have always impressed me and pushed me forward. Also thanks for the hours of manuscript reading, critique and for encouraging me back. Because of your guidance, I feel confident as I will continue my journey and scientific career. Thank YOU for everything.

I would also like to express my gratitude to Dr. Delphine Muriaux, for her supportive role she played in the shaping of my Ph.D. work. I have truly appreciated your endless help and support all these years beginning from my very first day in the lab. I hope that we will have more opportunities to work together in the future.

I am really grateful to Dr. Johnson Mak, Dr. Catherine Picart and Quentin Lubart for being our collaborators and supporting my thesis work. I also thank Dr. Catherine Picart & Dr. Vladimir Lorman (late) for being my thesis committee members for the past three years. Your thoughtful comments and suggestions given over the time were very helpful and proven important for the good progress of my project. I would also like to thank Dr. Patricia Bassereau and Dr. Agnès Girard Egrot for accepting to read and evaluate my work. I would also like to thank the Erasmus Mundus Svaagata program and their team who with their scholarship has contributed to the accomplishment of my Ph.D. project. Additionally, I would like to thank Dr. Johnson Mak's lab at Deakin University at Melbourne for the all-important Gag protein, Dr. Michel Franco's lab at Institute de Pharmacologie Moléculaire et Cellulaire at Valbonne, for EFA6-PH plasmid, Michael Summers's lab at Howard Huges Medical Institute at Baltimore for HIV-1 MA plasmid, and Olivier Coux's lab at Centre de Recherche de Biochimie Macromoléculaire at Montpellier for helping with protein purification.

I truly appreciate the kind of friends I am associated with during these three years, no one better deserves than Ayyappasamy Sudalaiyadum Perumal. More than you know, I always cherished your company and support. I will not forget how you selflessly stood up for me.

I take this opportunity to acknowledge my colleagues: Adeline Kerviel - I am sure that I won't be here if it is not you who motivated and inspired me to hang on till the end. Charlotte Floderer – My compatriot at work and in the zodiac. Firstly, thank you for bearing me and being a wonderful person. I once again thank you for your support at work, for clarifying my doubts and for encouraging throughout. Shantoshini Dash – You taught me a lot of things and helped me during our time at the lab. I always appreciate your friendly nature and supporting hand towards me. Finally, I truly thank all three of you for sharing the enjoyment and frustration in the office, constant encouragement and for always being there to listen and discuss.

Nathalie Gros – As a non-biologist, I don't even know how to make an SDS-PAGE gel. Being a lab engineer with loads of work in organising the lab, ordering required reagents and for practical and technical assistance all through my thesis work, you taught me a lot. I truly appreciate the help you provided.

Elise Kaplan – Thank YOU very much for being there for me when I desperately need someone to hear me. Your support is immense. I would like to extend my thanks to Peggy Marida, Eric Martinez, Luca Freddi, Jamal Alfaisal, Coralie Daussy, Celia Chamontin, Simon Lachambre and my Volleyball team.

I would like to take this opportunity to thank all my colleagues and friends, past and present, at CPBS for a relaxing and stimulating scientific environment. You've always been very nice and helpful.

I also thank all my friends Rishi Kishore Vishwakarma, Satish Sati, Ramhari Kumbhar, Payal Baheti, Parisha, Gaurav Chatterjee and Diwas Srivastava for being there and providing me with the perspective to the 'real world' outside CPBS. I thank you for never-ending kindness and countless memories. Lakshmi Pravallika Poka, thank you for being my side for all these years. To all of my friends back home and to my teachers who motivated me through lives and their thoughts, Thank YOU very much.

And last, to my family, I can never thank you enough: for all your support, now and always.

Abstract

Role of HIV-1 Gag protein multimerization in the generation of nanodomains in lipid membranes

By – Naresh Yandrapalli

Thesis Director – Dr. Cyril Favard

Gag polyprotein of HIV-1 is made of four main domains Matrix (MA), Capsid (CA), Nucleocapsid (NC), and P6 and is the prime orchestrator of virus assembly that occurs during the late phase of replication. It is well known that Gag interacts with host cell lipids while self-assembling along the inner leaflet of the plasma membrane in order to generate virus-like particles (VLPs). Budding of these VLPs out of the living cell is described to be ESCRT dependent. Structural, functional and simulation-based studies have shown that Gag membrane binding is mediated by a bipartite interaction: one specific electrostatic interaction, between the highly basic region (HBR) of its MA domain and the host cell acidic lipid phosphatidylinositol bisphosphate ($PI(4,5)P_2$), plus a hydrophobic interaction through Gag's myristate insertion in the plasma membrane. It is still an open question whether Gag would specifically recognise pre-existing lipid domains such as rafts to optimise its multimerization or, on the contrary, would reorganise lipids during its multimerization. During my Ph.D., I explored the second hypothesis using purified myr(-) Gag protein and model membranes containing fluorescently labelled $PI(4,5)P_2$.

Binding experiments have shown strong affinities of these purified proteins towards $PI(4,5)P_2$ containing lipid bilayers. Using $PI(4,5)P_2$ fluorescence self-quenching properties, I found that the multimerizing Gag generates $PI(4,5)P_2$/Cholesterol enriched nanoclusters. On the opposite, sphingomyelin was excluded from these nanoclusters. In addition to this, using a fluorescently labelled myr(-) Gag, I have observed its preferable partitioning into lipid disordered (L*d*) phases of the giant unilamellar vesicles (GUVs). Further, the possibility of whether HIV-1 Gag alone, as a minimal system, can induce the formation of vesicles on $PI(4,5)P_2$/PS containing supported

lipid bilayers (SLBs) & GUVs was tested. Using quartz crystal microbalance (QCM-D) and fluorescence microscopy techniques, I monitored the self-assembly of HIV-1 Gag with time and found that Gag is sufficient to generate membrane curvature and vesicle release. Moreover, using mutants of this protein, I found that having MA and CA domain is enough for Gag to produce vesicle-like structures. Taken together, these results suggest that binding and multimerization of Gag protein does not occur in pre-existing lipid domains (such as "rafts") and this multimerization is more likely to induce PI(4,5)P_2/Cholesterol nanoclusters. Finally, this nanophase separation could locally play a role in the membrane curvature needed for the budding of the virus.

Resumé

Rôle de la multimérisation de la protéine Gag du HIV-1 dans la génération de nanodomaines lipidiques membranaires

Par - Naresh Yandrapalli

Directeur de thèse - Dr. Cyril Favard

La polyprotéine Gag du VIH-1 qui contient quatre principaux domaines Matrix (MA), capside (CA), nucléocapside (NC), et P6) est l'orchestrateur privilégié de l'assemblage du virus HIV-1, assemblage qui a lieu pendant la phase tardive de la réplication. Il est bien connu que Gag interagit avec les lipides de la membrane plasmique de la cellule hôte et s'auto-assemble sur le feuillet interne de cette dernière afin de générer de nouvelles particules virales. Le bourgeonnement de ces particules virales hors de la cellule hôte est décrit comme étant dépendant de la machinerie cellulaire ESCRT. Différentes études structurales, fonctionnelles ainsi que des simulations de dynamique gros grain ont montré que la liaison de Gag à la membrane est médiée par une interaction duale. Une spécifique de nature eléctrostatique, qui associe une région hautement basique (HBR) du domaine MA de Gag au lipide acide, phosphatidyl inositol biphosphate ($PI(4,5)P_2$) du feuillet interne de la membrane plasmique. Une de type hydrophobe, qui consiste en l'insertion du myristate de Gag dans la membrane plasmique. Savoir si Gag reconnait spécifiquement des domaines lipidiques pré-existants de type « rafts » ou si, au contraire, Gag tri ses lipides et les réorganise latéralement afin d'optimiser sa multimérisation et son bourgeonnement est une question à la fois fondamentale et d'actualité en virologie.

Durant ma thèse, j'ai vérifié l'existence de la seconde hypothèse en utilisant des membranes modèles contenant du PI (4,5) P_2 marqué de façon fluorescente et différent mutants et produits de la protéine Gag non-myristoylée. Ces expériences ont montré de fortes affinités de ces protéines pour les membranes contenant du PI (4,5) P_2. S'appuyant sur les propriétés d'auto-extinction de fluorescence du marqueur choisit et à l'aide des différents variants de la protéine Gag, jai pu

montré que la multimérisation de Gag génére l'existence de nanodomaines contenant du PI (4, 5)P_2 et du cholestérol, la sphingomyeline étant au contraire exclue de ces domaines. En marquant la protéine Gag par un autre fluorophore, j'ai pu montrer par microscopie optique sur des vésicules lipidiques géantes (GUVs) que la protéine Gag partitionnait préférablablement dans des microdomaines lipidiques de type liquide désordonnés (L*d*).Par la suite, j'ai testé la capacité de la protéine Gag d'induire la formation de vésicules sur des membranes modèles (Bicouches supportés et GUVs) contenant du PI(4,5)P_2 et de la phosphatidylsérine (PS).En utilisant une microbalance à cristal de quartz (QCM-D) et des techniques de microscopie de fluorescence, j'ai suivi l'auto-assemblage de Gag dans le temps et ai montré que la protéine Gag était suffisante pour générer une courbure de la membrane et libérer des vésicules lipidiques. Grâce à différents produits de maturation de cette protéine, j'ai montré que la présence des domaines MA et CA est suffisante pour produire ces vésicules.

L'ensemble de ces résultats suggèrent que la liaison et la multimérisation de la protéine Gag ne se produit pas dans des domaines lipidiques préexistants de type « raft », mais, au contraire, que la liaison et multimérisation de la protéine Gag génére l'existence de domaines lipidiques enrichis en PI (4,5) P_2 et en cholestérol. La génération de ces domaines lipidiques pourrait participer à la courbure de la membrane plasmique nécessaire au bourgeonnement du virus.

Table of Contents

Abstract IV

Resumé VI

Table of Contents VIII

List of Figures XIV

List of Tables XVIII

List of Publications & Communications XIX

Abbreviations XXI

Chapter 1 1

Background and Significance 1

1.1 Introduction 2

1.2 Retrovirus 4

1.2.1 Human Immunodeficiency Virus (HIV) 4

1.2.2 Structure of HIV-1 Virus 5

1.2.3 Gag polyprotein – A structural and functional protein of HIV 6

1.2.3.1 Matrix (MA) 8

1.2.3.2 Capsid (CA) 9

1.2.3.3 Nucleocapsid (NC) 11

1.2.3.4 P6 11

1.2.3.5 SP1 and SP2 12

1.2.4 Replication Cycle 12

1.2.4.1 Early phase: 12

1.2.4.2 Intermediate phase: 14

1.2.4.3 Late phase: 14
1.3 Membrane Systems 15
1.3.1 Physicochemical properties of lipids 16
1.3.1.1 Fatty acid & head group modifications 17
1.3.1.2 Self-assembly of lipids 18
1.3.1.3 Phase transition in lipid membranes: 19
1.3.2 Plasma Membrane (PM) 22
1.3.2.1 Plasma membrane lipid organization 22
1.3.2.1 Lipid-Protein interactions 25
1.3.2.3 Curvature 27
1.4 HIV Gag interaction with plasma membrane 31
1.4.1 HIV-1 Lipidome 31
1.4.2 Phosphatidylinositol-4,5-bisphosphate ($PI(4,5)P_2$) 32
1.4.3 Gag – Plasma membrane interaction: 35
1.4.4 Gag & raft - like - micro domains: 36
1.4.3.1 Interplay between lipids and Gag during viral assembly: 38
1.5 Protein self-assembly at pre-existing lipid domains or protein self-assembly induced lipid domains: a chicken or an egg? 41
Chapter -2 43
METHODS 43
2.1 Model membranes 44
2.1.1 Model Membrane fabrication 46
2.1.1.1a Small Unilamellar Vesicles (SUVs) preparation: 46
2.1.1.1b Visualization and quantification of SLBs 48
2.1.1.2a Large Unilamellar Vesicles (LUVs) preparation-Extrusion method: 49

2.1.1.2b Phospholipid mole fraction quantification: 50
2.1.1.3 GUV preparation – Hydration method....50
2.1.1.3b Visualization of GUVs....52
2.1.1.3c GUV Control experiments:....54
2.2 Protein expression, purification and Labelling: 55
2.3 K*p* determination:....56
2.3.1 Co-sedimentation assay: 56
2.3.2 Multimerization assay on LUVs....57
2.3.3 Quartz Crystal Microbalance with Dissipation (QCM-D):....57
2.4 Fluorescence Self-quenching: 59
2.4.1 Fluorescence Quenching Measurements:....61
2.4.1.1 On LUVs: 61
2.4.1.2 On SLBs: 62
2.5 Confocal Microscopy: 62
2.5.1 Fluorescence Recovery After Photobleaching (FRAP): 63
2.5.2 Two-photon Laser Scanning TCSPC FLIM: 64
2.5.3 Fluorescence Correlation Spectroscopy (FCS): 65
Chapter-3 70
HIV-1 Gag is reorganising PI(4,5)P_2 during multimerization on model membranes....70
3.1 Introduction....71
3.2 Approach....71
3.3 Results & Discussions 73
3.3.1 Affinity studies of Gag towards PI(4,5)P_2 containing membranes: 73
3.3.2 Self-quenching of TopFluor® labelled lipids: 76

3.3.3 HIV-1 Gag Multimerization induces lateral reorganization and nanoclustering of PI(4,5)P_2 in model membranes (LUVs/SLBs/GUVs) 77

3.3.3.1 On LUVs 77

3.3.3.2 On SLBs: 80

3.3.4 Quantifying oligomerizing state of HIV-1 Gag and its multimerization mutant 80

3.3.5 Opposing effects on LUVs and SLBs by Gag multimerization 82

3.3.5.1 Effect of probe and probe concentration on fluorescence quenching 82

3.3.5.2 Quenching/Unquenching and membrane curvature 84

3.3.6 HIV-1 Gag Multimerization induces nanoclustering of PI(4,5)P_2 on model membranes 86

3.3.7 Line-Scan FCS on TF-PIP2 labelled basic SLBs 88

3.3.8 Multimerization property of Gag and its domains 90

3.3.9 Cholesterol but not sphingomyelin is sensitive to HIV-1 Gag multimerization 93

3.3.10 Co-clustering of lipids by Gag on SLBs 93

3.3.11 Gag interaction on complex lipid mixtures 96

3.3.12 HIV-1 Gag PI(4,5)P_2 and cholesterol nanoclustering mainly occurs in liquid disordered lipid phases 97

3.4 Conclusions: 99

Chapter-4 101

HIV-1 Gag protein multimerization induces vesiculation of PI(4,5)P_2 containing model membranes 101

4.1 Introduction 102

4.2 Approach 103

4.3 Results & Discussion 105

4.3.1 Protein - Membrane binding studies using QCM-D: 105

4.3.2 Interaction of non-multimerizing proteins with PI(4,5)P_2 containing SLBs: 106

4.3.2.1 EFA6-PH and MARCKS peptide: 106

4.3.2.2 Matrix protein: 110

4.3.2 Interaction of multimerizing proteins with PI(4,5)P_2 containing SLBs: 113

4.3.2.3 Gag and its mutants 113

4.3.5 Gag and its mutants induce membrane invaginations 123

4.3.6 Gag as a minimal system can induce vesiculation of membranes 124

4.4 Conclusion 127

Chapter-5 130

Conclusions and Future perspectives 130

5.1 Conclusions 131

5.1.1 Gag can bind to P(4,5)P_2 containing basic composition lipid membranes 132

5.1.2 Fluorescence quenching studies revealed the difference in the interaction of protein with PI(4,5)P_2 present in lipid bilayers with opposing curvature 132

5.1.3 Gag multimerization on lipid bilayers induced the formation of PI(4,5)P_2 nanodomains 133

5.1.4 Gag induces co-clustering of lipids, but excludes Sphingomyelin 134

5.1.5 Gag assembly occurs in the Liquid disordered phase of the membranes 134

5.1.6 QCM-D studies revealed a difference between non-multimerizing and multimerizing proteins 135

5.1.7 Gag as a minimal system can induce membrane vesiculation and multimerization is responsible for this lipid bilayer deformation. 136

5.2 Future Perspectives 136

5.2.1 Development of asymmetric lipid bilayers and actin reconstituted lipid bilayers 137

5.2.2 To study the formation of lipid domains and assembly platforms generated by HIV-1 Gag 138

5.2.3 Role of RNA in multimerization and thus, in the formation of lipid domains 140

5.2.4 Cell based studies with labelled lipids and Gag protein 140

References 142

List of Figures

Figure 1.1: HIV statistics 3

Figure 1.2: Schematic representation of HIV-1 virus 5

Figure 1.3: Model Gag poly protein, generated by I-TASSER suite 7

Figure 1.4: Structural illustration of HIV-1 Matrix protein (MA) 8

Figure 1.5: Structural conformation and assembly of HIV-1 CA protein 10

Figure 1.6: HIV-1 replication cycle, depicting from infection to viral particle release 13

Figure 1.7: Detailed schematic of a typical cell membrane 16

Figure 1.8: Schematic representation of mainly two different kinds of lipids with glycerol and sphingosine backbone 17

Figure 1.9: Schematic representation of different shapes of lipid molecules and the varying aggregates with change in the *P* factor 19

Figure 1.10: Scheme illustrating the different physical states adopted by a lipid bilayer in aqueous medium 20

Figure 1.11: Phase transition temperatures observed for lipid mixtures of different compositions 21

Figure 1.12 Asymmetric transbilayer distribution of phospholipids in red blood cell membranes given as a percentage of each phospholipid 23

Figure 1.13: Free energies of association of different lipid-modified protein groups with lipid bilayers, as estimated from measurements of the affinities of association of lipid-modified peptides with lipid vesicles 26

Figure 1.14: Lipid membrane curvature generation 28

Figure 1.15: Enrichment studies of $PI(4,5)P_2$ in the viral membrane of HIV viral particles produced from H9 cells to that of the total membrane and plasma membrane of H9 cells .32

Figure 1.16: Schematic representation of(A) L-α-phosphatidylinositol-4,5-bisphosphate and (B) its TopFluor® derivative 33

Figure 1.17: MA-PI(4,5)P2 interaction mechanisms reported 39

Figure 1.18: Illustration of HIV-1 Gag assembly on the inner leaflet of plasma membrane40

Figure 2.1: Model systems used to mimic cellular membranes 44

Figure 2.2: Schematic representation of chamber formation and housing on to a coverslip 47

Figure 2.3: Quality control of SLBs.....49

Figure 2.4: Domain visualization of Phase separated GUVs 53

Figure 2.5: GUV integration and partitioning of labelled components.....54

Figure 2.6: SDA-PAGE gels of purified proteins and labelled proteins.....55

Figure 2.7: Comparison of collisional and static quenching.....60

Figure 3.1: Purified proteins used in this study 71

Figure 3.2: Binding of FL-Gag and its mutants, Matrix, PH-EFA6 and MARCKS to "basic" lipid membranes 74

Figure 3.3: Concentration dependence of self-quenching property of TopFluor® labelled lipids in LUVs.....75

Figure 3.4: MARCKS peptide induced quenching of labelled PI(4,5)P_2 containing LUVs..76

Figure 3.5: PI(4,5)P_2 lateral reorganization induced by Gag multimerization on basic composition liposomes.....78

Figure 3.6: PI(4,5)P_2 lateral reorganization induced by Gag multimerization on basic composition SLBs.....79

Figure 3.7: Multimerization induces lateral reorganization of PI(4,5)P_2.....81

Figure 3.8: Quenching and unquenching observed for different Bodipy derivatives labelled lipids at different molecular ratio in LUVs and SLBs 83

Figure 3.9: TF-PI(4,5)P_2 fluorescence lifetime change upon FL-Gag addition 84

Figure 3.10: PI(4,5)P_2 nanoclusterization induced by Gag multimerization on basic composition lipid membranes (SLB/GUV).....87

Figure 3.11: Line-Scan FCS of TF-PIP$_2$ labelled basic SLBs before and after addition of FL-Gag 89

Figure 3.12: Comparing the distances of adjacent HBR regions in MA trimer and MA-CA dimer 90

Figure 3.13: Multimerization property of MLV Gag and its ability to quench TF-PI(4,5)P$_2$ 91

Figure 3.14: Gag multimerization is sorting cholesterol but not sphingomyelin 92

Figure 3.15: SLB TF-SPM fluorescence increase upon BT-PI(4,5)P$_2$ photobleaching 94

Figure 3.16: Co-clustering of PI(4,5)P$_2$ and Cholesterol by Gag 95

Figure 3.17: Gag PI(4,5)P$_2$ and Cholesterol nanoclustering in complex membrane models 96

Figure 3.18: Preferential partitioning of Gag on GUVs 98

Figure 4.1: Typical frequency shift and change in dissipation observed during the formation of SLB from LUVs 105

Figure 4.2: Binding of Gag to PI(4,5)P$_2$ containing SLBs 106

Figure 4.3: A typical sensorgram obtained after the injection of EFA6-PH protein 107

Figure 4.4: Sensorgram with multiple concentrations of protein interaction on PI(4,5)P$_2$ containing SLBs 108

Figure 4.5: ΔD - ΔF plots of EFA6-PH obtained on interaction with PI(4,5)P$_2$ containing basic composition SLBs 109

Figure 4.6: Patches of basic composition SLB labelled with 1% TF-PI(4,5)P$_2$ before and after interaction with EFA6-PH and MARCKS peptide, 1 µM 110

QCM-D results of MA protein interaction on PI(4,5)P$_2$ containing basic lipid composition SLB 111

Figure 4.8: Fluorescence Microscopy of MA interaction on PI(4,5)P$_2$ containing basic lipid composition SLB 112

Figure 4.9: Inverse Frequency shift plots of various proteins interaction on PI(4,5)P$_2$ containing basic lipid composition SLBs 113

Figure 4.10: Sensorgrams depicting the effect of crosslinking or oligomerization on proteins 114

Figure 4.11: ΔD - ΔF plots for various concentrations of FL-Gag interaction with PI(4,5)P_2 containing basic composition SLBs 116

Figure 4.12: Comparing the ΔD - ΔF plots and frequency shift of Gag and its mutants (P39 and WM) upon interaction with PI(4,5)P_2 containing basic composition SLBs 117

Figure 4.13: Comparing the Morphology of TF-PI(4,5)P_2 labelled basic composition SLBs before and after the interaction with various proteins 119

Figure 4.14: Morphology of various TF-PIP_2 labelled basic composition SLBs treated with various concentration of FL-Gag 120

Figure 4.15: FRAP experiments on formed vesicles upon interaction of Gag with PI(4,5)P_2 containing basic SLBs 121

Figure 4.16: Gag induced budding 122

Figure 4.17: Time profile of GUV vesiculation by Gag 123

Figure 4.18: GUV incubation in Alexafluor-594 labelled BSA 124

Figure 5.1: Schematic representation of possible assembly mechanism of HIV-1 Gag 137

Figure 5.2: svFCS correlograms obtained for TF-PIP_2 present in basic SLBs 138

Figure 5.3: svFCS diffusion time of TF-PIP_2 in basic composition SLBs with respect to varying waist radii 139

List of Tables

Table 1.1: Apparent binding constants of viral matrix proteins of various retroviruses that have specificity towards PI(4,5)P_2 lipid 34

Table 2.1: Different lipid composition of LUVs, SLB and GUV used in the single labelled lipid experiments 45

Table 2.2: Different SLB lipid composition used for the dual labelled lipid experiments 45

Table 3.1: Apparent K*p* of the different proteins used in this study 74

Table 3.2: Monomer-dimer equilibrium of MLV Gag and HIV-1 Gag proteins 91

List of Publications & Communications

Naresh Yandrapalli, Quentin Lubart, Hanumant Tanwar, Catherine Picart, Johnson Mak, Delphine Muriaux, and Cyril Favard, 2016. "***Self-assembly of HIV-1 Gag Protein on Lipid Membranes Generates PI(4,5)P_2/Cholesterol Nanoclusters***." Scientific Reports 6, Article number: 39332 (2016) doi:10.1038/srep39332

Naresh Yandrapalli, Delphine Muriaux, and Cyril Favard, 2014. "***Lipid Domains in HIV-1 Assembly***." Frontiers in Microbiology 5 (May). Page: 220. doi:10.3389/fmicb.2014.00220.

Sébastien Balme, Pierre Eugène Coulon, Mathilde Lepoitevin, Benoît Charlot, **Naresh Yandrapalli**, Cyril Favard, Delphine Muriaux, Mikhael Bechelany, and Jean-Marc Janot. 2016. "***Influence of Adsorption on Proteins and Amyloid Detection by Silicon Nitride Nanopore***." Langmuir 32 (35): 8916–25. doi:10.1021/acs.langmuir.6b02048.

Eric Martinez, Julie Allombert, Franck Cantet, Anissa Lakhani, **Naresh Yandrapalli**, Aymeric Neyret, Isobel H. Norville, Cyril Favard, Delphine Muriaux, and Matteo Bonazzi. 2016. "***Coxiella Burnetii Effector CvpB Modulates Phosphoinositide Metabolism for Optimal Vacuole Development***." Proceedings of the National Academy of Sciences 113 (23): E3260–69. doi:10.1073/pnas.1522811113.

Selected talk entitled, "***HIV-1 Gag redistributes PI(4,5)P_2 during multimerization on model membranes.***" Joint Meeting of the Membrane Sections of the French and German Biophysical Societies "Biophysics of Protein–Membrane Interactions: From Model Systems to Cells" April 11 to 14, 2016 - Bad Herrenalb, Germany.

Poster presentation entitled, "***HIV-1 Gag protein multimerization induces vesiculation of PI(4,5)P2 containing model membranes***." in 10th International Retroviral NucleoCapsid protein and Assembly Symposium, September 18 to 21, 2016 - Montpellier, France.

Poster presentation entitled, "***How PI(4,5)P2 is segregated by Gag protein of HIV-1 in model membranes?***" in Joint Meeting of the GDRi PHYSICS OF LIVING SYSTEMS and the GRISBI network, June 1-3, 2015 - Montpellier, France.

Poster presentation entitled, *"**How PIP2 is segregated by HIV-1 Gag protein during assembly?**"*2nd Labex Inform Conference, 2015 - Cargèse, France

Poster presentation entitled, "***Revisiting the mechanism of membrane anchoring of the hiv-1 matrix protein by a molecular modeling approach and fluorescence quenching***." Annual congress of French Biophysics Society, 2014 - Guethary, France.

Abbreviations

acc – accessible

AIDS – Acquired Immune Deficiency Syndrome

ANTH – Amino-N-Terminal Homology

APD – Avalanche photodiode

ARF6-PH – ADP-Ribosylation Factor 6-PH

BAR – Bin/Amphiphysin/Rvs

BPS – brain PS

BSA – Bovine Serum Albumin

BT – Bodipy TMR

CA – Capsid

CCR – C-C chemokine Receptor

CD4 – Cluster of differentiation 4

CDC – Center for Disease Control

CDP-DAG – Cytidine Diphosphate Diacylglycerol

Chol– Cholesterol

COP – Conserved coat protein complex

CTD – C-terminal Domain

CXCR – CXC chemokine Receptor

CypA – Cyclophilin A

DIlC18 – 1 1 dioctadecyl 3 3 3 3 tetramethylindocarbocyanine perchlorate

DMPC – 1,2-Dimyristoyl-sn-glycero-3-phosphocholine

DNA – Deoxyribonucleic acid

DOPC – Dioleoylglycerophosphocholine

DPPC – Dipalmitoylphosphatidylcholine

DRM – Detergent Resistant Membranes

DSPC – Distearoylglycerophosphocholine

E.coli - *Escherichia coli*

EDTA - Ethylenediaminetetraacetic acid

EEA1 – Early Endosome Antigen 1

EFA6 – Exchange Factor for ARF6

EGTA – Ethylene glycol-bis(β-aminoethyl ether)-N,N,N',N'-tetraacetic acid

EIAV – Equine Infectious Anemia Virus

Em – Emission

ENTH – EpsinN-Terminal Homology

Env – Envelope

EPC – egg PC

ER - Endoplasmic reticulum

ESCRT - Endosomal Sorting Complexes Required for Transport

ESR – Electron Spin Resonance

Ex – Excitation

FCS – Fluorescence Correlation Spectroscopy

FERM – four point one/ezrin/radixin/moesin

FL Gag/FL-Gag- Gag Full length

FLIM – Fluorescence lifetime microscopy

FRAP – Fluorescence Recovery After Photobleaching

FRET – Fluorescence Resonance Energy Transfer

GaAsp – Gallium arsenide phosphide

Gag - Group-specific antigen

GFP – Green Fluorescent Protein

GM1 – Monosialotetrahexosylganglioside

GOLPH3 – Golgi phosphoprotein 3

gp – glycoprotein

GPi – Glycosylphosphatidylinositol

GUV – Giant Unilamellar Vesicle

HAART – Highly Active AntiRetroviral Therapy

HBR – Highly Basic Region

HEPES – 4-(2-hydroxyethyl)-1-piperazineethanesulfonic acid

HIV – Human Immunodeficiency Virus

HRP – Horseradish Peroxidase

I-domain – Interaction domain

IN – Integrase

IP – Inositol Phosphate

IPTG – Isopropyl β-D-1-thiogalactopyranoside

K_B – Boltzmann constant

KCl – Potassium Chloride

K*p* – Apparent partitioning constant

L*d* – Liquid disordered

L*o* – Liquid ordered

LUV – Large Unilamellar vesicles

MA – Matrix

MARCKS – Myristoylated Alanine-Rich C-Kinase Substrate

Mefp-1 – Mussel Adhesive protein-1

MHR – Major Homology Region

MLV – MultiLamellar Vesicles/Murine Leukemia Virus

mRNA – messenger RNA

MSD – Mean square distance

MVB – MultiVesicular Bodies

NaCl – Sodium Chloride

$NaIO_4$ – Sodium Iodate

NC – Nucleocapsid

Nef – Negative Regulatory Factor

Ni-NTA – Nickel-NitriloTriacetic Acid

NMR – Nuclear magnetic resonance

NTD – N-terminal domain

PA – Phosphatidic acid

PC – Phosphatidylcholine

PCP – Pneumocystis carinii pneumonia

PCR – Polymerase chain reaction

PDMS – Polydimethylsiloxane

PDZ – acronym combining the first letters of three proteins postsynaptic density protein (PSD95), Drosophila disc large tumor suppressor (Dlg1), and zonula occludens-1 protein (zo-1)

PE – Phosphatidylethanolamine

PG – Phosphatidylglycerol

PH domain – Pleckstrin Homology domain

PI – Phosphatidylinositol

$PI(4,5)P_2/PIP_2$ – Phosphatidylinositol phosphate

PIC – Pre-Integration Complex

PKC – Protein Kinase C

PLCΔ - Phospholipase C delta

PM – Plasma Membrane

PMT – Photo-multiplier tube

Pol – Polymerase

POPC – 1-palmitoyl-2-oleoyl-sn-glycero-3-phosphocholine

POPS – 1-palmitoyl-2-oleoyl-sn-glycero-3-phosphoserine

PS – Phosphatidylserine

PTB – Phosphotyrosine binding

PVA – Poly-Vinyl Alcohol

QCM-D – Quartz Crystal Microbalance with Dissipation

Rev –Regulator of expression of virion proteins

R_h – Hydrodynamic radius

RNA - Ribonucleic acid

ROI – Regions Of Interest

RSV – Rous Sarcoma Virus

RT – Reverse Transcriptase

SDS – Sodium Dodecyl Sulfate

SDS-PAGE – Sodium Dodecyl Sulfate-PolyAcrylamide Gel Electrophoresis

SLB – Supported Lipid Bilayer

SM/SPM – Sphingomyelin

So – Solid ordered

SP – Spacer Peptide-1/2

SUVs – Small Unilamellar Vesicles

svFCS – spot variation FCS

Tat – Transactivator of transcription

TCSPC – Time-Correlated Single Photon Counting

TEM – Tetraspanin-enriched micro-domain

TF – TopFluor®

T_g – Glass transition

T_m – Melting Temperature

TMR –Tetramethylrhodamine

TNBS - 2,4,6-trinitrobenzen sulfonic acid

TRIM – Tripatriate motif family

tRNA – Transfer ribonucleic acid

TSG101 – Tumor susceptibility gene101

UEV – N-terminal ubiquitin E2 variant

Vif – Viral infectivity factor

VILIP-1 – Visinin-Like Protein-1

VLP – Virus-Like Particle

Vpr – Viral protein r

Vpu – Viral protein u

VSV – Vesicular Stomatitis Virus

WHO – World Health Organization

ZF – Zinc finger

ϩ – Solution Viscosity

Chapter 1

Background and Significance

1.1 Introduction

Circle of life is complete only when death is followed by life and vice versa. An ever-increasing consciousness of humans and their efforts to control the nature has shifted this circle of life and thus the many consequences. While this new-found ability to manipulate nature gave fruitful results - when put to good use, there is always the dark side. In this fight for survival & dominance, a lot was studied and achieved, but there is an ocean of it still remains. If Darwin's "**survival of the fittest**" (Spencer1864) has any impact on the world, all research work in the name of science can be attributed to it. Here I present two beings that strive to survive in this struggle: HUMANS and VIRUSES.

From time immemorial, viruses plagued humans in one or the other way: either by infecting the food sources (plants, avian and cattle) they eat or by infecting them directly. While the earlier one poses only an indirect threat to survival, the later one is both direct and very imminent. So it became very important to study these beings in detail and so they can be countered. In the process, during 1898 the first identification was made by Martinus Beijernck as ***contagium vivum fluidum*** (soluble living organism), later termed as **Virus**. This was followed by the discovery of many viruses infecting all kind of life forms from the single cell to complex multicellular organisms. The virus was defined as,

"***a small infectious agent that can only replicate inside a living host cell***"

In the course of time, over 5000 types of virus were discovered and classified. Based on shape, size and the type of nucleic acid molecule present, these non-living beings were classified into many groups. Among many viruses and the infections they cause, one particular virus that belongs to the family, Retroviridae, caused a huge impact on the lives of human beings and still remained as a serious public health challenge even after 30 years of epidemic set in 1920 (Faria et al. 2014). In this work, much will be discussed regarding Human Immunodeficiency Virus (HIV) as I try to understand the assembly of the viral protein on artificial lipid membrane systems using fluorescent techniques.

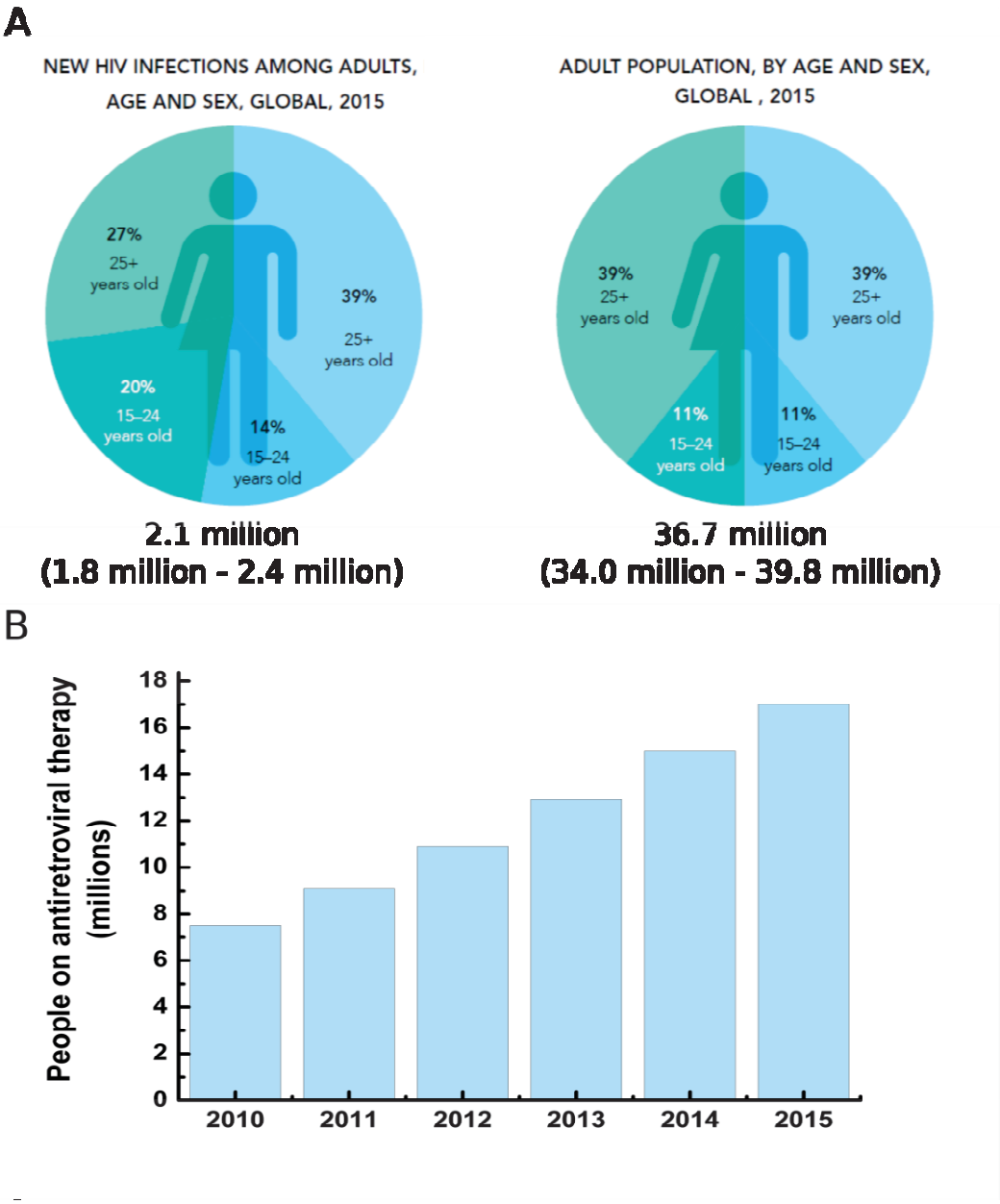

Figure 1.1: HIV statistics. (A) New (left) and Global (right) distribution of HIV infected population by age and sex. (B) A number of people living with HIV on antiretroviral therapy, global, 2010-2015. Data obtained from the Global AIDS response progress report (GARPR), 2016 by UNAIDS.

1.2 Retrovirus

Any enveloped virus with a single-stranded and positive-sense RNA (ribonucleic acid) can replicate through reverse transcription in a living host cell. The title "retro" comes from the ability of the virus to convert genomic RNA into DNA (deoxyribonucleic acid) using its own reverse transcriptase (RT) enzyme which is in reverse to usual DNA to RNA conversion that takes place in cells. At this point, the new DNA is incorporated into host cell genome using integrase enzyme. Once done, the viral genome is referred as a provirus and expressed like other host cell genes. Thus produced viral proteins from the expression of the viral genome, assemble to form new copies of the virus. Belonging to this family, there are many potentially dangerous viruses that are in circulation. Of them, Human Immunodeficiency Virus-1 (HIV-1) is the prime virus that created a greater impact on our lives. Figure 1.1 depicts the span of HIV-1 infection all over the world and the number of people still living with it as of 2014, according to Joint United Nations Programme on HIV/AIDS (UNAIDS).

1.2.1 Human Immunodeficiency Virus (HIV)

Human Immunodeficiency Virus belongs to the family *Retroviridae* and *Lentivirus* genus. It is a ~120 nm diameter spherical enveloped virus. HIV virus was supposed to be originated in Kinshasa, the Democratic Republic of Congo at 1920 when it transmitted from chimpanzees to humans. Only during the 1980s, there was a dramatic increase in the number of people reporting a rare lung infection, Pneumocystis carinii pneumonia (PCP) and a very aggressive connective tissue cancer, Kaposi's sarcoma (Hymes et al. 1981)(Centers for Disease Control (CDC) 1981). After this and several similar events reported abroad, Center for Disease Control (CDC) coined the term "**AIDS**" (Acquired Immune Deficiency Syndrome) that is linked to the health condition of people infected with HIV. The virus is responsible for the decreased immunity of the infected person and thus paving way for opportunistic infections leading to PCP, Kaposi's sarcoma, and other co-infections. Indeed, HIV infects CD4+ T-Cells (cluster of differentiation) very efficiently and results in the drop of their count. In time, HIV evolved to give four main groups with slightly different genetic make-up, they are: M, N, O and P. Of those, HIV-1 of type M has spread all

around the world and is responsible for most of the infections till date; evidently it is also the most studied HIV type. Although a lot of progress has been achieved in finding a cure if not prevention, yet so much has to be studied. A brief overview of the virus and its components are described below.

1.2.2 Structure of HIV-1 Virus

HIV virus is an enveloped virus with a genomic RNA dimer that encodes into DNA by viral reverse transcriptase (RT). The proviral DNA has nine genes of which three are common to most retroviruses: Group-specific antigen (Gag), Pol and Env genes. Gag precursor protein forms the major structural unit that is responsible for assembling at the plasma membrane to form new particles. Env forms the envelope (Env) protein that helps the virus to enter the host cell/infection. Various enzymes like protease, reverse transcriptase (RT) and integrase (IN) are encoded by Pol genes. Apart from these, Tat (Trans-Activator of Transcription) and Rev (Regulator of expression of virion proteins) forms the regulatory proteins and Vif (Viral infectivity factor), Vpr (Viral protein r), Vpu (Viral protein u) and Nef (Negative Regulatory Factor) as accessory proteins. Once all viral components are assembled, the released viral particle from the surface of the host cell plasma membrane will be ~120 nm size in diameter. Figure 1.2 depicts the immature and mature viral particles. An immature particle is a non-infectious viral particle that later matures into an infectious one. A central capsid cone formed after the protease enzymatic activity differentiates the immature from the mature particle. This is achieved by Gag proteolysis and redistribution of cleavage products within the viral particle over a half-time of 29±8 min (Janina Hanne et al 2016).

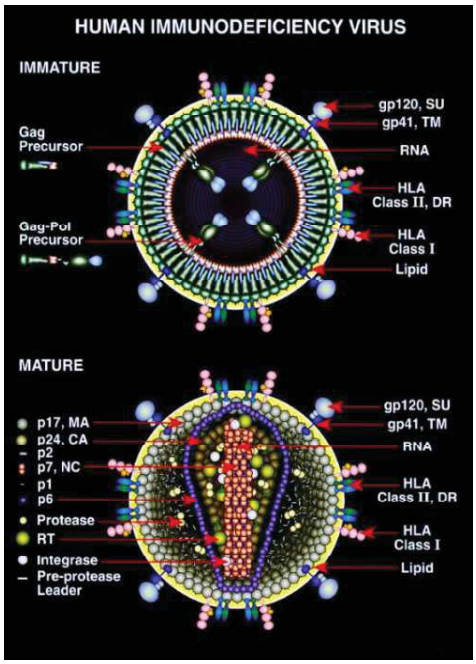

Figure 1.2: Schematic representation of HIV-1 virus, both immature and mature viral particles.

Above mentioned viral protein and components form a formidable outer protein coat, encompassing two single-stranded RNA molecules and the three enzymes encoded by Pol gene. Covering the entire viral particle is the lipid membrane derived from the host cells from which the virus has been produced.

1.2.3 Gag polyprotein – A structural and functional protein of HIV

Gag polyprotein is the key component in the virus structure which orchestrates the sequestration of various other viral components while it assembles along the plasma membrane of the host cell. A Pr55 Gag is a full-length Gag protein that is of 55kDa in molecular weight and has four domains with specific roles. The four domains from N-terminus to C-terminus: (a) Matrix (MA), (b) Capsid (CA), (c) Nucleocapsid (NC), and (d) P6. Below is the structure of the full-length protein (figure 1.3(A)) generated using I-TASSER suite (Roy, Kucukural, and Zhang 2010).This polyprotein is horse-shoe shaped (Munro et al. 2014), but it was known to take an extended conformation in the presence of IP5/6 (Inositol phosphate) and genomic RNA (Datta, Zhao, et al. 2007)(Datta, Curtis, et al. 2007a). Figure 1.3(B) presents the amino acid sequence of this polyprotein. Demarcated are the specific sequences unique to each domain and do participate in the assembly process of the Gag protein along the inner leaflet of the plasma membrane. Much will be discussed on the role of these amino-acid patches in the sections below.

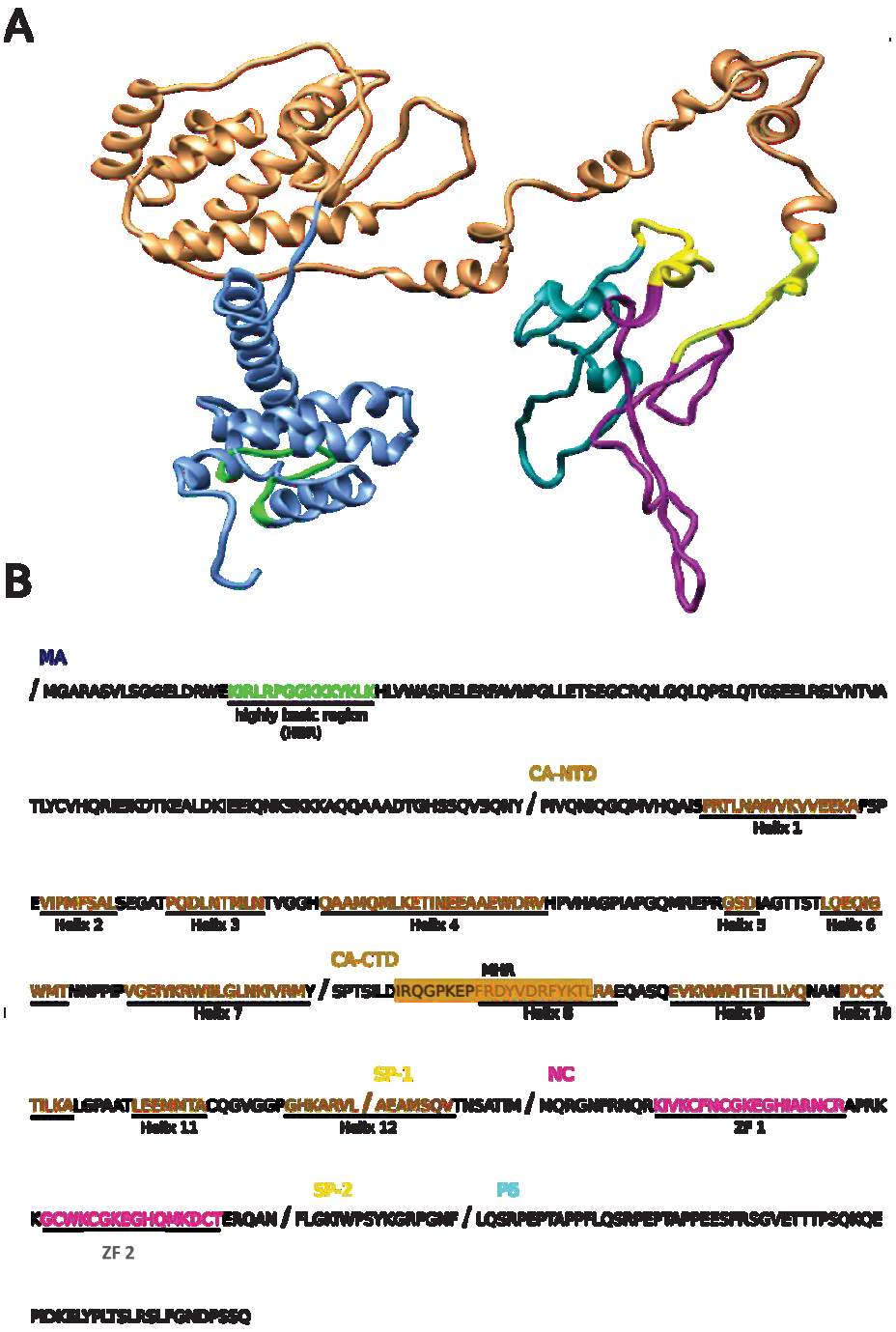

Figure 1.3: Model Gag poly protein, generated by I-TASSER suite (A)Blue – Matrix domain with green HBR patch, Gold – Capsid, Magenta – Nucleocapsid, Cyan – P6 domain and Yellow – spacer proteins (SP1 and SP2).(B)HIV-1 Gag polyprotein amino-acid sequence demarcated with its domains and specific sequences that have a major role during the assembly of the protein along the inner leaf-let of the plasma membrane.

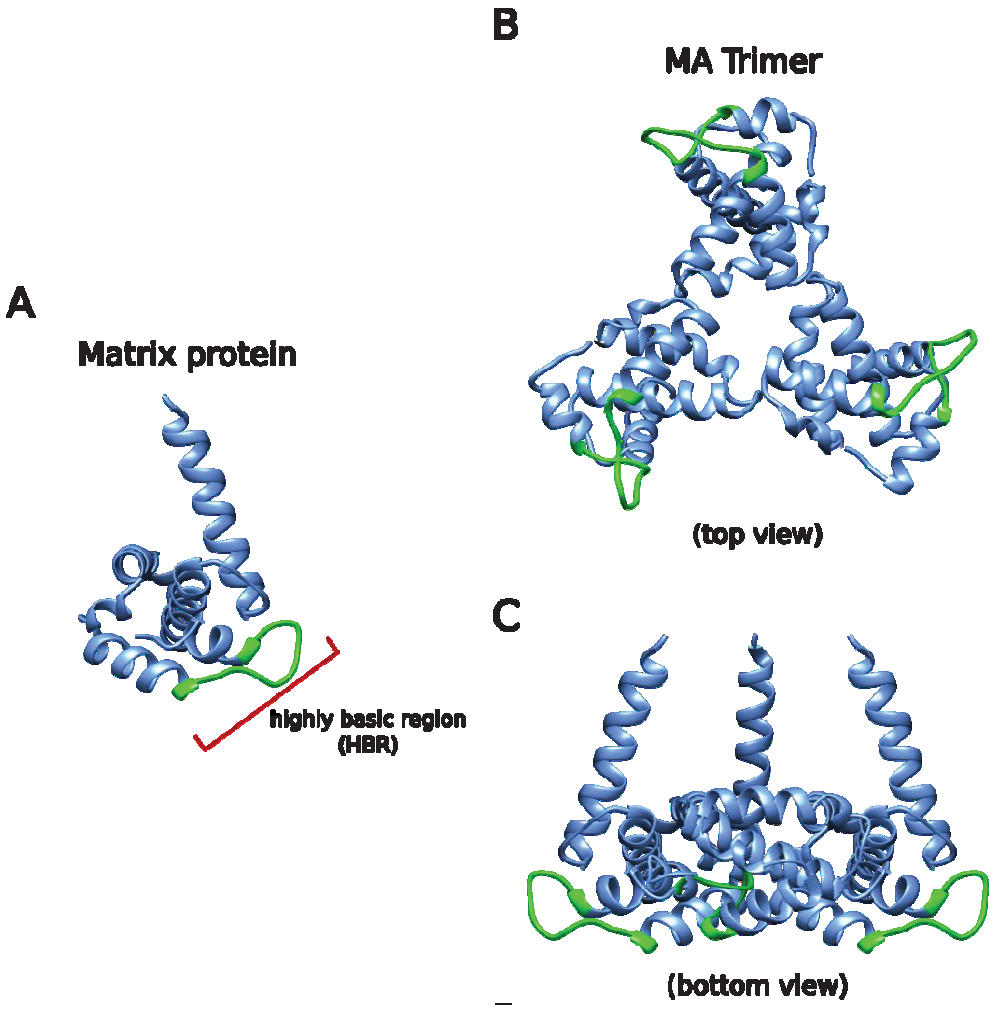

Figure 1.4: Structural illustration of HIV-1 Matrix protein (MA) (A) MA protein highlighted with HBR region (green). (B) and (C) Depicting MA trimer formation of MA protein (top view and bottom view) with upon assembly at high concentrations. Structures are obtained from the protein data bank and modified where required.

1.2.3.1 Matrix (MA)

The Matrix protein of Pr55Gag is a 131 amino acid long domain (depicted in blue in figure 1.3(A) and 1.4(A)) that is responsible for targeting and binding of the Gag protein along the inner leaflet of the plasma membrane. To achieve this, the protein is equipped with two structural entities at the N-terminus: (a) highly basic region (HBR) formed by 17-31 amino acid sequence (green color-figure 1.3 and 1.4) that can interact with the acidic lipids present in the plasma membrane, (b) a myristoyl chain that can help with the stabilization of the interaction. These two structural moieties help in targeting and binding of the Pr55Gag to the plasma membrane,

especially acidic lipids such as PI(4,5)P_2 (Phosphatidylinositol (4,5) phosphate) and PS (Phosphatidylserine) lipid present in the inner leaflet of the plasma membrane (PM) (Akira Ono et al. 2004). Minor modifications in either HBR region or the myristate have shown to affect this interaction (Bryant and Ratner 1990; Chukkapalli and Ono 2011). Structural studies revealed that MA domain as such can form trimers (Hill et al. 1996) at sufficient concentrations (see figure 1.4(B) and 1.4(C)) and further super assemble into hexamer of trimers (Alfadhli, Barklis, and Barklis 2009). On a membrane, a typical trimer occupies an area of 15.68 nm^2 with a volume of 180 Å x 180 Å x 100 Å (Alfadhli et al. 2009). Although this area spans quite a number of lipids, the protein's ability to choose specific lipids elicited a new direction in the research of HIV. Recent NMR (Nuclear magnetic resonance) and simulation studies revealed the specific interaction of the HBR region of the matrix protein and the PI(4,5)P_2 lipid (Charlier et al. 2014; Chukkapalli et al. 2008; Mercredi et al. 2016; Saad et al. 2006). The intricate interaction between specific lipids of the plasma membrane and HBR region of matrix domain will be dealt in detail later on.

1.2.3.2 Capsid (CA)

CA is the multimerizing domain present between the MA and the first spacer peptide (SP1). It is 231 amino acids long & is responsible for forming dimers of Pr55Gag in solution (depicted in gold, figure 1.3(A)). Structurally, CA is distinguished into two domains: an N-terminal domain (NTD) and a C-terminal domain (CTD) specified in figure 1.3(B) and figure 1.5(A). The C-terminal domain with its four alpha helixes has a functional property that has been identified by introducing a point mutation in the second alpha-helix. These mutations resulted in the inhibition of CA dimerization and eventual HIV-1 replication (Gamble et al. 1997). Apart from this, a major homology region (MHR), highly conserved region among many retroviruses - also exists within the C-terminal domain of CA (Wills and Craven 1991). Furthermore, any alterations in this MHR region resulted in an abnormal or no Gag assembly (Provitera et al. 2001). During maturation of the newly formed viral particle, CA gets cleaved to form a conical core (figure 1.5 (C)) around the viral genome and this proteolytic cleavage has been found important for the infectious nature of the matured viral particle (Arts and Hazuda 2012). As a major anti-retro viral drug target, structural biology of the CA protein has been extensively studied. Figure 1.5

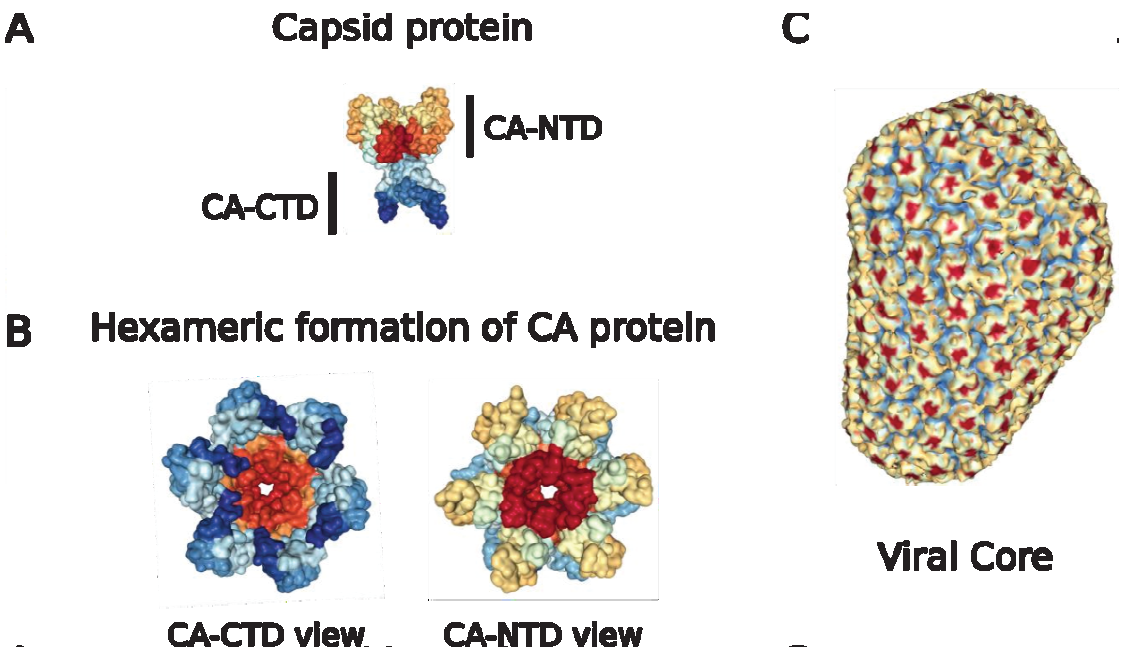

Figure 1.5: Structural conformation and assembly of HIV-1 CA protein(A) Crystal structure of HIV-1 CA protein (PDB ID: 5L93) (Schur et al. 2016) (B) Hexameric structure of full-length CA protein (PDB ID: 3J4F) (Zhao et al. 2013) (C) Atomistic structure of HIV-1 viral core as revealed by cryo-electron microscopy (PDB ID: 3J3Q) (Zhao et al. 2013).

presents the structural conformation revealed through X-ray diffraction or cryo-electron microscopy. It was found that CA can form hexamers (figure 1.5(B)) by interacting with the CA domains of adjacent Gag molecules (Zhao et al. 2013). Very recently, it was also revealed that CA-CTD region of the CA domain is responsible for these hexamers and the dimerization property of CA-NTD helps connect these adjacent hexamers to form an intact core (Lingappa et al. 2014). Before forming this core, in an immature CA protein assembly, the arrangement of CA-CTD within the immature-like lattice can be formed independently of the arrangement of the CA-NTD and that the linker between them is highly flexible (Bharat et al. 2014). Furthermore, the authors have shown that the CA-NTD assemble independently and can oligomerize in three different ways to form curved lattices. This suggests a greater role for CA-NTD during the assembly and maturation of the new viral particle.

1.2.3.3 Nucleocapsid (NC)

NC is a 55 amino acids long basic protein with two zinc fingers (magenta in figure 1.3(A) and 1.3(B)). NC has multiple roles in viral RNA metabolism, binding and thus in Gag assembly. It was found that NC with its basic residues can bind to any negatively charged entity, especially viral RNA via its two zinc fingers (ZF 1 and ZF 2 depicted in figure 1.3(B)) and also to charged lipids but without any specificity towards a particular lipid (Kempf et al. 2015b). Nevertheless, NC role in Gag assembly and packaging is of huge interest to the scientific community. It was speculated that NC can indeed help in the tight packaging of Gag molecules through its interaction domain (I-domain) (Bowzard et al. 1998)(Burniston et al. 1999).

1.2.3.4 P6

As shown in figure 1.3 (in cyan), P6 is a 52 amino acids long protein with proline-rich motifs. Also called as Late domain/ L domain of Gag polyprotein, it plays a role in the late stages of viral life cycle. Major understanding of this domain came through the work of Göttlinger et al. 1991 where mutations in P6 domain found to affect the release properties of newly formed HIV-1 particles. Subsequent findings revealed that at least two short peptide motifs of P6 can affect the new viral particle release (Huang et al. 1995; Sakaguchi et al. 2005) and their phosphorylation could be essential for this functionality (Müller, Patschinsky, and Kräusslich 2002). Motifs such as P(T/S)AP motif (second amino acid is Thr or Ser) bind directly to the UEV domains of TSG101 to recruit ESCRT-I (Endosomal Sorting Complexes Required for Transport-I) (VerPlank et al. 2001). Another motif being, YPXL, initially discovered in equine infectious anemia virus (EIAV) is also present in HIV-1 P6 domain. It is known to interact with ALIX that in turn facilitates virus budding (Fujii, Hurley, and Freed 2007). Later, it was established that P6, indeed, interacts and recruits various cellular factors such as ESCRT-I/II&III components that could help in the viral release - detailed review for the same can be found here (Usami et al. 2009; Votteler and Sundquist 2013).

1.2.3.5 SP1 and SP2

The two yellow color patches in figure 1.3 are 14 and 15 amino acids long small spacer peptides existing within the Gag polyprotein along with the four major domains, MA, CA, NC, and P6. From what is known, these spacer peptides form continuous helixes with the C-terminal of the major domains and thus have a function regarding Gag structure. SP1 which forms such alpha helixes in continuation with the C-terminal of the CA (see figure 1.3) can thus regulate HIV-1 assembly in three distinct ways: Gag multimerization (Levin et al. 2005), viral production (Kräusslich et al. 1995)(Accola, Strack, and Göttlinger 2000) and maturation (Gay et al. 1998)(Wiegers et al. 1998)(Gross et al. 2000). In the case of SP2, it was understood that deletion of this peptide or induced mutations could result in a decreased Vif encapsulation (Huvent et al. 1998) and can also affect the morphology of the Gag particles (Gay et al. 1998).

1.2.4 Replication Cycle

Typically, the HIV-1 virus replication cycle involves a series of events that can be categorized into three different phases: (a) an initial early phase including binding and genome integration, (b) intermediate phase comprising viral component expression and (c) a late phase made up of assembly and budding of the new viral particles. The same was depicted clearly in figure 1.6, showing various events taking place from viral infection to new viral particle release.

1.2.4.1 Early phase: Binding and Genome integration

$CD4^+$ T-cells, the main target cell types of HIV-1, expresses three different receptors that help dock HIV-1 virus on to the surface of the cell: CD4 receptors and two chemokine receptors, CCR5 (C-C chemokine receptor 5) and CXCR4 (CXC chemokine receptor 4).
Of them, primary lymphocytes express both the chemokine receptors, CCR5 and CXCR4, while the macrophages only express CCR5. One of the two non-covalently associated subunits of the HIV envelope glycoprotein (Env), glycoprotein (gp) 120, docks with the CD4 receptor to reveal its variable domain, V3, that in turn interacts with the chemokine co-receptors (Trkola et al. 1996), (L. Wu et al. 1996). This secondary interaction triggers a conformation change within

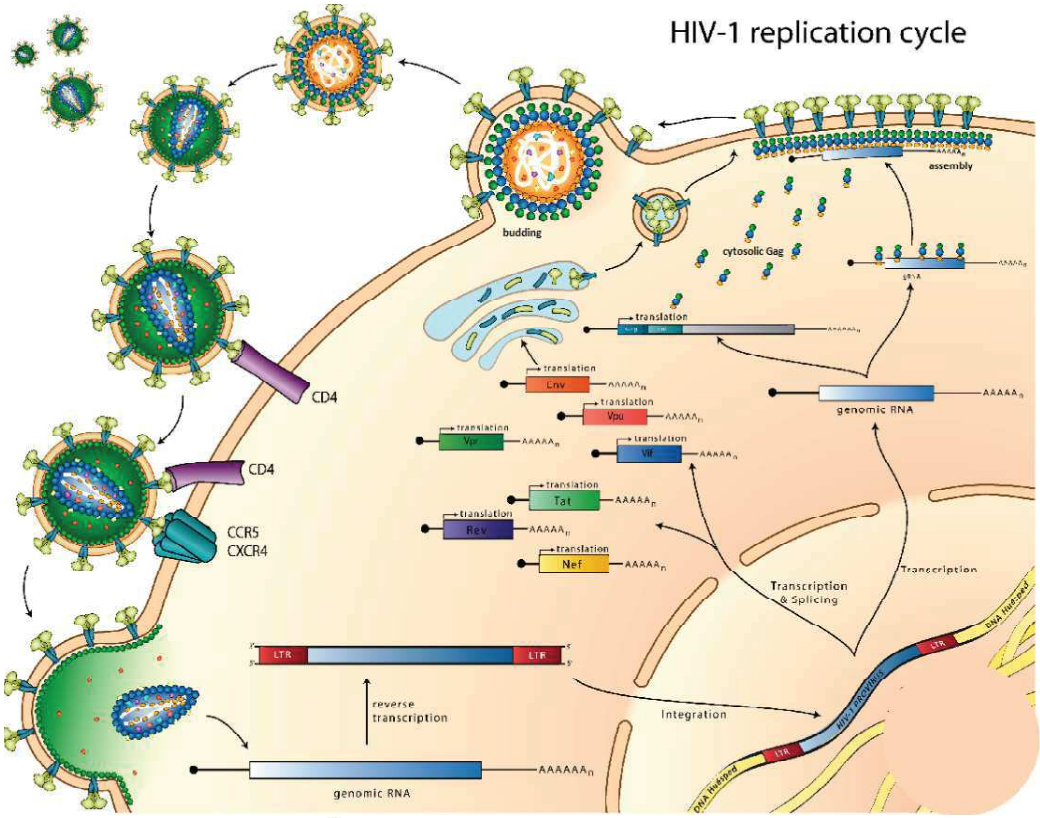

Figure 1.6: HIV-1 replication cycle, depicting from infection to viral particle release. Modified and obtained under creative commons (credits: Pablo Ramdhor) [https://www.flickr.com/photos/opiado/4191226676]

gp120 (glycoprotein 120) to expose a fusogenic peptide at the amino-terminus of gp41. These series of events led to a fuso-active gp41 that inserts into the membrane of the host cell (Kwong et al. 1998) and eventually releases the viral core into the cytoplasm of the host cell. After entering the host cell cytoplasm, the viral core is partially opened to convert the genomic RNA into a double-stranded viral DNA by RT. Cellular factors, such as TRIM-CypA (Tripatriate motif family-Cyclophilin A) and TRIM5α, have been proposed to modulate HIV-1uncoating (Diaz-Griffero et al. 2007; Forshey et al. 2002). Recently, new data suggest that 60-120 min after infection, the viral core starts to disintegrate only to release the contents of the core (Yingxin Ma et al. 2016). This event is followed by the formation of a viral pre-integration complex (PIC), containing viral DNA, Integrase (IN) with Gag, Pol proteins and some cellular factors assisting the transportation and integration of the viral DNA with that cellular genetic material to form what is called as “a Provirus” (Roger H. Miller and Sarver 1995), (Thomas et al. 2006).

1.2.4.2 Intermediate phase: Viral gene expression and components generation

Even in a non-dividing cell, HIV-1 can replicate - an advantage that can help the virus by expressing the viral DNA into RNA using host cellular machinery. Once the proviral DNA is expressed, the RNA is spliced into various intermediate mRNAs (messenger RNA): (i) a ~2kb multiply spliced RNA that codes for viral regulatory proteins, Tat, Rev, and Nef, (ii) a ~4.2kb single spliced RNA encodes Vpu, Vpr, Vif and Env proteins, and (iii) a ~9.2kb unspliced RNA translating into Gag and Pol proteins. While regulatory proteins help in the activation of provirus transcription and direct the export of genome length RNA/ Env RNA, accessory proteins like Vpr help in arresting the infected cells in G2/M phase to ensure high Gag and Gag-Pol production. More detailed review about the HIV-1 gene expression can be found here (Y. Wu 2004).

1.2.4.3 Late phase: Viral assembly and release

Viral assembly and release is supposedly the most complex process in the replication cycle, as all the required components have to be assembled in appropriate proportions to make a viable infective virus. The assembly of type C retrovirus and lentiviruses occur at the plasma membrane. Gag polyprotein – lipid interaction is the major prerequisite for the assembly of various viral components to form a viral particle. More details about the Gag protein-lipid interactions will be dealt in the coming sections. Subsequently, the recruitment of Env protein takes place by a series of transportation, cleavage, and trafficking along the cell membrane (Murakami 2012). Once internalized at the assembly site, a new viral particle starts to bud out of the cell membrane. At this stage, the virus-like-particle (VLP) is immature and non-infectious, but over the course of time, the Gag protein is cleaved by the proteases entrapped during assembly to form an inner conical shaped core and an outer protein coat layered by the host cell plasma membrane. A complete mature particle was depicted in figure1.2. Even though Gag alone can form virus-like-particles, it needs other components to be infectious and replication ready (Freed 2015). So to form a successful viral particle, all the components should be at the right place and at the right time. While Gag assembles along the membrane, rest of the components has to be recruited to form an infective and replicable viral particle. Thus, Gag interaction with

the lipid to form assembly platforms is the crucial step in the late phase of the viral replication cycle.

1.3 Membrane Systems

Historically, simple membrane systems are the walls that can delineate the cellular content from the external environment. Both prokaryotes and eukaryotes possess these membranes. Prokaryotes like *Escherichia coli* (*E.coli*) are surrounded by an outer rigid and porous cell wall (composed of polysaccharides and peptides) and an inner plasma membrane, which is a bilayer of phospholipids and associated proteins. This plasma membrane can act as a selective barrier for the passage of molecules. Indirectly, the plasma membrane determines the composition of the cytoplasm and so determines the identity of the cell itself. But as the systems evolved, the membranes started to play complex roles and become more crucial for the overall functioning of the cells or organelles they encapsulate, in the case of eukaryotes. Complex roles required complex components, eventually making the membranes more complex and highly dynamic. Figure 1.7 depicts a highly complex and evolved cellular plasma membrane of a typical eukaryotic cell. In general, membranes are made of lipids and proteins that have specific roles for the membrane to function as a unit. Indeed, the first evidence of lipid bilayer nature of biological membranes came from the study of two Dutch scientists (Edwin Gorter and Grendel) on red blood cells. Such as it, lipids and proteins formed the building blocks of cellular systems. Around 5% of the genetic material is responsible for the lipid metabolism and activities; this suggests the significance of lipids in the evolution of cellular systems. In addition to this, compartmentalization of organelles in eukaryotes further increased the role of membranes by many folds. Other than being a part of membranes, lipids also act as energy reserves, co-factors, and even hormones. In this dissertation, I shall exclusively deal with plasma membrane lipids and introduce a simple notion of understanding the organization of lipids and their potential role in HIV-1 assembly (section 1.4).

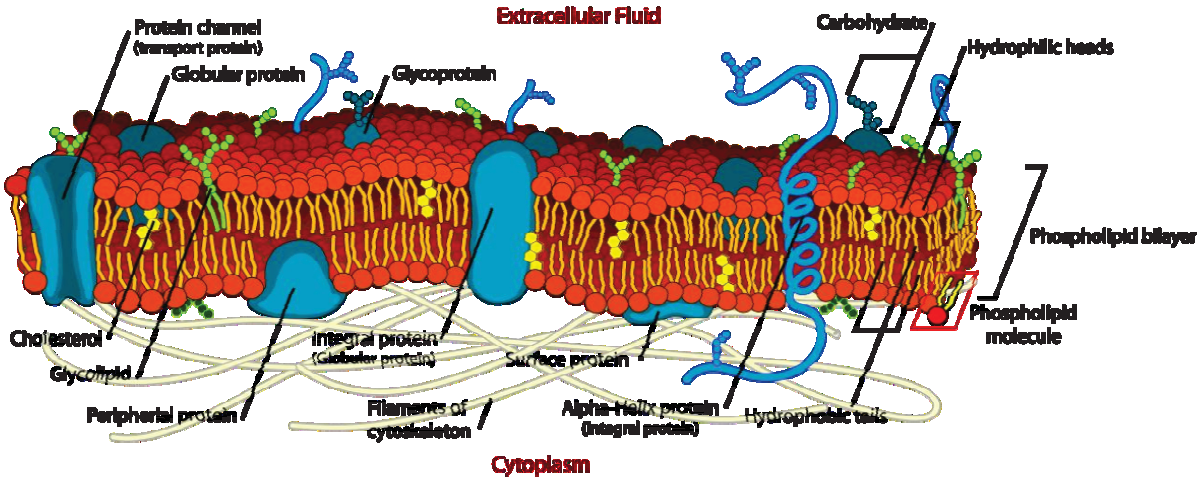

Figure 1.7: Detailed schematic of a typical cell membrane. (Credits: Lady of Hats Mariana Ruiz), [https://commons.wikimedia.org/w/index.php?curid=6027169]

1.3.1 Physicochemical properties of lipids

Lipids are amphipathic molecules that have a hydrophilic head and a hydrophobic tail bound to either a glycerol backbone or a sphingosine (figure 1.7). Because of this amphiphilic nature, they tend to self-assemble - maintaining a lower entropy and are governed by weak and non-covalent interactions. It leads to varied structures of lipid bilayers. In biological context, two important features of lipid bilayers are critical, (a) structure of phospholipids, as this amphipathic nature is responsible for its function as a barrier to water soluble molecules and (b) as these natural lipids form viscous fluids, not solids is important for a soft and flexible form allowing the diffusion of both lipids and proteins, laterally. So, both lipid composition and lipid structural differences affect the physicochemical properties of the membrane. Importantly, fatty acid & head group modifications and backbone diversity resulted in a diverse set of lipids.

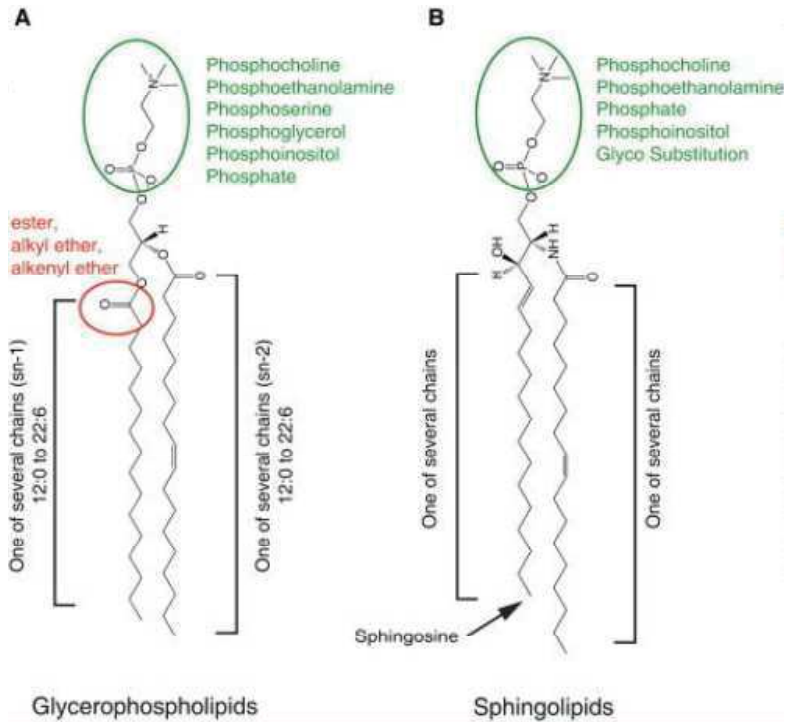

Figure 1.8: Schematic representation of mainly two different kinds of lipids with glycerol and sphingosine backbone. Variations are brought about by a change in their head group or the acyl chain length or unsaturation or type of bonding between the acyl chain and the glycerol backbone. (Reproduced with permission from Cell Membranes: The Lipid Perspective Coskun, Ünal et al. Structure, Volume 19, Issue 11, 1543 – 1548.)

1.3.1.1 Fatty acid & head group modifications

In a lipid, fatty acyl chains form the hydrophobic region and the head group is the hydrophilic entity. To oversimplify, one can say that fatty acid chains determine the permeability and viscosity of the membrane, while head groups provide the much-needed charge for interacting with various cytosolic proteins. Fatty acyl chains can be either saturated or unsaturated. For equivalent polar heads, lipids with saturated fatty acyl chains are linear and form compact structures that have high phase transition temperatures and less permeability. On the contrary, unsaturated acyl chains with their double bonds form loose structures that are more permeable and have low phase transition (see section 1.3.1.3 for the definition of phase transition). Indeed, lipids can have their acyl chains that are either saturated (like Dipalmitoylphosphatidylcholine (DPPC)) or unsaturated (like Dioleoylglycerophosphocholine (DOPC)) or even both (like brainPalmitoyl Oleyl Phosphatidyl Choline (POPC)). In eukaryotic cell membranes, and specifically, the plasma membrane, two main groups of lipids can be distinguished as a function

of their connection between the polar head and the acyl chains. The glycerolipids that contain a glycerol as the connector (see figure 1.8 left) and the sphingolipids that contain a sphingosine as the connector (see figure 1.8 right). The huge diversity of lipid chemical compositions starts with the possibility of having different acyl chains (as mentioned earlier) and further with different polar heads.

These combinations will result in lipid bilayers with varied structures and properties. The most common head groups are either neutral or negatively charged moiety. These can be an unmodified phosphatidic acid or a -choline/ -ethanolamine/ -serine/ -glycerol/ -inositol group or other complex branched sugars, in the case of sphingolipids. Finally, the head groups can be diversely charged: PC and PE are neutral, PS & Phosphatidylglycerol (PG) are mono-charged, but PI with varying number of phosphate groups can have mono to hexa charge. Together, all these variations form a diverse set of lipids that add unique physicochemical properties and functionality to the cellular membranes.

1.3.1.2 Self-assembly of lipids:

Geometry and inter-molecular forces between the head groups and fatty acid chains of various lipids present in the membranes play a key role in the overall structure. These forces, along with the geometry of the lipids, between the adjacent lipids can induce lateral pressure within the membrane affecting the entropy of the entire structure. To keep the system stable, the membrane bends and so giving itself a curvature that can be named as spontaneous curvature (SC). This suggests that the mean curvature of the membrane is a direct outcome & contribution of each and every lipid it is comprised of. Figure 1.9 depicts the shape of different lipids and the various shapes they can form at critical micellar concentrations. In a way, packing of the lipids in the bilayer forces the membrane to take a shape. Israelachvili-Mitchell-Ninham packing parameter:

$$P = {}^{v}/_{al} \qquad \textit{Eq: 1}$$

where v is the molecular volume, a is the cross-sectional area of the head group and l being the length of the molecule (Israelachvili 1977) has been proposed and the value of P can emphasize the structure of the lipid assembly. Based on the P value, there are two kinds of lipids (figure 1.9). Bilayer prone lipids are those that have a P value close to 1. These are cylindrical lipids that pack tightly and partitions preferably into liquid-ordered (Lo) regions. Non-bilayer prone

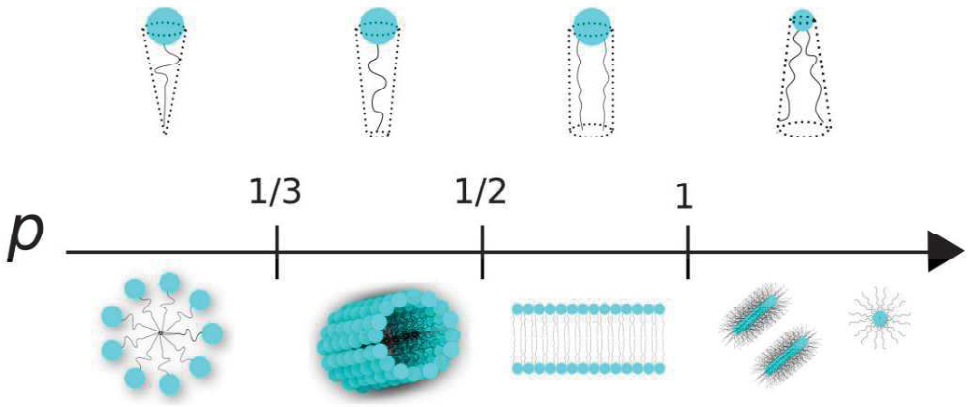

Lysophospholipids (sphingosine etc.) Detergents	PC, SM, PS, PI PG, PA	PE, Cholesterol (Chol)

Figure 1.9: Schematic representation of different shapes of lipid molecules and the varying aggregates with a change in the *P* factor.

lipids are those with a packing parameter value far from 1. A lipid whose *P* value is less than one induces positive curvature and form micelles in water. On the opposite, when the value is greater than one, they induce negative curvature and form inverted micelles.

1.3.1.3 Phase transition in lipid membranes:

The physical state of lipids and lipid membranes varies with temperature, volume (area) and pressure (surface pressure). Model membranes are excellent models to study the phase transition temperatures of mono, binary and even ternary mixtures, as the composition of these membranes can be controlled. Basically, a lot of pure lipids can undergo a transition from solid state (S_0 also named L_β) to liquid disordered state (L_d also named L_α) along with a range of temperatures (from -20 to +50°C) (see figure 1.11). Melting temperature (T_m) is defined for single lipid, but as the complexity increases there occurs the formation of coexisting phases. The pure lipid T_m depends not only on the acyl chain length and saturation but also on the nature of the polar head (figure 1.11(B)).

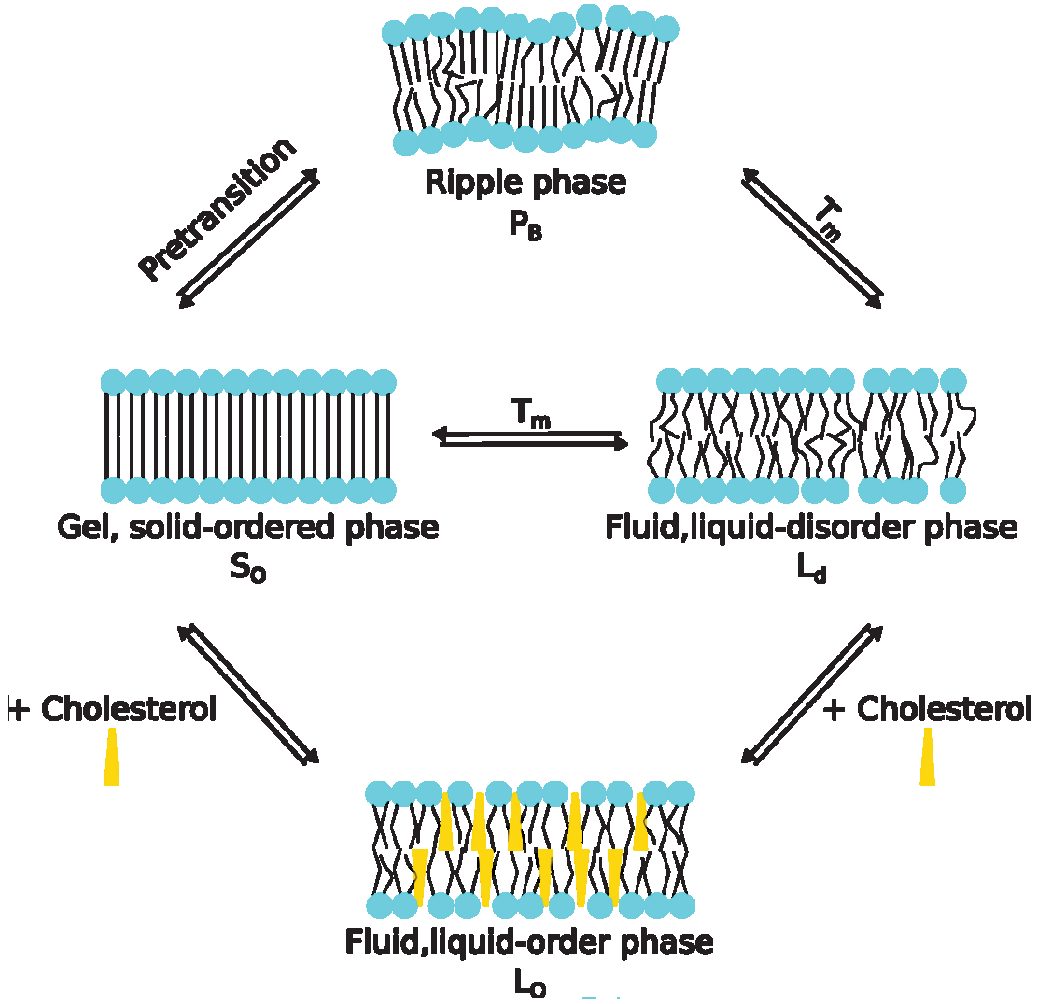

Figure 1.10: Scheme illustrating the different physical states adopted by a lipid bilayer in an aqueous medium.

These two states can be characterized by many different parameters, amongst which the lateral diffusion coefficient is one (Vaz, Melo, and Thompson 1989).But, when it comes to more complex mixtures of lipids, phase diagrams are helpful to describe their physical states.

For example, a binary mixture of high and low melting temperature lipids can be liquid and homogenous above the T_m of high melting lipid, solid and homogenous at temperatures below the T_m of low melting lipid and in co-existing phases when temperatures lie in between of the two individual T_m. (Feigenson 2007; Veatch and Keller 2005). This is illustrated in figure 1.11(A) in the case of the simple DMPC/DSPC mixture. Interestingly, the configuration where

fluid and gel coexist in membrane leads to the lateral phase separation and the generation of micro to macro domains.

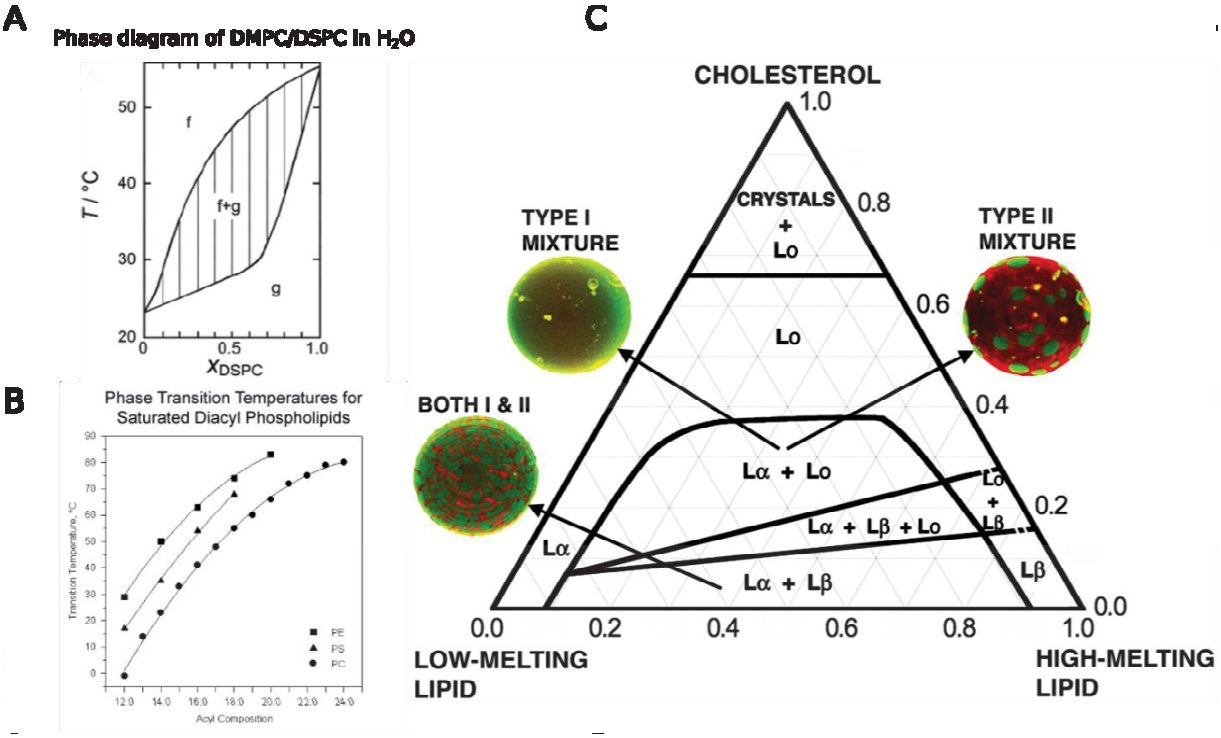

Figure 1.11: Phase transition temperatures observed for lipid mixtures of different compositions. (A) Phase diagram of DMPC/DSPC in H_2O (f, fluid phase; g, gel phase; f+g, gel–fluid two-phase coexistence region) (reproduced from (Janosch et al. 2004)), (B) Phase transition temperatures for saturated diacyl phospholipids (https://avantilipids.com/tech-support/physical-properties/phase-transition-temps/), and (C)Phase diagram of three component bilayer mixtures with cholesterol (reproduced from (Feigenson 2009)).

Phase transition in cholesterol-containing lipid membrane: Cholesterol (Chol) is the single most abundant lipid species in mammalian cell membranes. Interestingly, 90% of all cellular cholesterol resides in the plasma membrane. Ipsen et al. described the effect of cholesterol on the phase behavior of pure lipids by introducing a new type of phase namely the liquid ordered phase (L*o*) (Hjort Ipsen et al. 1987) (figure 1.10).

To simplify this, liquid ordered phase is lying somewhere between the solid phase and the liquid-disordered (fluid) phase (figure 1.10). Almost every experimental study on cholesterol containing different lipid mixtures has shown to produce these co-existing phases. For example, binary mixtures of high-T_m PC and Chol, as well as ternary mixtures of low-T_m PCs, cholesterol, and high-T_m PCs or SM, exhibit coexisting L*d* and L*o* phases (Crane and Tamm 2004; John R.

Silvius 2003) (figure 1.11(C)). Cholesterol is described to play a major role in the phase separation occurring in the plasma membrane. The existence of these co-existing phases has been implicated in biological functions and is usually designated as lipid rafts.One characteristic of this liquid ordered state is to exhibit a mean lateral diffusion coefficient only ~2-3 folds lower than L*d* phase (Veatch and Keller 2005), which makes it be directly observed in cell membranes (Bacia et al. 2004).

1.3.2 Plasma Membrane (PM)

Structurally speaking, a plasma membrane is a ~60 Å thick with a hydrophobic core that is flanked on its either sides by polar head groups and spanned by various transmembrane proteins and peripheral proteins (W. Cho and Stahelin 2005). Singer and Nicholson described plasma membrane as a fluid-mosaic where proteins are floating in a sea of lipids(Singer and Nicolson 1972). Although this model is still relevant, it underestimates the complex nature of the plasma membrane. The general view of the plasma membrane has been changed to a more heterogeneous, asymmetric and dynamically compartmentalized bilayer. In this new view, extracellular proteins, actin meshes, sugar-sugar and protein-sugars interactions also play a role in its organization (figure 1.7).

1.3.2.1 Plasma membrane lipid organization

In a typical human cell membrane, there exists ~1000 different kind of lipids (van Meer 2005). Lipids in the membrane do show a great level of mobility by changing their conformational, rotational, lateral diffusion and even by flip-flopping between the monolayers (Mouritsen 2005). The plasma membrane is known to be highly heterogeneous and asymmetric. Heterogeneous, for it has a wide variety of lipids and asymmetric, for the vastly different composition of the monolayers it comprises.

Axial asymmetry: Cell plasma membrane comprises of two monolayers with different compositions. While PC and SM form the neutral lipids existing predominantly in the outer

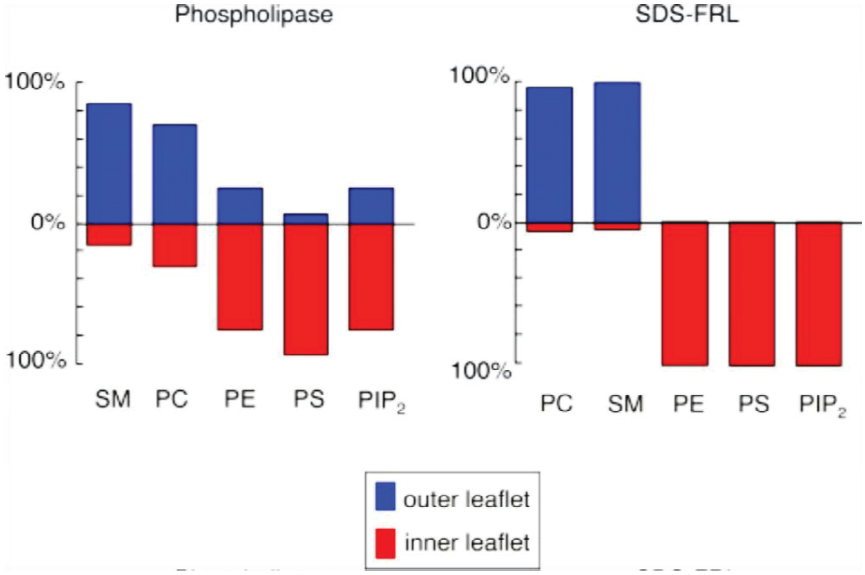

Figure 1.12 Asymmetric trans-bilayer distributions of phospholipids in red blood cell membranes given as a percentage of each phospholipid. (Left) Lipid distribution measured using phospholipases and TNBS. (Right) Lipid distribution measured by SDS-FRL(reproduced from (Murate and Kobayashi 2016).

leaflet, charged lipids like phosphatidylserine and phosphatidylinositol phosphates are located in the inner leaflet of the cell plasma membrane (see figure 1.12). Contrary to this asymmetric distribution, cholesterol exists in both the leaflets – bringing flexibility to the membrane. By varying cholesterol/phospholipid ratio, the cell can regulate membrane fluidity in eukaryotes (Bastiaanse, Höld, and Van der Laarse 1997).Further, cholesterol is also known to stabilize phospholipid domains that can play a role in the functioning of the plasma membrane (Jiang et al. 2014; Ohvo-Rekilä et al. 2002).

Lateral Organization: Based on the phase behavior of lipid mixtures, a lot of effort was put into identifying lateral domains in cell plasma membranes using either biochemical or biophysical techniques since the early 70s. In the late 90s, the lipid domains concept has been revitalized by the emergence of "rafts". As elaborated earlier, a complex mixture of lipids in membranes can have both L*d* and L*o* phases. Typically, biological membranes exist in fluid phase (L*d*) where transient local lateral liquid ordered domains exist by means of lipid-lipid interactions or lipid-protein interactions (Simons and Ikonen 1997).Cholesterol-lipid interactions play a key role in the formation these rafts (Brown and Rose 1992; John R. Silvius 2003). Membrane rafts are

defined as being transient, heterogeneous, highly dynamics, sterol and sphingolipid-enriched domains with lipid-anchored proteins (L J Pike 2006a).Rafts are described to play an active role in numerous cellular processes. They were primarily identified as insoluble fractions of the membranes solubilized with Triton-X100 at low temperature and originally named as DRM for Detergent-Resistant Membranes (K Simons and Ikonen 1997). Although some of the researchers were able to extract native raft-like structures using this methodology (Brown and Rose 1992)(Hanada et al. 1995), the possibility of this method resulting in the generation of artificial raft composition which might not be present in native live cells has raised concerns (Lingwood and Simons 2007)(Lichtenberg, Goñi, and Heerklotz 2005)(Shogomori and Brown 2003). For that reason, the search for rafts in living cells started. But, visualizing rafts is a daunting task, owing to their transient delicateness, metastable and nanoscale nature. Nevertheless, recent developments in imaging technologies have revealed few glimpses of how these lipids behave along the plasma membrane in the presence and absence of external stimulants like other lipids or proteins (Sezgin and Schwille 2011). Due to the axial heterogeneity, a question can be immediately raised. Since rafts are enriched in SM and cholesterol, they are supposed to exist almost exclusively in the outer leaflet of the plasma membrane. How can “rafts” exist in the inner leaflet of the plasma membrane then? How can some inner leaflet binding proteins partition into rafts?

To overcome that problem, biologists use the term “raft-like”, this, in turn, meant “everything that is not soluble after membrane solubilization with any detergent at a given temperature”. As already stated by Edidin, “membrane are not just rafts” (Shaikh and Edidin 2006).It was speculated that domains of different lipid compositions can exist in the inner leaflet that can be coupled with the rafts of the outer leaflet. Studies performed on an asymmetric model system at the thermodynamic equilibrium end up in a coupled macroscopic phase separation (L*o*/L*d*) on both leaflets (Allender and Schick 2006; Kiessling, Wan, and Tamm 2009; Wan, Kiessling, and Tamm 2008). It is also important to state that, as originally proposed by Sackmann (1995), cytoskeleton (Ehrig et al., 2011a; Sens and Turner, 2011) as well as trafficking (Turner et al., 2005) could play a major role in the lateral segregation of lipids. This more generalized view opened a new field in understanding the role of trans-bilayer domains coupling with the functionality (Raghupathy et al. 2015).

1.3.2.1 Lipid-Protein interactions

Lipid-protein interactions along the plasma membrane form the basis for cellular communications with the external environment and vice-versa. There are mainly two types of protein based interactions occur with the lipids present in the plasma membrane: (i) membrane protein based interactions and (ii) peripheral or cytosolic protein based interaction.

Membrane proteins form the crucial basis for many functional cellular signaling pathways. Proteins like potassium ion channels & GPi anchored proteins (Glycosylphosphatidylinositol anchored proteins) embed themselves into the cellular plasma membrane with their membrane penetrating domains. The surrounding lipids that closely interact with the protein are necessary for proper functioning of these proteins (Sackmann 1984, Kinnunen et al. 1994)). The first layer of lipids that bind closely to the membrane protein are called annular lipids and have a very low diffusion constant (Lee 2011). These interactions could be due to hydrogen bonding or hydrophobic attraction or electrostatic interaction. The tight interactions of lipids with transmembrane proteins lead to the concept of "hydrophobic mismatch". Such proteins direct the lipid composition around them (Gil et al. 1998) and any alterations with respect to lipid composition due to thermodynamic conditions or membrane altering molecules or protein conformational changes (Cantor 1997) can activate or de-activate a protein (Sackmann 1984). Some proteins might have a high preference for specific lipids and thus can play a regulatory role on the functionality of the membrane proteins (Gonen et al. 2005). In that respect, the hydrophobic mismatch is one way to generate lipid nanodomains around proteins.

Other types of lipids which exist in small pockets or clefts that are formed by membrane spanning proteins are called non-annular lipids. These lipids can also be a part of a regulatory function, for example, cytochrome bc1 complex has PI lipids in their inter-helical position that help in the assembly of the complex (Palsdottir and Hunte 2004).

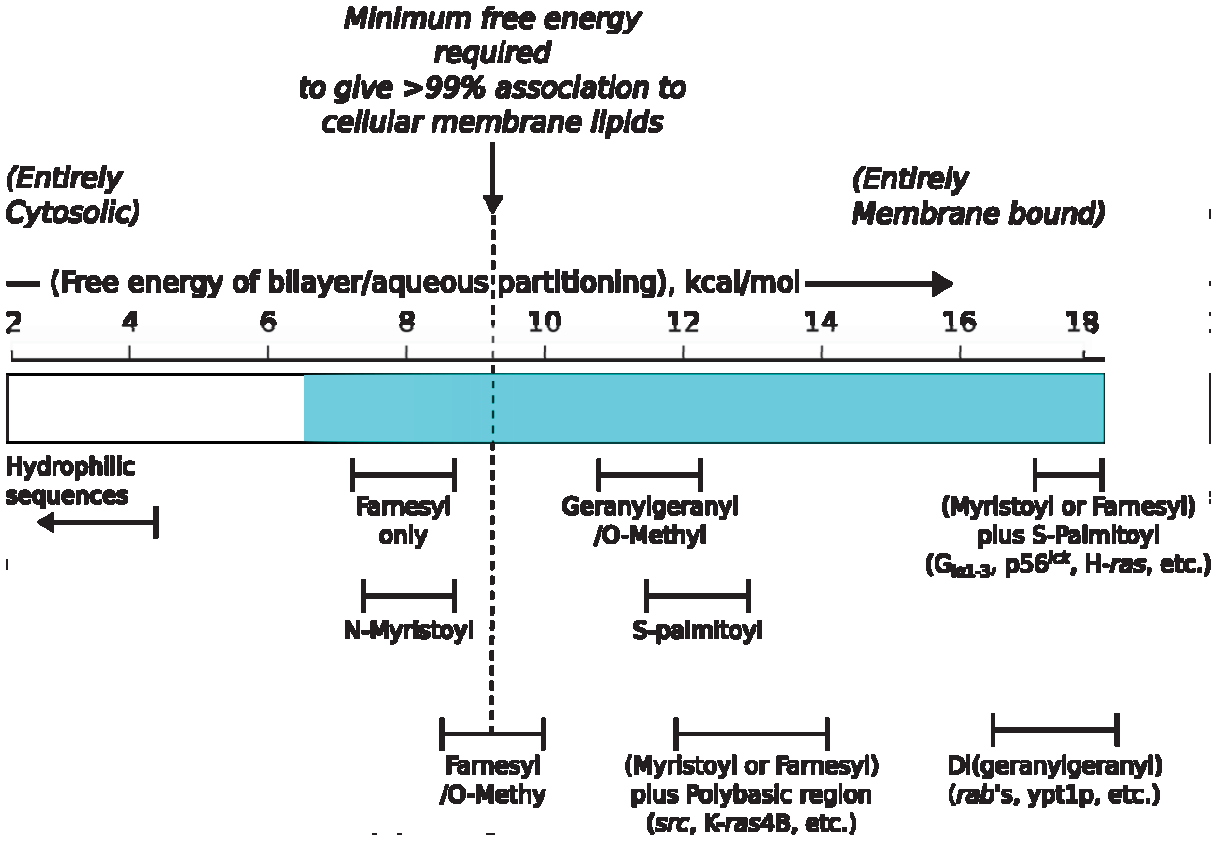

Figure 1.13: Free energies of association of different lipid-modified protein groups with lipid bilayers, as estimated from measurements of the affinities of association of lipid-modified peptides with lipid vesicles. (modified and reproduced from (J.R. Silvius 2002)). The vertical dashed line represents the calculated minimum free energy of membrane binding required to give >99% membrane association of an intracellular protein if the concentration of membrane lipids exposed to the cytoplasm lies in the low millimolar range, as has been estimated for a typical mammalian cell, Shading schematically illustrates the predicted distribution of a protein between the aqueous and membrane phases under intracellular conditions (white, entirely aqueous; black, entirely membrane-bound) if the protein binds to membranes with the indicated free energy.

Diffusion and electrostatic forces are primarily responsible for membrane targeting of peripheral proteins (Murray et al. 2002). Initial membrane absorption is followed by specific lipid interactions and further membrane penetration depending on the protein structure. Indeed, while negatively charged lipids facilitate the electrostatic binding of oppositely charged proteins, acylation of these proteins can help them anchor tightly to the lipid membrane by incorporating into the hydrophobic acyl-core (see figure 1.13) (Heimburg, Angerstein, and Marsh 1999).

Based on the membrane localization, there are three types of peripheral proteins: (i) S-type proteins – predominantly interact with the polar heads, (ii) I-type proteins – partially penetrate

into the lipid bilayer, and (iii) H-type proteins – significantly penetrate into the hydrophobic core of the lipid bilayer. While possession of unique structural components (lipid binding domains/lipidation/aromatic aminoacids) enhances the membrane-binding ability of the proteins, but the specificity to a particular lipid majorly depends on the structural conformations of the protein. For example, pleckstrin homology (PH) - domain containing phospholipase C delta (PLCΔ) (C. Zhou, Akhtar, and Abdel-latif 1993)&exchange factor for ARF6-PH (EFA6-PH) (Macia et al. 2008b)domain bind to PI(4,5)P_2 with high specificity because of the structural conformation that allows it to pocket PI(4,5)P_2 head group. Contrary to this, myristoylated proteins like alanine-rich C-kinase substrate (MARCKS) peptide can bind to both PS &PI(4,5)P_2 (Gambhir et al. 2004) majorly due to electrostatic attractions. Apart from this, a series of many other cellular proteins interact with the lipids present in the plasma membrane (W. Cho and Stahelin 2005). One such example is the myristatedVisilin-like-Proteins 1 & 3 (VILIP-1 &3) that are found to bind highly negatively charged lipids in the presence of calcium which helps in membrane anchoring by inducing a myristoyl switch (Rebaud, Simon, et al. 2014; Rebaud, Wang, et al. 2014).

Like cellular proteins, viral proteins can also bind to lipids. For example, Elise et al., 2014 has shown that murine leukemia virus Gag protein can bind to the host membrane initially driven by electrostatic forces and then anchor itself by incorporating the myristoyl (Elise Hamard-Peron and Muriaux 2011). The case of HIV-1 Gag will be detailed in section 1.4.3.

1.3.2.3 Curvature

Membrane curvature can be a resultant of either spontaneous curvature (SC) of the bilayer or the induced one. SC is influenced by the curvature of all its components and further depends on each monolayer SC (figure 1.14(A)). For example, monolayers comprised of cylindrical molecules whose SC is zero (0.5<P<1) will form zero curvature membranes. Physical properties of lipid bilayers play a greater role in defining the shape of membranes. To understand the induced curvature, it is important to acknowledge the role of the two competing physical properties of lipid bilayers: (a) homogeneous lipid bilayers tends to remain flat and are resilient towards

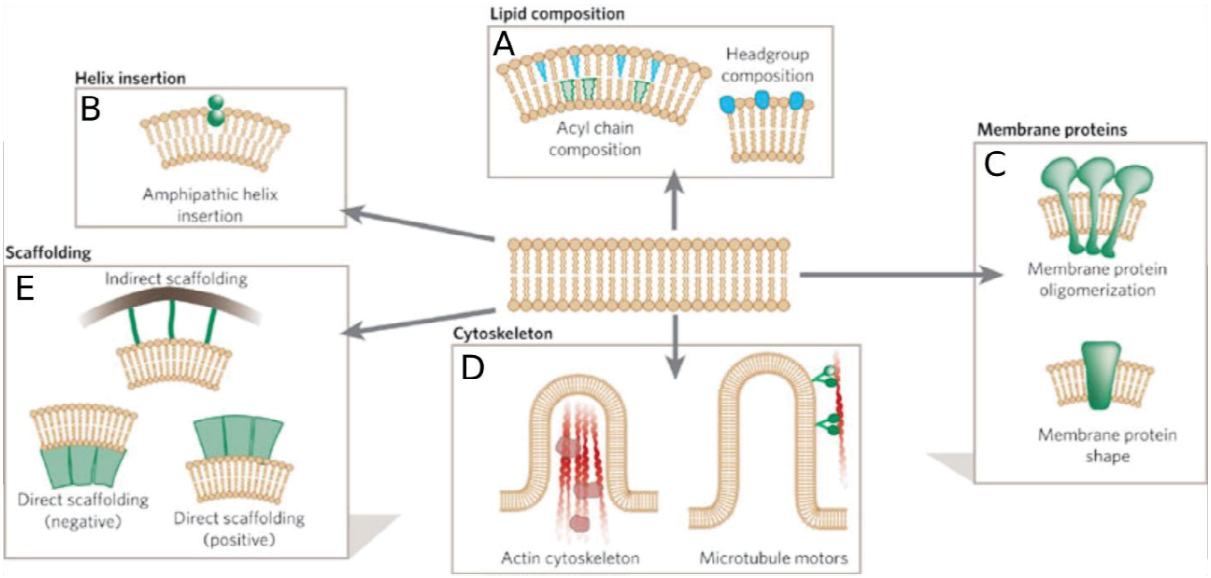

Figure 1.14: Lipid membrane curvature generation. (A) Spontaneous curvature due to the asymmetrically enrichment of shaped lipids, (B) Protein hydrophobic moiety insertion, amphipathic helix, C2 domain or loop insertion, (C) Membrane proteins affecting curvature to the lipid bilayer. (D) Bundles of protein filaments stabilizing or affecting the membrane curvature. (E) Scaffolds of proteins that bind to the membrane through adaptor proteins inducing curvature. Reproduced from (McMahon and Gallop 2005).

bending. This tendency of the bilayers to remain flat or resistance towards bending is dictated by the symmetry of monolayers and by the intra-molecular interactions present between lipid molecules. Surprisingly for a 4 nm thick film, the bending rigidity (κ) of the lipid bilayer is about 15-30 k_BT (Marsh 2006), ie., much higher than the energy provided by thermal fluctuations. This suggests that the latter cannot determine the membrane shapes. (b) Lipid bilayers tend to be continuous to avoid having edges that can arise due to ruptures or structural defects. In the case of an edge, the bilayer tends to avoid it by adopting a closed shape – unavoidably accompanied by bilayer bending. These competing physical properties – membrane rigidity and the tendency to prevent edge formation force any bilayer larger than 200 nm to adopt a closed spherical shape. The bending energy of this spherical bilayer is about $8\pi\kappa = 500k_BT$, independent of the sphere radius(Helfrich 1986). Thus, a homogeneous and symmetric lipid bilayer tends to adopt closed sphere shapes. Further inducing a deformation to the spherical shape will require, either to make it structurally asymmetric or to apply energies in the range of tens of hundreds of k_BT. Below are the mechanisms that can achieve membrane deformation or reshaping:

Lateral Domain driven shape: Domain boundary can provide the necessary driving force for membrane budding even in symmetric lipid bilayers. This is brought about by the ability of lipids to phase separate into co-existence regimes. Domain-driven budding predicted theoretically (R Lipowsky 1993) has been studied in different lipid systems and the involvement of fluid domains in protein driven membrane morphogenesis has also been shown (Shnyrova et al. 2007; Shnyrova, Frolov, and Zimmerberg 2009). Does lipid polymorphism play any role in this process? SC of lipids is an important parameter in regulating the main driving force of the domain-driven budding, the line tension (Döbereiner et al. 1993; Staneva, Angelova, and Koumanov 2004). Co-existing phases in lipid bilayer marks with the presence of thicker fluid ordered regions and thinner fluid disordered regions which lead to membrane height mismatch at the phase boundaries (Kuzmin et al. 2005). This difference in thickness between the membrane regions is smoothed out by non-bilayer lipids, thus lowering the energy of this mismatch. The stimulating effect of domain budding by lipids with large SC has been reconstructed experimentally (Döbereiner et al. 1993). It is becoming clear that a 100-nm vesicle derived from the cell has a distinct lipid composition than its parent membrane. Moreover, the degree of lipid ordering in those derived vesicles is different. This suggests that phase separation and its consequent line tension between domains results in budding and lipid sorting (Klemm et al. 2009). This "boundary" effect plays an important role in cellular membrane morphogenesis through membrane transformations: it is called "topological remodeling".

Tuning shape:

Protein domain insertion: Amphipathic or hydrophobic protein domain insertion into the lipid bilayer largely perturb the structure of the membrane. This leads to the generation of local membrane curvature when the perturbation is asymmetric (figure 1.14(B)). The effectiveness of this mechanism depends on the extent of the insertion into the membrane matrix. It was found that shallow protein insertions to be more powerful in generating a membrane curvature over the integral insertion or membrane spanning (figure 1.14(C)). The high effectiveness of curvature generation by shallow insertions has been suggested by previous computational modeling of the embedding N-terminal amphipathic helices of ENTH domains and of N-BAR domains(Henne et al. 2010; Madsen et al. 2010).

Forcing Shape:

Push-pull: Cellular organelles have complex membrane shapes. For example, peripheral endoplasmic reticulum (ER) Golgi complex and mitochondria have an elaborate 3D network of 10-50 nm tubules that bend to form compartments within the organelle (Mironov et al. 2003; Palade 1953; Shibata, Voeltz, and Rapoport 2006). It can be possible that ensembles of polymerizing actin filaments or groups of molecular motors such as kinesins or dyneins can help stabilize the structures (figure 1.14(D)). The required force (f) can be estimated by dividing the membrane bending rigidity (κ) by membrane curvature radii (r~20nm), which gives $f = k/r \approx 10$ pN (Kozlov et al. 2014). While the force necessary to stabilize is high, bundles of actin filaments and molecular motors can provide enough stabilizing force as the minimal force generated by one molecular motor or an actin filament is 1pN (Kull and Endow 2013; Mogilner 2006).Further, this force has to be exerted perpendicularly to the plane of the membrane for maximal effect.

Protein scaffolds: Another form of membrane asymmetry, achieved through the binding of hydrophilic proteins to tone side of the bilayer, can result in membrane curvature. Such proteins or oligomers of proteins, referred as scaffolds, can bend the membrane most efficiently if their membrane interaction faces are curved or when they polymerize with a curved architecture. By imposing their curvature to the interacting membrane face, they can curve the membranes into different shapes (figure 1.14(E)). For example, COPI, COPII, and Clathrin can form spherical scaffolds (Faini et al. 2013), dynamin family proteins involved in endocytosis can form cylindrical scaffoldings (Ferguson and De Camilli 2012; Roux et al. 2010). But for these scaffolds to effectively bend the membranes, the energy of binding and scaffold rigidity must exceed the membrane bending energy and rigidity, respectively. In the case of monomeric cylindrical scaffolds of some BAR domain proteins (Daum et al. 2016; Itoh and De Camilli 2006), the efficiency depends on the contact area. The larger the membrane contact surface – the closer the generated membrane curvature to that of the proteins intrinsic curvature.

Protein domain bound to the membrane surface has been suggested to generate membrane curvature by crowding mechanism. The essence of this mechanism is that hydrophilic protein domains undergo a thermally driven lateral diffusion and collide with each other in a plane, which is parallel to, but remote from, the membrane plane by a distance equal, approximately, to

the domain size. A stunning example of such a behavior was demonstrated by (Stachowiak et al. 2012). Using his-tagged green fluorescent protein (GFP) and Nickel-Nitrilotriacetic acid (Ni-NTA) lipids containing giant unilamellar vesicle (GUV), they were able to show that non-membrane binding protein like GFP that is tethered peripherally can also induce membrane bending. Authors hypothesized that the high local surface density of proteins is responsible for this effect and the membrane bends to dilute the high local surface density of proteins. Nevertheless, such an effect has yet to be observed *in vivo*.

1.4 HIV Gag interaction with plasma membrane

1.4.1 HIV-1 Lipidome

Protein binding to lipids can induce a wide range of structural and conformational changes in the protein, lipid and even the membrane in entirety. Many retroviral proteins are known to be enveloped by host cell membrane during the process of budding out from the cell surface. This suggests that not only the viral particle has the traces of host cell on it, but also specific lipid interactions of the viral protein can be known as the viral particles budding from these assembly platforms could retain all the trapped lipids. In cells, it was shown that HIV-1 particles and HIV-1 Gag co-localize with raft markers (Nguyen and Hildreth 2000)(O W Lindwasser and Resh 2001)(A Ono and Freed 2001a)(Bhattacharya, Repik, and Clapham 2006).When probed for membrane phase properties and fluidity, it was revealed that the viral membrane is in a liquid-ordered-like state (Aloia et al. 1988; Aloia, Tian, and Jensen 1993; Lorizate et al. 2009). These results directed to hypothesize that HIV-1 viral particles bud from raft-like structures of the plasma membrane. In support of this hypothesis, scientific findings suggest that the viral membrane is rich in lipids those are present in cell-derived raft membrane domains (Linda J Pike et al. 2002; Zech et al. 2009). Finally, lipidomic studies by Chan et al. and Lorizate et al. suggested that viral membrane composition is enriched with cholesterol, sphingolipids and PI(4,5)P_2 (figure 1.15) when compared with that of the host cell plasma membrane (Chan et al. 2008a; Lorizate et al. 2013). Further, Chan et al. 2008 also found that when cells are expressed

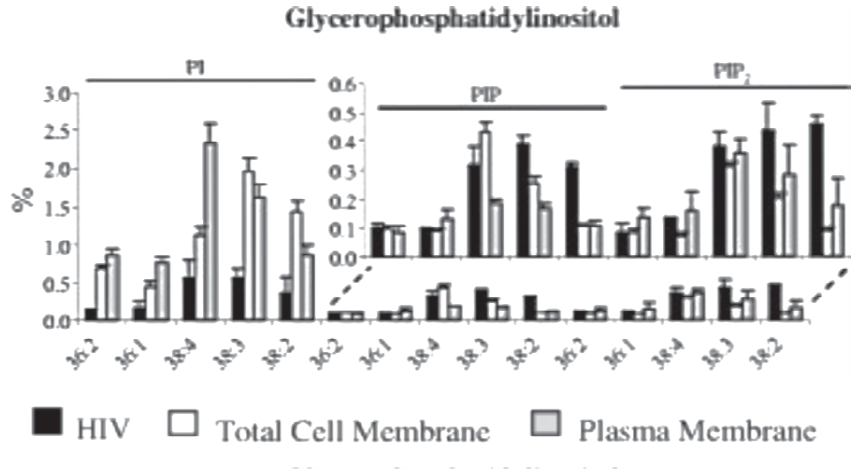

Figure 1.15: Enrichment studies of $PI(4,5)P_2$ in the viral membrane of HIV viral particles produced from H9 cells to that of the total membrane and plasma membrane of H9 cells (reproduced from Chan et al. 2008a).

with Gag protein lacking the MA domain - the enrichment of $PI(4,5)P_2$ in the viral membrane is reduced by two folds. This suggests that MA domain is responsible for the enrichment of $PI(4,5)P_2$.

1.4.2 Phosphatidylinositol-4,5-bisphosphate ($PI(4,5)P_2$)

As previously stated, cellular lipid membranes are dynamic structures that contain >1000 different lipid species(van Meer 2005). Among the many lipids that are present in the plasma membrane, one lipid that is unique in both physio-chemical properties and functional significance is phosphatidylinositol phosphates (PIPs). PIPs are derived from phosphatidylinositol (PI), synthesized in the ER by a PI synthase enzyme that utilizes both Cytidine Diphosphate Diacylglycerol (CDP-DAG) and myoinositol. PI is then transported from the ER by PI transfer proteins(Cockcroft 2007) and possibly vesicular trafficked to different cellular membranes. Recently, the PI synthase enzyme was found localized in a highly mobile organelle originating from the ER (Kim, et al. 2011). The discovery of this organelle harboring PI synthase suggests that PI may be dynamically disseminated throughout the cell via this machinery. Once distributed, PI can

be reversibly phosphorylated on the3, 4, and/or 5 hydroxyl group yielding seven different PIP species. These include the monophosphorylated(PI(3)P, PI(4)P, and PI(5)P) as well as the bis ($PI(3,4)P_2$, $PI(3,5)P_2$, and $PI(4,5)P_2$(figure 1.16) and trisphosphorylated ($PI(3,4,5)P_3$ forms. Having such a phosphorylated head group, not only make the lipid bulky with ~75$Å^2$/molecule footprint but also gives a charge that is highly negative, ~-3 to -4 (Toner et al. 1988; J. Wang et al. 2002). $PI(4,5)P_2$ estimated to be in the range of 5000–20,000 molecules/m^2 in the PM cytosolic leaflet (Falkenburger, Jensen, and Hille 2010). It can attract and bind nearly 280 different intracellular proteins (Catimel et al. 2008; Gericke et al. 2013). Although most of the interactions are well documented using *in vitro* and *in vivo* studies, the role played by the $PI(4,5)P_2$ during signaling events in cells is yet to be deciphered in-depth. Lipid lateral organization could be decisive to execute signaling responses as the movement of the lipids are highly regulated due to many diffusion barriers (Trimble and Grinstein 2015). But, enrichment in the form of domains is largely disputed (van Rheenen et al. 2005) as the high negative charge of this lipid head group could essentially hinder the formation of such enrichment under natural conditions/no external influence. Nevertheless, recent coarse-grained simulation studies revealed the presence of tiny clusters of $PI(4,5)P_2$ (Ingólfsson et al. 2014). This finding neither right off the presence of monomeric $PI(4,5)P_2$, nor the presence of $PI(4,5)P_2$ clusters but only increases the complexity of the system (Kolay, Basu, and Raghu 2016). For example, MARCKS peptide is shown to cluster freely diffusing $PI(4,5)P_2$ on model membranes (Gambhir et al. 2004). On the other hand, plasma membrane and actin bridging proteins like vinculin are known to bind only $PI(4,5)P_2$ clusters but not monomeric $PI(4,5)P_2$ (Saarikangas, Zhao, and Lappalainen 2010).

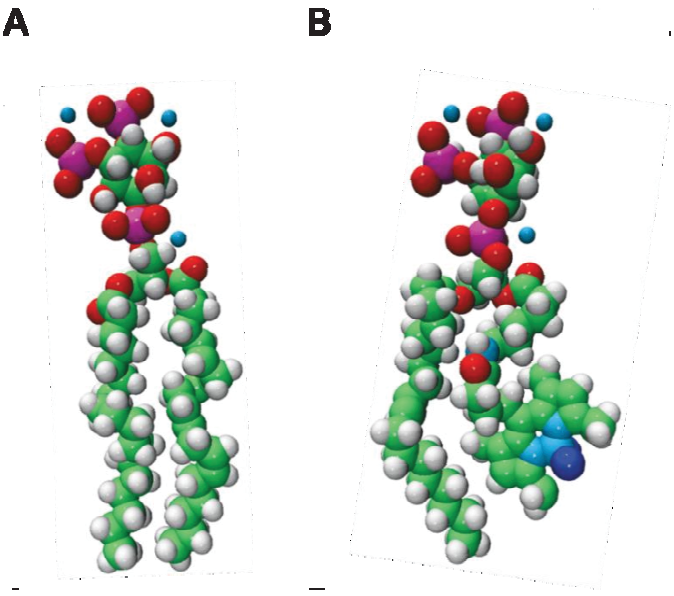

Figure 1.16: Schematic representation of

(A) L-α-phosphatidylinositol-4,5-bisphosphate and

(B) its TopFluor® derivative

Table 1.1: Apparent binding constants of viral matrix proteins of various retroviruses that have specificity towards $PI(4,5)P_2$ lipid

Virus Matrix protein	HIV-1	MLV	EIAV	RSV
$K_{p\ (co\text{-}sedimentation\ assay)}$	8.2±0.7 μM (Barros et al. 2016)	5.4±1.7 μM (E Hamard-Peron et al. 2010b)	NA	100 μM (Dalton et al. 2005)
$K_{p\ (NMR)}$	240±6 μM (Saad et al. 2006)	NA	182±56 μM (K. Chen et al. 2008)	NA

It could be true that both monomeric and clustered $PI(4,5)P_2$ exist and exchanged, dynamically. Phosphoinositides are enriched with polyunsaturated fatty acids at the sn-2 position and mainly contain 1-stearoyl and 2-arachidonoyl chains in the cellular setting. When PIPs are mixed with other lipids in cellular membranes, they can form PIP-enriched regions (Levental, and Janmey 2008; Y. H. Wang, Slochower, and Janmey 2014) that can be further stabilized by peripheral proteins that cluster PIPs (Gambhir at al. 2004; Saarikangas et al. 2009).

These PIP-binding structural modules, also known as membrane-targeting domains, include proteinkinase C (PKC) conserved 2 (C2) (Corbalan-Garcia and Gómez-Fernández 2014); pleckstrin homology (PH) (Lemmon 2010; Macia et al. 2008a; Rebecchi, Peterson, and McLaughlin 1992); Fab1, YOTB, Vac1, and EEA1 (FYVE) (Kutateladze 2010); Phox (PX) (Ponting 1996; Ellson et al., 2001; Seet and Hong, 2006; Kutateladze, 2010); epsin amino-terminal homology (ENTH) (Horvath et al. 2007); AP180 amino-N-terminal homology (ANTH) (Legendre-Guillemin et al. 2004); Bin amphiphysinRvs (BAR) (Saarikangas et al. 2009); band 4.1, ezrin, radixin, moesin (FERM) (Mani et al. 2011); phosphotyrosine binding (PTB) (Alajlouni et al. 2011); postsynaptic density 95, disk large, zonula occludens (PDZ) (Y. Chen et al. 2012; Wawrzyniak, Kashyap, and Zimmermann 2013); and Golgi phosphoprotein 3 (GOLPH3) (Dippold et al. 2009). $PI(4,5)P_2$ has also been successfully shown to be an important

secondary messenger in many signaling cascades. A detailed review can be found elsewhere (Gamper and Shapiro 2007). So far, viral matrix proteins of HIV-1 (Mercredi et al. 2016) , MLV (Hamard-Peron et al. 2010b), Equine infectious anemia virus (EIAV) (Chen et al. 2008), Rous sarcoma virus (RSV) (Inlora et al. 2014) and Ebola virus (K. A. Johnson et al. 2016) were detected showing affinity for $PI(4,5)P_2$. Table-1.1 comparing the apparent binding constants (*Kp*) of these viral proteins to $PI(4,5)P_2$ containing liposomes is provided above.

1.4.3 Gag – Plasma membrane interaction:

Gag assembly starts with the trafficking of Gag polyprotein from the cytosol to the membrane. Once in the cytosol, the MA domain is responsible for the membrane interaction and targeting to the plasma membrane (A. Ono, Orenstein, and Freed 2000), this was confirmed by point mutations in the HBR region of the MA domain - resulted in Gag binding to late endosomes or multivesicular bodies (MVB) (A Ono and Freed 2004). Furthermore, deprivation of $PI(4,5)P_2$ from the plasma membrane also leads to a similar fate to Gag i.e., mistargeting to endosomes (Akira Ono et al. 2004). Although MA alone seems to exhibit a lower affinity for membrane than Gag (W. Zhou and Resh 1996), above findings conclude that MA domain of Gag and $PI(4,5)P_2$ has specific interaction. The highly basic region of MA domain is responsible for the primary interaction with the acidic lipids of the membrane, especially $PI(4,5)P_2$ (Chukkapalli et al. 2008; E Hamard-Peron et al. 2010b; W. Zhou et al. 1994). Apart from $PI(4,5)P_2$, phosphatidylinositol 3,4 bisphosphate ($PI(3,4)P_2$) or phosphatidylinositol 3,4,5 triphosphate ($PI(3,4,5)P_2$) also bind efficiently (Anraku et al. 2010).Similarly, it was shown that Gag protein of HIV-1 virus can bind to both PS and $PI(4,5)P_2$ containing model membranes (Dick et al. 2012) as this was also observed for MLV Matrix protein(Elise Hamard-Peron and Muriaux 2011). This seems to be a generalized mechanism for poly-basic proteins (Ben-Tal et al. 1997). Moreover, through lipidomic analysis, it was known that retroviral Gag proteins not only just interact with specific lipids; indeed virus-like particles are enriched with different lipid compositions when compared to the composition of their host plasma membrane (Lorizate et al. 2013).

MA domain has a myristoylation at its N-terminus that supposedly has an exposed conformation only after the HBR – $PI(4,5)P_2$interaction (Saad et al. 2006). And this exposure might facilitate

its insertion into the inner leaflet and further stabilize Gag – lipid interaction. However, new evidence suggested that myristoyl trigger might not require a specific lipid interaction but trimerization of the protein or non-specific electrostatic interactions can also help (Charlier et al. 2014; Valentine et al. 2010). Especially, coarse-grained molecular simulations revealed that any non-specific interactions can trigger myristoyl exposure and thus allow the protein to further orient itself to capture $PI(4,5)P_2$ head group. Notably, structural studies of MA – soluble form of $PI(4,5)P_2$ (diC4$PI(4,5)P_2$ or diC8$PI(4,5)P_2$) interactions were studied in detail to give an insight into specific interaction sites. Recent NMR data by Vlach and Saad (2013) revealed that other acidic lipids (PS & PE) and even neutral lipid-like PC could bind directly to a different site of Gag and thus reinforce its interaction with the plasma membrane (Vlach and Saad 2013).Although MA has specific interaction with $PI(4,5)P_2$, as a poly-basic protein, long-range electrostatic interactions can attract various other acidic lipids and that can also help in the initial targeting to the plasma membrane. But considering the early findings of Gag mistargeting in the absence of $PI(4,5)P_2$ suggests that even though initial targeting can be of non-specific in nature, a stable interaction might occur only in the presence of $PI(4,5)P_2$.

In addition to MA interaction with the lipids, researchers have also studied the interaction of other domains of Gag with specific lipids. Capsid and NC domains were shown to interact with different lipids. While CA protein was able to bind only negatively charged lipids (phosphatidic acid and phosphatidylserine) (Barrera et al. 2006), NC could bind both charged and neutral lipids (PC). In the same study, NC was also shown to bind nucleic acid (RNA) with greater affinity and has less preference for $PI(4,5)P_2$ (Kempf et al. 2015b). This behavior is completely opposite to MA protein which has high preference for $PI(4,5)P_2$ over RNA (Chukkapalli, Oh, and Ono 2010).

1.4.4 Gag & raft - like - microdomains:

Over a number of years, many researchers have found that the retrovirus viral membrane composition is distinct from that of the host PM (Aloia, R. C., Curtain, C. C. & Jensen 1992). Unlike Semliki-Forest and vesicular stomatitis viral membrane which is not-so-distinct from host PM, Influenza and HIV-1 viral membrane have high concentrations of raft-specific lipids such as

SM &Chol(Blom et al. 2001; Kalvodova et al. 2009; Lorizate et al. 2013). These observations led to a hypothesis that the viral assembly and budding may occur in raft components. However, Gag association to "rafts" is a long-standing debate. Rafts are described to be transient nano-domains made of sphingomyelin, cholesterol, and other glycolipids and are hard to be spotted by conventional or even super-resolution microscopes (K Simons and Toomre 2000). Nevertheless, different experiments based on:

- Detergent solubilization(Hogue, Llewellyn, and Ono 2012; O W Lindwasser and Resh 2001; Nguyen and Hildreth 2000; A Ono and Freed 2001a)
- Cholesterol depletion (A Ono and Freed 2001a; Akira Ono, Waheed, and Freed 2007)
- Lipidomics (Brügger et al. 2006; Chan et al. 2008b; Lorizate et al. 2013)
- Immunofluorescence colocalization(Kirsi Holm et al. 2003; Nguyen and Hildreth 2000; Akira Ono et al. 2005)

have suggested a potential role of "rafts" in the assembly of Gag.

Recently, Dick et al. 2012 suggested that Gag precursor protein can sense cholesterol and acyl chain unsaturation. Their study revealed that Gag has a higher affinity for unsaturated lipids containing LUVs than those with saturated versions. Further, binding studies with cholesterol containing (0-60%) liposomes revealed that increasing cholesterol content positively assists in this process for all liposome types, independently of their acyl chains. Interestingly, electron spin resonance (ESR) studies revealed that, although, Gag binding to liposomes increases with increased cholesterol content, but cannot be attributed as a result of liquid ordering. Likewise, Gag preference for unsaturated acyl chain lipid, brain/DO PI(4,5)P_2, was shown by Olety et al, 2015 (Olety, Veatch, and Ono 2015). This paper also positions the role of genomic RNA in the selection of unsaturated acyl chain containing lipids by Gag. This role will not be addressed in my work.

Adding to this, lipidomic studies have mainly shown that HIV lipid envelope was highly enriched in PIPx, but also in sphingomyelin& cholesterol (Chan et al. 2008b; Lorizate et al. 2013). Consolidating all these results lead to a strong hypothesis that HIV-1 Gag protein prefers

raft-components enriched membrane microdomains that have PI(4,5)P_2. However, PI(4,5)P_2 is not a saturated lipid and it is unlikely that it will preferentially partition into L*o* phase/sphingomyelin and cholesterol-enriched phases.

1.4.3.1 Interplay between lipids and Gag during viral assembly:

Gag polyprotein binding to raft-like microdomains is a hypothesis generated out of many results: (i) HIV-1 lipidome is enriched in raftcomponents like Cholesterol, Sphingomyelin & GM3 (Chan et al. 2008b; Lorizate et al. 2013), (ii) Gag protein can sense cholesterol (Dick et al. 2012), (iii) Not only that tetraspanin-enriched microdomain (TEM) were shown to co-localize with Gag (Grigorov et al. 2009; Jolly and Sattentau 2007), but also tetraspanin components are found to be incorporated into HIV-1 particles, especially CD81 (Grigorov et al. 2009). Further, Hogue et al., 2011 suggested that at the site of HIV assembly, Gag could induce coalescence of rafts and TEMs. To consider that Gag binds to raft-like structures, it's important to understand the concept of rafts as such. As mentioned earlier, "Raft" is a transient structure enriched in sphingomyelin, cholesterol and saturated lipids. But, the findings of Olety et al., 2015, Dick et al., 2012 suggested that Gag protein doesn't prefer saturated lipids in natural conditions. Olety et al., 2015 rather clearly showed that in the absence of RNAase, Gag doesn't bind to DPPI(4,5)P_2, a saturated variant of PI(4,5)P_2. However, in natural conditions, PI(4,5)P_2 has an unsaturated acyl chain at its sn-2 position that essentially doesn't partition into L*o* phase. Combining both saturated lipids of rafts & natural unsaturated nature of PI(4,5)P_2, a rather convincing & constructive model was suggested by Saad et al. 2006 based on NMR data. Experiments on MA protein with di-C8PI(4,5)P_2 in solution revealed that the unsaturated acyl chain of PI(4,5)P_2 has inserted itself into a hydrophobic pocket of MA (figure 1.17(A))**.** From this result, authors proposed that a similar switching might happen during Gag -PI(4,5)P_2interaction on membranes and this will be followed by a myristate switch, whilst the saturated sn-1 acyl chain remains in the plasma membrane (illustrated in the figure 1.18(A)). This mutual switching will remove the unsaturated acyl chain from the membrane and is replaced by a saturated myristate. Thus the MA-PI(4,5)P_2 complex result in a saturated acyl chain structure that can readily partition into rafts(Akira Ono 2011; Kai Simons and Gerl 2010). In addition to this, new NMR data re-enforced the above theory by suggesting the presence of a secondary lipid binding site, which can

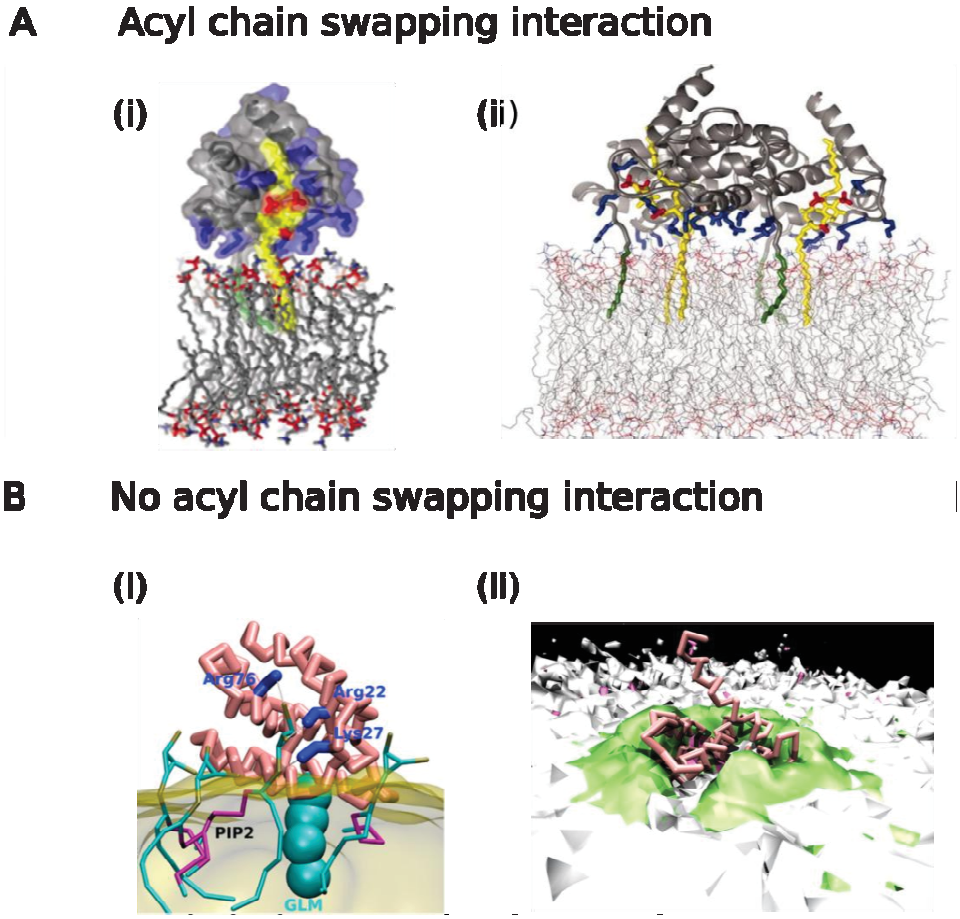

Figure 1.17: MA-PI(4,5)P_2 **interaction mechanisms reported**. (A) NMR data based interaction model generated for a truncated PI(4,5)P_2 that has its sn-2 acyl chain swapped into the hydrophobic pocket of the MA protein (i) and the MA trimer model (ii). (B) Coarse grain simulation model showing zero swapping of the acyl chains and specific interaction of the full-lengthPI(4,5)P_2 head group with the acidic arginine groups (i) and the over the top view of the interaction observed during simulation where the PI(4,5)P_2 is enriched around the MA protein (ii).

accommodate an unsaturated sn-2 acyl chain from different types of lipids like PS, PE and even PC (Vlach and Saad 2013). This mechanism could potentially deplete the unsaturated acyl chains at the site of MA interaction and thus partition primarily into rafts. But the inevitable drawback of this study being the use of truncated PI(4,5)P_2 and the medium of interaction between the lipid and MA; in solution but not on lipid bilayer. Further, considering that if switching of acyl chains does occur during the protein-lipid interaction, such flip might induce negative curvature of the membrane and can potentially inhibit budding.

Nevertheless, recent findings strongly support an alternate hypothesis presented based on the coarse-grained simulations performed using a full-length PI(4,5)P_2 on simulated lipid bilayers.

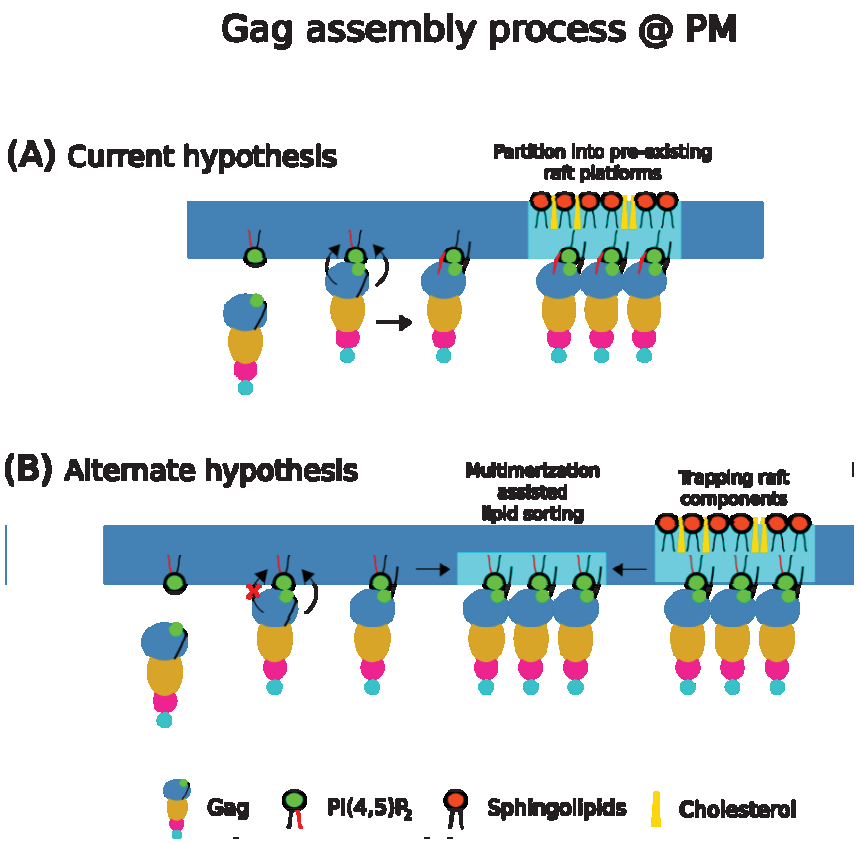

Figure 1.18: Illustration of HIV-1 Gag assembly on the inner leaflet of theplasma membrane. (A) The current hypothesis was based on the NMR data obtained for the interaction between truncated $PI(4,5)P_2$ and MA protein where a swapping of acyl chain was proposed for spontaneous partitioning into raft domains. (B) The alternate hypothesis proposed on the basis of coarse-grain simulations that doesn't detect any extended $PI(4,5)P_2$conformation up on MA interaction.

Supporting data includes: recent results on multimerize MA protein partitioning on phase separated GUVs revealed that the protein is strictly colocalizing with the $PI(4,5)P_2$ lipid that is present in the L*d* region of the GUVs ((Keller, Kräusslich, and Schwille 2013), coarse-grained simulations revealing the non-occurrence acyl chain swapping during the interaction of MA with full-length $PI(4,5)P_2$ (Charlier et al. 2014) (figure 1.17(B)) and finally, latest NMR data confirmed that there is no such swapping of lipid acyl chains into the hydrophobic pocket of the MA protein (Mercredi et al. 2016); confirming the results obtained from the simulations. Knowing that $PI(4,5)P_2$ can spontaneously aggregate into nano-sized domains (Ellenbroek et al. 2011; C. M. Johnson, Chichili, and Rodgers 2008; Salvemini et al. 2014) and also be sequestered by proteins in cells (McLaughlin et al. 2002), the assembly could induce the formation of lipid domains (Zimmerberg and Kozlov 2006) and not the opposite. In the light of all these, an

alternative hypothesis has been proposed by our team (Kerviel et al. 2013a)shown in figure 1.18(B). It was hypothesized that Gag binds to acidic lipids that are followed by multimerization, potentially creating acidic lipid enriched domains. As this assembly traffic the lateral diffusion of the lipids in the inner leaflet, they can, in turn, affect the diffusion of lipids/proteins in the outer leaflet of the membrane such as rafts & TEMs which can get trapped into to the slow diffusing acidic lipid enriched domains. In support of this hypothesis, coarse-grained molecular dynamics by Charlier et al., 2014 revealed that there is $PI(4,5)P_2$ enrichment at the site of protein interaction (figure 1.17(B)). Even more, it was already shown that Gag co-localizes with TEMs in T-cells (Grigorov et al. 2009; Jolly and Sattentau 2007) and Gag multimerization is responsible for trapping CD9 (raft component) at the site of assembly but not the other way around (Krementsov et al. 2010). Put together, the latest developments suggest that it is not Gag that is being trapped at pre-existing domains. On the contrary, Gag is trapping various components as it multimerizes along the surface of the plasma membrane. Overall, these opposing theories built out of the results obtained need to be tested in depth to understand the true mechanism occurring during HIV-1 Gag assembly. And this is the main topic of my thesis.

1.5 Protein self-assembly at pre-existing lipid domains or protein self-assembly induced lipid domains: a chicken or an egg?

Although it has recently been shown that HIV assembly may be initiated in the cytosol (Hendrix et al. 2015), it is commonly accepted that the formation of large HIV-1 assembly complexes mainly occurs at the plasma membrane (PM) of the virus producing cells.

Historically, Gag has been shown to associate with the detergent-resistant membrane (DRM) by cell membrane fraction assays (Callahan and Wills 2000; A Ono and Freed 2001b). Nevertheless, the exact composition of these "rafts" or DRM is controversial (Shahan Campbell et al. 2004; K Holm et al. 2003). Indeed, many different types of rafts may exist within the plasma membrane as long as they are enriched in cholesterol and sphingolipids (Pike 2006b). However, Gag self-assembly occurs at the inner leaflet of the cellular PM where sphingolipids are poorly present. Therefore, the ability of the Gag/$PI(4,5)P_2$ complex to partition preferentially

into "raft" domains and more generally into PM pre-existing domains to enhance virus assembly is still a matter of controversy (Kerviel et al. 2013a).

In order to control and decipher the respective roles of lipid domains and protein self-assembly, I used different types of lipid bilayers with different lipid compositions. In this study, I have also used different maturation products of Gag (FL-Gag, P39, MA) to see the respective roles of each domain, as well as a dimerization-deficient mutant (WM) to examine the role of self-assembly. In this manuscript, I shall answer the following questions:

- **Is Gag able to sequester/redistribute/sort various lipids, especially** $PI(4,5)P_2$**, cholesterol, and sphingomyelin:**
    - Do Gag and different mutants of Gag protein bind to $PI(4,5)P_2$ containing model membranes?
    - Does Gag multimerize on model membranes? If so, is there lipid redistribution during Gag interaction & multimerization?
- **Is there a role of pre-existing membrane domains in self-assembly?**
    - If Gag redistributes $PI(4,5)P_2$, where does the re-distribution occur - liquid ordered phase or liquid disordered phase?
- **Will this sequestration of lipids, along with protein self-assembly, trap liquid ordered components?**
    - Does multimerization of Gag protein induce membrane bending/curvature?
    - Can this multimerization trap liquid ordered components such as Cholesterol or Sphingomyelin?

Chapter -2

METHODS

2.1 Model membranes

Many factors contribute to the biophysical properties of membranes. In a dynamic system such as live cells, understanding the role of lipids in the activity of particular protein becomes difficult. Simplified systems such as artificial models of cell membranes are of great use in such a scenario. The ability to closely control their composition is proving to be a great tool to study the role of different kind of lipids in the interaction and assembly of a protein(s).

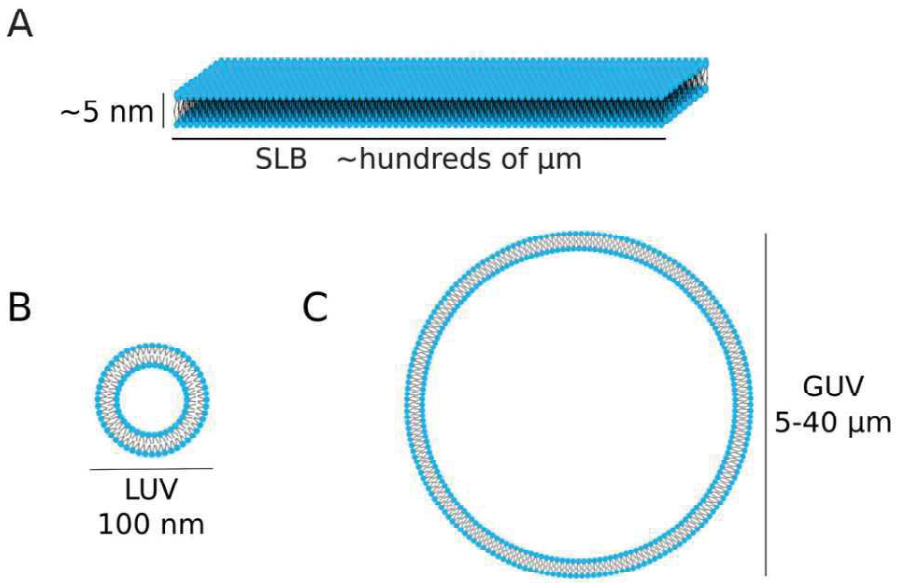

Figure 2.1: Model systems used to mimic cellular membranes. (A) Supported lipid bilayers (SLB); (B) Large unilamellar vesicles (LUV), and (C) Giant unilamellar vesicles (GUV).

Model membrane systems such as supported lipid bilayers (SLB), large unilamellar vesicles (LUV), and giant unilamellar vesicles (GUV) have been used in this study to understand the role of specific lipids in the interaction and assembly of Gag proteins. Figure 2.1 depicts the generalized view of all the three kinds of model systems used in this study, along with their dimensions, while tables 2.1 and 2.2 describe the lipid compositions used in this study.

Table 2.1: Different lipid composition of LUVs, SLB, and GUV used in the single labelled lipid experiments

	Basic		Substituted Basic		Inner Leaflet		Rafts	
	Lipid	Mol%	Lipid	Mol%	Lipid	Mol%	Lipid	Mol%
Model Membrane	Egg PC	70	Egg PC	68	Egg PC	17	DOPC	31
	Brain PS	30	Brain PS	30	Brain PS	17	DOPS	6
			Brain $PI(4,5)P_2$	2	Brain SM	9	Brain SM	30
					Cholesterol	30	Cholesterol	25
					Liver PE	25	GM1	1
LUV	Brain $PI(4,5)P_2$	0 or 1.5			Brain $PI(4,5)P_2$	0	Brain $PI(4,5)P_2$	5
	TF-$PI(4,5)P_2$	2 or 0.5			TF-$PI(4,5)P_2$	2	TF-$PI(4,5)P_2$	2
SLB	Brain $PI(4,5)P_2$	1	Brain SM or Chol	1	Brain $PI(4,5)P_2$	1	Brain $PI(4,5)P_2$	6
	TF-$PI(4,5)P_2$	1	TF-SM or TF-Chol	1	TF-$PI(4,5)P_2$	1	TF-$PI(4,5)P_2$	1
GUV	Brain $PI(4,5)P_2$	1			Brain $PI(4,5)P_2$	1	Brain $PI(4,5)P_2$	6
	TF-$PI(4,5)P_2$	1			TF-$PI(4,5)P_2$	1	TF-$PI(4,5)P_2$	1

Table 2.2: Different SLB lipid composition used for the dual labelled lipid experiments

TF-SPM Labelled						TF-Chol Labelled					
Substituted basic		Inner Leaflet		Rafts		Substituted Basic		Inner Leaflet		Rafts	
Egg PC	66	Egg PC	17	DOPC	31	Egg PC	66	Egg PC	17	DOPC	31
Brain PS	30	Brain PS	17	DOPS	6	Brain PS	30	Brain PS	17	DOPS	6
Brain $PI(4,5)P_2$	1	Brain $PI(4,5)P_2$	1	Brain $PI(4,5)P_2$	6	Brain $PI(4,5)P_2$	1	Brain $PI(4,5)P_2$	1	Brain $PI(4,5)P_2$	6
Brain SM	1	Brain SM	8	Brain SM	29	Chol	1	Brain SM	9	Brain SM	30
		Cholesterol	30	Cholesterol	25			Cholesterol	29	Cholesterol	24
		Liver PE	25					Liver PE	25		
BT-$PI(4,5)P_2$	1	BT-$PI(4,5)P_2$	1	BT-$PI(4,5)P_2$	1	BT-$PI(4,5)P_2$	1	BT-$PI(4,5)P_2$	1	BT-$PI(4,5)P_2$	1
TF-SPM	1	TF-SPM	1	TF-SPM	1	TF-Chol	1	TF-Chol	1	TF-Chol	1

2.1.1 Model Membrane fabrication

2.1.1.1a Small Unilamellar Vesicles (SUVs) preparation:

SUVs of 30 nm in diameter were prepared for the formation of SLBs. In a clean and dry 10 mL round bottom flask, lipid mixtures of various compositions at 0.1 mg/mL concentration was added. To form a thin lipid film, the round-bottomed flask was fixed to a rotary vacuum evaporator and was allowed to rotate at 90rpm @40°C under high vacuum pressure. In the case of lipid mixtures that have ≥30% cholesterol, the temperature was set at 50°C. After 2h, a thin film of lipid layer formed was hydrated using warm citrate buffer (NaCitrate10mM, 100mM NaCl, and 0.5mM ethylene glycol-bis (β-aminoethyl ether)-N,N,N',N'-tetraacetic acid (EGTA), pH 4.6) (50°C) at room temperature for overnight. The following day, the hydrated lipid layer was suspended into the buffer using a shaker to form a multi-lamellar vesicle (MLV) suspension. For better retrieval of lipids, 2 min bath sonication with 30s interval was employed. Thus obtained MLV suspension was pipetted into an Eppendorf tube and used within 15 days. To assist the formation of SUVs using extrusion and to decrease the loss of lipids, freeze (-80°C) – thawing (50°C) was performed for 10 cycles, followed by continuous bath sonication for 15 min. After this, the MLV suspension was allowed to settle at 4°C for one hour before extruding to produce 30 nm sized liposomes. A 30 nm graded Whatman Nucleopore Track-Etched membrane filter was fitted to Avanti mini-extruder and 21 cycles of extrusion were performed. In the case of lipid composition with ≥30% cholesterol, extrusion was performed on a hot-plate which was set at 50°C to assist the process. Finally, SUVs were kept at 4°C for 30 min and just before injecting into the chamber for SLB formation they were heated to 37°C for 10 min.

Cover-slip preparation: Clean cover-slips for SLB formation were prepared by adding initially to a 5% SDS solution and bath sonicated in a beaker at maximum amplitude for 1h. Later, the coverslips were washed rigorously with Milli-Q water. In the second step, the same glass coverslips were immersed in a freshly prepared Piranha solution (3:1 v/v H_2SO_4: 35 wt% H_2O_2). After 20 min, the coverslips were washed again rigorously in Milli-Q water and were kept under water until use.

Chamber formation: Individual polymerase chain reaction (PCR) tubes of 300µL capacity were used to form chambers. The tubes were devoid of the cap and 40µL volume length was severed from the bottom of the tube. Thus obtained open-ended tube was used to stick on the cleaned coverslips.

PDMS glue: For every 700 µL of Polydimethylsiloxane (PDMS), 100µL of the radical solution was added and mixed well. The mixture was then allowed to settle for 30 min, before using as a glue to stick the cut-PCR tubes onto the cleaned coverslips.

Housing: Freshly cleaned coverslips were dried using compressed air/argon gas and were settled on a hot plate (70°C). Using the brush, a thin film of PDMS glue was smeared onto the defect-free front-end of the cut-PCR tube and stuck onto the surface of the coverslip. The process was repeated for as each coverslip can accommodate two to three chambers. A typical chamber fixed on a coverslip is illustrated in figure 2.2. The system was covered to avoid settling of dust while it was left on the hot-plate for three hours. At the end, the chambers were gently filled with ultra-pure water and the remaining PDMS glue was applied to the cover-slip-tubing contact point. Care was taken not to disturb the contact while smearing. The system was left totally covered and undisturbed overnight, at room temperature. Thus formed chambers filled with ultra-pure water were stored and further processed before the formation of SLBs.

Pre-step: Before making the SLBs, fresh piranha solution was prepared. Around 100µL of ultra-pure water was left in the chamber, to which 100µL of the piranha solution was added. After 10 min, the chambers were gently washed with excessive amounts of ultra-pure water (10 cycles).

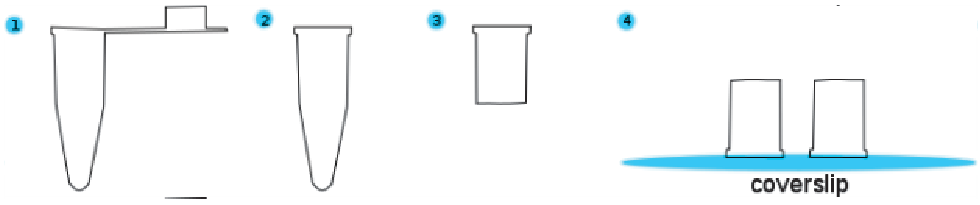

Figure 2.2: Schematic representation of chamber formation and housing onto a coverslip. (1) 500 µl capacity DNA/RNAase free tubes. (2) and (3) sectioning of the tube that can hold 300 µl of water. (4) the housing of the tubes onto the coverslips to form chambers.

SLB formation: At 37°C, ultra-pure water present in the chamber was replaced with 40µL of 30 nm SUV suspension. Once the chamber was covered, SLB formation was allowed to take place for the first 20 min at 37°C and the second 20 min at room temperature. After this, 100µL of citrate buffer was introduced very gently, in a drop-wise fashion, close to the water surface without touching either the tube or the cover-slip. Now, the SLB was rinsed for 10 times with citrate buffer and later withHepes buffer (4-(2-hydroxyethyl)-1-piperazineethanesulfonic acid (HEPES)-10mM, KCL-150mM, and2mM ethylenediaminetetraacetic acid (EDTA), pH 7.4)(50µL each time) (10 times). In the end, ~250µL of Hepes buffer was allowed to stay in the chamber. Thus formed SLBs were used within 6 hours.

Large area SLBs: Cleaned coverslips were dried and fixed to the Atto® cell chamber. Immediately after that, 200µL of the SUV suspension was added. Usually, 300µL of liquid is required to fill the entire coverslip in the Atto® chamber. Since the cover-slip was made very hydrophilic, 200µL was enough to spread all over the cover-slip. The process of alternate temperatures for SLB formation was carried out. This was followed by multiple washing steps and final equilibration with Hepes buffer.

2.1.1.1b Visualization and quantification of SLBs

SLB visualization was done using ZEISS LSM780 confocal microscope (Carl Zeiss, Inc.) equipped with a 63x, 0.75 NA objective and Zeiss definite focus system. Either 2-photon excitation (930nm) or single-photon excitation (488 nm) was used to excite the TF-labelled SLBs. A typical SLB is shown in figure 2.3(A). Qualities of the SLBs were confirmed initially by manually hovering over the entire SLB and also by performing FRAP measurements that detail the diffusion properties of the lipids present in the SLB (figure 2.3(B)).

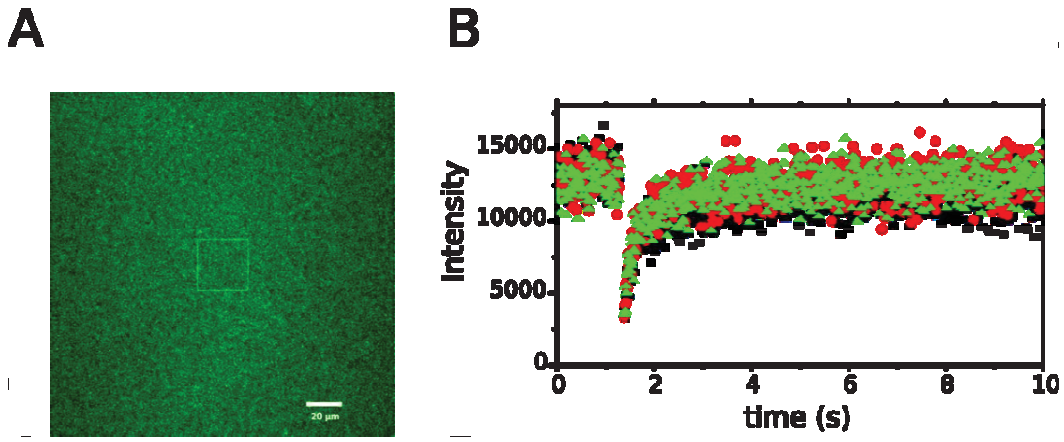

Figure 2.3: Quality control of SLBs: (A) Image of a typical SLB labelled with TF-PI(4,5)P_2. (B) FRAP studies defining the quality of the SLB through measurements of the diffusion of lipids. Scale corresponds to 20 µm.

2.1.1.2a Large Unilamellar Vesicles (LUVs) preparation-Extrusion method:

In a clean and dry 10 mL round bottom flask, mole-per-mole concentrations of lipid mixtures of a specific composition comprising to 45µM were added. To form a thin lipid film, the round bottom flask was fixed to a rotary vacuum evaporator and was allowed to rotate at 90rpm @40°C under high vacuum pressures. In the case of lipid mixtures that have a≥30% cholesterol, the temperature was set at 50°C. After 2h, a thin film of lipid layer formed was hydrated using a Hepes buffer(Hepes-10 mM, KCL-150 mM, and2 mM EDTA, pH 7.4) (50°C). The system was then allowed to hydrate in dark at room temperature for overnight. The following day, the hydrated lipid layer was suspended into the buffer using a shaker or 2 min bath sonication for 30s - for better retrieval of lipids. Thus obtained MLV suspension was pipetted into an Eppendorf tube and processed further to produce 100 nm size lipids. To assist the formation of LUVs using extrusion and to decrease the loss of lipids, freeze (-80°C) – thawing (50°C) was done for 10 cycles, followed by continuous bath sonication for 15 min. After this, the MLV suspension was allowed to settle at 4°C for one hour before extruding to produce 100 nm sized liposomes. A 100 nm grade Whatman Nucleopore Track-Etched membrane filter was fitted to Avanti mini-extruder and 21 cycles of extrusion were performed. In the case of lipid composition with ≥30% cholesterol, extrusion was performed on a hot-plate which was set at 50°C to assist the process. Finally, LUVs were kept at 4°C for 30 min and were brought to room temperature using them for any experiments.

2.1.1.2b Phospholipid mole fraction quantification:

Phospholipid assay was performed as directed by the manufacturer's protocol. Briefly, choline measuring high-throughput assay kit was obtained from Sigma-Aldrich. Initially, phosphatidylcholine standard curve was obtained by colorimetric detection using 0, 60, 120 and 200 µM from manufacturer's sample. Liposomes with various compositions were measured for their choline-containing lipids after the extrusion process. While the starting concentration of the 'basic' composition liposomes was 45 µM; placing the eggPC concentration at 30 µM. Through the phospholipid assay, it was found that 7% of the lipids were lost after extrusion with eggPC at 27 µM. Thus, giving the total lipid concentration at 42 µM and total $PI(4,5)P_2$concentration at 0.84 µM. Dilutions were done to obtain a fluorescence intensity of 1000K units for 2% labelled $PI(4,5)P_2$ under fluorescence spectrofluorometer. At this point, the total lipid concentration was 14 µM and the total $PI(4,5)P_2$ concentration is 0.28 µM. In conjunction to this quantification, Beer-Lambert's law of absorbance measurements was done while assuming the excitation coefficient (ε) of the dye as ~80000/cm.M. The sample whose fluorescence intensity was 1000K where used for absorbance measurements and the concentrations were estimated using Beer's law. Triplicates gave a measure of ~0.23 µM concentration for 2% labelled $PI(4,5)P_2$ containing liposomes. For the LUV experiments performed thereafter, liposome samples were measured for their fluorescence intensity and diluted appropriately to obtain 1000K units. Lamp correction was done by recording the Raman spectra of pure water before every experiment. All experiments were performed at room temperature.

2.1.1.3 GUV preparation – Hydration method

5% Poly-vinyl alcohol (PVA) Solution: 2.5g of Mowiol® 28-99 was added to 50 mL of Milli-Q water in a beaker. The mixture was heated to 90°C on a hot plate under stirring until there observed no visible polymeric particles/ a clear solution.

Coating on cover-slips: Using the home-made spin-coater, the 5% PVA solution was deposited as a thin film on a clear cover-slip (diameter - 25 mm). Using a double-sided tape, cover-slip was fixed to the spin-coater. 700 uL of hot 5% PVA solution was deposited on the cover-slip in such

a way that the entire surface was covered. Later, the cover-slip was allowed to spin gradually to yield a very thin film of PVA. After 2 min, the coverslip was removed and kept in an incubator at 50°C for 1 h and was left alone at room temperature, overnight. Thus formed PVA coated coverslips were stored in dark, before use.

GUV lipid concentrations: 1mg/mL mole per mole concentrations of lipid mixtures were made in chloroform was used for the formation of GUVs. Typically, 30µL of the above-mentioned concentration was used for a single experiment.

Lipid coating: 5% PVA coated coverslips prepared using the above said method was placed on the hot-plate (50°C). 15 µL of the lipid mixture was gently spread all over the PVA coated side of the cover-slip. The process was repeated for the other 15µL of the lipid mixture. In between the successive lipid coatings, 15 µL of pure chloroform was applied to form a uniform lipid layer. Later, the coverslips were fixed in the Atto® cell chamber and kept under vacuum for 2h in dark at room temperature to remove any traces of chloroform.

GUV production: To be relevant in the cellular context, buffer with 230 mOsm was used to form and dilute GUVs. 700µL of hot HEPES buffer (20 mM Hepes 180 mM sucrose solution, pH – 7.4) (40°C) was gently added to hydrate the dried lipid film deposited on the 5% PVA coated coverslips. After addition of the buffer, the chamber was kept in a dark and humidified incubator (to avoid evaporation of the water present in the buffer) at room temperature for overnight incubation. If the lipid mixture deposited contains ≥30% cholesterol, the incubator was initially set at 37°C for 2h and then left at room temperature, overnight.

GUV retrieval: Following day, the chamber was gently shaken by tapping on the sides to detach the GUVs from the surface. Using a 200 µL pipette, loaded with a cut tip, the GUVs suspension was drawn from the chamber.

GUV storage: To avoid the splashing of GUVs upon touching the bottom of an Eppendorf tube, 20 uL space was left at the bottom of the tube while loading the GUV suspension. Thus, the GUVs kept in a suspended state were stored in dark at room temperature until further use.

GUV concentration: A buffer of low density but of equal osmolality was prepared to concentrate the GUVs. 20 mM HEPES & 180 mM sucrose solution in which the GUVs were made were diluted in a 20 mM Hepes 100 mM KCL and 0.5 mM EDTA pH – 7.4 buffer that has same osmolality, 230 mOsm. To concentrate the GUVs, 300µL of the low-density buffer was loaded in a suspended state, and then add 50/100 µL of the GUV suspension from above was added drop-wise. After 15 min, 50uL of the solution from the bottom of the tube was retrieved for the experiment.

GUV mounting: Starting with, 2 mg/mL casein solution was added to an Atto® cell chamber fixed with a glass coverslip. After 5min, the solution in the chamber was gently removed and replaced with 250 µL of low-density buffer (20 mM HEPES, 100 mM KCL and 0.5 mM EDTA). Once the chamber was mounted on the microscope, 50 µL of the concentrated GUV suspension was deposited. After 20 min stabilization, GUVs were visualized using a microscope.

Labeling Phase-separated-GUVs: Phase-separated GUVs were labelled with Cholera toxin-B-647. 1% Monosialotetrahexosylganglioside (GM1) lipid was added to the phase-separating lipid mixture while spreading on the 5% PVA-coated coverslips. 1µL of 1mg/mL Cholera toxin B-647 was added to the stabilized GUVs and let the label bind GM-1 for 15 min, before adding Gag.

2.1.1.3b Visualization of GUVs

Visualization of GUVs was done using ZEISS LSM780 Confocal microscope (Carl Zeiss, Inc.) equipped with a 63x, 0.75 NA objective. On the microscope, GUVs were added to the Attofluor cell chamber (Thermo Fisher Scientific, Inc.) fitted with casein (2 mg/ml) coated coverslip (25 mm, Deckgläser). Upon stabilization, labelled proteins were added to the medium and imaged. Images were acquired with 512x512 pixels and 16 bit at constant intensity keeping the green channel at ex488/em498-555 nm & red channel at ex561/em600-660 nm. For Spectral imaging, the excitation was set at 488 and 561 nm for green and red fluorescence respectively, the spectral range was set from 496 to 660 nm. Linear Unmixing of the images was done to avoid the bleed-through from Topfluor® to Alexafluor-594 channel using ZEISS 2012 software. In case of

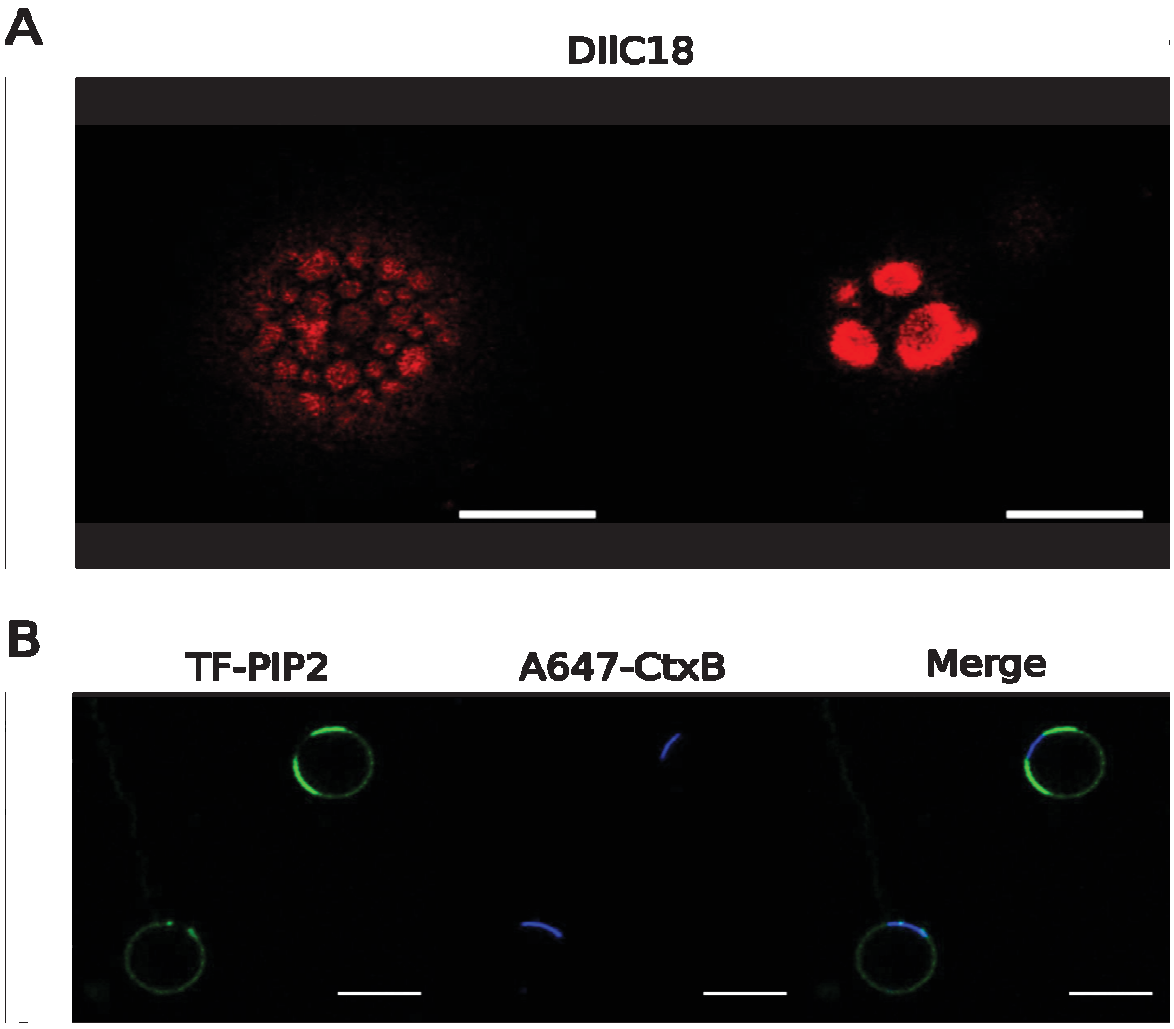

Figure 2.4: Domain visualization of Phase separated GUVs. (A) Initial experiments on production of phase separated GUVs labelled with Ld marker, DIIC18 (dopc 17%, dops 17%, SPM 25%, Chol 30%, BrainPI(4,5)P_2 7.5% and DIIC18 1%). (B) Dual labeling of Phase separated GUVs: Ld phase is labelled with TF-PI(4,5)P_2 and Lo phase was labelled with A647-Cholera toxin-B. Scale bar corresponds to 10 μm

GUVs labelled with cholera toxin B-647, the ex was set at 488/561/630 nm for green, red & far red channels. Further, images were treated using Image J software. All experiments were conducted at room temperature unless otherwise specified. Multi-color images of phase separated GUVs were done. An example of the phase separated GUVs were represented in figure 2.4. Figure 2.4(A) depicts the domains formed on GUVs with phase separation composition that was labelled with DIIC18 in the L*d* phase. Multi-color images of phase separated GUVs labelled with TopFluor-PI(4,5)P_2 and A647 Cholera toxin-B were shown in figure 2.4(B) and TF-PI(4,5)P_2 essentially staying in the L*d* phase of the GUV.

Quantification of GUV intensity

To establish the spatial autocorrelation of the fluorescence intensity of TF-PI(4,5)P_2 or A594-FL-Gag on basic composition GUVs, the change in intensity was plotted along the GUV using the following integration:

$$I(r,\theta) = \frac{1}{N}\sum_{dr=r-2\Delta r}^{dr=r+2\Delta r}\sum_{\theta=\theta}^{\theta=\theta+\Delta\theta} I_N(r+dr,\theta+\Delta\theta) \quad Eq: 2$$

Intensity was plotted with r.sin θ as the length unit. The obtained curve was autocorrelated using either the autocorrelation or the cross-correlation function of Matlab R2015 (Mathworks®). Intensity partition of each label in the case of raft GUVs was determined using the following equations:

$$I_{in} = \sum_{\theta=\theta_i}^{\theta=\theta_0} I(r_{GUV},\theta)\Delta\theta \Big/ \sum_{\theta=0}^{\theta=2\pi} I(r_{GUV},\theta)\Delta\theta, I_{out} = 1 - I_{in} \quad Eq: 3$$

θ_i and θ_0 were determined with the help of Alexa647-CtxB intensity circular profile.

2.1.1.3cGUV Control experiments:

Before incubating GUVs with Alexa Fluor-594 labelled proteins, the integrity of the GUVs over time was checked by incubating the GUVs with Alexafluor-594 dye alone for 1h, at salt concentrations equivalent to the labelled protein experiment. Figure 2.5 shows that the GUV is quite stable and not labelled by theAlexaFluor-594 dye. Further, to understand the TF-PI(4,5)P_2 partitioning into phase-separated GUVs, (1 1 dioctadecyl 3 3 3 3 tetramethylindocarbocyanineperchlorate) DIlC18 labelled-GUVs were incubated with TF-PI(4,5)P_2 for 2h and imaged.

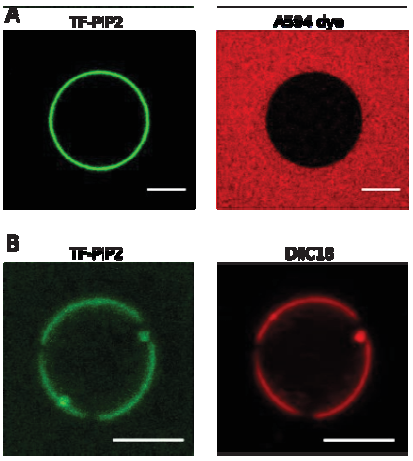

Figure 2.5: GUV integration and partitioning of labelled components. (A) TF-PI(4,5)P_2 labelled basic composition GUVs were incubated in Alexa fluor-594 dye alone. (B) Phase partitioning of TF-PI(4,5)P_2 was studied by adding it to DIlC18 labelled phase separated GUVs. Scale bar 10 µm.

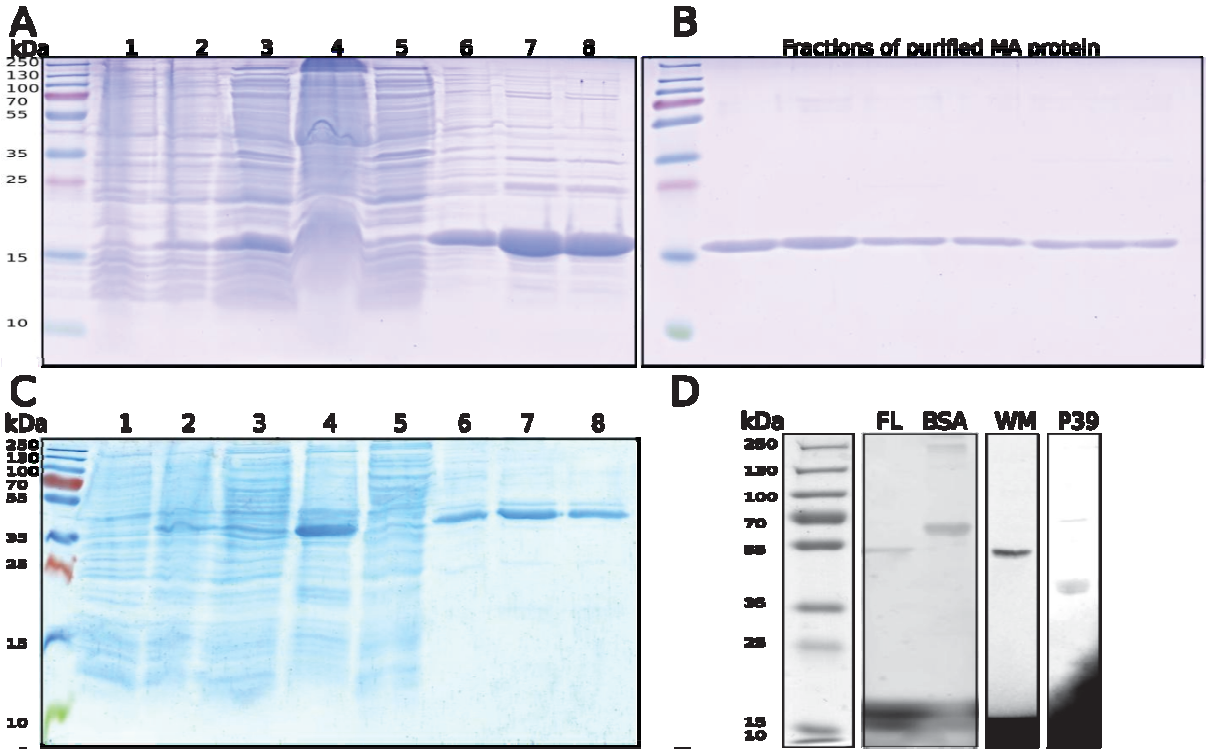

Figure 2.6: SDA-PAGE gels of purified proteins and labelled proteins(A) Expression profile and purification of HIV-1 Matrix protein in prokaryotic BL-21 *E.coli* cells in a 16% gel. (B) Highly purified fractions of MA protein used for the experiments in a 16% gel. (C) Expression profile and purification of EFA6-PH with thecoiled coil in a 16% gel. (D) 10% Gel of labelled proteins imaged with 561 nm excitation. (1) Pre-incubation (2) post-incubation (3) supernatant for MA gel (4) pellet for MA gel (reversed in thecase of EFA6-Ph-Cter) (5) flowthrough (6) resin (7) elution (8) PD-10 exchange.

2.2 Protein expression, purification, and Labeling:

Matrix protein (MA) and PH-EFA6 were purified in-house using a standard protocol. Briefly, prokaryotic expression of both the proteins was done by transfecting the vectors into BL-21 *E.coli* cells. A 500 mL culture was allowed to grow and protein expression by IPTG induction was done for 4h at 37°C. On expression, bacteria was pelleted and lysed using a wash/lysis buffer (50 mM Sodium Phosphate, 250 mM NaCl, 10 mM Imidazole and 0.02% -mercaptoethanol with pH 7.0), followed by sonication for 2 min in the presence of protease inhibitors and DNAase. The cell lysate was centrifuged at 20,000 g for 15 min at 4°C, to separate the debris from the expressed protein. The supernatant containing his-tagged protein was added to Ni-NTA agarose beads and left at least for one hour at 4°C on a rocker. After incubation, the supernatant was passed through propylene column and washed with wash/lysis buffer. To free

the protein bound to Ni-NTA agarose beads, they were incubated in elution buffer (wash/lysis buffer + 250mM imidazole, pH 7.0) for 1h at 4°C on a rocker. Finally, PD-10 column was used to change

the buffer to 100 mM Tris, 0.5 M NaCl, 0.02% -mercaptoethanol, pH 7.4. Purified proteins were analyzed using sodium dodecyl sulfate-polyacrylamide gel electrophoresis (SDS-PAGE) and stored at -80°C, until use. Protein labeling was done for Gag mutants with Alexafluor® 594 C5-maleimide according to manufacturer's guidelines. Excess dye has been removed either by PD-10 column or by Slide-A-Lyzer™ MINI Dialysis Device, 20K MWCO, 0.5 mL, Thermo Fisher scientific. Figure 2.6 reveal the purity of expressed proteins used in the study and the labelled proteins, as well. All the proteins produced were stored at -80°C in aliquots and thawed just before the experiment. Labeling of the proteins was performed at 4°C to avoid any impact of temperature variations on its stability.

2.3 K*p* determination:

2.3.1 Co-sedimentation assay:

K*p* were determined on basic lipid composition (EPC 68%, BPS 30% &PI(4,5)P_2 2% for LUVs or POPC 68%, POPS 30% &PI(4,5)P_2 2% for SLBs). Methods used were either cosedimentation assays for LUVs or QCM-D experiments on SLBs. Co-sedimentation assays were made at 1 µM protein concentration with varying concentrations of total accessible lipids from 0.07 to 2250 µM in 100 µl, according to the protocol in Hamard-Peron et al. 2010. After 15 min of incubation at room temperature, samples were centrifuged at 220,000 g for 1 h at 4°C using a Beckman Coulter's TLA 100 rotor. The top 80 µL was considered as supernatant (S) and the remaining 20 µl diluted with 60 µL of working buffer as a pellet (P). Pellet and supernatant were analyzed on a 10% SDS-PAGE and stained using Coomassie blue. Quantifications were made using Image J software (National Institutes of Health, MD, USA). SLBs were prepared with 0.1 mg.mL−1 liposomes flowing at 10 µL.min−1 for 10-20 min on an UltraViolet-treated SiO_2 surface of Q-sensor fixed in a Q-Sense Flow module, QFM 401 Biolin Scientific, Sweden). Stable SLBs were rinsed with citrate buffer (NaCitrate 10 mM, 100 mM NaCl, and 0.5 mM EGTA, pH 4.6) and then with injection buffer (5 mM Tris& 100 mM NaCl pH 7.4). At equilibrium, 200 µL of

increasing protein concentration was successively injected into the flow chamber followed by rinsing steps in between. The same was repeated with increasing protein concentrations until saturation. Sensorgrams were normalized to the third harmonic in the case of varying harmonic curves. F (plateau values) was used to measure the lipid SLB surface fraction of protein bound. In order to compensate the dilution of the pellet, the true intensity of the pellet was set by, $I_{Pellet} = I_P\ 0.2*I_S$, while I_P& I_S being experimental intensities obtained for pellet and supernatant, respectively. From this, affinity constants for all the proteins were calculated using the Eq. 4, where the percentage of protein bound (PB) to the LUVs is $[PB] = I_{Pellet}/(I_P + I_S)$. The fraction of protein bound from the total protein (PT) added is related to an apparent association constant K (i.e, the reciprocal of apparent partitioning constant (K*p*), following the equation:

$$\frac{[PB]}{[\mathrm{PT}]} = \frac{K[L]_{acc}}{1+K[L]_{acc}} \qquad \textit{Eq: 4}$$

2.3.2 Multimerization assay on LUVs

A 100 μL of the basic composition LUVs was incubated at room temperature for 15 min with either 0.9 μM (P/L* - 2) or 4.5μM (P/L* - 5) of FL-Gag or WM. After centrifugation at 10,000 g for 5 min, 20μL of the supernatant was loaded on a 10% native-PAGE and proceed for immunoblot as in (Hamard-Peron et al. 2010a). FL-Gag and WM were detected by a primary anti-capsid antibody (HIV-1 p24 NIH AIDS Reagents) followed by secondary antibody conjugated with anti-mouse HRP. The membrane was revealed by Femto substrate (Thermo-scientific) and imaged under G: Box (Syngene).

2.3.3 Quartz Crystal Microbalance with Dissipation (QCM-D):

QCM-D is an ultra-sensitive mass sensor that works on the principle of converse piezoelectric effect. While the piezoelectric effect is induced by mechanical deformation of materials like Quartz crystal, QCM works on the opposite principle: applied electric field on piezoelectric materials induces a strain, which under alternating current produces oscillations with a Q factor

(frequency/bandwidth) as high as 10^6. QCM exploits this high Q-factor that leads to the accurate determination of a resonance frequency. And also based on Sauerbrey's findings of change in frequency is directly proportional to change in mass, QCM technique gives a very accurate measurement of the amount of mass bound to the surface of the sensor.

$$\Delta m = -C\frac{1}{n}\Delta f \qquad \textit{Eq: 5}$$

Where Δm & Δf is changed in mass & frequency, n is harmonic overtone &C is the mass sensitivity constant, 17.7ngcm^{-2}s^{-1}

A typical QCM sensor is made of AT-cut Quartz crystal that is sandwiched between gold electrodes. When a constant AC current was applied, at t=0, the voltage (U) was allowed to decay as an exponentially damped sinusoidal which relays in time. And this decay curve was fitted to determine the resonant frequency and dissipation factor simultaneously.

$$U_t = U_0 e^{-t/\tau} \cdot \sin(2\pi f t + \emptyset) \qquad \textit{Eq: 6}$$

Where τ corresponds to the decay time constant and ϕ is the phase. And the dissipation factor being inversely proportional to τ was determined using the equation

$$D = \frac{1}{\pi f \tau} \qquad \textit{Eq: 7}$$

When we considered all three equations, one can deduce the adsorbed amount with Δf and ΔD providing information on the rigidity of the adsorbed material. Finally, using a multiple frequency modeling one can also get information on the visco-elastic properties of the adsorbed layer, swelling/hydration properties and even insights into structural changes.

Experimental Setup: SLBs for QCM-D measurements were prepared with a lipid composition of 68% POPC, 30% POPS & 2% PI(4,5)P_2. For this, 0.1mg/mL concentration of liposomes was passed over Ultra Violet-treated SiO_2 surface of Q-sensor in a Q-Sense Flow module, QFM 401 BiolinScientific, Sweden) at 10μL/min flux and for a period of 10-20 min.

Thus formed stable SLBs were rinsed initially with Citrate buffer (10 mM NaCitrate, 100 mM NaCl, and 0.5 mM EGTA, pH 4.6) and then with diluted protein buffer (5 mM Tris& 100 mM NaCl). At equilibrium, 200 μL of the protein solution (specific concentration) was injected into the flow chamber encompassing the Q-sensor. After reaching a plateau in the signal, the system

was rinsed with 5 mM Tris& 100 mM NaCl buffer pH 8. The same was repeated with increasing protein concentrations until there observed saturation. Obtained sensorgrams were normalized to the third harmonic in the case of varying harmonic curves. Consequently, Eq. 8 was used to generate apparent K*p* values from the plots of ΔF (plateau values) *vs* protein concentrations.

$$Y = \frac{B_{max} \cdot X}{K_p + X} \qquad Eq: 8$$

Where, X is the protein concentration

2.4 Fluorescence Self-quenching:

Fluorescence Self-quenching is one the major methods that are being used to study the lipid clustering ability of proteins on model membranes. In our study, we also used the same technique to understand the PI(4,5)P_2 clustering by Gag protein. Fluorescence self-quenching is used to ensemble studies of protease and nuclease activities (Jones et al. 1997), membrane fusion (Weinstein et al. 1984)), and protein dimer formation (Wendt et al. 1995). Typically, quenching is a decrease in fluorescence intensity as a result of multiple phenomena like excited state reactions, collisional interactions, complex formation & energy transfer. In this study, self-quenching properties of Topfluor®/Bodipy-FL labelled lipids were analyzed before using in the protein-lipid interaction assay. As the name suggests, it is an interaction between two molecules of same species within a reasonable concentration range. That interaction can occur either by collision at the excited state, Collisional/Dynamic quenching or complex formation due to hydrophobic attractions in the ground state itself, Static quenching. Either scenario, the fluorophore has to be in contact with each other. Typically, both collisional and static quenching can be explained using Stern-Volmer equation:

$$\frac{F_0}{F} = 1 + k_q \tau_0 [Q] = 1 + K_D [Q] \qquad Eq: 9$$

Where F_0 and F are the fluorescence intensities before and after the collision, respectively; k_q is the bimolecular quenching constant; τ_0 is the lifetime of the fluorophore before the collision, and Q is the concentration of the fluorophore. Finally, K_D is the Stern-Volmer quenching constant.

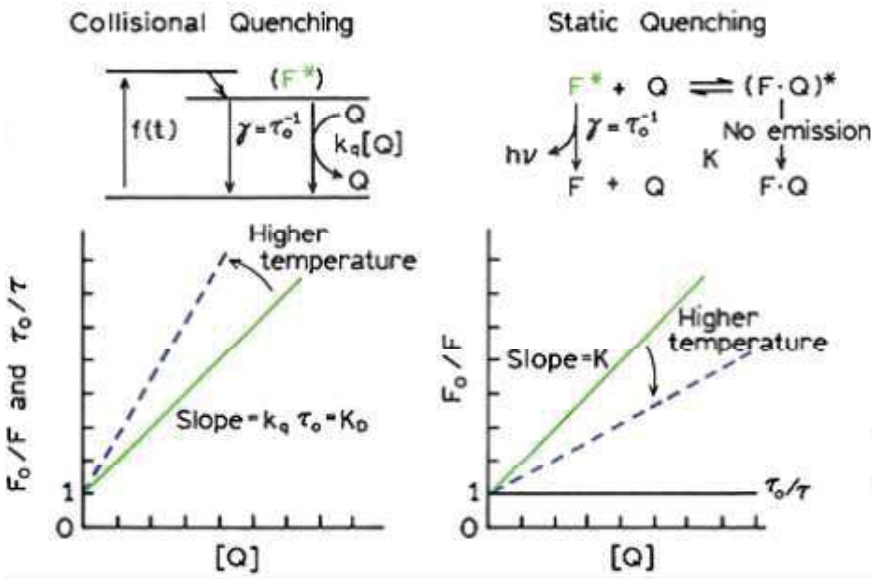

Figure 2.7: Comparison of collisional and static quenching (adapted from Principles in Fluorescence Spectroscopy edited by Joseph R.Lakowicz)

Similarly, static quenching can also be deduced using a modified Stern-Volmer equation:

$$\frac{F_0}{F} = 1 + K_S[Q] \qquad \textit{Eq: 10}$$

Where K_s is the Stern-Volmer association constant given by: $K_s = \frac{[F-Q]}{[F][Q]}$; [F-Q] is the concentration of the complex. Importantly, in both cases, F_0/F dependence on [Q] is linear. This suggests that only by intensity measurements it is not possible to deduce the dynamic or static nature of self-quenching.

From figure 2.7, while fluorescence intensity measurements remain linear for both of the quenching processes, high temperatures, and lifetime measurements showed differences with increasing concentrations. At high temperatures, the complexes can dissociate when the fluorophores are weakly bound. This shall result in lower static quenching. In the case of collisional quenching, high temperatures increase the number of collisions and so the shift towards y-axis. But when the bonding is strong and to maintain physiologically relevant conditions, lifetime measurements are more accurate and preferable. One of the main characteristics of collisional quenching is $^{F_0}/_{F} = {}^{\tau_0}/_{\tau}$, there will be an equivalent decrease in

fluorescence intensity and a lifetime as the number excited states decreases with increase in collision rates. On the contrary, a fraction of fluorophores are unavailable for fluorescence excitation at the ground state due to static quenching and during excitation, the emission population remains constant. Meaning, even though the fluorescence emission decreases with concentration – the lifetime remains constant: ${}^{\tau_0}/_{\tau} = 1$.

In model membranes, when lipids are labelled with self-quenchable fluorophores, the 2D diffusion of lipids can result in self-quenching mainly by the collision. On the other hand, lipids labelled with TopFluor® are known to undergo static quenching because of the strong hydrophobic attractions between the bodipydyes.

Self-quenching was measured using the spectrofluorometer (Photon Technologies International, Inc.)) for TF-PI(4,5)P_2 (ex 495 nm/ em 510 nm). Amount of self-quenching due to the proximity of neighboring labelled lipid was determined by comparing the fluorescence intensity of LUVs containing increasing percentages of TF-PI(4,5)P_2 lipids (from 0 to 2% of FL-PI(4,5)P_2, over a total PI(4,5)P_2 concentration of 2%, I_p) and of the same lipids after perturbation of the LUVs membrane by addition of 1% Triton X100 (I_0). The total lipid concentration was 45 µM. Percentage of self-quenching was calculated using the equation:

$$\%\, Self - quenching = \left(1 - \left(\frac{I_p}{I_0}\right)\right).100 \qquad \textit{Eq: 11}$$

2.4.1 Fluorescence Quenching Measurements:

2.4.1.1 On LUVs:

Effect of different proteins on TopFluor ® (TF) labelled PI(4,5)P_2 quenching in LUVs were monitored with a fluorescence spectrometer (Photon Technologies International, Inc.) using λ_{exc} = 485nm and λ_{em} = 510 ± 10 nm. Excitation lamp intensity was calibrated using the Raman spectrum of pure water and its fluctuations corrected every second. For the interaction assay, the concentration of protein injected was adjusted to have desired protein/accessible PI(4,5)P_2 lipid

ratio (named P/PI(4,5)P_2^{acc} in the figures). For every interaction assay, the obtained intensity curve was corrected for both bleaching and dilution (by the addition of protein solution) effect and then, normalized to the mean intensity before injection.The normalized curve was then treated using an arbitrary bi-exponential growth process:

$$\frac{F}{F_0} = A_0 + A_1[1 - e^{-(t/\tau_1)}] + A_2[1 - e^{-(t/\tau_2)}] \qquad \textit{Eq: 12}$$

Here, A_0, A_1, and A_2 correspond to initial intensity, the intensity at the time, τ_1 and intensity at the time, τ_2, respectively.

2.4.1.2 On SLBs:

Time-lapse fluorescence measurements of labelled SLBs before and after the addition of the proteins (FL/P39/WM/MA/EFA6-PH) or buffer were recorded using ZEISS LSM780 confocal microscope (Carl Zeiss, Inc.) with a 63x, 0.75 NA objective. To avoid any z-drift, Zeiss definite focus system was employed in conjunction with a 2-photon excitation (930nm).Images were acquired for every 5s in order to strongly reduce photobleaching. A typical time-lapse fluorescence measurement was recorded at 512x512 pixels and 16 bit at a constant intensity. In the case of a dual color acquisition, green channel was set at ex488/em498-500 nm and red channel at ex 561/em 600-660 nm. To negate the bleaching effect in the overall quenching measurements, a 2 min acquisition was done before addition of the protein. The sequential acquisition was then done for a period of 10 min or till there observed a plateau in the signal. Obtained time-lapse was corrected for bleaching if any. The mean intensity of each image was normalized to the intensity before injection.

2.5 Confocal Microscopy:

Visualization of GUVs was done using ZEISS LSM780 Confocal microscope (Carl Zeiss, Inc.) using a 63x, 0.75 NA objective. On the microscope, GUVs were added to the Attofluor cell chamber (Thermo Fisher Scientific, Inc.) fitted with casein (2mg/ml) coated coverslip (25 mm, Deckgläser). On stabilization, labelled proteins were added to the medium and imaged. Images

were acquired with 512x512 pixels and 16 bit at constant intensity keeping the green channel at ex488/em498-555 nm & red channel at ex561/em600-660 nm. For Spectral imaging, the excitation is set at 488 and 561 nm for green and red fluorescence, the spectral range was set from 496 to 660 nm. Linear Unmixing of the images was done to avoid the bleed-through from Topfluor® to Alexafluor-594 channel using ZEISS 2012 software. In the case of GUVs labelled with cholera toxin B-647, ex was set at 488/561/630 nm for green, red & far red channels. Further, images were treated using Image J software. All experiments were conducted at room temperature.

2.5.1 Fluorescence Recovery After Photobleaching (FRAP):

FRAP is a facile and reproducible method to elucidate the quality of the supported bilayers with fluorescently labelled lipids as the method gives the diffusion of the laterally moving lipids in this thin lipid bilayer. A typical experiment involves before and after the recording of fluorescence intensity of a bleached region over time. For a good quality SLB, the recovery of the fluorescent intensity should be 100%. In our study, we employed this technique to understand the lipid trapping nature of the protein, assuming a trapped lipid will have a crippled diffusion and the overall recovery will be less than 100% on the same time-scale.

FRAP experiments were performed on labelled lipid containing SLBs using a Zeiss LSM-780 confocal microscope. The image sequence was acquired at a 20 Hz frequency using the 488 nm line of an argon ion laser at a very low power to avoid photobleaching during recording. After 50 images, 3 regions of interests (ROI), of 1 μm radius each, which correspond to 0.236 μm waist of a Gaussian beam were rapidly photobleached ($t < 60$ ms) at maximal laser power. Fluorescence recovery was monitored at 20 Hz by acquiring successive images during 15 s. The recovery curves were obtained by plotting the mean fluorescence intensity as a function of time in this three ROI, and were corrected for fluctuations in axial position by another ROI located far from the bleached areas and finally normalized to the mean value of each ROI before photobleaching. The curves were fitted using Eq.13 which is a slightly modified 2D diffusion model for FRAP taking into account normalization and fractional recovery (M):

$$F(t) = M\sum_{n=1}^{\infty}\frac{(-K)^n}{n!}\frac{1}{1+n+2n\frac{t}{t_{1/2}}} + (1-M)F_0 \qquad \textit{Eq: 13}$$

In eq. 13, K measures the deepness of the bleach, $t_{1/2}$ corresponds to the time where half the fluorescence has been recovered and is linked to the two-dimensional diffusion coefficient D, F_0 is the fluorescence intensity immediately after the end of the bleach, i.e. at t = 0. Equation 13 was used to its 20th order limited development for data fitting (n=20). The fractional recovery (M) is defined as:

$$M = \frac{F_{15s}-F_0}{1-F_0} \qquad \textit{Eq: 14}$$

2.5.2 Two-photon Laser Scanning TCSPC FLIM:

By calculating the exponential decay rate of a fluorescence emitted by an excited fluorophore, Fluorescence lifetime imaging technique (FLIM) can calculate the lifetime of these fluorophores and can generate an image based on the lifetime itself. In simple terms, the fluorescence decay time is written as

$$I(t) = I_0 e^{-t/\tau} \qquad \textit{Eq: 15}$$

Where $1/\tau = \Sigma\, k_i$. I_0&I(t) is the fluorescence intensity at the time, t, k_i is the decay rate and τ is the fluorescence lifetime. As τ is independent of concentration, molecular information at different environments can be measured simultaneously despite the difference in the concentration from one region to the other. In this study, this is achieved by time-correlated single photon counting (TCSPC) method where the time of detection of the individual photons by a photo-multiplier tube (PMT) was recorded. Further, a histogram of the entire event as across the recorded time points was fit to extract the lifetimes of the fluorophore at the pixel level.

Fluorescence lifetime images were acquired with the Zeiss LSM 780 confocal microscope equipped with a not-descanned output with a fast hybrid photomultiplier (HPM-100-40) and SPC-830 time-correlated single photon counting (TCSPC) electronics (Becker &Hickl). A 40x, NA 1.3 objective was used to image the sample. An excitation wavelength of a Chameleon

Ultra-II (Coherent Inc.) was tuned to 900 nm and used at low intensity to avoid photobleaching. The acquisition time was variable ($5 < t < 20$ min) in order to keep the number of photons above 3000 for each decay in each pixel of the image. This authorizes to keep the fluorescence lifetime measurement accuracy constant (<2%) in the presence or absence of quenching and strongly decreases the contribution of the background. Moreover, confocal model and two-photon excitation method almost completely negate the background. Finally, the number of photons acquired per second was kept under the pile-up threshold (106 cts.s^{-1}). Fluorescence decays were fitted with a single exponential and a generated instrument response function (IRF) using the SPCImage software of Becker &Hickl.

2.5.3 Fluorescence Correlation Spectroscopy (FCS):

FCS is a fluorescence fluctuation based technique where the fluorescence intensity recorded over time in a confined volume will be correlated by itself or in cross-correlation to provide details about the local concentrations, molecular weights, translational and rotational diffusion coefficients, chemical rate constants, association and dissociation constants, and photodynamics *in vitro* as well as *in vivo*.

Background: To measure the dynamic properties of molecules it is important to understand the diffusion property of a particle. Simply put, diffusion can be described as a random walk of a molecule which is measured with a coefficient, Diffusion coefficient, with μm^2/ sec as its unit. While the trajectory over time of a diffusing particle is defined as the mean square distance (MSD) (r^2), it primarily depends on the diffusion coefficient of the molecule which in turn, depends on various other factors related to the molecule and the surrounding medium. Stokes-Einstein equation presents this in an elegant manner:

$$D = {k_B T}/{6\pi.\eta.R_h} \qquad \textit{Eq: 16}$$

Where Boltzmann's constant k_B = 1.3806504. 10^{-23} J/K, T is the absolute temperature, η is the solution viscosity and R_h is the hydrodynamics radius.

Studying the diffusion of a molecule using this equation is facile at large volumes. But is not practical for biological systems where the components are confined to micro-nanometer scale range. Nevertheless, fluorescence fluctuation based techniques like FCS can be of great help in these cases, where a fluorescently tagged molecule can be studied at nanometer scale range.

Based on the method employed there are different FCS based methods. In this study, we have employed spot variation FCS and linescan FCS to understand the assembly of HIV-1 Gag interaction with PI(4,5)P_2 containing lipids.

Theory: As explained earlier, the technique employs correlating the change in fluorescence intensity fluctuations over time, I(t). For example, in a defined homogenous volume, the average number of diffusing particles (N) over time (N(t)) should be constant at equilibrium. So, the intensity (I) should remain constant. As the particles move out and inside of the observation volume, the change in fluorescence intensity due to change in a number of particles over time is calculated δN(t). Giving the overall number of particles over time as

$$N(t) = (N) + \delta N(t) \qquad \textit{Eq: 17}$$

In FCS, the fluctuations δN(t) or δI(t) is analyzed while keeping the average (N) or (I) out of it. Since the number of particles cannot be calculated directly, the change in fluorescence intensity emitted by the particles is analyzed. As a particle enters the focal volume, it gets excited by the laser and the constant cycle of excitation and emission occurs. Thus emitted photons are detected on an Avalanche photodiode (APD)/ Gallium arsenide phosphide (GaAsp) detector. In terms of fluorescence intensity:

$$I(t) = (I) + \delta I(t) \qquad \textit{Eq: 18}$$

To know how fast the particle fluctuates, the intensity fluctuations (δI(t)) are mathematically treated using autocorrelation analysis tool. This gives the autocorrelation function g(τ) that measures the self-similarity of the fluorescence fluctuations δI(t) with time t and a lag time τ. To

have a high autocorrelation, the lag time should be lower than the average retention of the particle in the focal volume. This will give a fair amount of self-similarity between δI(t) and δI(t+τ) that is used to generate g(τ).

$$g(\tau) = \frac{(\delta I(t).\delta I(t+\tau))_t}{(I(t))_t^2} \qquad \textit{Eq: 19}$$

As these fluctuations occur because the volume is defined (V_{obs}), it is imperative to pre-calibrate the observational volume using a known fluorescent molecule such as Rhodamine B. This will help in calculating the diffusion coefficient of the molecules. As the system used here is a confocal microscope which has an ellipsoid focal volume with a width in xy-axis (ω_{xy}) and a length (z_o). In addition to the autocorrelation curve obtained from FCS measurements, further evaluation has to be done by fitting with theoretical models that can provide with the diffusion time (τ_D). A theoretical model for a single diffusing species can be as simple as

$$g(\tau) = \frac{1}{N} . (1 + \frac{\tau}{\tau_D})^{-1} . (1 + \frac{\tau}{\gamma^2 \tau_D})^{-1/2} \qquad \textit{Eq: 20}$$

Where γ is the structural factor, z_0/ω_{xy}.

Adding to the complexity, during the excitation-emission cycle, molecules can crossover into triplet state (T) rather than directly returning into the ground state. But the eventual relaxation from triplet state to ground state results in a blinking process with a characteristic lifetime τ_T. This leads to an additional factor in the correlation function:

$$g(\tau) = \frac{1}{N} . \frac{1 - F_T + F_T . e^{-\tau/\tau_T}}{1 - F_T} (1 + \frac{\tau}{\tau_D})^{-1} . (1 + \frac{\tau}{\gamma^2 \tau_D})^{-1/2} \qquad \textit{Eq: 21}$$

Where F_T is the fraction of particles in the triplet state T

Finally, using the obtained τ_D and ω^2_{xy} one can calculate diffusion coefficient, D and also the concentration, c:

$$D = {\omega_{xy}^2}\Big/{4\tau_D} \qquad \textit{Eq: 21}$$

$$c = \frac{N}{V_{eff}} \qquad \textit{Eq: 23}$$

WhereV_{eff} is Effective Volume = $\pi^{3/2}.\gamma.\omega^3_{xy}$

Measurements: In our experiments, both svFCS and line-scan FCS was employed. FCS measurements were performed using Zeiss LSM780 with an FCS module installed. Using an x40 water objective with a ring set at 0.17, both svFCS and line FCS were done. For svFCS, the acquisition was made with repetition of 10 over 10s for every pupil radii (100, 70, 50, and 30) using a GaAsp detector. The obtained correlation data was fitted with pycorr fit software for calculating the diffusion coefficient of the labelled lipid. In the case of linescan FCS, laser scan speed of 1.6KHz with a pixel dwell time of 0.5 µsec and a scan length of 13.3 µm was used to record 50000 images through a GaAsp detector. Analysis of the recorded images was done to generate autocorrelation using custom made software. In the analysis, the initial bleached part was removed to avoid the discrepancies. Thus obtained autocorrelation curves were fitted with a single or two component models, wherever required. An average of the obtained correlation curve was plotted and fitted to give the final diffusion time and to further calculate the diffusion coefficient.

Chapter-3

HIV-1 Gag is reorganising $PI(4,5)P_2$ during multimerization on model membranes

3.1 Introduction

In order to elucidate whether Gag would bind to preexisting raft or lipid domains in the PM or generate its own lipid domains while assembling, we have monitored the lateral reorganization of $PI(4,5)P_2$, cholesterol (Chol) and sphingomyelin (SPM) upon Gag multimerization. Above question was addressed on different lipid mixtures, from the simplest ($PC/PS/PIP_2$, called basic composition) to more complex compositions mimicking either the inner leaflet cell plasma membrane (Ingolfsson et al. 2014) or the "lipid rafts" domains (i.e. two separated phases, a liquid disordered (L*d*) and a liquid ordered (L*o*) enriched in cholesterol and sphingomyelin) (Keller, Kräusslich, and Schwille 2013) (See SI tables S1 and S2 for detailed lipid compositions).

3.2 Approach

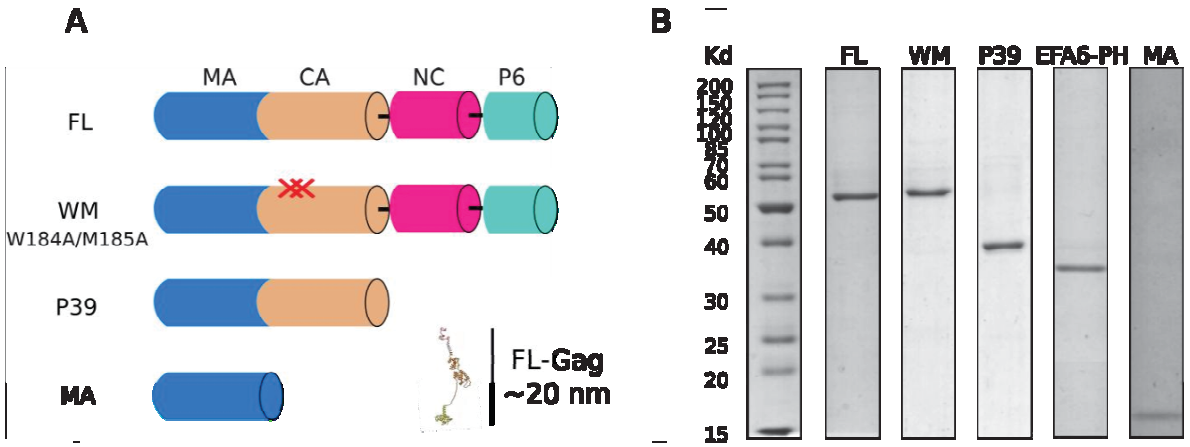

Figure 3.1: Purified proteins used in this study. (A) Schematic representation of Gag full-length protein and various mutants used in this study. Inset, shown the length of an open conformation FL-Gag protein ie., ~20 nm. (B) All the different proteins purified were run through 10% SDS-PAGE and stained with coomassie brilliant blue.

For this study, highly purified Gag proteins (FL-Gag, P39, WM, & MA) (figure 3.1(B)) were used as it was known that any polybasic protein can interact electrostatically with the lipid bilayer and so are undesirable. For a multimerizable protein, the presence of unwanted proteins might affect the availability of specific lipid and membrane surface. To understand the role of different domains in the interaction with lipids & the effect of multimerization efficiency we

have chosen various mutants of Gag, apart from the wild type (see figure 3.1). We compared MA domain, P39 (lacking NC & P6 domains) and WM (multimerizing mutant) with that of the wild type in their ability to interact and assembly on lipid bilayers. Finally, to study the interaction of Gag protein with lipids, we choose to use model membranes as interaction substrate.

Model membranes for their simplistic nature and a possibility to control precisely the lipid composition can help understand the role of specific lipids in the assembly of Gag protein along the plasma membrane. Using model membranes with a difference in curvature like LUVs – significant curvature, GUVs – less curvature & SLBs – zero curvature will provide the opportunity to understand their interaction and assembly of proteins. Overall, this study uses different types of model membranes and biophysical tools – initially to validate the methodology binding ability and affinities of the proteins towards $PI(4,5)P_2$ containing LUVs were performed followed by quenching experiments on liposomes and SLBs. The property of the protein multimerization in the observed effect was even answered. Further to this, as mentioned earlier, the role of specific rafts lipids in Gag assembly was probed in different lipid composition environments. Finally, GUVs were employed to visualize the binding and assembly of Gag and to ascertain the L*d*/L*o* nature of assembly platforms.

3.3 Results & Discussions

3.3.1 Affinity studies of Gag towards PI(4,5)P_2 containing membranes:

Gag protein binding to the plasma membrane is considered as a bipartite mechanism that involves (a) interaction of the HBR region with the PI(4,5)P_2 present in the inner leaflet & (b) insertion of the N-terminal myristate into the hydrophobic core of the plasma membrane. From many studies, it was understood that the N- terminal myristyl group functions in concert with the HBR to maintain membrane binding (Saad et al. 2006; Zhou and Resh 1996). However, some retroviruses, such as Rous sarcoma virus (RSV)(Dalton et al. 2005; Inlora et al. 2014) and Equine infectious anemia virus (EIAV) (Chen et al. 2008), despite lacking a myristate anchor, Gag can bind to the PM merely by electrostatic interactions. Moreover, it was also shown that the driving force for membrane association, in the case of myr MA, stems largely from ionic interactions(Dalton et al. 2007). Therefore, in order to understand a potential role of HIV-1 Gag in the lateral reorganization of PI(4,5)P_2, we first tested the ability of the HIV-1 myr(-)Gag and its mutants to bind model membranes containing PI(4,5)P_2. These mutants include: (1) a mutant of CA involved in CA-CA interaction and Gag multimerization (WM) (2) Gag lacking the C-terminus NC-sp2-p6 domains that are involved in NC-RNA association (P39). The membrane binding domain alone of Gag (MA) was also tested (see figure 3.1(A)). Results were compared to the one obtained for a specific cellular PM PI(4,5)P_2 binding protein, the PH domain of EFA6 (PH-EFA6) (Macia et al. 2008b) and a peptide, MARCKS (151-175) that is known to laterally redistribute PI(4,5)P_2on model membranes (Gambhir et al. 2004). In order to understand the potential role of HIV-1 Gag in the lateral reorganization of lipids, its affinity towards to the "basic" lipid membranes was first assessed. For that purpose, we performed Large Unilamellar Vesicles (LUV) co-sedimentation assays (figure 3.2(A)) with increasing lipid concentrations and keeping the protein concentration at 1µM. In parallel with Quartz Crystal Microbalance (QCM-D), by monitoring the association of increasing protein concentrations (from 10^{-2} to 10 µM) to Supported Lipid Bilayers (SLB) at constant lipid concentration (figure 3.2(B) and (D)). Plots of lipid-bound proteins as a function of increasing concentrations of lipids (figure 3.2(C)) or protein (figure 3.2(D)) allowed determination of apparent partition coefficients (K_p) for the different proteins used. Except for MA, K_p obtained for other proteins were less than 1µM.

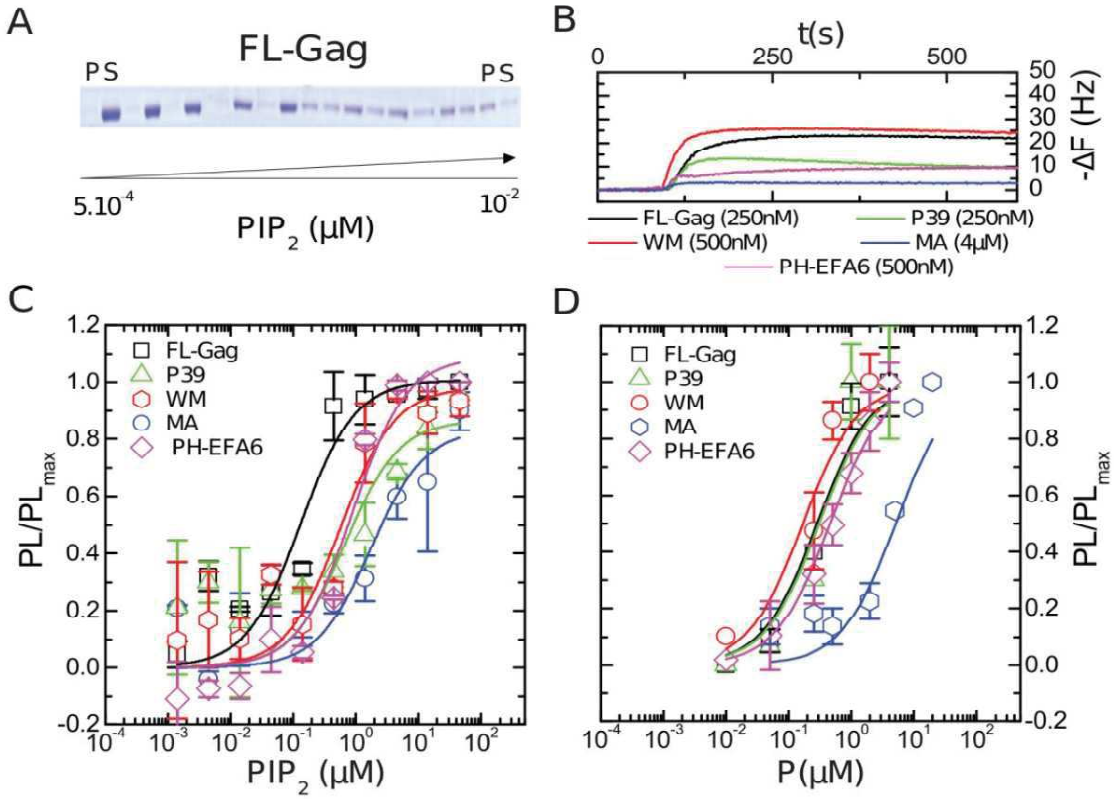

Figure 3.2: Binding of FL-Gag and its mutants, Matrix, PH-EFA6 and MARCKS to "basic" lipid membranes
Part A: An example of co-sedimentation assay obtained for FL-Gag with increasing concentrations of 2% mol $PI(4,5)P_2$ containing LUVs. Part B : Typical change in resonance frequency observed during QCM-D experiments after addition of different proteins at different concentrations on a basic composition SLB. Part C and D : Binding isotherm curve obtained from different co-sedimentation assays (Part C, n=3) and different QCM-D experiments (Part D, n=2) for the different proteins used in this study. Experimental values were fitted using equation 4 for cosedimentation assay and equation 8 for QCM-D results., *Kp* obtained from these binding isotherms are summarized in table

Table 3.1: Apparent K*p* of the different proteins used in this study

Method	FL	P39	WM	MA	PH-EFA6	MARCKS
Cosedimentation assay	0.13±0.05	0.66±0.44	0.56±0.26	1.72±1.05	0.88±0.27	-
QCM-D	0.40±0.11	0.47±0.26	0.26±0.13	7.16±3.33	0.68±0.03	0.65±0.23

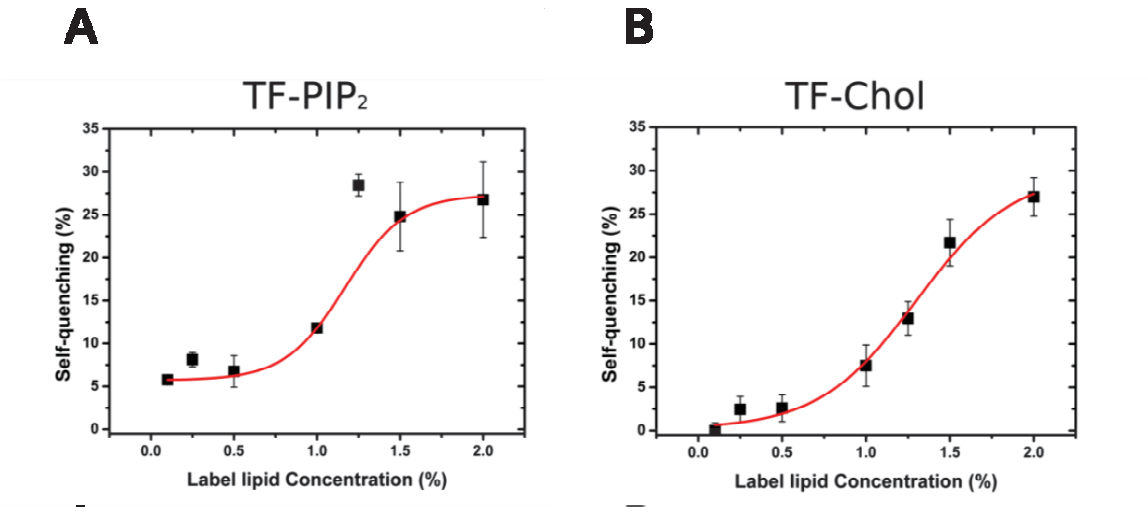

Figure 3.3: Concentration dependence of self-quenching property of TopFluor® labelled lipids in LUVs (A) TopFluor® PI(4,5)P_2 (B) TopFluor® Chol

Interestingly, the K*p* values of MARCKS and PH-EFA6 ($0.7 < Kp < 0.8\mu M$) were found to be in the range of the one obtained for Gag (FL) and its mutants ($0.2 < Kp < 0.8\mu M$). This suggests that the ratio of membrane-bound over total protein will be approximately equivalent for all these proteins, allowing direct comparisons of their respective roles in the lateral sorting of PI(4,5)P_2. A higher affinity for FL-Gag as compared to its mutants can be justified by the recent finding: NC domain of Gag can bind to lipid membranes with an apparent K*p* as high as 7 µM on LUV containing 5% of PI(4,5)P_2(Kempf et al. 2015b). Oligomerization state can also be a contributing factor towards higher affinities. Recent studies using LUV with the same lipid composition as that of this study have also suggested that this increase in binding for FL Gag compared to MA may reflect an oligomerization state of Gag. Moreover, this result also emphasizes that the driving force for membrane association stems largely from ionic interactions between multimerized Gag and negatively charged phospholipids than from myristate insertion(Dalton et al. 2007). This is consistent with the differences of K*p* values seen with the mutants of Gag protein. Myr(-) FL-Gag with its HBR region, NC domain and the high oligomerizing property has higher affinity for the LUVs than myr(-)Gag WM (HBR, NC domain & mild oligomerizing property) & myr(-)Gag P39 (HBR & oligomerizing property). Myr(-) MA being the crippled off NC domain & CA domain (for oligomerization) has a distinctively lower affinity.

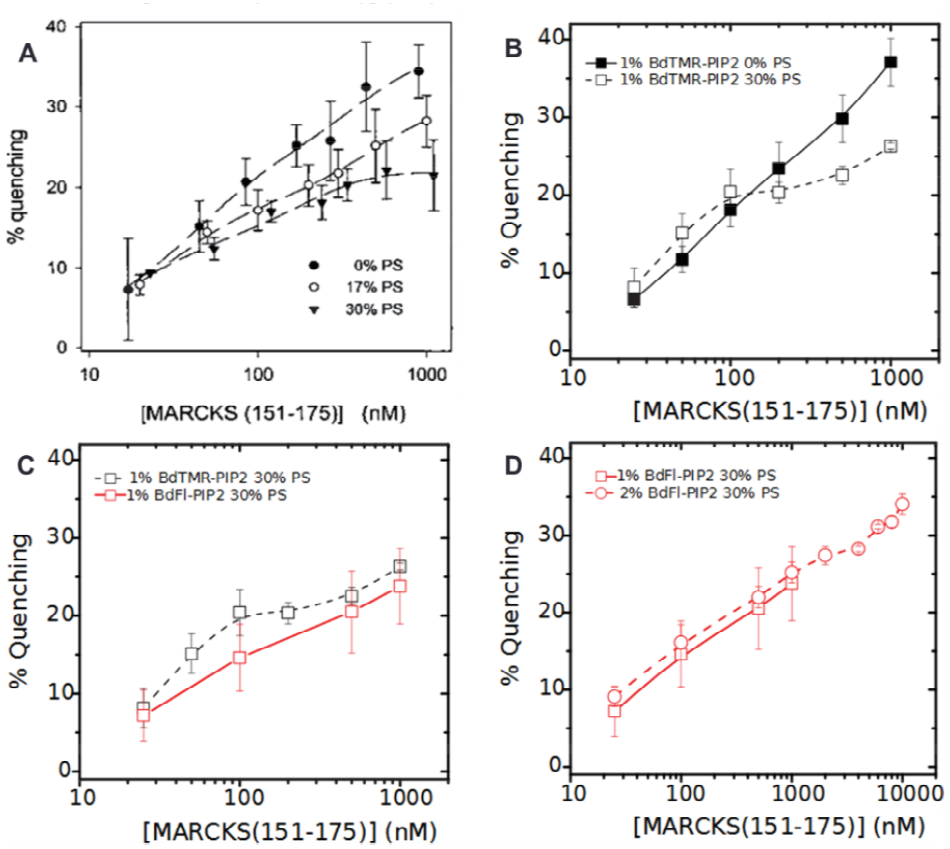

Figure 3.4:MARCKS peptide induced quenching of labelled PI(4,5)P_2 containing LUVs (A) Figure obtained from (Gambhir et al. 2004) for comparison, (B) Our data showing the results of MARCKS peptide induced quenching of BT-PI(4,5)P_2 labelled PI(4,5)P_2 containing liposomes, in direct comparison with the 30% PS variant of already published data. (C) Similar quenching profile observed when Bodipy-TMR is replaced with TopFluor®, showing dye independent nature of MARCKS peptide in PI(4,5)P_2 clustering and (D) No significant difference in the extent of MARCKS induced quenching with varied labelled TF-PI(4,5)P_2 concentration.

Overall, these findings emphasize that various domains & properties of the protein can affect the overall affinity of the Gag protein towards the inner-let of the plasma membrane, especially towards PI(4,5)P_2.

3.3.2 Self-quenching of TopFluor® labelled lipids:

To understand the lipid lateral redistribution property of Gag, we employed quenchable variants of lipids. As explained in the Methods section, self-quenching process occurs when two dye molecules align close enough (<50Å) to quench and it is an efficient way to study the

protein-lipid interactions. So, as the concentration of the dye molecules increases, the probability of one molecule encountering the other also increases – inducing quenching. In this study, the degree of self-quenching of TopFluor PI(4,5)P_2 in LUVs of basic composition (EPC, BPS & PI(4,5)P_2 at 68%, 30% & 2%, respectively) was estimated by employing varied percentage of labelled PI(4,5)P_2(from 0.1, 0.25, 0.5, 1, 1.25, 1.5 & 2 while keeping the overall percentage of PI(4,5)P_2 at 2%) containing LUVs. The data obtained clearly suggests that TopFluor PI(4,5)P_2 does self-quench quite effectively as the concentration of the labelled dye increases within the liposomes. Self-quenching of TopFluor PI(4,5)P_2 is in good agreement with the previously published data for Bodipy-FL PI(4,5)P_2(Blin et al. 2008). Similarly, self-quenching properties of the TopFluor labelled Cholesterol was also studied (figure 3.3(B)). Both the lipids have shown a similar profile, suggesting the quenching properties are similar and comparable.

To compare the self-quenching properties of Bodpiy-TMR PI(4,5)P_2 with that of TF-PI(4,5)P_2 used in this study, quenching experiments on LUVs using MARCKS peptide was performed. The initial attempt was to reproduce the earlier work of Gambhir et al. 2004 (figure 3.4(A)) by using increasing concentrations of MARCKS peptide on Bodipy-TMR/TopFluor® labelled PI(4,5)P_2 containing LUVs (figure 3.4). We found that by substituting BT-PI(4,5)P_2 by TF-PI(4,5)P_2 does not change the effect observed after addition of MARCKS peptide (figure 3.4(C)) (neither at 1% or 2% molar concentration of the TF labelled lipid (figure 3.4(D)), confirming that the interaction is dye independent.

3.3.3 HIV-1 Gag Multimerization induces lateral reorganization and nanoclustering of PI(4,5)P_2 in model membranes (LUVs/SLBs/GUVs)

3.3.3.1 On LUVs

Lateral redistribution of lipids along the membrane is the hallmark of various proteins that have an affinity for a specific lipid types. Proteins like AnnexinA2-p11 (Gokhale et al. 2005), MARCKS peptide (Gambhir et al, 2004) & Profilin (Krishnan et al. 2009) were proven to cluster PI(4,5)P_2 on model membranes. Although, in most PI(4,5)P_2 clustering protein studies, self-quenching dyes labelled variants of PI(4,5)P_2 were used, only MARCKS peptide & Profilin were

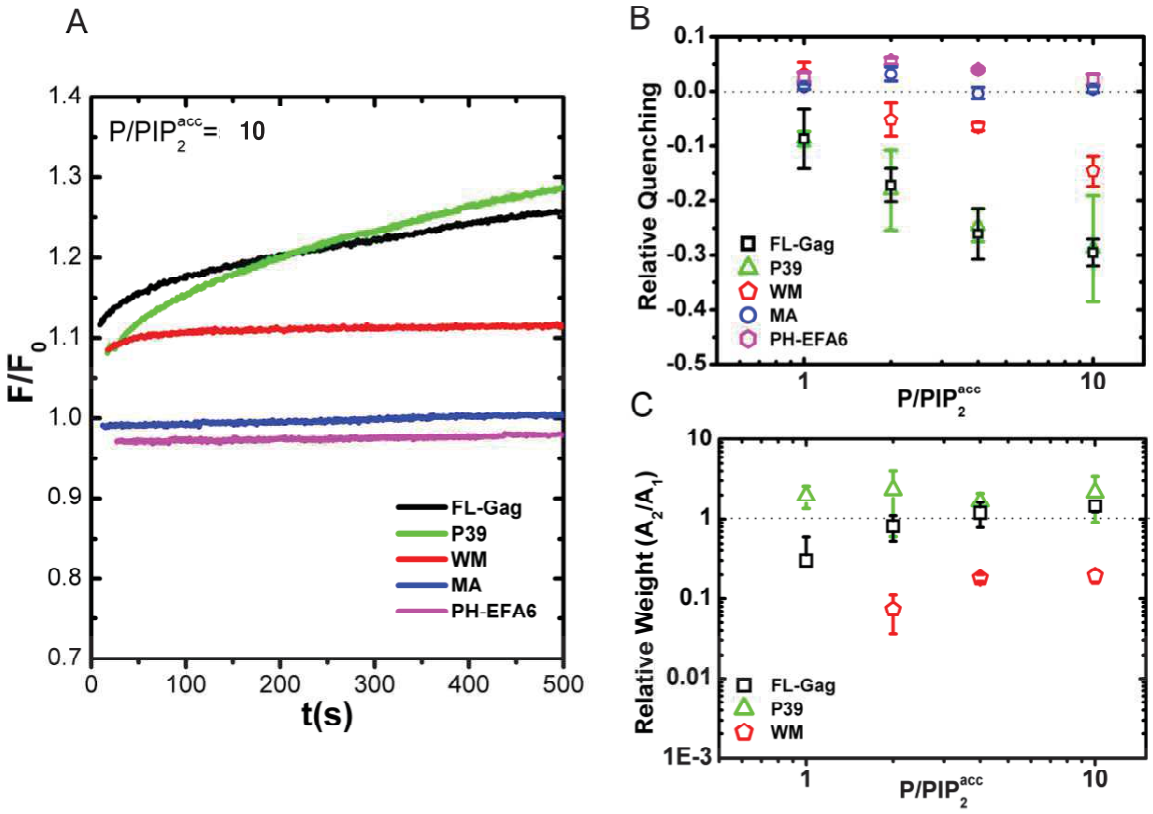

Figure 3.5:PI(4,5)P_2 lateral reorganization induced by Gag multimerization on basic composition liposomes
(A) Typical time course of TF-PI(4,5)P_2 fluorescence on LUVs after addition of the different proteins or peptide at a P/PIPacc2 = 10. (B) Relative quenching values observed for FL-Gag, its mutant, MA and PH-EFA6 onLUVs (mean ± s.d. values of $n \geq 3$ for each P/PIPacc2 conditions, except P39($2 < n < 3$)). (C) Relative weights from the bi-exponential fit of fluorescence time course obtained for various P/PI(4,5)P_2^{acc} of FL-Gag, WM & P39.

able to induce self-quenching by closely clustering Bodipy-TMR labelled PI(4,5)P_2. Keeping this in mind, we have performed quenching based experiments to study the myr(-) FL-Gag ability to sequester TopFluor® labelled PI(4,5)P_2 on model membranes.

In order to understand the possible lateral reorganization of PI(4,5)P_2 during Gag interaction & multimerization, we then performed acquisition of fluctuations in the intensity of overall fluorescence with time upon protein interaction with the TF-PI(4,5)P_2 containing LUVs. When monitoring the change in TF-PI(4,5)P_2 fluorescence after addition of Gag or its mutant for "basic" LUVs, we observed an increase in TF-PI(4,5)P_2 fluorescence (figure 3.5(A)) opposite to that of MARCKS peptide. From figure 3.5(A), it was evident that addition of increasing concentrations of FL-

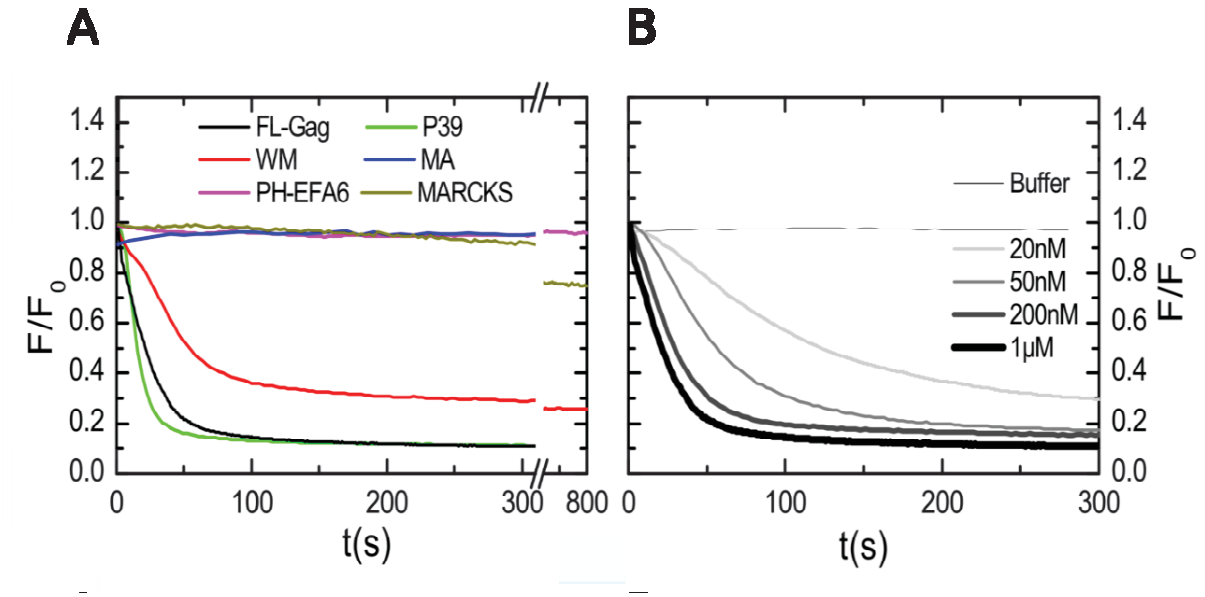

Figure 3.6: PI(4,5)P_2 lateral reorganization induced by Gag multimerization on basic composition SLBs(A) Typical time course of TF-PI(4,5)P_2 fluorescence on SLBs after addition of the different proteins or peptide at 1 µM. (B) Fluorescence time course of TF-PI(4,5)P_2 after addition of increasing FL-Gag concentrations on different SLBs.

Gag, P39 and WM induced an increasing fluorescence unquenching of TF-PI(4,5)P_2. On the other hand, adding increasing concentrations of MA did not generate any change in the fluorescence of TF-PI(4,5)P_2. Identically, PH-EFA6, known to specifically bind PI(4,5)P_2 without reorganising its lateral distribution, did not produce any effect either (figure 3.5(A) or (B)). Figure 3.5(C) is depicting a characteristic change in fluorescence intensity over time for a 5:1 P/PI(4,5)P_2acc ratio. A fit of these fluorescence time courses with an arbitrary bi-exponential increase (see material and methods) was used to determine the presence or absence of a two-step process and to measure, when present, their respective weights (namely A_1 for the short life- time (1 <50s) and A_2 for the long lifetime (200< 2 <500s)). As stated previously, one would expect multimerization to occur after binding. In that perspective, we plotted the ratio A_2/A_1 of PI(4,5)P_2 de-quenching as a function of P/PI(4,5)P_2acc for FL-Gag and WM (the multimerization mutant). Interestingly, FL-Gag overcame a A_2/A_1= 1 threshold at P/PI(4,5)P_2acc = 2 ratios, showing that the long lifetime step of the unquenching process occurs even at low concentrations of FL-Gag. On the opposite, within the range of protein concentrations used in this study, WM, A_2/A_1 never reached one even at the highest concentration, P/PI(4,5)P_2acc = 10. A major difference between the MA and the precursor proteins (FL-Gag, P39 and WM) is their capacity to form large oligomer complexes via the CA-CA interactions (Datta, Curtis, et al. 2007a), although WM is

less efficient (two orders of magnitudes in solution) in supporting this oligomerization (Fung and Stryer 1978). Interestingly, this fluorescence unquenching was always less efficient in the case of WM compared to FL-Gag (from 3 to 5 times), indicating that this fluorescence variation could be an outcome of the Gag to multimerization capacity.

3.3.3.2 On SLBs:

Although LUVs provided a simple, reliable and easy to control model membranes, the Gag multimerization usually occurs on membranes with zero or no radius of curvature. Therefore, time course fluorescence quenching of TF-PI(4,5)P_2 was also conducted on "basic" SLBs that resemble the real world scenario. For FL-Gag and P39, the TF-PI(4,5)P_2 fluorescence intensity changed on SLBs (figure 3.6) and was opposite to the one observed with LUVs (figure 3.5) while still being a function of the protein concentration (figure 3.6(B)). As it was the case for LUV, the TF-PI(4,5)P_2 quenching induced on SLBs after the addition of WM mutant was less efficient than in the case of FL-Gag. While PH-EFA6 and MA did not induce any changes in TF-PI(4,5)P_2 fluorescence (figure 3.6(A)), interestingly, the same figure depicts that MARCKS peptide addition induced the same TF-PI(4,5)P_2 quenching on SLBs, as it was the case on LUVs (see figure 3.4). These results conclude that despite the opposite effects observed with change in model membrane curvature, multimerization of HIV-1 Gag is laterally reorganising TF-PI(4,5)P_2.

3.3.4 Quantifying oligomerizing state of HIV-1 Gag and its multimerization mutant

Apparent affinity studies on HIV-1 myr (-) Gag mutants (FL, MA, P39 & WM) revealed the role of NC domain and oligomerizing capability of the protein in enhancing the affinities of the protein towards LUVs with basic lipid composition. While NC domain's ability to bind lipids has been established very recently, the oligomerization properties are not well characterized. Although in the presence of high ionic strength buffer; isolated CA can self-assemble into hollow

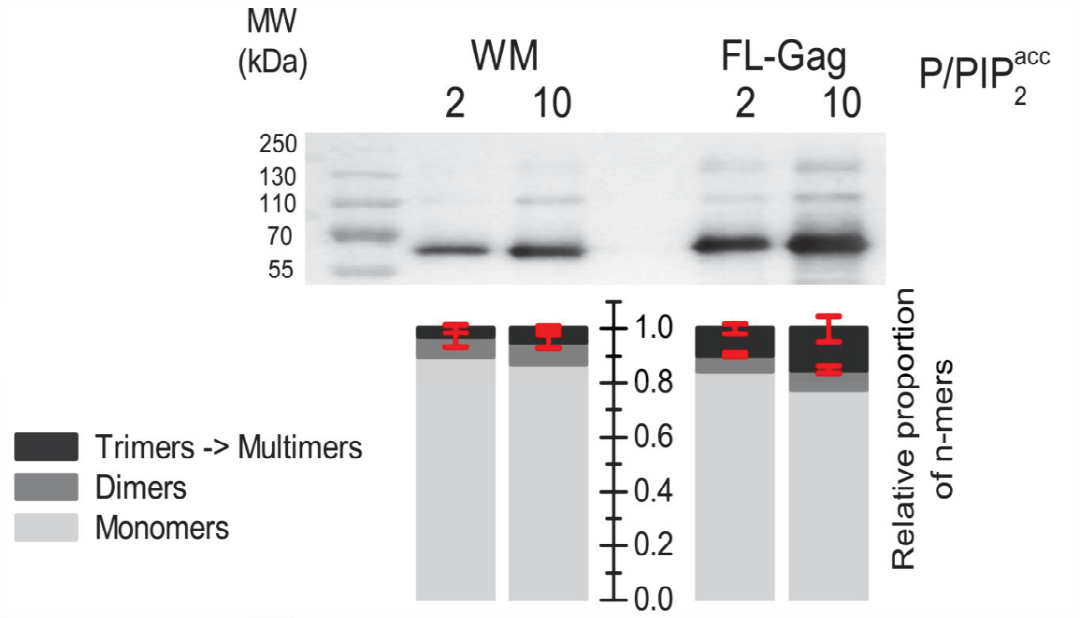

Figure 3.7: Multimerization induces lateral reorganization of PI(4,5)P_2. Typical blot observed for WM and FL-Gag at two different P/PI(4,5)P_2^{acc} and its quantification in terms of the relative proportion of n-mers in the total protein (mean ± s.d., n=3).

cylinders (Ganser-Pornillos et al. 2004), Gag requires low ionic strength (≤ 300 mM sodium chloride) to oligomerize and subsequently assemble. In vitro studies revealed that myr(-) GagΔp6 exists at a monomer-dimer equilibrium in solution (Datta, Zhao, et al. 2007)(Deshmukh, Ghirlando, and Clore 2015)& in the presence of IP6, it shifts to a monomer-trimer equilibrium (Datta, Zhao, et al. 2007). Further, in a similar study, the myr(-)GagWMΔp6 was shown to exist primary as a monomer and its dimerizing capacity has been found to be ~100 folds lower when compared to FL-Gag(Datta, Curtis, et al. 2007a). Apart from the oligomerization state in solutions & IP6, no study has been done on the oligomerization state in the presence of actual lipids and on bilayers. In this study, we tried to differentiate the oligomerizing capability of myr(-) FL-Gag& myr(-) Gag WM in the presence of LUVs with basic lipid composition using a non-denaturating gel electrophoresis. From figure 3.7, it is evident that myr(-) FL-Gag can even oligomerize at lower P/$L_{(PI(4,5)P_{2)(acc)}}$ concentrations compared to myr(-) Gag WM. But when compared to the difference found in solution (~100 folds), the difference sensed in the presence of actual lipids is rather low. This could be because the apparent concentration on the surface of a 100 nm vesicle must be way larger than in solution and the probability of encountering a partner to form a dimer or trimer is high. Considering the results from interaction with IP6, in the

presence of actual lipid, PI(4,5)P_2, one can obtain more than just dimers or trimers– even multimers. The result obtained for WM was only two times less efficient than FL-Gag in multimerization capacity (figure 3.7). Furthermore, this ratio was in the range of the relative efficiency of TF-PI(4,5)P_2 unquenching observed between FL-Gag and WM – supporting the role of Gag multimerization in the observed TF-PI(4,5)P_2 fluorescence changes.

3.3.5 Opposing effects on LUVs and SLBs by Gag multimerization

3.3.5.1 Effect of probe and probe concentration on fluorescence quenching

We tried to study the possible role of dye and dye concentration on the opposing effects we observed on model membranes with a difference in curvature. We first conducted experiments on the same "basic" composition LUVs but with a different labelled PI(4,5)P_2 (BT-PI(4,5)P_2) and compared to the results obtained with LUVs containing TF-PI(4,5)P_2. Figure 3.8(A) shows a good reproduction of the BT-PI(4,5)P_2 quenching published in (Gambhir et al. 2004). In the same figure, substituting BT-PI(4,5)P_2 by TF-PI(4,5)P_2 does not change the effect observed after addition of MARCKS peptide, either at 1% or 2% molar concentration. Knowing that TopFluor labelled PI(4,5)P_2 does self-quench and its dependence on concentration, we also tested the quenching concentration dependency of TF-PI(4,5)P_2 upon addition of different FL-Gag concentrations (figure 3.8(B)). Again, we did not observe any drastic change with different dye molar ratios. All these results show a weak dependency of the induced PI(4,5)P_2 clustering upon the nature of the fluorescent dye and its molar concentration in the LUVs. We then performed a similar experiment on SLBs to ascertain that the opposing effect is not due to the dye concentration. Figure 3.8(C) and (D) show the change in fluorescence of either TF- or BT-labelled PI(4,5)P_2 after FL-Gag addition at different concentrations. At low FL-Gag concentration (i.e. equivalent to small FL-Gag/PI(4,5)P_2^{acc}), we could see differences depending on the molar concentration and the nature of the fluorophore in the normalized fluorescence value (0.4 for TF-PI(4,5)P_2 and 0.2 for BT-PI(4,5)P_2). Importantly, these differences faded with increasing FL-Gag concentration. At FL-Gag concentrations above 200 nM, the fluorescence of either different dye molar ratio (figure 3.8(D)) or chemical nature always fall down to 0.2 ±0.1. We concluded that at labelled lipid saturating FL-Gag

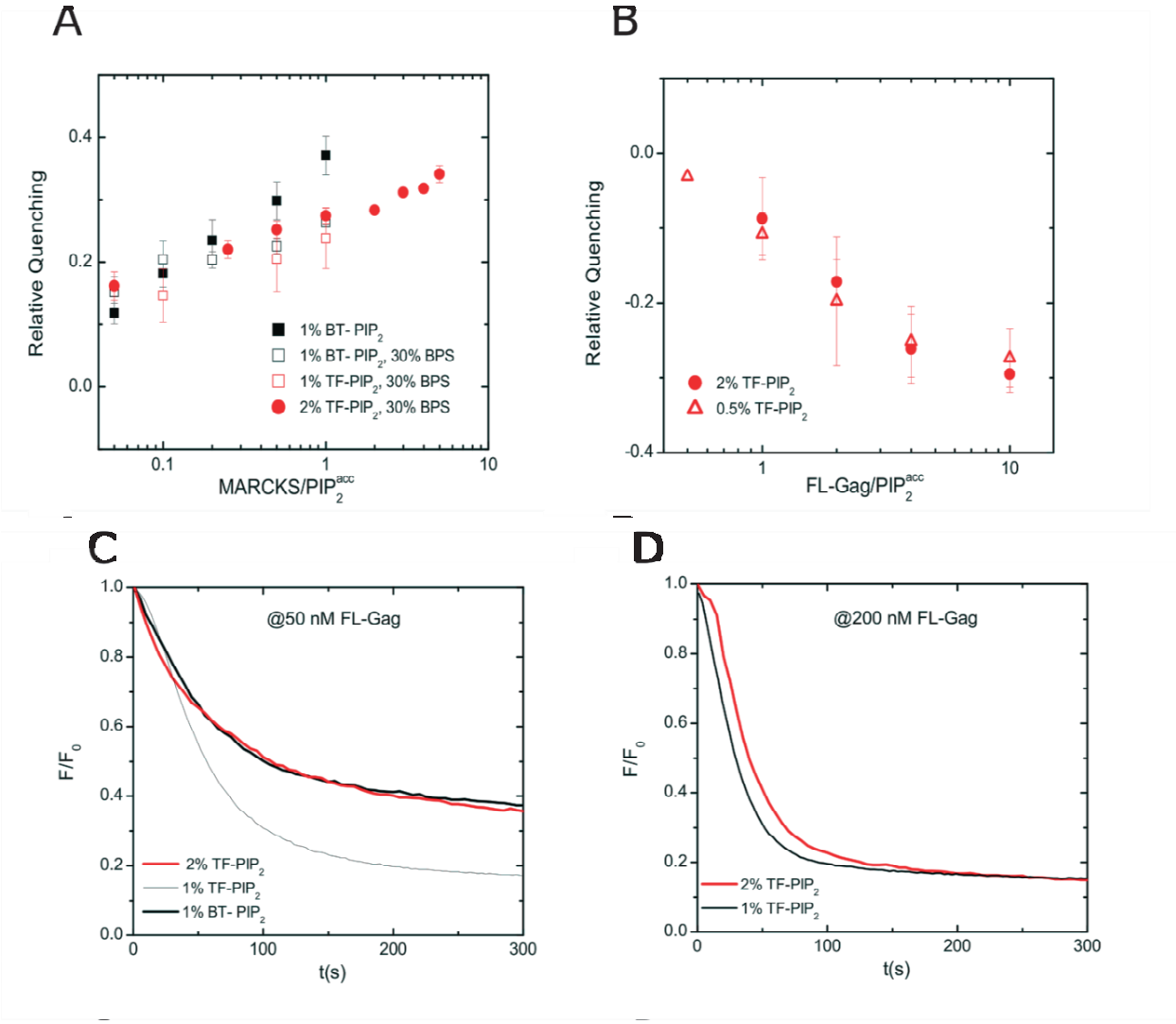

Figure 3.8: Quenching and unquenching observed for different Bodipy derivatives labelled lipids at different molecular ratio in LUVs and SLBs (A) Effect of MARCKS peptide on fluorescence quenching of Bodipy derivatives labelled lipids in LUVs. Black : Relative quenching of BT-PI(4,5)P_2 in different LUVs (Closed square, 98% PC, 1% PI(4,5)P_2,Open square : basic composition. Red : Relative quenching of TF-PI(4,5)P_2 at 1% mol (open square) or 2% mol(closed circle) in basic LUVs. (B) Effect of two different TF-PI(4,5)P_2molar concentrations (2% and 0.5%) on the fluorescence unquenching induced by FL-Gag in basic LUVs. (C) and (D) : Typical fluorescence change after addition of 50nM (C) or 200nM (D) FL-Gag of different Bodipy derivatives labelled PI(4,5)P_2 at different molar concentrations (1% or 2%) on basic SLBs

concentrations, the nature and the concentration of the dye do not have any influence on the relative fluorescence decrease nor on the opposing effects observed between LUV and SLB upon Gag interaction.

3.3.5.2 Quenching/Unquenching and membrane curvature

BT-labelled lipids clustering generally induce fluorescence quenching on LUVs (figure 3.4(A)), i.e. fluorescence decrease (Gambhir, et al. 2014). Therefore,

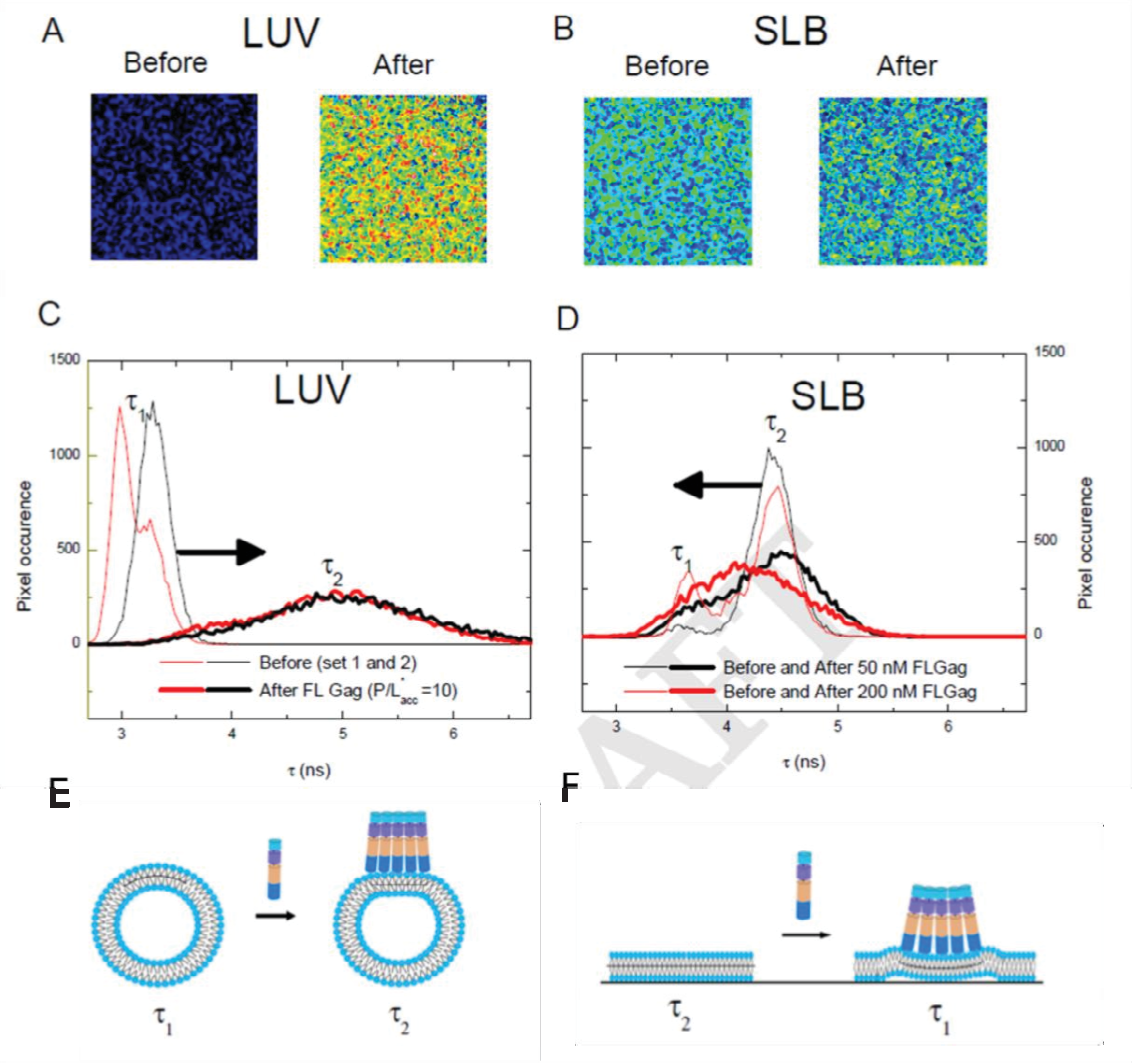

Figure 3.9:. TF-PI(4,5)P_2 fluorescence lifetime change upon FL-Gag addition (A) and (B): Fluorescence lifetime images before and after addition of FL-Gag in a LUV solution ((A), P/L*$_{acc}$= 10) or on SLB ((B), 200nM). (C) and (D): Fluorescence lifetime distributions before and after addition of FL-Gag. Part C exhibits two different measurements (red and black) in two different LUV solutions before (thin line) and after (thick line) addition of FL-Gag at P/L*$_{acc}$= 10 ratio. Black arrows show the direction of the change in the mean lifetime from short (τ_1) to long (τ_2). Part D exhibits two different measurements on two different SLBs before (thin line) and after (thick line) addition of FL-Gag at 50 nM (black) or 200 nM (red). Black arrows show the direction of the change in the mean lifetime from long (τ_2) to short (τ_1). (E): Schematic explanation of the opposite change in fluorescence lifetimes upon addition of FL-Gag for LUV and SLB containing TF-PI(4,5)P_2.

unquenching observed in this study upon Gag and its mutant addition was unexpected. Nevertheless, this TF-PI(4,5)P_2unquenching result has also been observed with another viral protein, Newcastle disease virus M protein (Shnyrova et al. 2007). Shnyrova et al. suggested that the decrease of dynamic quenching due to lipid clustering upon addition of virus M protein could be responsible for this unquenching (Shnyrova et al. 2007). So, a possible role for the dynamic quenching to produce opposite effects on LUVs and SLBs has been examined.

Two different types of fluorescence quenching may occur, i.e. the dynamic quenching (Qd) and the static quenching (Qs). Overall, the total quenching (QT) can be simply described by:

$$Q_T = Q_d + Q_S \qquad \textit{Eq: 24}$$

To simplify, dynamic quenching reflects the possibility of the quencher to collide with an excited fluorescent molecule. It is proportional to the quencher concentration (here TF-PI(4,5)P_2) and the temperature. Static quenching reflects the possibility of the quencher to form a complex with the quenched molecule at the ground state. This complex then becomes non-fluorescent. Both types of quenching (dynamic and static) induce fluorescence intensity that decrease with increasing concentration of the quencher. But, only an increasing dynamic quenching will result in decreasing the fluorescence lifetime of the quenched molecule (for more details, see section 2.4).Therefore, to understand the respective role of dynamic and static quenching of the TF-PI(4,5)P_2 after FL-Gag self-assembly on SLBs and LUVs, we acquired fluorescence lifetime images. The fluorescence lifetime of a dye exposed to dynamic quenchers is expected to decrease with increasing quencher concentration. Figure 3.9 (A) to (D), depicts the change in lifetime observed on LUV (part A and C) or SLB (part B and D) upon FL-Gag addition. Interestingly an opposite tendency has been observed. In the case of LUV, before addition of FL-Gag, the lifetime distribution is centered at τ_1 = 3.2 ± 0.1 ns and it is moved to a higher lifetime valueτ_2 = 5.1 ± 0.8 ns after FL-Gag addition (FL-Gag/TF-PIPacc2 =10). On the opposite, SLB already exhibit two different lifetimes, respectively centered at τ_1= 3.6 ± 0.3 and τ_1= 4.4 ± 0.4 before FL-Gag addition. The first lifetime centered at 3.6 ± 0.3 is close to the one observed for LUVs and is likely due to the presence of vesicles not totally fused with the rest of the SLB. Upon FL addition, the mean lifetime decreases slightly in the case of SLB instead of increasing. The photophysics of TF lipid derivatives is poorly documented (Boldyrev et al. 2007). Nevertheless, Karolin et al. measured lifetimes of tetra-methylbodipy (3,3',4,4'-difluoro-1,3,5,7-

tetramethyl-4-borato-3a-azonia-4a-aza-s-indacene) which is the closest chemical structure to the TF label in lipid derivatives. They have shown the existence of two different lifetimes τ_1 = 5.3 ns, in acetone and 3.0 $\leq\tau_2\leq$ 3.7 ns, when the dye was quenched with different dynamic quenchers (Karolin et al. 1994). The fluorescence lifetimes obtained in this study are consistent with these values and suggest that before FL-Gag addition, the dynamic self-quenching contribution to the total self-quenching is higher in curved membranes (LUVs *vs* SLBs) than after FL-Gag addition. As represented in the scheme of figure 3.9(E), multimerizing Gag and its mutants can impose a strong local curvature to the membranes. This curvature is opposite to the one of LUVs and could have therefore induced a local "flattening" of LUVs, whereas on the opposite it will induce a local curvature on flat SLBs. Formulated in terms of respective quenching type contributions, it can be written as:

$$Q_{Gag} = Q'_d + Q'_s \; with \begin{cases} Q'_d << Q_d, & for\ LUV \\ Q'_d > Q_d, & for\ SLB \end{cases} while\ Q'_s > Q_s\ for\ LUV\ and\ SLB \qquad Eq: 25$$

The two components of quenching are additive in the case of SLBs and opposite in the case of LUVs. This could explains why the fluorescence changes seen with TF-PI(4,5)P_2 are inverted in membranes with opposite curvature upon Gag addition and why their absolute value is more important in SLB than in LUV. Supporting this hypothesis, MARCKS peptide, which is not inducing any curvature lead to the same overall quenching of TF-PI(4,5)P_2 on flat and curved membranes.

3.3.6 HIV-1 Gag Multimerization induces nanoclustering of PI(4,5)P_2 on model membranes

To emphasize the quenching effect observed in this work, Gag interaction on SLBs was further monitored using FRAP experiments – before and after addition of FL-Gag to assess clustering of PI(4,5)P_2. The upper limit of Gag multimer diffusion coefficient (D) was assumed to be 0.01 $\mu m^2.s^{-1}$(Hendrix et al. 2015). Considering that clustered PI(4,5)P_2 in Gag multimer will diffuse with the same coefficient, the fluorescence of TF-PI(4,5)P_2 in a 1µm radius bleached area containing multimers should not totally recover after 15s (figure 3.10(A)). In the absence of FL-Gag, fractional fluorescence recovered to 1, as expected for freely diffusing lipids (figure 3.10(B)). On the opposite, addition of increasing FL-Gag concentrations induced a decrease in PI(4,5)P_2 fluorescence fractional recovery, corresponding to the observed fluorescence

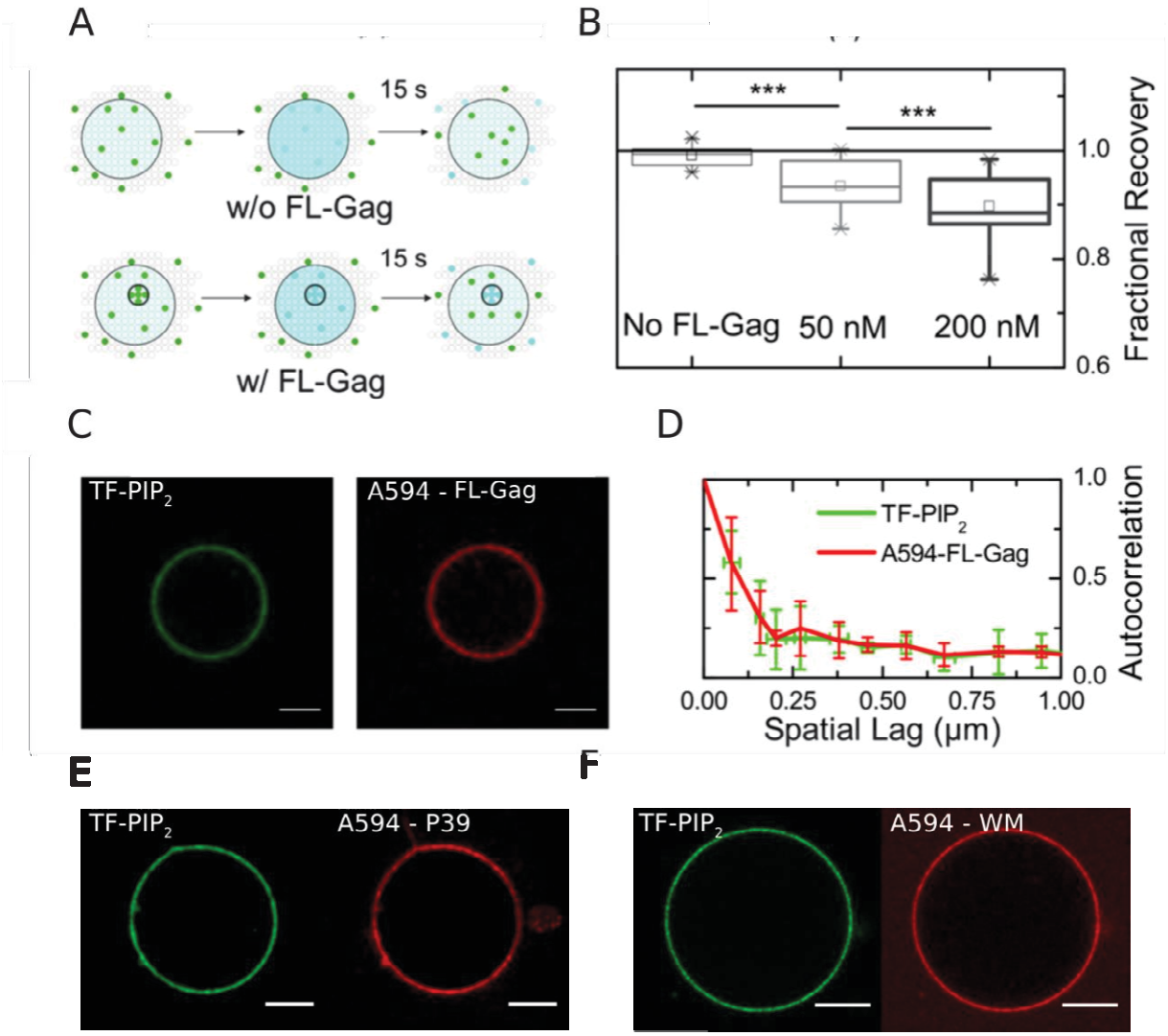

Figure 3.10: PI(4,5)P_2 nanoclusterization induced by Gag multimerization on basic composition lipid membranes (SLB/GUV). (A) Schematic representation of the effect of an immobile fraction on the fractional recovery. Upper part, without FL-Gag, 15s after bleaching, the concentration of fluorescent TF-PI(4,5)P_2 fully recovers, i.e. the fractional recovery = 1. Lower part, 15min after Gag addition, 15 s after bleaching the Gag trapped PI(4,5)P_2 appears immobilized leading to a fractional recovery less than 1. (B) Plot box of the fractional recoveries obtained from FRAP measurements before and after addition of increasing concentration of FL-Gag on the same SLB (Boxes are 25, 75% with bars max and min values of $n \geq 15$, *** : $p \leq 10^{-3}$ for Student t-test at 0.01 confidence level). (C) Left, localization of TF-PI(4,5)P_2 (in green) and Alexa 594 FL-Gag(A594-FL-Gag) (in red) in a basic composition GUV. Scale bar is 5µm. (D) Right, autocorrelation of the fluorescence intensities of TF-PI(4,5)P_2 (in green) and A594-FL-Gag (in red), (mean ± s.d, n=4) (E) A594-tagged P39 binds to TF-PI(4,5)P_2 labelled GUVs (F) A594-tagged WM binds uniformly on TF-PI(4,5)P_2 containing GUVs with basic composition. Scale bar corresponds to 10 µm.

quenching (figure 3.6(B)). This clearly confirms that Gag multimerization generates $PI(4,5)P_2$ clusters. In order to visualize these clusters, we imaged the surface distribution of TF-$PI(4,5)P_2$ and a fluorescently labelled FL-Gag in "basic" GUVs. Both $PI(4,5)P_2$ and FL-Gag showed a uniform distribution over the surface of the GUV (figure 3.10(C)). Moreover, fluorescence spatial auto-correlation of both $PI(4,5)P_2$ and FL-Gag (figure 3.10(D)) exhibited a fast decorrelation. This shows that the cluster sizes are less than 200 nm. Our data clearly suggest that HIV-1 Gag is sorting $PI(4,5)P_2$ in the lipid membrane and that Gag multimerization is responsible for generating these $PI(4,5)P_2$ nanoclusters in model membranes. This is significant because we found a difference in the efficiency of quenching/unquenching when we employed a non-multimerizing protein like EFA6-PH. Despite affinity studies revealed that the EFA6-PH does interact with the model membranes with similar affinities like that of Gag and its mutants, we haven't observed any quenching/unquenching on LUVs or SLBs by EFA6-PH. This confirms that it is the multimerizing property of Gag that is responsible for this quenching/unquenching of labelled $PI(4,5)P_2$. Further, other Gag mutants, P39 and WM were also labelled and checked for their ability to bind $PI(4,5)P_2$ containing GUVs. Figure 3.10(E) and (F) demonstrates that the mutants do bind the basic composition GUVs.

3.3.7 Line-Scan FCS on TF-PIP2 labelled basic SLBs

More strong evidence for the lipid binding & clustering can be obtained by studying the diffusion of those lipids before and after protein interaction. From the figure 3.11, it is evident that the addition of Gag decreases the diffusion of the TF-$PI(4,5)P_2$ present in the SLB. While correlation carpets are visibly distinct from each other (figure 3.11 (a) and (c)), the autocorrelation curves derived from these carpets exhibited a single component (figure 3.11(b)), when there is no Gag and two components (figure 3.11(d)), in the presence of Gag. Histograms of the diffusion time revealed that the diffusing components changed from a highly monodisperse group (black) to a polydisperse group (red) after the addition of Gag (figure 3.11(C)). In this polydispersity, the minimum diffusion time of the lipid (0.1 μm^2/sec) is 10 times more than the diffusion of the lipids before the addition of Gag (1.19 μm^2/sec). Further, there are two distinct groups with one peak having a diffusion coefficient of 0.1 μm^2/sec and the other at

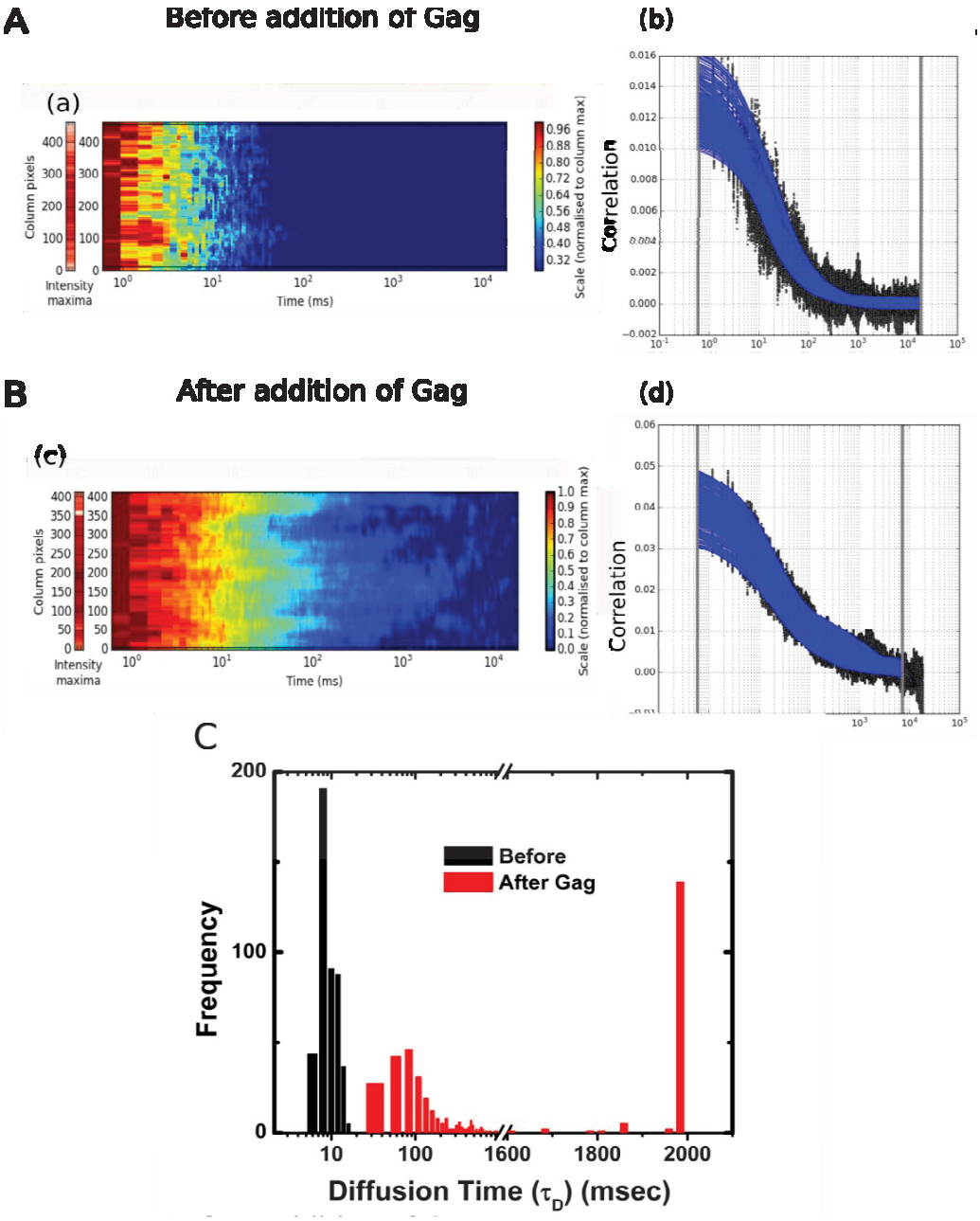

Figure 3.11: Line-Scan FCS of TF-PIP$_2$ labelled basic SLBs before and after addition of FL-Gag. (A) Before addition of FL-Gag and (B) After addition of FL-Gag. (a) and (c) correlation carpet, (b) and (d) the fitting of the autocorrelation curves generated out of the correlation carpet. (C) the histograms of lipid diffusion before and after addition of FL-Gag (n=5).

0.004 μm^2/sec. This suggests that there are multiple diffusing components after the addition of FL-Gag. Finally, the data from line-scan FCS & FRAP experiments concludes that Gag is trapping TF-PI(4,5)P_2.

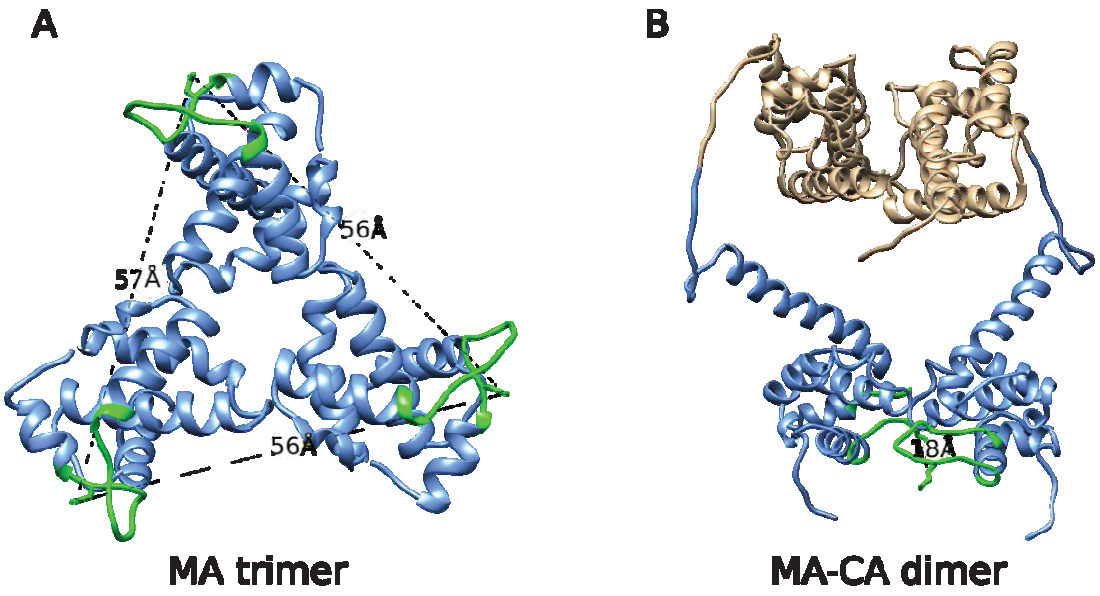

Figure 3.12: Comparing the distances of adjacent HBR regions in MA trimer and MA-CA dimer. (A) MA trimer obtained from PBD, ID-1h1w, showing the distances from adjacent HBR regions. (B) MA-CA dimer generated using I-TASSER suite, Spring software at 4Å RMSD, spring score of 16.8 and TM score above 0.5.

3.3.8 Multimerization property of Gag and its domains

CA-CA interaction is considered as the prime multimerizing initiation factor during the assembly of the HIV-1 Gag. CA domain is known to form hexamers and pentamers, apart from dimers (Pornillos et al. 2009; Zhao et al. 2013). From the literature, it is evident that not only ionic interactions of protein domains with lipid molecules help in membrane association but also the multimerization of these domains do play a role in the membrane attachment (van den Bogaart et al. 2011; Dalton et al. 2007). From the results obtained here, all the proteins that have a CA domain were able to cluster $PI(4,5)P_2$ molecule, irrespective of the efficiency of multimerization (figure 3.6). This suggests that multimerization is a crucial property that has a significant effect in the Gag assembly. Nevertheless, another Gag domain that is also known to form multimers is the Matrix domains. MA domain of HIV-1 Gag alone can form trimers (Hill et al. 1996) and even hexamer of trimers at high concentrations (Alfadhli et al. 2007). In spite of its ability to form trimers and even having the HBR region, our results suggest that the domain is not efficient in clustering $PI(4,5)P_2$ as reported through quenching experiments (figure 3.5 (A) and 3.6(A)). Typically, for quenching to occur the foster radius has to be less than 50Å. When we measure the distance between the HBR regions in trimer of MA produced from

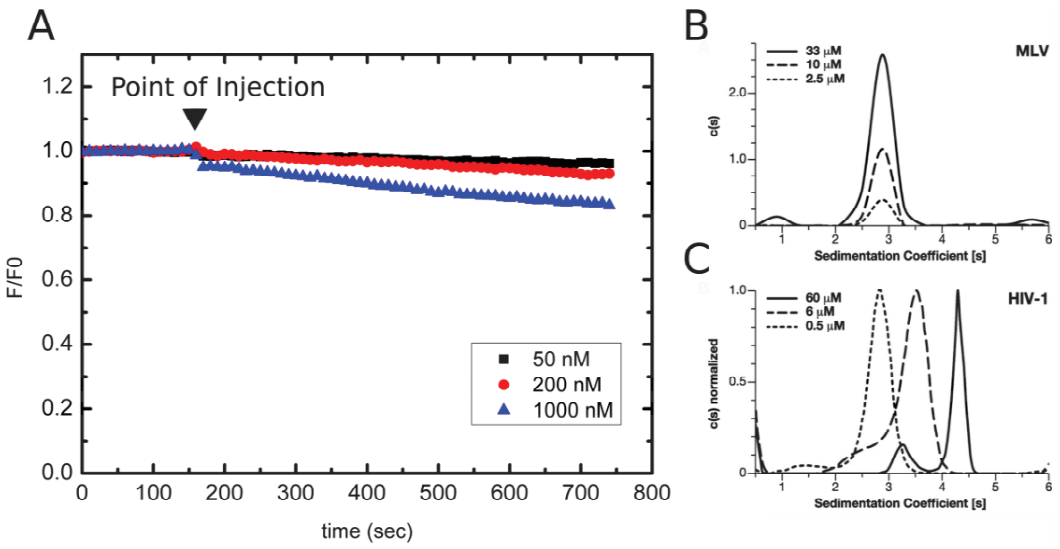

Figure 3.13: Multimerization property of MLV Gag and its ability to quench TF-PI(4,5)P_2. (A) Concentration-dependent quenching of TF-PI(4,5)P_2 by MLV Gag on basic composition SLBs (n=2). (B) and (C) Sedimentation analysis of MLV gag and HIV-1 Gag at various concentrations using analytical ultra-centrifugation, reproduced from (Datta et al. 2011).

Table 3.2: Monomer-dimer equilibrium of MLV Gag and HIV-1 Gag proteins

Gag Protein	K*d* (µM)
HIV-1	~5
MLV	~400

NMR data, they lie as far as 57Å from each other (see figure 3.12(A)). On the contrary, a dimer of MA-CA generated using Spring protein-protein interactions software has it HBR regions rather closer than in MA trimer ie., the HBR regions are separated by 18Å, only in case of MA-CA dimer (figure 3.12(B)). At this distance, it is highly likely that the lipids clustered by CA containing Gag proteins can undergo quenching. In support of the multimerization role in effecting the nano-clustering and thus quenching of TF-PI(4,5)P_2, we have performed experiments with MLV Gag protein on SLBs (figure 3.13(A)). When compared with that of HIV-1 Gag quenching results (figure 3.6(A)), MLV Gag has not affected significant quenching to the TF-PI(4,5)P_2 containing SLBs. Interestingly, Datta et al. 2011 have compared the multimerizing capacities of the two proteins of the viruses. Figure 3.13 (B) and(C) represent the multimerizing efficiency of the two proteins when studied using analytical centrifugation technique.

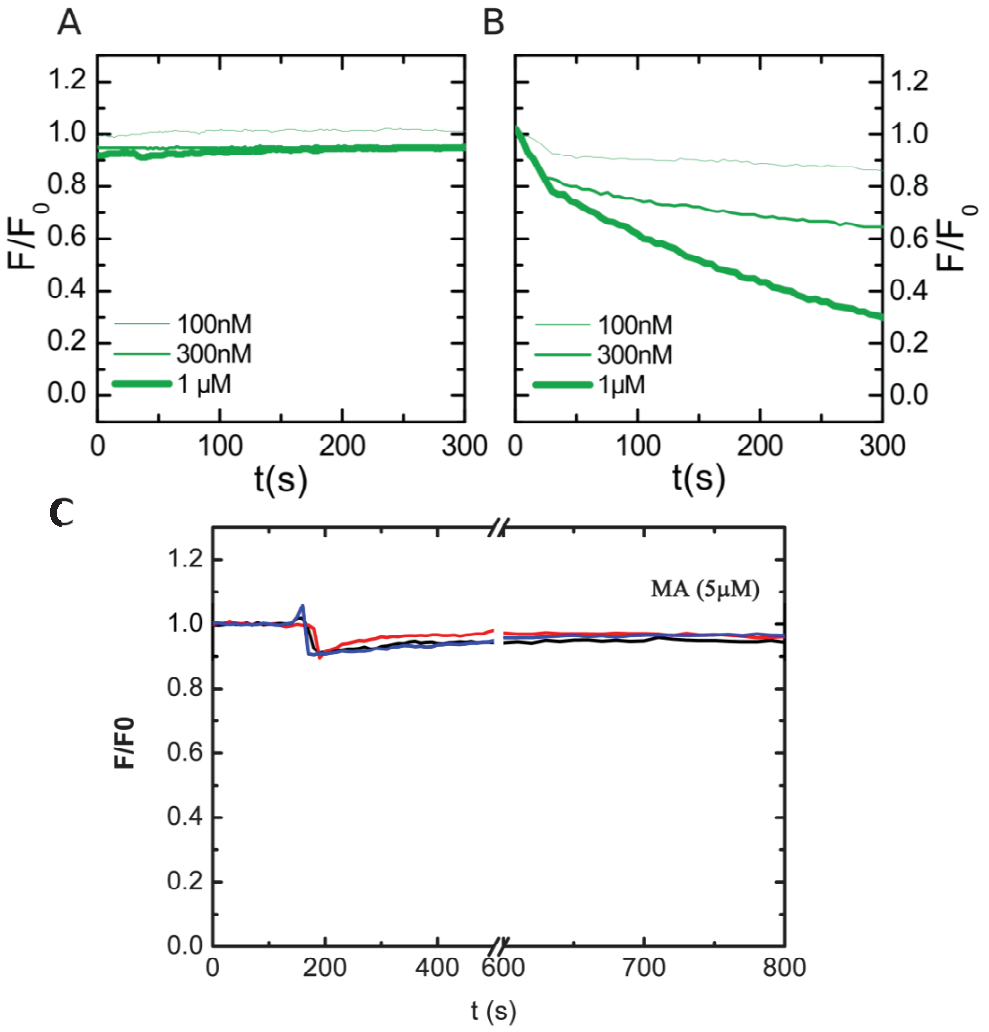

Figure 3.14: Gag multimerization is sorting cholesterol but not sphingomyelin. A and B: Typical fluorescence time course after addition of increasing FL-Gag concentrations on substituted basic SLBs labelled with TF-SPM (A) or TF-Chol (B) (n=2) (C) Fluorescent intensity time course of high concentration (5 µM) MA interaction with basic SLBs labelled with TF-Chol (n=3).

Sedimentation velocity data reveals that at all concentrations tested there observed only a single peak in case of MLV Gag (suggesting a monomeric state) but in the case of HIV-1 Gag there is always a short peak and a long peak (suggesting a multimeric state). Moreover, the authors calculated that the monomer-dimer equilibrium is very high for MLV Gag when compared to that of HIV-1 Gag – making it difficult to multimerize (table 3.2). These results further confirm that it is the multimerization property that is responsible for the quenching observed in case of HIV-1 Gag protein.

3.3.9 Cholesterol but not sphingomyelin is sensitive to HIV-1 Gag multimerization

Many findings on HIV-1 assembly process support the involvement of Cholesterol (Chol) and Sphingomyelin (SPM) in the form of rafts. Literature evidence like the enrichment of cholesterol and sphingomyelin in the envelope of produced virus and cholesterol induced enhancement of protein targeting to the plasma membrane helped promote the idea of HIV-1 Gag assembly towards raft domains. Since Chol and SPM are the main components of raft domains, their enrichment into the Gag multimerization induced $PI(4,5)P_2$ nanoclusters was assessed. 2% mol of egg phosphatidylcholine (EPC) present in our "basic" lipid composition, were substituted either by SPM or by Chol with half of them being labelled with TF derivatives (see table 2.1). This substitution allowed the net surface charge and the $PI(4,5)P_2$ content to be maintained, limiting any drastic change in the partitioning constant (K*p*). Time course fluorescence change of either TF-SPM or TF-Chol was then monitored after FL-Gag addition. Figure 3.14(A) shows that FL-Gag addition had no effect on TF-SPM fluorescence whereas there observed an increasing quenching of TF-Chol with increasing concentrations of FL-Gag (figure 3.14(B)), as it was the case for TF-$PI(4,5)P_2$ (figure 3.6(B)). While the protein is known to have an affinity for cholesterol (Dick et al. 2012), this is the first time anyone has ever shown a direct proof of cholesterol clustering by Gag. However, when a similar experiment was performed with high concentrations of MA protein (5 μM), there observed no change in the fluorescence intensity of the SLB (figure 3.14(C)). Once again confirming that multimerization property of Gag is responsible for this clustering of lipids.

3.3.10 Co-clustering of lipids by Gag on SLBs

Co-clustering of different lipids was assessed by simultaneously monitoring the change in fluorescence upon addition of FL-Gag with either TF-SPM and BT-$PI(4,5)P_2$ or TF-Chol and BT-$PI(4,5)P_2$ labelled SLBs.TF-Chol and BT-$PI(4,5)P_2$ have been recently shown to exhibit Forster resonance energy transfer (FRET) (Wang YH, Bucki R 2016). We examined the possibility for TF-SPM (donor) and BT-$PI(4,5)P_2$ (acceptor) to achieve FRET in the "basic" SLB used (figure 3.15). A typical x, y image of a basic SLB labelled with TF-SPM (green) and BT-$PI(4,5)P_2$ (red) shows the good mixing properties of both dyes (figure 3.15(A)). To test the

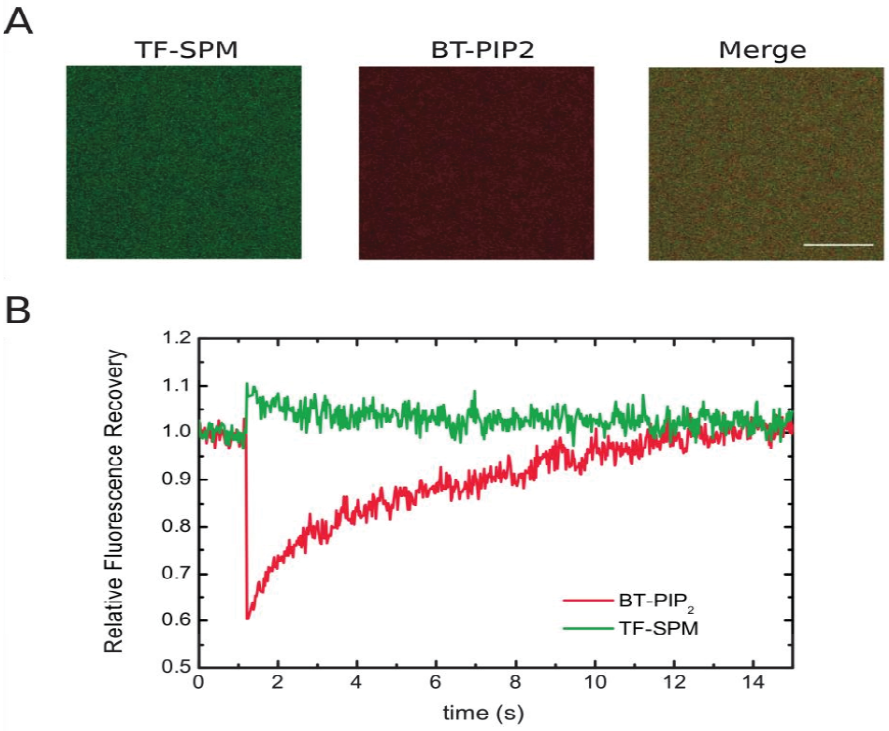

Figure 3.15: SLB TF-SPM fluorescence increase upon BT-PI(4,5)P_2 **photobleaching** (A) Confocal Laser Scanning images of basic SLB (part A) labelled with TF-SPM (green), BT-PI(4,5)P_2 (red) and their overlay showing a good miscibility at a sub-micrometer scale. (B) Mean recovery curve (n= 20 on 4 different SLBs) obtained after pulsed photobleaching of BT-PI(4,5)P_2.

occurrence of FRET in these SLBs, we repeated photobleaching of the acceptor (BT-PI(4,5)P_2) and monitored the fluorescence changes of both TF-SPM and BT-PI(4,5)P_2 (n=20 on 4 different SLBs). As depicted in figure 3.15(B), BT-PI(4,5)P_2 exhibits a fluorescence recovery after bleaching with a fractional recovery close to 1. Interestingly, immediately after the end of the acceptor photobleaching pulse, TF-SPM exhibited an apparent increase in fluorescence which is a characteristic of loss in FRET. Moreover, this increased TF-SPM fluorescence decreases with increasing fluorescence of BT-PI(4,5)P_2 showing that FRET increase again with unbleached lipid remixing. This clearly confirms the existence of FRET between TF-SPM and BT-PI(4,5)P_2 when these two lipid derivatives are present in the SLB. Donor FRET efficiency is a function of acceptor concentration in the lipid bilayer (Fung and Stryer 1978). FRET decreases when acceptor concentration decreases, leading to donor fluorescence increases. TF-Chol and BT-PI(4,5)P_2 exhibited simultaneous quenching after addition of various concentration of FL-Gag, suggesting

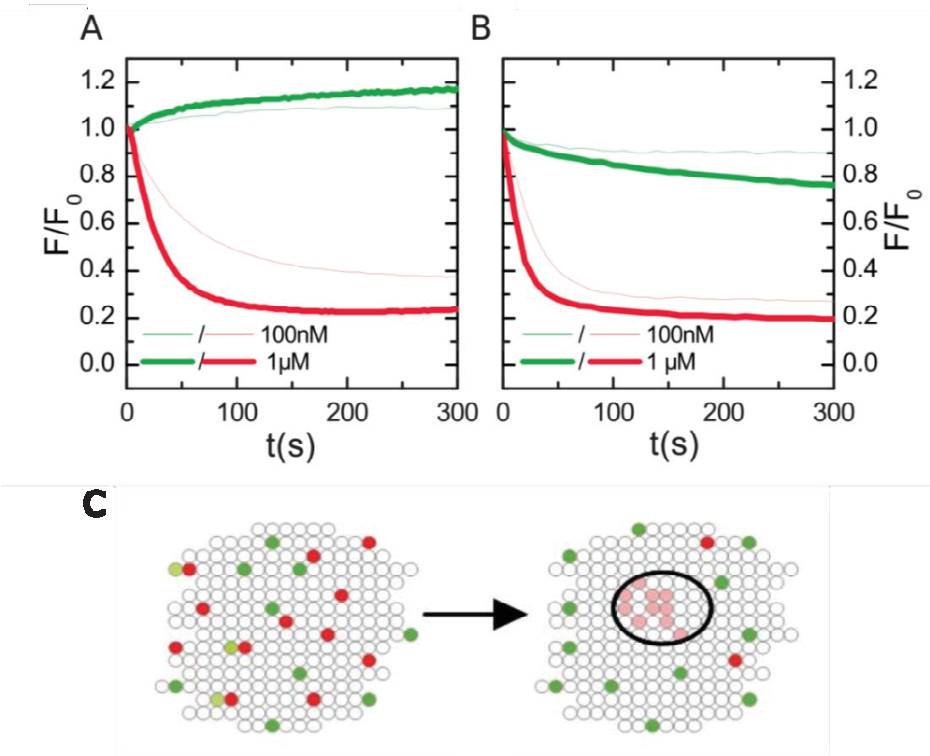

Figure 3.16: Co-clustering of PI(4,5)P_2 and Cholesterol by Gag(A) and (B): Simultaneous fluorescence time course after addition of increasing concentrations of FL-Gag on substituted basic SLBs labelled with TF-SPM (in green) and BT-PI(4,5)P_2 (in red) (A) or TF-Chol (in green) and BT-PI(4,5)P_2 (in red) (B). (C) Schematic representation of un-mixing due to FL-Gag multimerization. Concentration of BT-PI(4,5)P_2 out of the clusters is decreasing, inducing an increase in fluorescence of TF-SPM.

that TF-Chol and BT-PI(4,5)P_2 are co-clustered in Gag multimerization induced nanodomains. Interestingly, TF-SPM exhibited an apparent unquenching after Gag addition while BT-PI(4,5)P_2 was still quenched. Apparent unquenching of TF-SPM upon addition of FL-Gag only occurred when BT-PI(4,5)P_2 was present in the lipid composition (figure 3.16(A) vs figure 3.14(A)). We, therefore, examined whether TF-SPM (as a donor) and BT-PI(4,5)P_2 (as an acceptor) were exhibiting Forster type energy transfer (FRET) (figure 3.15(B)). This is what we observed in figure 3.16(A), and, more interestingly, this is also what is seen in figure 3.16(B). This shows that during PI(4,5)P_2 clustering, the outside BT-PI(4,5)P_2 (acceptor) concentration is decreasing, while the outside cluster TF- SPM (donor) concentration remained unchanged. This can be interpreted as a nano-unmixing of SPM and PI(4,5)P_2 during FL-Gag multimerization (figure 3.16(C)). Since donor FRET efficiency is a function of acceptor concentration in the lipid bilayer, FRET will decrease when acceptor concentration decreases. This loss in FRET will induce an

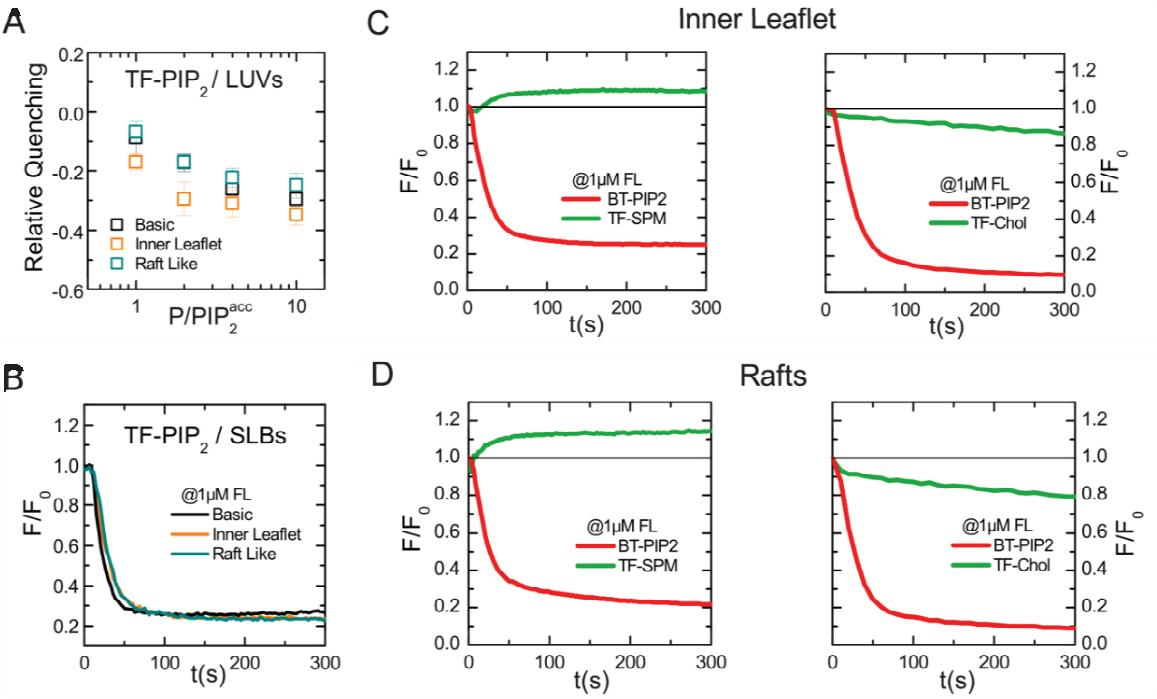

Figure 3.17: Gag PI(4,5)P_2 and Cholesterol nanoclustering in complex membrane models(A) relative quenching of at different P/PI(4,5)P_{2acc} ratio. Mean ± s.d., n≥3) or SLBs ((B) Typical time course of TF-PI(4,5)P_2 fluorescence addition of 1 µM FL-Gag. (C) Simultaneous fluorescence time course obtained on "inner leaflet" SLBs for BT-PI(4,5)P_2 (in red) and in green TF-SPM (left panel) or TF-Chol (right panel). (D) Simultaneous fluorescence time course obtained on "raft" SLBs for BT-PI(4,5)P_2 (in red) and in green TF-SPM (left panel) or TF-Chol (right panel).

increase in the donor fluorescence (TF-SPM). Because Gag multimerization only clusters BT-PI(4,5)P_2, the BT-PI(4,5)P_2 concentration out of these clusters is decreasing. This decrease is responsible for the apparent unquenching of TF-SPM fluorescence. Altogether, these results show that HIV-1 Gag multimerization is generating PI(4,5)P_2 and cholesterol nanodomains while excluding sphingomyelin.

3.3.11 Gag interaction on complex lipid mixtures

Cell PMs are complex lipid mixtures. The presence of other lipids can potentially affect the interaction or the partition of the protein. This lead us to examine the possible role of lipid complexity on the lateral sorting of PI(4,5)P_2, Chol and SPM during HIV-1 Gag (FL-Gag) multimerization. For that purpose, we used two different lipid mixtures mimicking either the

inner leaflet of cells PM ("inner-leaflet") or a "raft" containing lipid mixture (table 2.2). We first compared the effect of FL-Gag multimerization on $PI(4,5)P_2$ clustering for all the three different lipid compositions used in this study. No change in TF-$PI(4,5)P_2$ fluorescence unquenching (LUVs, figure 3.17(A)) or quenching (SLBs, figure 3.17(B)) could be clearly detected. This showed that Gag has the ability to equivalently cluster the $PI(4,5)P_2$, independently of the surrounding lipids chemical nature. We then tested Chol and SPM ability to partition into these FL-Gag induced $PI(4,5)P_2$ nanoclusters either using "inner leaflet" SLBs (figure 3.17(C)) or "raft" containing SLBs (figure 3.17(D)). TF-Chol, TF-SPM and BT-$PI(4,5)P_2$ exhibited the same fluorescence time course upon FL-Gag addition as the one observed in the "basic" SLBs. These results showed that Gag multimerization induced $PI(4,5)P_2$ nanoclusters in complex lipid mixtures were also enriched in Chol, but not in SPM.

3.3.12 HIV-1 Gag $PI(4,5)P_2$ and cholesterol nanoclustering mainly occurs in liquid disordered lipid phases

Finally, as observed for "basic" lipid composition GUVs (figure 3.10(C)), the surface distribution of labelled FL-Gag and $PI(4,5)P_2$ on "inner leaflet" GUVs (figure 3.18(A)) did not exhibit any phase separation above the diffraction limit. On the opposite, labelled FL-Gag was essentially restricted to L*d* phases in the "rafts" GUVs (figure 3.18(C) and (B)). Since these three lipid compositions are favorable to FL-Gag multimerization, it seems reasonable to expect that the multimerization will mainly occur in the L*d* phase. Further ascertaining the preference of Gag for L*d* regions, we have carried out temperature induced partitioning of the bound Gag on GUVs (figure 3.18(D)). Initially, the protein was allowed to bind TF-labelled GUVs at 37°C. Later, the GUVs were cooled down gradually to lower temperatures. At around 31°C, A594-FL-Gag bound GUVs of phase separating composition started to partition into L*d* and L*o* domains. Importantly, Gag bound to the TF-$PI(4,5)P_2$ (1%) or un-labelled $PI(4,5)P_2$ (6.5%) partitioned only into L*d* phase of the GUV. For the same lipid composition, a multimerizable derivative of MA protein preferentially partitioned into L*d* phase (Keller, Kräusslich, and Schwille 2013) like that of FL-Gag. These results emphasize that Gag protein interacts with $PI(4,5)P_2$ in the L*d* phase but not L*o* phase.

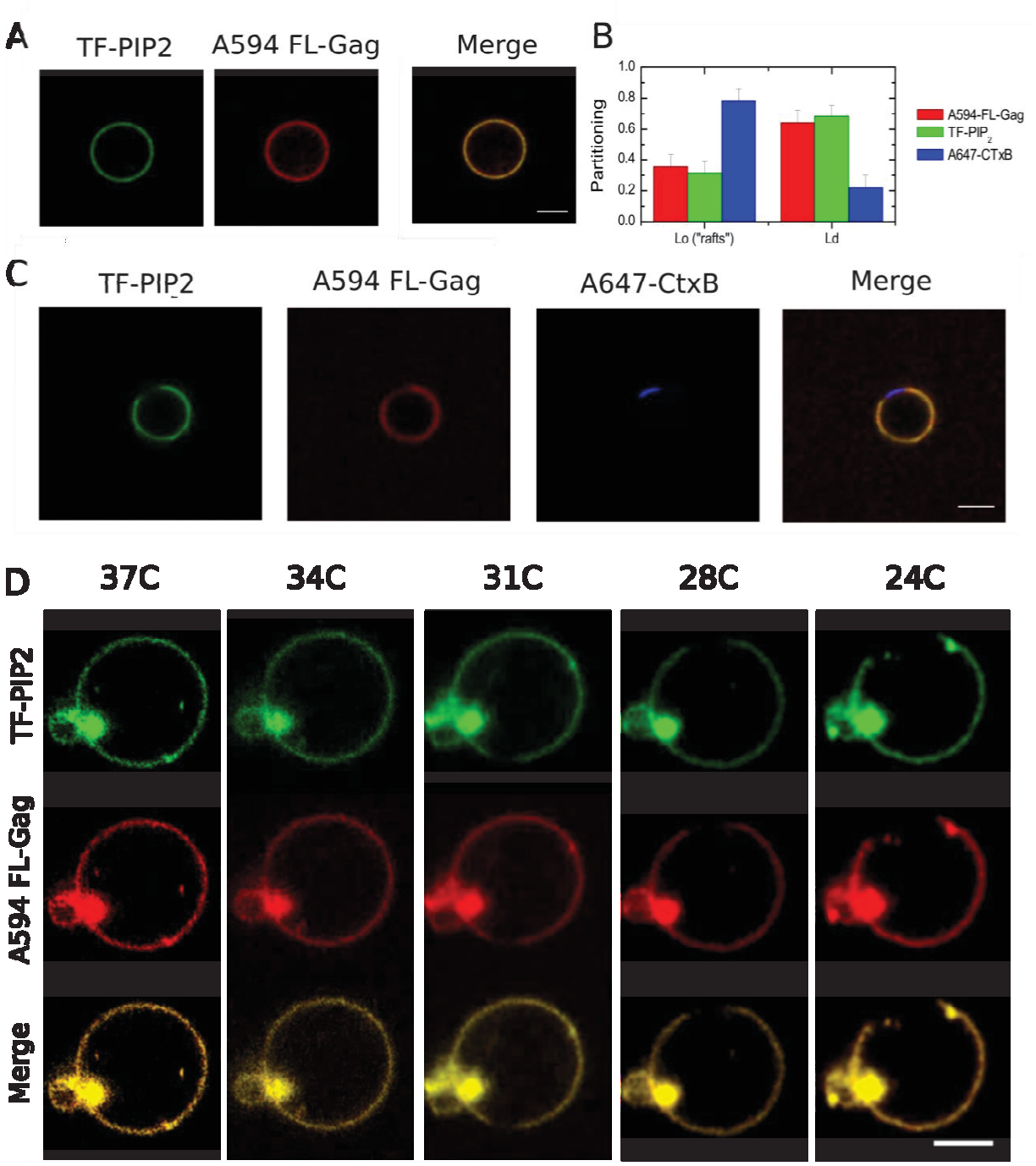

Figure 3.18: Preferential partitioning of Gag on GUVs. TF-PI(4,5)P_2 fluorescence changes in lipid membranes of different composition (basic, Inner Leaflet, Raft) using LUVs (A) and (C) Localization in "inner leaflet" GUVs (Part A) or "Raft" GUVs (Part C) of TF-PI(4,5)P_2(in green), A594 FL-Gag (in red) and GM1, a raft partitioning ganglioside, labelled with Alexa 647 cholera toxin B (A647 Ctx-B) (in blue) and images overlay (Merge). Scale bar is 5µm. (B) Partitioning in L*o* and L*d* phase of "raft" GUVs for A594 FL-Gag, TF-PI(4,5)P_2 and A647-CtxB mean ± s.d., n=25 GUVs. (D) Partitioning of A594 FL-Gag and TF-PI(4,5)P_2 into Ld phases upon cooling from 37C to 24C Scale bar is 5µm (n=4).

3.4 Conclusions:

Although the MA domain is primarily responsible for HIV-1 Gag binding to the PM, the ten times higher apparent affinity for membrane models observed here, in the case of FL-Gag, P39 and WM, confirms that the NC domains and CA-CA multimerization of Gag are involved in efficient membrane binding. Indeed, the NC domain of Gag alone has recently been described to bind to $PI(4,5)P_2$ containing lipid membranes with an apparent K_D as high as 7 μM (Kempf et al. 2015a). It has also already been shown that the driving force for membrane association stems largely from the ionic interactions between multimerized Gag and negatively charged phospholipids (Dalton et al. 2007). Here, we show that FL-Gag multimerization not only plays a role in membrane binding but, more importantly, in generating $PI(4,5)P_2$ and cholesterol enriched lipid nanodomains in the membrane. Supporting this theory, a similar view on the role of multimerization in reorganising micro-domains has been discussed earlier elsewhere (Hogue, Llewellyn, and Ono 2012). As a general mechanism, proteins with basic interfaces can recruit acidic lipids that, in turn, can facilitate recruitment and clustering of these proteins into nanodomains (van den Bogaart et al. 2011). A similar cooperative mechanism could also happen when HIV-1 Gag binds to $PI(4,5)P_2$ during viral assembly at the plasma membrane. Cytoplasmic proteins such as ezrin (Al-Momany et al. 2014; X. Chen et al. 2015), syntaxin-1 (Honigmann et al. 2013) have also been described to induce or interact with $PI(4,5)P_2$ nanoclusters. Interestingly, the matrix domain of Gag is not able to induce this $PI(4,5)P_2$clusterization, suggesting that after maturation and particle release, the inner leaflet lipids of the virus envelope might be free to diffuse again. It has been shown that cholesterol may facilitate Gag membrane binding and that Gag could sense cholesterol (Barros et al. 2016; Dick et al. 2012). Moreover, cholesterol has also been shown to be crucial for virus infectivity (Shahan Campbell et al. 2004; Hawkes et al. 2015). Although there are still remaining critical issues about the $PI(4,5)P_2$ role in the formation of cholesterol-dependent lipid domains, $PI(4,5)P_2$ could form clusters in the presence of cholesterol alone (Jiang et al. 2014). Our results also show that cholesterol is laterally redistributed during Gag assembly and participates in the formation of cholesterol/$PI(4,5)P_2$/Gag enriched domains. In contrast, sphingomyelin is not sorted during HIV-1 Gag multimerization. The Gag multimerization and the associated $PI(4,5)P_2$ enriched nanoclusters mainly occur or, at least, initiate in Ld phases, i.e., more likely outside of lipid raft

domains. The lack of myristate in the different Gag variants tested here could explain the Gag L*d* phase localization (Wolf Lindwasser and Resh 2002). Nevertheless, our results are consistent with the L*d* phase GUV localization of multimerizable myr(+)MA protein observed by Keller et al. (Keller, Kräusslich, and Schwille 2013). Since HIV-1 Gag has been often found into detergent resistant membranes (DRM) (Ono and Freed 2001), Gag multimers could partition into rafts after assembly, or rafts could be trapped by these nascent PI(4,5)P_2-Gag nanodomains through transbilayer lipid interaction, as we already proposed (Kerviel et al. 2013b) or as it has been recently shown for GPi anchored proteins (Raghupathy et al. 2015).

In conclusion, we have shown using simple and complex lipid composition model membranes that Gag multimerization is inducing nanoclusters enriched in PI(4,5)P_2 and cholesterol. This lipid nano-clusterization does not require sphingomyelin and mainly occurs out of the raft phases in GUVs. Further, the different lipid composition tested here does not strikingly affect the capacity of Gag to induce these lipid nanoclusters.

Chapter-4

HIV-1 Gag protein multimerization induces vesiculation of PI(4,5)P_2 containing model membranes

4.1 Introduction

In retroviruses, protein oligomerization is a key aspect for the formation of assembly platforms, required to recruit all the necessary components for a new viral particle formation. HIV-1 Gag protein with multiple domains can play more than one role in orchestrating the assembly that leads to budding event (Freed 2015). While the Gag protein is addressed to the inner leaf-let of the plasma membrane – defined by MA-HBR region and polar head of $PI(4,5)P_2$ (Chukkapalli and Ono 2011; Akira Ono et al. 2004), formation of assembly platforms along the plasma membrane is achieved through hydrophobic interactions of CA domain present in the adjacent Gag proteins (Bocanegra et al. 2013; Mateu 2009; Yu and Hagan 2012). In earlier chapter, oligomerization of the HIV-1 Gag protein can induce the formation of $PI(4,5)P_2$ and cholesterol clusters has been demonstrated. In the process, WM mutant which has ~100 times less multimerizing efficiency than Gag-FL in solution (Datta, Curtis, et al. 2007b) was found to show an improved multimerization efficiency of ~2-4 times in the presence of model membranes (see section 3.3.4 in Chapter 3).

In general, Gag protein assembly along the inner leaf-let of PM is followed by or induces membrane bending of the lipid bilayer and end up in a budding event in order to release a new viral particle. Some researchers have reported the presence of cellular proteins such as annexins and various ESCRT factor proteins that can help in membrane bending and assist in the release of new viral particles. (Drücker et al. 2013; Harrist et al. 2009; Hurley et al. 2010; Votteler and Sundquist 2013). This recruitment of cellular factors has raised a question of the role of the multimerization of the capsid domain in inducing membrane curvature. Von Schwedler et al. 2003have shown that the mutations in the capsid region resulted in irregular Gag assembly and thus lacked proper curvature to form closed particles. Furthermore, mutated CA-NTD domain, P99A, has been shown to be unable to induce membrane budding as well as co-patching of lipid raft and TEM markers (Hogue et al. 2011). Adding to this observation, Grover et al found that CA mutations affecting the multimerization (CA P99A (40) and CA EE75,76AA) resulted in the formation of electron-dense patches underneath the plasma membrane and decreased the VLP release (Grover et al. 2013). All these findings tentatively suggest that multimerization property of HIV-1 Gag protein has a role to play in the formation of new viral buds. However, so far, no

study has been performed in establishing the bud formation by HIV-1 Gag protein alone. In this work, we aim to understand the ability of Gag itself, as a minimal system, to generate lipid vesicles and the role of multimerization property of this protein in affecting the same.

4.2 Approach

Quartz crystal microbalance is an ultrasensitive and accurate mass measurement technique that can be used to understand the intimate interactions between the adsorbent and the adsorbate. Mass adsorbed on the vibrating surface of the sensor is recorded as change in the frequency (frequency shift). Not only the mass and the trapped solvent, but also the change in the conformation of the molecules can be studied using this technique. Dissipation (D) is defined as the loss of energy per oscillation period divided by the total energy stored in the system. A change in the dissipation (ΔD) is measured simultaneously along the change in the frequency (ΔF) detected after the adsorption of components. This gives the advantage of knowing the amount of substance adsorbed to the surface and also the viscoelastic properties of the adlayer formed (Dixon 2008). Visco-elastic properties such as rigidity and softness of the adlayer can be detected as the adsorbed molecule undergoes various structural conformations during the interaction process. Other techniques like surface plasmon resonance spectroscopy, dual polarization interferometry and ellipsometry can only provide information on the adsorption kinetics but not the visco-elastic properties of the adlayer. Many studies have been done using QCM-D to understand the biomolecular interaction between different molecules or between substrate and molecules. Biomolecular components like DNA, proteins, and even cells interaction on various substrates have been studied (see this review (Cheng, Chang, and Chu 2012; Cooper and Singleton 2007).

Recently, biomolecular interaction with cellular plasma membrane models like liposomes and SLBs have grabbed the interest of the research community. After the successful understanding of the mechanics of SLBs formation on QCM-D substrates (N.-J. Cho et al. 2010), many interaction studies on this biologically relevant substrate have been conducted (Cheng, Chang, and Chu 2012). For example, interaction of nanoparticles (Bailey et al. 2015; Van Lehn et al. 2014),

antimicrobial peptides (K. F. Wang, Nagarajan, and Camesano 2015), poly-electrolytic materials (Alves et al. 2009; Rossetti et al. 2004) , and even viral components (N.-J. Cho et al. 2007; Nam-Joon Cho et al. 2016) have been studied. In this work, we have tried to study the interaction of Gag and other proteins on $PI(4,5)P_2$ containing SLBs using QCM-D technique.

Complementing the QCM-D study, fluorescence microscopic visualization of the Gag-$PI(4,5)P_2$ interaction was studied on TF-labelled $PI(4,5)P_2$ containing SLBs. The data obtained from both the techniques have been used to understand the complex interaction process of HIV-1 Gag protein with $PI(4,5)P_2$ lipid and the role of its multimerization during this interaction.

4.3 Results & Discussion

4.3.1 Protein - Membrane binding studies using QCM-D:

Quartz Crystal Microbalance is one of the accurate ways to measure the binding properties of the proteins to physiologically relevant lipid bilayers, flat supported lipid bilayers with zero curvature. Detailed procedure for the preparation of the supported lipid bilayer was mentioned in the Methods section of this work. From figure 4.1, it is clear that the produced supported lipid bilayers are of good quality. A frequency shift from 0 to -25Hz and $\Delta D*10^{-6}$ equals zero; signify the quality of the SLB to be good. Care was taken to produce similar SLBs that are to be used in the interaction of proteins. All the experiments were done at room temperature and in duplicates.

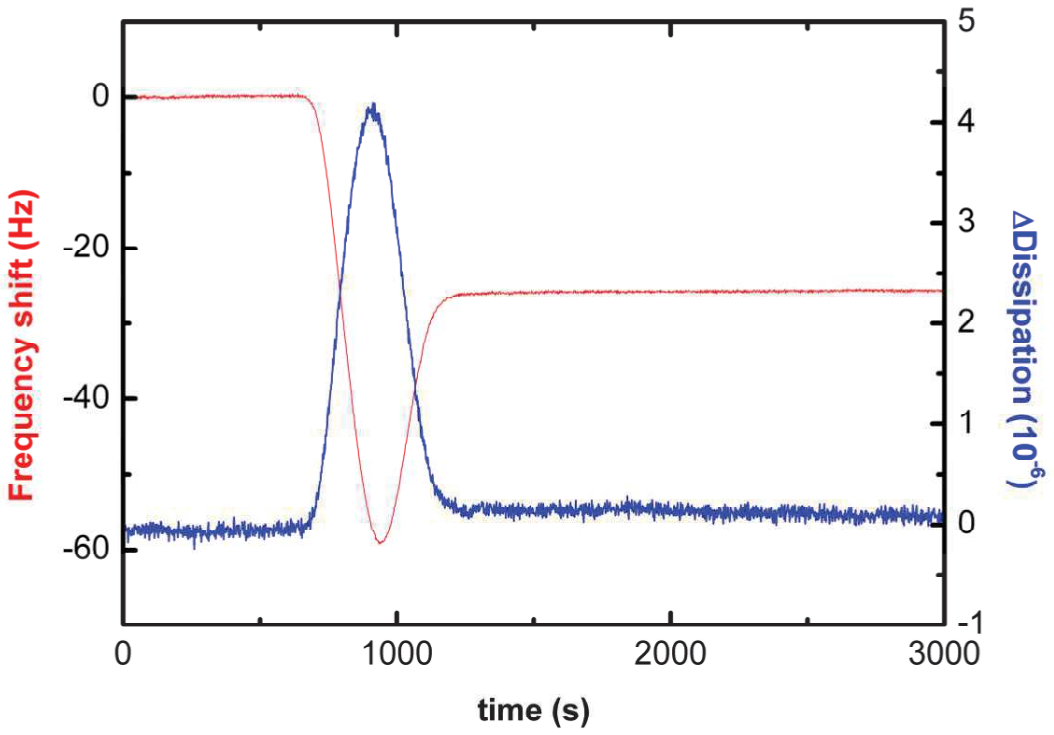

Figure 4.1:Typical frequency shift and change in dissipation observed during the formation of SLB from LUVs.

For the different proteins used in this study, we have determined their affinity towards simple basic supported lipid bilayers (PC 68%, PS 30% and PI(4,5)P_2 2%) from the frequency shift

obtained after the injection of increasing concentrations of a protein. As presented in the table-3.1 of the Chapter-3, the K*p* values obtained with QCM-D are well within the range of the values obtained for co-sedimentation assay. Despite the fact that the curvature of the model membranes is completely different from each other, a similar K*p* values suggests no role of curvature on the binding affinity of the protein.

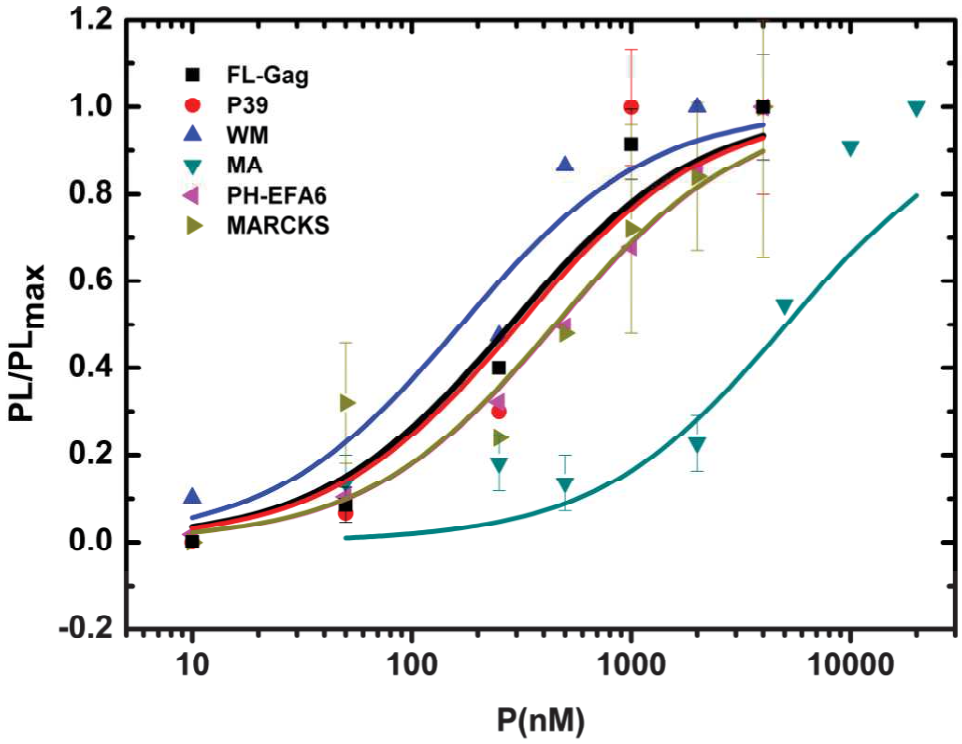

Figure 4.2: Binding of Gag to PI(4,5)P_2 containing SLBs.QCM-D based K*p* measurements of Gag and its mutants. For the K*p* values see table 3.1in Chapter 3.

4.3.2 Interaction of non-multimerizing proteins with PI(4,5)P_2 containing SLBs:

4.3.2.1 EFA6-PH and MARCKS peptide:

QCM-D measurements: Specific proteins were known to interact with high affinity towards certain lipids. EFA6 protein with its PH domain has been shown to bind to PI(4,5)P_2 (Macia et al. 2008a) in cells. On the other hand, MARCKS peptide (151-175) can bind to both PS and PI(4,5)P_2 (Gambhir, et al. 2004). But, both the proteins are not known to self-assemble or bend

the membrane locally. Figure 4.3 & figure 4.4(A) depicts the change in frequency shift and dissipation observed upon injection of EFA6-PH into the SLB containing chamber. Within the 60 sec period of injection, the binding of the protein was rather instant and resulted in a spiked response in the frequency shift followed by a steady decay and plateau. At plateau, a rinse step was performed which resulted in no change in the adsorbed protein level – suggesting that the protein has high affinity for the lipid and bound strongly to the $PI(4,5)P_2$ present in the membrane.

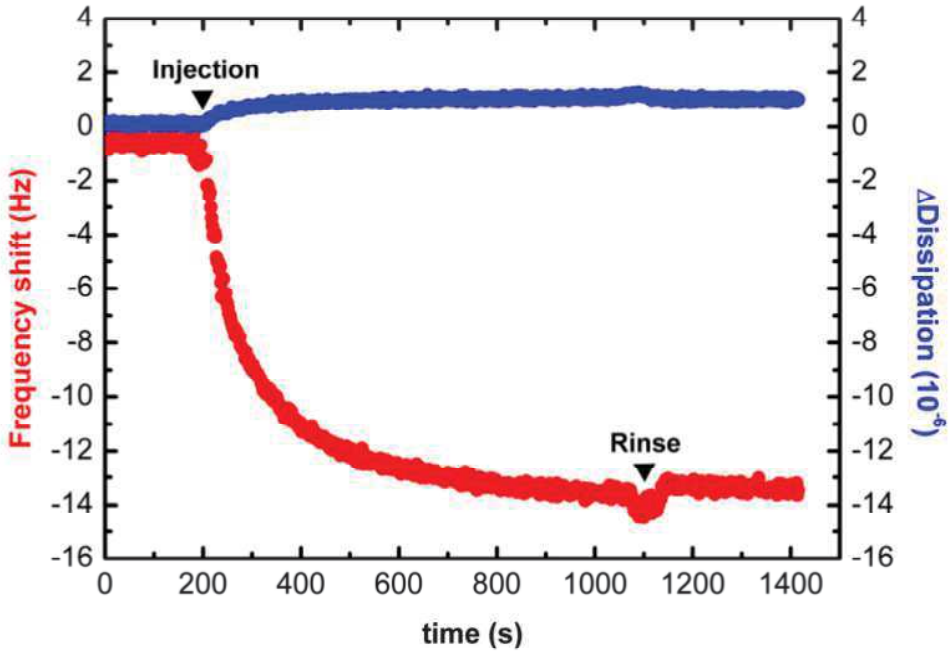

Figure 4.3: A typical sensorgram obtained after the injection of EFA6-PH protein. Both Injection and rinse steps were depicted in the plot. Protein cocentration – 250 nM.

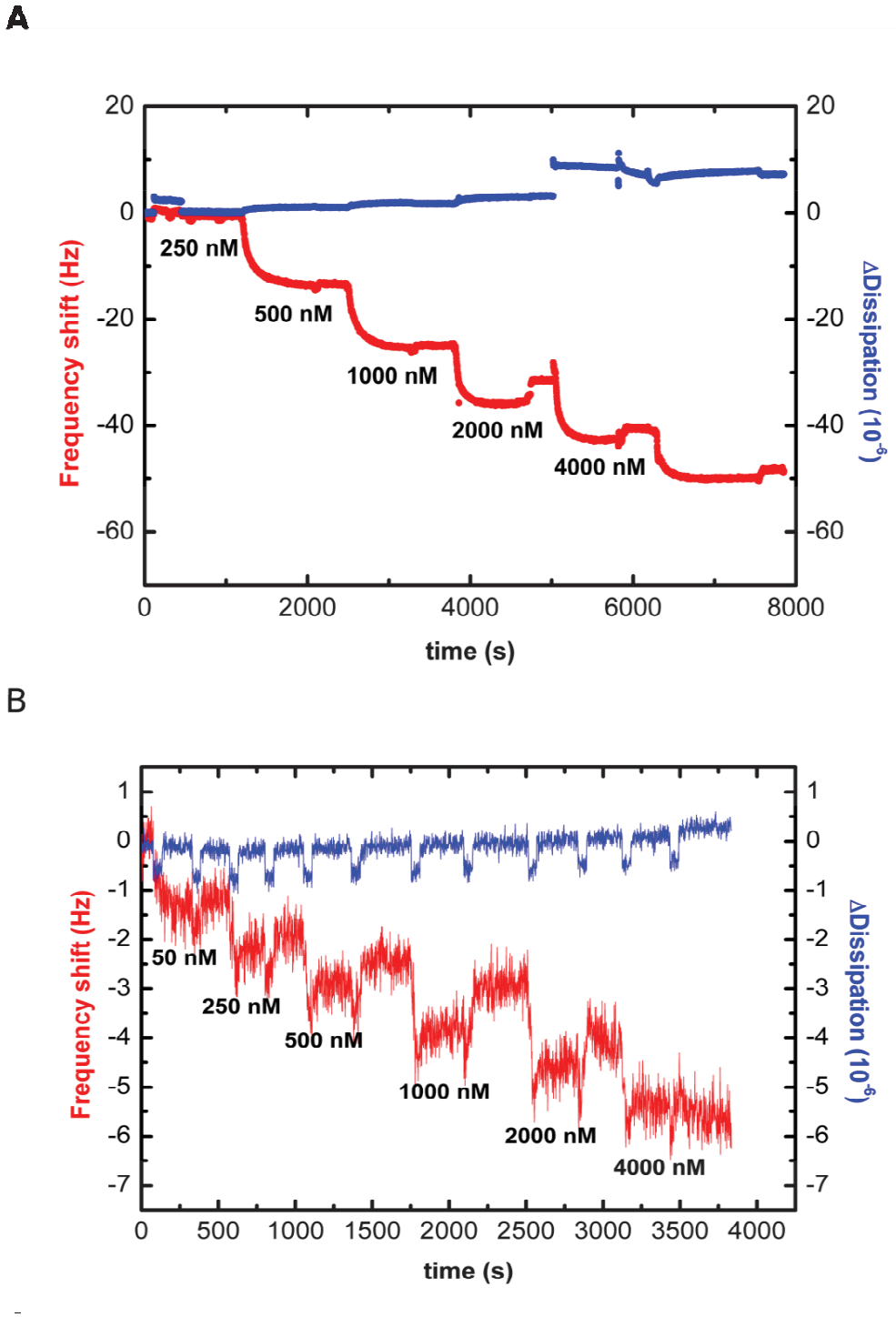

Figure 4.4: Sensorgram with multiple concentrations of protein interaction on PI(4,5)P_2 containing SLBs. (A) EFA6-PH and (B) MARCKS peptide (151-175)

Similarly, MARCKS peptide which is known to cluster PI(4,5)P_2 without even oligomerizing on the surface of the lipid membrane was used. Figure 4.4 reports the obtained sensorgrams for all

the different concentrations of both EFA6-PH and MARCKS peptide. It is evident from the plots that even at same concentrations; the shift in frequency is completely different amongst both the proteins, despite having similar K*p* values (~0.6 μM) (figure 4.2, table 3.2). As mentioned earlier, QCM-D measures the mass of the adsorbed molecules – that is represented in the form of frequency shift. Even with same affinity, EFA6-PH (42 kDa) is heavier than MARCKS peptide (~3kDa) and so higher shift in frequency. The change in dissipation is higher for EFA6-PH, but almost remained at zero for MARCKS peptide – even at high concentrations. This could be because EFA6-PH used in this study has a long C-terminal ie., a coiled-coil C domain that is flexible and thus will lead to high dissipation values. Figure 4.5 depicts the change in dissipation (ΔD) *vs* frequency shift (ΔF) plots of EFA6-PH. Such a plot is helpful for understanding the nature of the adlayer formed on the surface of the SLB. A linear curve depicts that neither the protein nor the lipid bilayer encountered significant morphological changes during the interaction. Finally, EFA6-PH not only interacts strongly with $PI(4,5)P_2$ (K*p* – 0.6 μM) but also induce membrane ordering by forming a rigid layer, but a flexible c-terminal is responsible for the increased dissipation. With no change in the dissipation, a similar plot for MARCKS peptide has not been produced.

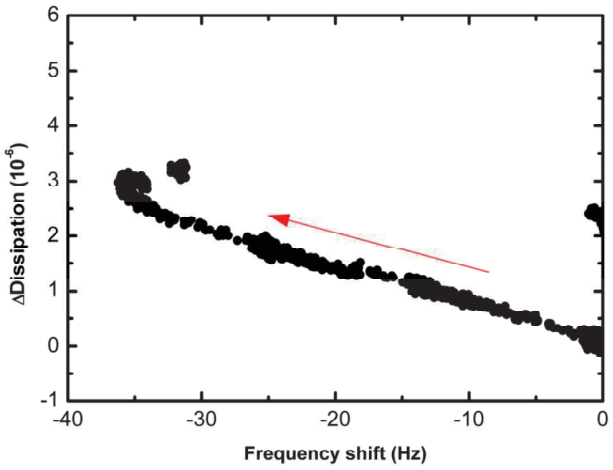

Figure 4.5: ΔD - ΔF plots of EFA6-PH obtained on interaction with $PI(4,5)P_2$ containing basic composition SLBs. Plotted data was from all the concentrations depicted in figure 4.4(A) for EFA6-PH

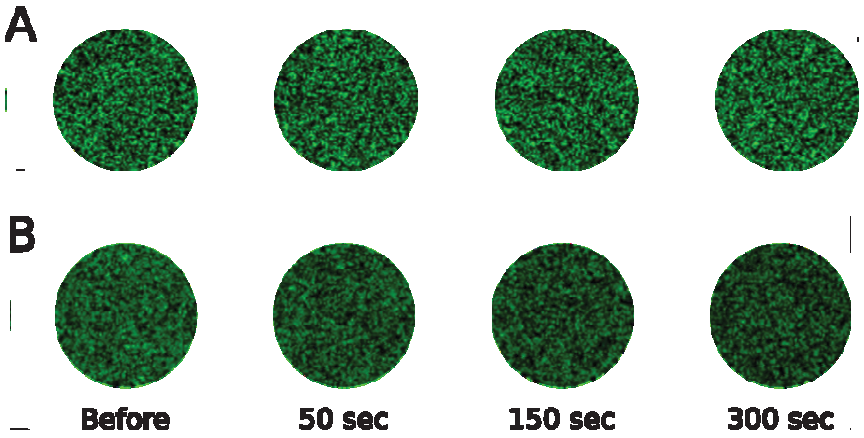

Figure 4.6: Patches of basic composition SLB labelled with 1% TF-PI(4,5)P_2 before and after interaction with EFA6-PH and MARCKS peptide, 1 µM. (A) EFA6-PH interaction (B) MARCKS peptide interaction.

Fluorescence Microscopy: It was shown in figure 3.5(A) and figure 3.6(A) of Chapter 3 that the interaction of EFA6-PH with TF-PI(4,5)P_2 labelled SLBs does not affect the fluorescence intensity and even the morphology of the SLB, as seen in figure 4.6(A). On the contrary, MARCKS peptide's interaction resulted in decreased fluorescence intensity (figure 3.4 and 3.6(A)) but without any change in the morphology of the SLB (figure 4.6(B)). Correlating the data from fluorescence measurements on SLBs with that of QCM-D, it can be concluded that EFA6-PH can bind PI(4,5)P_2 containing SLBs with high affinity but doesn't affect the morphology of the SLB. Instead, the observed increase in the dissipation values is merely due to the presence of a flexible C-terminal ie., a coiled coil C domain. In case of MARCKS peptide, the protein is able to cluster PI(4,5)P_2 which is evident from the decreased fluorescence intensity of the SLB and from previously published data (Gambhir et al. 2004). But, no change in dissipation from QCM-D and no visible morphological changes of the SLB suggest non-curvature inducing nature of the peptide.

4.3.2.2 Matrix protein:

***QCM-D measurements*:** MA of HIV-1 Gag is the major domain that is responsible for the membrane targeting of the protein. In support of this, the domain as such is capable of binding to lipid bilayers through its HBR region and so have yielded a K*p* of ~7.16 ± 3.3 µM in our studies using QCM-D (figure 4.2 and table 3.1). In figure 4.7 below, the QCM-D profile obtained for the MA protein interaction on SLB is depicted.

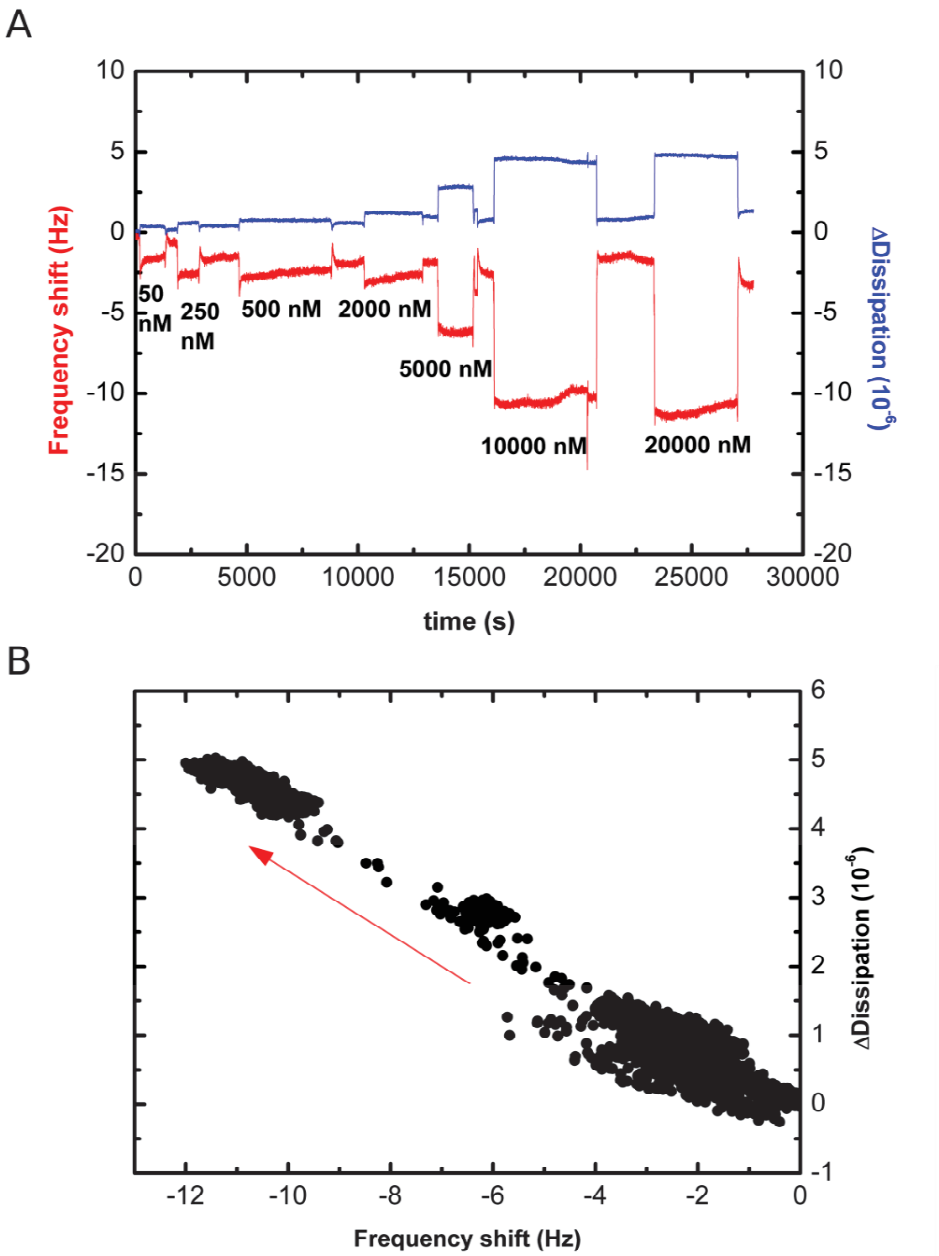

Figure 4.7: QCM-D results of MA protein interaction on PI(4,5)P_2 containing basic lipid composition SLB. (A) Sensorgram of increasing concentrations of MA protein on SLB in QCM (B) ΔD - ΔF plots of and Matrix protein obtained on interaction with PI(4,5)P_2 containing basic composition SLBs.

Note that the transient spikes observed in ΔF and ΔD are attributed to the fluctuation of temperature during the solution exchange.

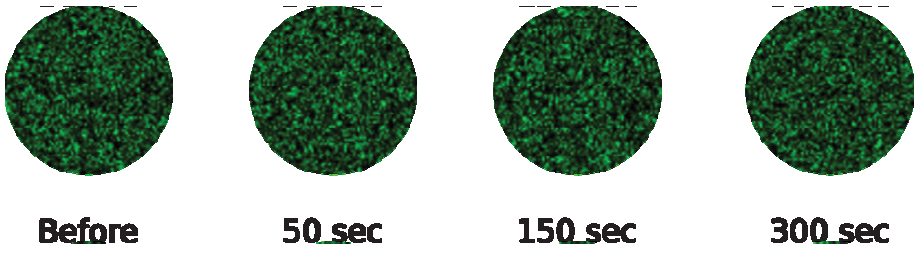

Figure 4.8: Fluorescence Microscopy of MA interaction on PI(4,5)P_2 containing basic lipid composition SLB. (A) Fluorescence microscopic images of MA interaction (1 μM) on SLB at various time intervals.

As expected from its binding affinity value, the binding ratio is significant only at higher concentrations.

From the sensorgram profile (figure 4.7(A)), MA protein binds to the membrane and stabilizes immediately. But the loss of protein after the rinse step, for all the concentrations, emphasize that the interaction is only electrostatic. Figure 4.7(B) depicts ΔD *vs* ΔF plot for MA protein. Noticeably, the profile is similar to that of EFA6-PH ie., a straight line with no deviation for all the different concentrations tested. As stated earlier,a straight curve for ΔD *vs* ΔF plot represents a single adlayer adsorbed on the surface of the SLB. Further, the K value (slope = ΔD/ΔF) for EFA6-PH (0.06) is lower than that obtained for MA protein (0.45). Suggesting that EFA6-PH not only interacts strongly with PI(4,5)P_2 (K_D – 0.6 μM), but also induce membrane ordering by forming a rigid layer compared to a protein like MA – whose interaction is weak (K_D - ~7 μM) and only electrostatic in nature.

Fluorescence measurements: Fluorescence microscopic visualization of the MA protein interaction on PI(4,5)P_2 containing basic composition SLBs revealed that the morphology of the SLB remained the same before and after the addition of the protein (figure 4.8), without affecting the fluorescence intensity of the SLB (figure 3.6(A) and 4.8). While QCM data confirms that the protein interacts with the SLB even at lower concentrations, no quenching of TF-PI(4,5)P_2 observed in fluorescence microscopy suggests that either the protein is unable to cluster PI(4,5)P_2 or the needed concentration of membrane-bound MA that can induce multimerization and TF-PI(4,5)P_2 quenching is not reached.

4.3.2 Interaction of multimerizing proteins with PI(4,5)P_2 containing SLBs:

4.3.2.3 Gag and its mutants:

QCM-D measurements: FL-Gag and its two mutants, P39 and WM were studied for their affinity towards PI(4,5)P_2 containing SLBs and the effect of multimerization upon binding to the membrane. Figure 4.9 reports the typical time course of interaction with the SLB for FL Gag and its mutants (WM, P39), MA and PH-EFA6. The ΔF time course profile for Gag and its mutants is different from any of MA, EFA6-PH or MARCKS

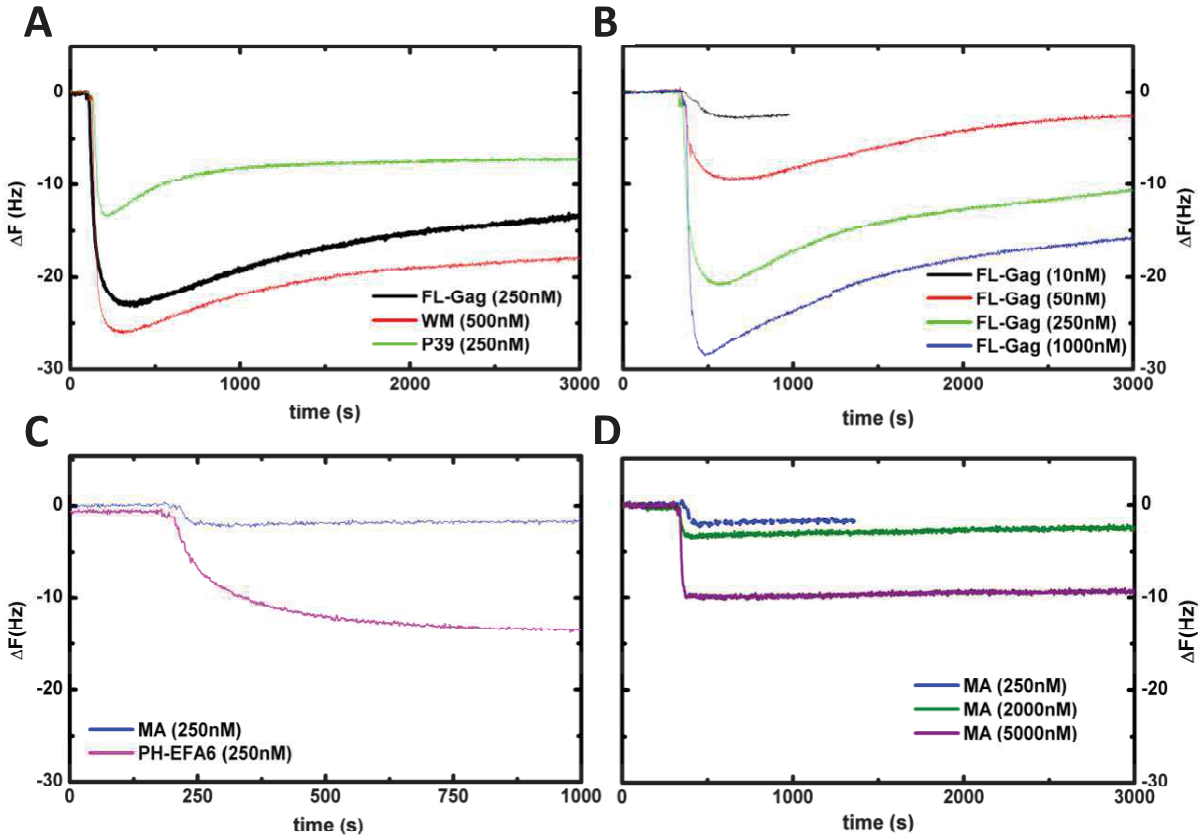

Figure 4.9: Inverse Frequency shift plots of various proteins interaction on PI(4,5)P_2 containing basic lipid composition SLBs. (A) Frequency shift of observed for FL Gag and its mutants. (B) Varied concentrations of Gag, (C) comparing EFA6-PH with that of MA at 250 nM concentration, and (D) various concentrations of MA protein. For all the experiments n=2.

peptide. In figure 4.9(A), the shift in frequency is more of a three-step process; an initial fast protein binding onto the surface of the SLB is followed by a gradual decrease in the frequency

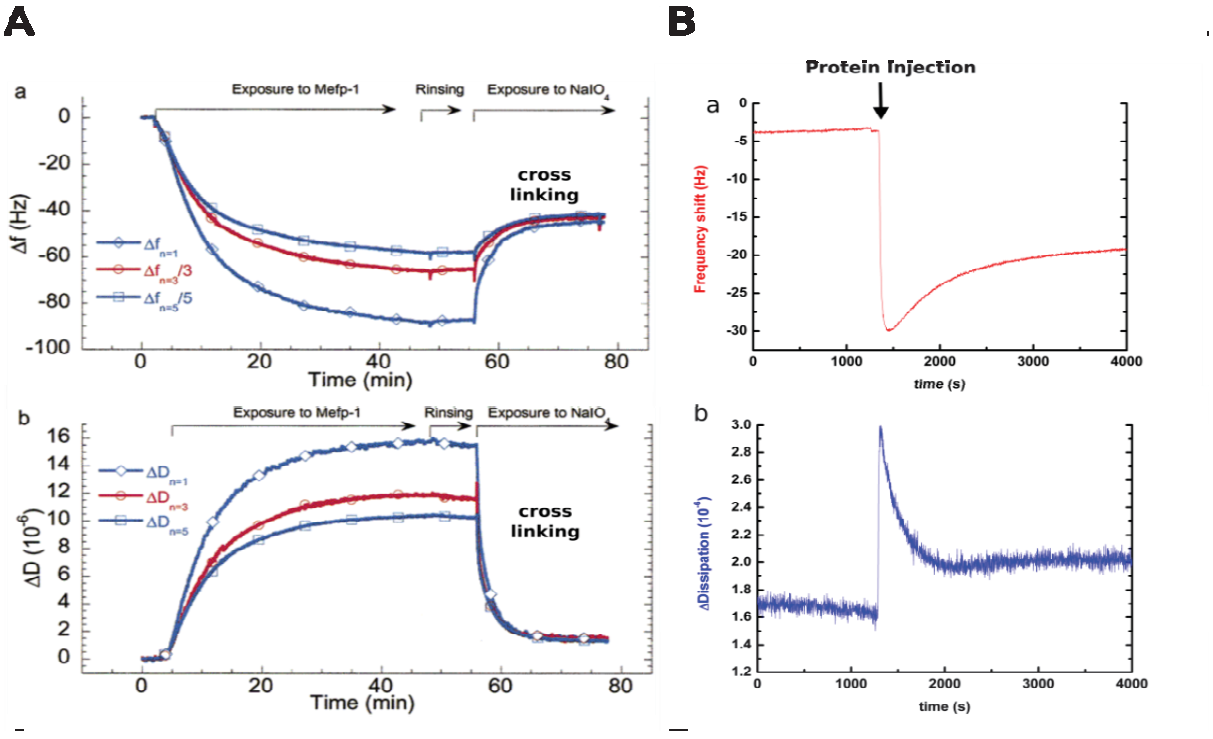

Figure 4.10: Sensorgrams depicting the effect of crosslinking or oligomerization on proteins. (A) Gradual binding and cross linking of Mefp-1 protein on a methyl-terminated non-polar surface (reproduced from (Fredrik Höök et al. 2001) and (B) Innate protein oligomerization resulting in a drastic change in the frequency shift and dissipation observed for FL Gag protein on $PI(4,5)P_2$ containing basic composition SLBs, concentration of the protein, 1 µM.

shift and end in a plateau. This behavior is very much evident in the figure 4.9(B) for FL-Gag protein; all the concentrations depicted have similar profile except for 10 nM. When the profile of FL-Gag is compared to that of the sensorgrams of MA, the difference is profound. Indeed, figures 4.9(B) and (D) show that whatever was the protein concentration used, there observed a clear difference between the sensorgram profiles of FL-Gag and MA – even for expected identical membrane bound protein concentrations i.e., MA 5000 nM as compared to FL-Gag 250 nM). MA protein is only binding to the SLB and reaches plateau immediately, like EFA6-PH, but surprisingly FL-Gag and its mutants has a decreasing frequency shift after the initial binding event. Different explanations could stand for this unexpected result.

A first scenario could be a non-specific association of the protein to the supported lipid bilayer. This would lead to a protein release after a given time (Baumann et al. 2011). In this case, one expect the ratio of the ΔF value (immediately after the injection) as to the ΔF value (at plateau) to

increase with increasing concentrations of protein. This isn't what observed, neither for FL-Gag (figure 4.9(B)) nor for P39 or WM mutants. Another possibility is the formation of highly ordered multimers on the surface of the SLB. For example, proteins like Mussel Adhesive protein-1 (Mefp-1) that exist in monomeric state under normal conditions, when allowed to oligomerize using a cross-linker such as sodium iodate ($NaIO_4$) has shown a sudden shift in the frequency (figure 4.10(A)) (Fredrik Höök et al. 2001)– like the one observed in this study for Gag and its mutants (figure 4.10(B) for FL-Gag). In case of Mefp-1, the sudden increase in the frequency shift and a drop in dissipation is explained as the crosslinking of the protein followed by the removal of the bound water from the surface of the proteins as they stack closer to one another. When compared this to the result observed for Gag proteins, unlike Mefp-1, Gag multimerize naturally upon binding to the surface of the lipid bilayer, thanks to CA-CA interactions. The sensorgram depicted in figure 4.10(B) justifies this statement. After injection, the sudden spike in the frequency shift is associated to the binding of the protein to the SLB which is later followed by natural oligomerization resulting in a significant increase in the frequency shift and a drop in the dissipation due to the removal of bound water on the membrane, between protein-protein and in-between the bilayers. A similar scenario of increasing frequency shift upon crosslinking of chitosan was observed elsewhere (Alves, Picart, and Mano 2009). These results suggest that crosslinking or oligomerization could yield in this sudden change in frequency shift, after an initial binding event.

FL-Gag in solution is a horse-shoe shaped protein (Datta, Curtis, et al. 2007a; Munro et al. 2014). Conformational changes in the structure can be brought about by binding to the polar head group of $PI(4,5)P_2$(Datta, Zhao, et al. 2007). QCM with dissipation has a distinct advantage of revealing the molecular conformational changes during the interaction process. A plot of ΔDissipation (10^{-6}) - ΔFrequency gives information about the membrane ordering property due to the formed adlayer and conformational changes of the protein. For example, changing directions of the arrows, as observed in figure 4.11, can be related to several different processes occurring on the surface of the membrane(Wang et al. 2015). The slope of the curves (K) is indicative for changes in the kinetic and conformational processes during the interaction. Theoretically, a small value of K indicates a rigid layer, whereas high value indicates a soft and water rich layer.

FL-Gag binding to SLB is immediately followed by multimerization. But multimerization can occur only when sufficient concentration of the protein is available on the surface of the lipid bilayer. Clearly, except for 10 nM concentration (figure 4.9(B) and 4.11(A)), rest of the concentrations have very distinct profile. A straight curve for 10 nM (figure 4.11(A)) meant that the concentration of FL-Gag protein bound to the surface is not enough for forming detectable oligomers and so the profile remained similar to that of the ΔD-ΔF plot of MA protein (figure 4.7(B)). In fact, the slope of the 10 nM FL-Gag curve (0.22) is half-way in-between to EFA6-PH (0.06) and MA (0.45). But, at higher concentrations, it is a different scenario. For example, at 50 nM concentration, ΔD-ΔF plot first increases fast and linear towards a negative ΔF (addition of mass) - indicated by thin linear curve and suggesting the formation of a compact layer (figure 4.11(B)). As the frequency shift increased (towards positive value) after point 'a', the

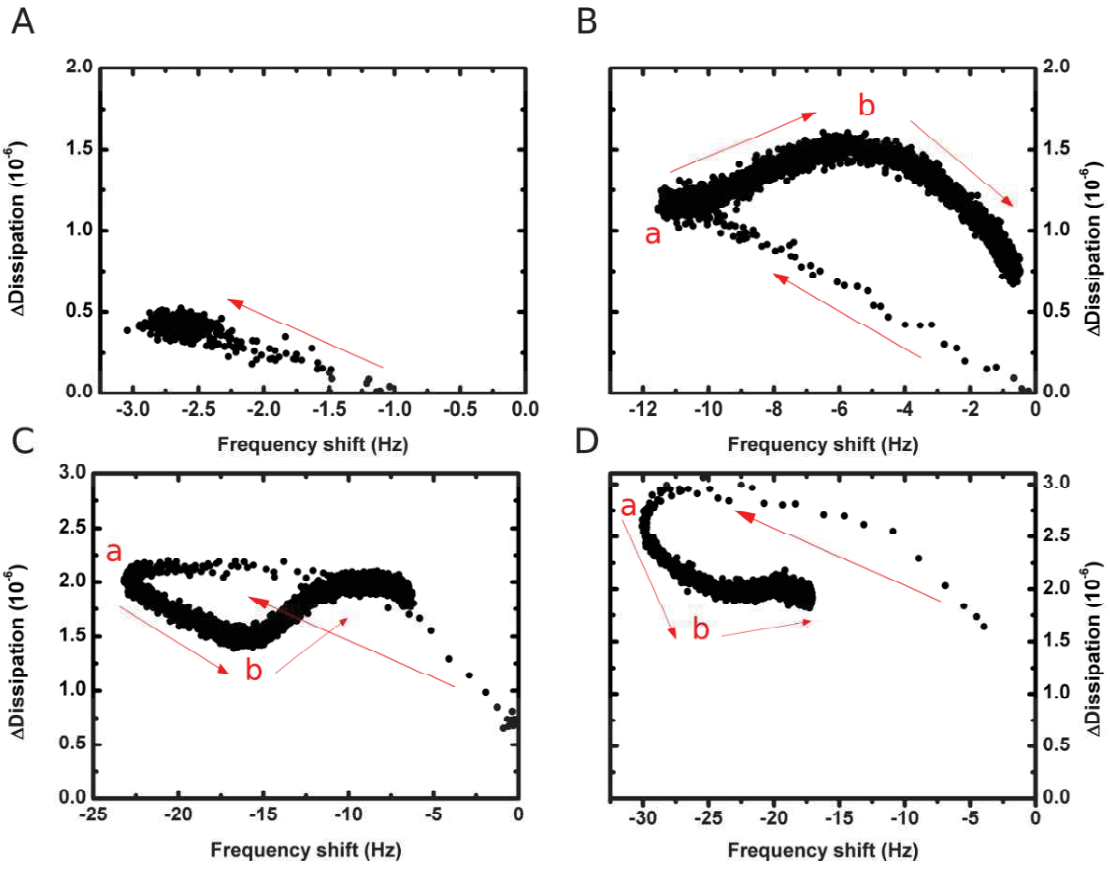

Figure 4.11: ΔD - ΔF plots for various concentrations of FL-Gag interaction with PI(4,5)P_2 containing basic composition SLBs. (A) 10 nM, (B) 50 nM, (C) 250 nM, and (D) 1000 nM, n=2. Red color arrow depicts the progression of the curve with time and transition points are labelled with a/b/c emphasizing the structural changes occurred.

formed protein adlayer can be concluded as a single layer (F Höök et al. 1998). Later, the kink at point 'a' is followed by a steady increase in the frequency shift (towards positive value), but ΔD varied with an increasing first and then decreased steeply later on. This behavior is unique and different from that of 10 nM Gag or MA (for all concentrations) or EFA6-PH (for all concentrations). Such a marked behavior suggests that after point 'a', there is a conformational change in the protein that could be attributed to multimerization after a transition from horse-shoe shape to a more linear structure upon binding to the head group of $PI(4,5)P_2$. Moreover, this kind of behavior is seen only from 50 nM concentration but not at 10 nM concentration. Low concentration result resemblance to MA and EFA6-PH implies that higher concentrations resulted in the multimerization of the protein in 50 nM and thereafter.

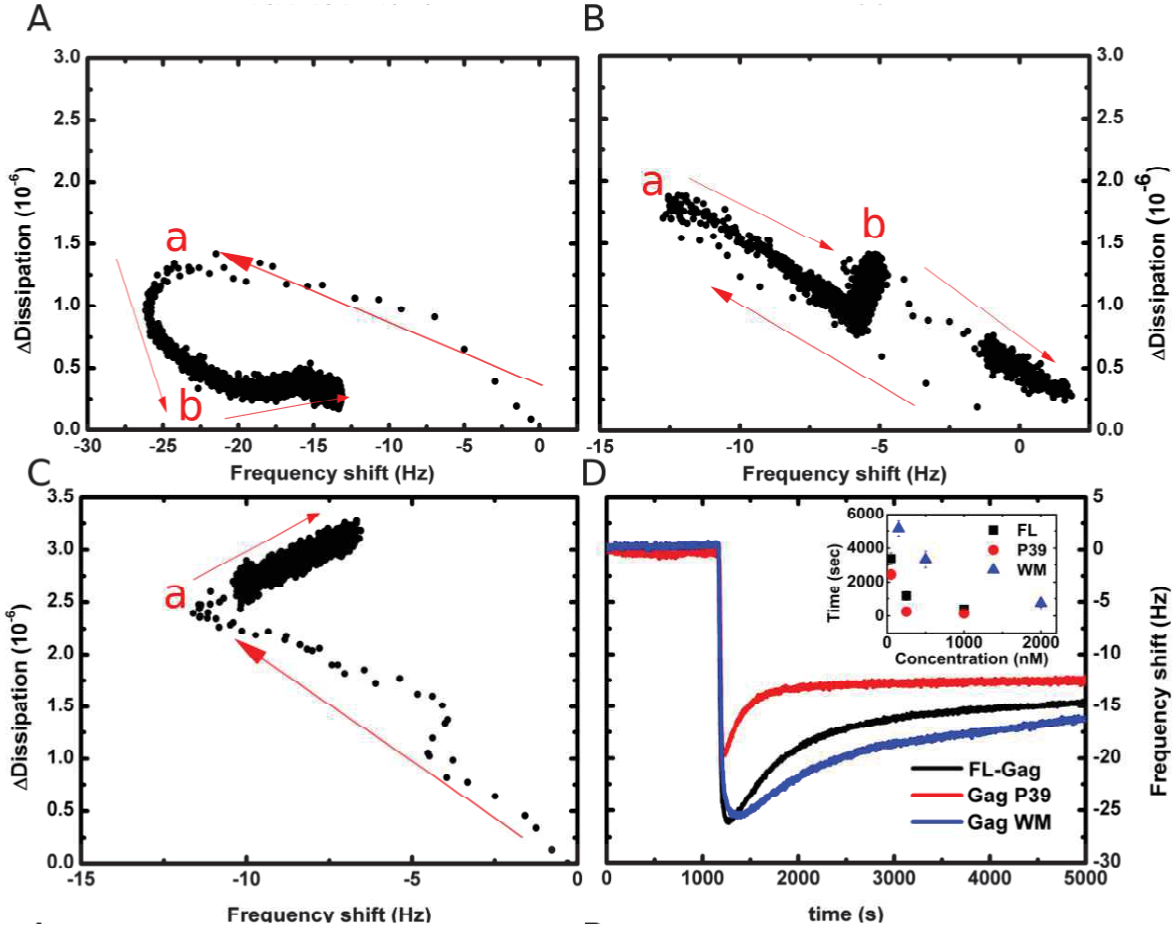

Figure 4.12: Comparing the ΔD - ΔF plots and frequency shift of Gag and its mutants (P39 and WM) upon interaction with $PI(4,5)P_2$ containing basic composition SLBs. (A-C) Normalized ΔD - ΔF plots of FL-Gag, P39 and WM, respectively. (D) Comparing Frequency shift of Gag and its mutants. Concentrations of FL-Gag and P39 are 1 μM, WM is 2 μM. Inset represents the slopes of the decreasing frequency shift obtained for FL-Gag and its mutants at various concentrations. n=2

With respect to Gag mutants, P39 (lacking both NC and P6 domain ie., no NC-lipid interactions (Kempf et al. 2015a) should be a better multimerizing protein compared to that of FL-Gag or WM. This is because the FL-Gag and WM are full length proteins with a bent conformation in solution and so require a conformational alteration step to form oligomers – leading to the conclusion that the order of multimerizing capacity might be P39>FL-Gag>WM. Considering that multimerization is responsible for the sudden change in the frequency shift after binding, the slopes of the increasing frequency shift (towards positive value) should be in the same order as their multimerizing capacity, while the time to reach a plateau for the three proteins should be in the opposite order. This trend is clearly visible from the figure 4.12(D). Even at a higher concentration (2000 nM), WM has a slope lesser than both FL and P39 that are at a lower concentration (1000 nM). A similar trend is obtained from the slopes calculated at various concentrations (inset in figure 4.12(D)). These results emphasize that (a) the assumption made earlier regarding the order of multimerization capacity is true, P39>FL>WM, (b) multimerization capacity of WM is lower as detected before (figure 3.7) and (c) bent conformation of the Gag protein decreases the efficiency of the protein to multimerize and to form compact/ordered structures. Further, the plot in figure 4.12(B) suggests that after P39 exposure there resulted in a fast increase in mass and dissipation followed by a kink at point 'a' (figure 4.12(B)) paving to rapid decrease in both mass and dissipation. WM being a multimerizing mutant is less efficient than FL-Gag or P39. Moreover, requirement of conformation alteration further delayed its multimerization capacity. Consequently, the slope of the increase in frequency shift (towards positive values) is more gradual (blue, figure 4.12(D)) when compared to FL-Gag or P39. Knowing that the concentration represented here for WM is double to that of P39 or FL-Gag, this reassures the poor multimerizing property of Gag WM. Overall, for Gag and its mutants, it is observed a three different profiles in the ΔD-ΔF plots for all the concentrations from 50 nM: an initial fast and linear step (spaced dots/thin region) – suggesting the fast binding of the protein, a slow process (thicker regions) is marked with increasing frequency shift (towards positive values). But, the ΔD value wavered i.e., either increasing (coupled with hydrated layer) or decreasing (coupled with rigid layer) or both after first transition point, 'a' (Voinova et al. 1999). This primary transition point 'a' could be due to the conformation change occurring with the

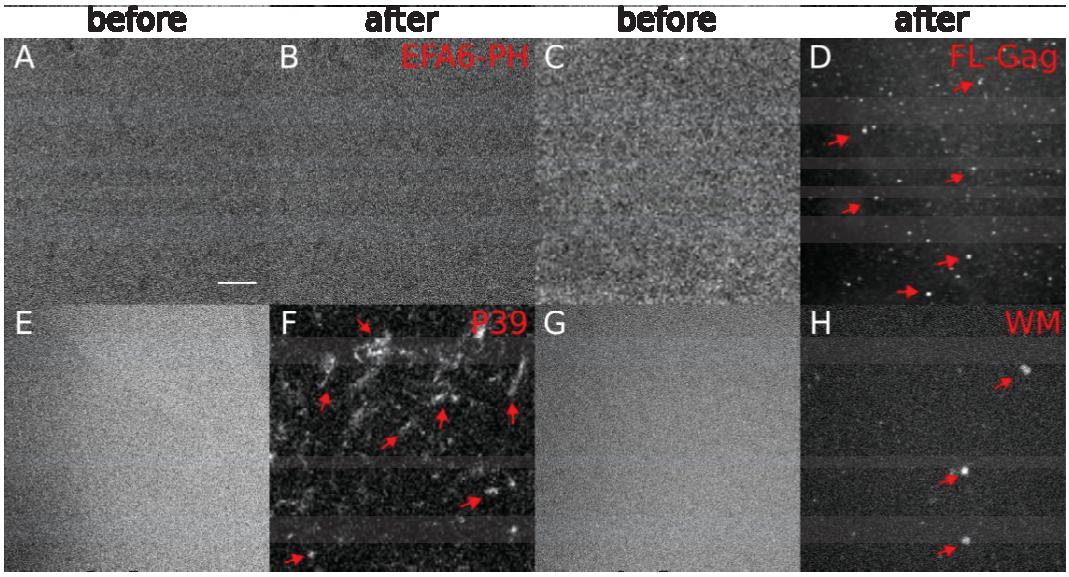

Figure 4.13: Comparing the Morphology of TF-PI(4,5)P_2 labelled basic composition SLBs before and after the interaction with various proteins. (A-B) EFA6-PH, (C-D) FL-Gag, (E-F) Gag P39 and (G-H) Gag WM. All the concentrations are at 1 μM.

protein upon multimerization, and later transitions in the curve could be the result of a higher ordering. However, the results obtained for Gag protein interaction on SLBs under fluorescence microscope gave a clear insight into the higher ordering of the protein and the resulting consequences of such an ordering.

Fluorescence Microscopy: We performed fluorescence microscopy of Gag interaction with SLB as a complementary method to better understand the results from QCM-D. While QCM-D provides information of an intimate interaction occurring at the interface with high resolution, fluorescence microscopy can let visualize the same process, albeit at lower resolutions. Nevertheless, it can provide information on the morphological and fluorescence changes upon protein interaction with the SLB. Non-multimerizing proteins, figure 4.6 and 4.8 revealed that EFA6-PH, MARCKS peptide and HIV-1 MA protein doesn't affect the morphology of the SLB at the resolutions observed. With no deviations in ΔD - ΔF plots for these proteins (figure 4.5 and 4.7(B)) and no visible morphological changes within the SLB, it is safe to conclude that the proteins doesn't induce any curvature even at resolutions below the diffraction limit. On the contrary, a significant change in the morphology of the "basic" composition SLBs has been Figure 4.13 report the morphological changes induced upon protein interaction with PI(4,5)P_2

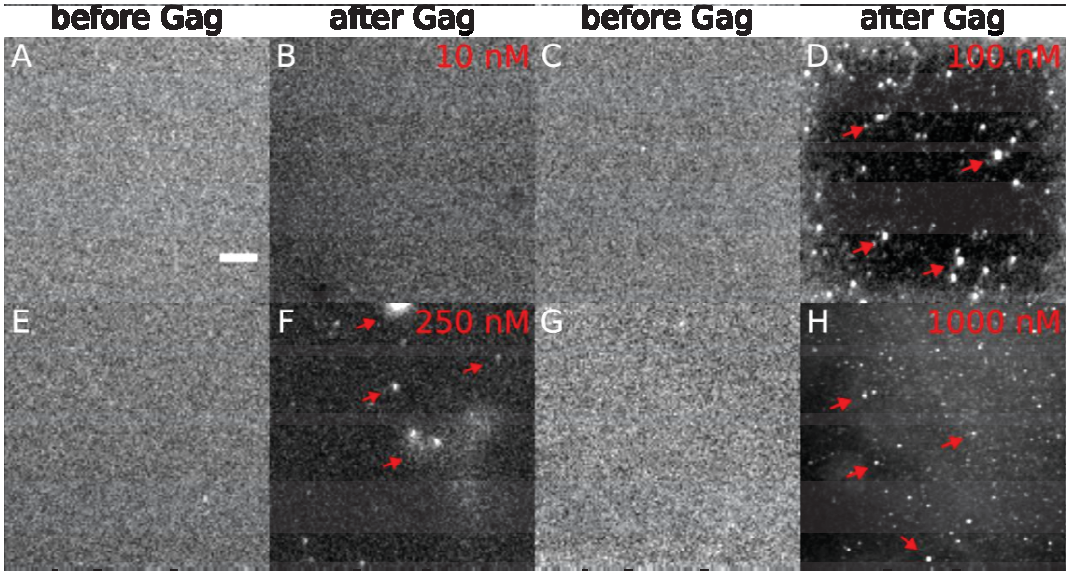

Figure 4.14: Morphology of various TF-PIP2 labelled basic composition SLBs treated with various concentration of FL-Gag. (A-C-E-G) are SLBs before addition of the FL-Gag. (B) 10nM, (D) 100 nM, (F) 250 nM, and (H) 1000 nMFL-Gag treated SLBs.

observed for Gag and its mutants – complementing the unique deviations in the ΔD - ΔF plots containing SLBs. Among the four different proteins presented in the figure 4.13, except for EFA6-PH, all the other proteins altered the morphology of the lipid bilayer. Correlating the linear ΔD - ΔF curve (figure 4.5) obtained from QCM-D data, the EFA6-PH interaction result (figure 4.12(B)) from fluorescence microscopy confirms that as a non-multimerizing protein binds to the $PI(4,5)P_2$ present in the SLB without inducing or undergoing any morphological and structural changes. However, from the figure 4.12, it is evident that vesicle-like structures (red arrow) appeared on the SLBs after their interaction with the proteins – FL-Gag (D), Gag P39 (F) and Gag WM (H). Bright spots formed on the surface of the SLB are representative of the deformation of the bilayer by Gag proteins and its mutants. Correlating this vesicle creation to the sharp increase observed in the frequency shift after an initial binding event gives a better understanding of the mass decrease detected by QCM. This mass decrease can be attributed to the lipid bilayer lift-off ie., local membrane curving by the interacting protein oligomer. A similar decrease in mass and vesicle creation has been detected elsewhere(Rossetti et al. 2004). Unlike the polymer used in that study, each Gag protein is a single unit. To be able to induce such a curvature, multimers of the protein is essential. In addition to this, concentration is a factor that can affect the multimerizing efficiency of the protein. Earlier, lower concentrations of

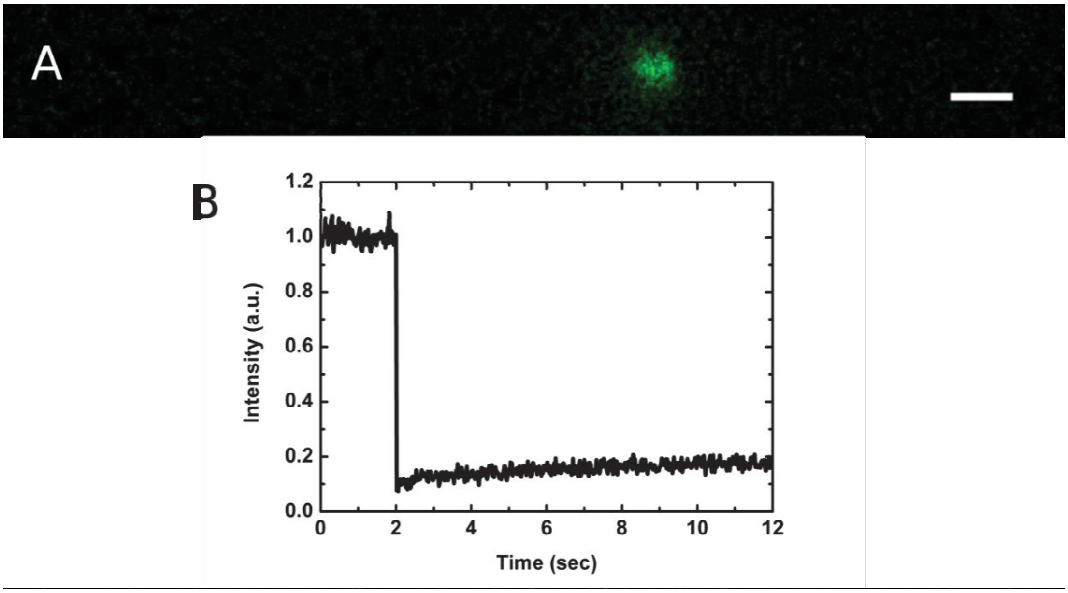

Figure 4.15: FRAP experiments on formed vesicles upon interaction of Gag with PI(4,5)P_2 containing basic SLBs. (A) Vesicle formed on the surface of the SLB (scale bar corresponds to 2 μm). (B) A very low recovery in the FRAP profile of a vesicle formed on the surface of the SLB, suggested no connections of the newly formed vesicules with the SLB (n=5).

Although FL-Gag is a multimerizing protein, at that lower concentration (10 nM) the morphology of the SLB remain unchanged (figure 4.14 (B)). But the higher concentrations of FL-Gag reported a decrease in the frequency shift (figure 4.9 (B)) and appearance of bright spots corresponding to membrane deformation and vesicle formation (figure 4.14 (D) (F) & (H)). These results further emphasize the role of multimerization capacity in vesicle formation by these proteins. Figure 4.15(A) is depicting the vesicles induced by the Gag protein after interaction with the TF-PI(4,5)P_2 labelled basic composition SLBs. While the image suggests the formation of large sized vesicles that are bigger than the actual size of the HIV-1 virus, it can't be ruled out that there is no formation of smaller vesicles close the actual size of the viral particles. It was visualized earlier by Campbell et al. using electron microscopy that Gag protein alone can form immature VLPs as small as 50 nm to 100 nm in the presence either tRNA (S Campbell and Rein 1999) or IP6 alone (S Campbell et al. 2001a) in solution. But, on model membranes it was shown very recently that Gag protein with RNA in urea medium produced vesicles as large as the once observed in this study (Gui et al. 2015). FRAP experiments on these formed vesicles resulted in almost no recovery in their fluorescence (figure 4.15(B)). This result reconfirms the previously shown PI(4,5)P_2 trapping property of Gag in figure 3.10(B), in

Chapter-3. Note that the vesiculation of the membranes by protein interaction is fascinating, but it is not uncommon that only 40% of SLBs treated with the proteins here were positive for vesiculation. Care was taken while presenting the self-quenching data from the non-deformed SLBs upon Gag interaction (under chapter 3).

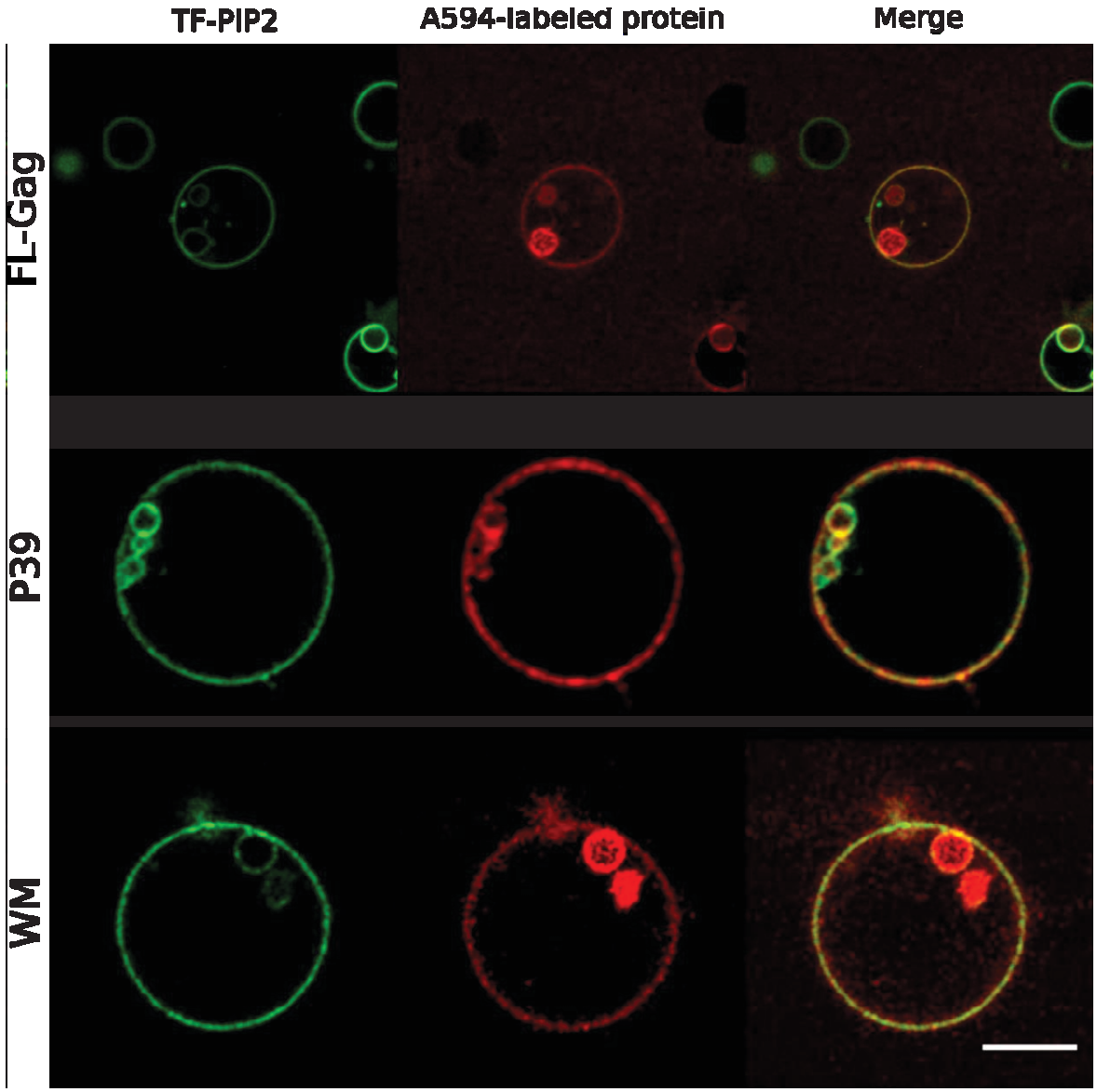

Figure 4.16: Gag induced budding. 1% TF-PIP_2 labelled GUVs were incubated with FL-Gag/P39/WM tagged with Alexa fluor-594. Images were acquired after 30 min of the incubation. Linear Unmixing of the images were performed using the Zeiss software after acquiring the spectral image of the respective GUVs. Note the co-localization of the labelled Gag protein and negatively charged TF-PIP_2 at the invaginations on the GUV under Merge. Scale bar corresponds to 10 μm.

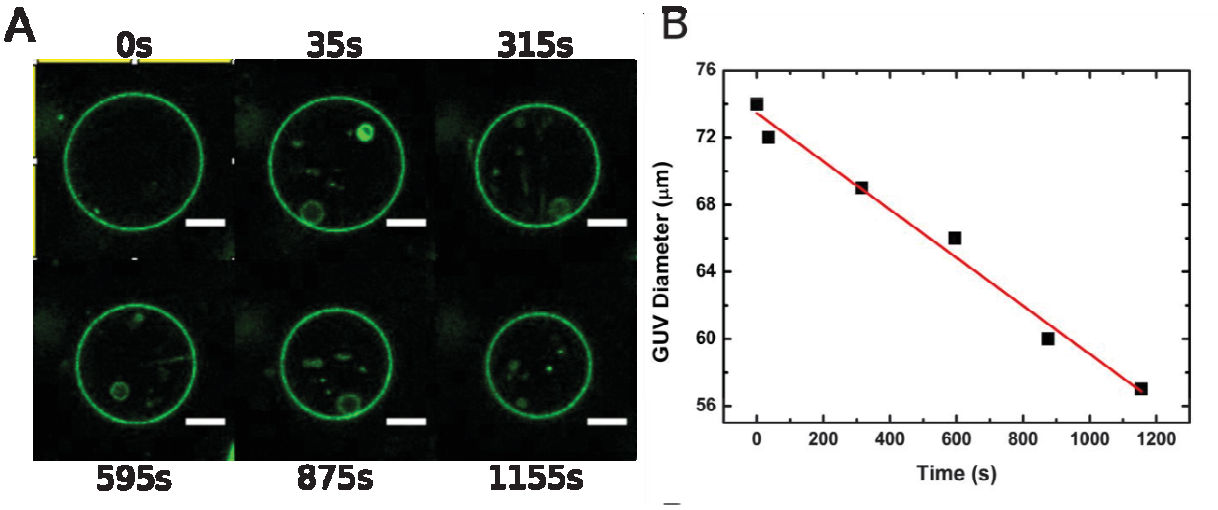

Figure 4.17: Time profile of GUV vesiculation by Gag. (A) GUV shrunk over time upon interaction with Gag protein. Scale bar corresponding to 10 μm. (B) GUV diameter decreased as a function of time linearly due to the formation of membrane invagination and vesicles.

While there are many parameters that can affect the vesiculation (Rossetti et al. 2004), having defective SLBs could be one reason as put forth by Rossetti et al. However, in our study the ability of the protein to induce vesiculation was also studied using GUVs.

4.3.5 Gag and its mutants induce membrane invaginations

Interactions of the labelled Gag protein with TF-PIP_2 labelled GUVs resulted in good binding of the protein all over the membrane and also resulted in the formation of membrane invaginations (figurer 4.16). Both Alexafluor-594 tagged FL-Gag and TF labelled PIP_2 lipids are colocalizing along the surface of the GUV membrane. A similar trend is observed for both the Gag mutants; P39 and WM (figure 4.16). Further, figure 4.17 presents the decrease in the diameter of the GUV upon interaction with FL-Gag protein. Over the course of time, the GUV diameter decreased from 74 μm to 57μm due to the constant membrane invagination induced by bound Gag. This decrease corresponds to a rate of 10 vesicles of 120 nm diameter produced every second. Interestingly, the size of the vesicles generated out of Gag-$PI(4,5)P_2$ interactions are larger in size and not necessarily ~120 nm as expected for a new viral particle of HIV-1 (S Campbell et al. 2001b; Gentile et al. 1994). Similar kind of large membrane invaginations were reported for vesicular stomatitis virus M protein interaction on GUVs (Solon et al. 2005).

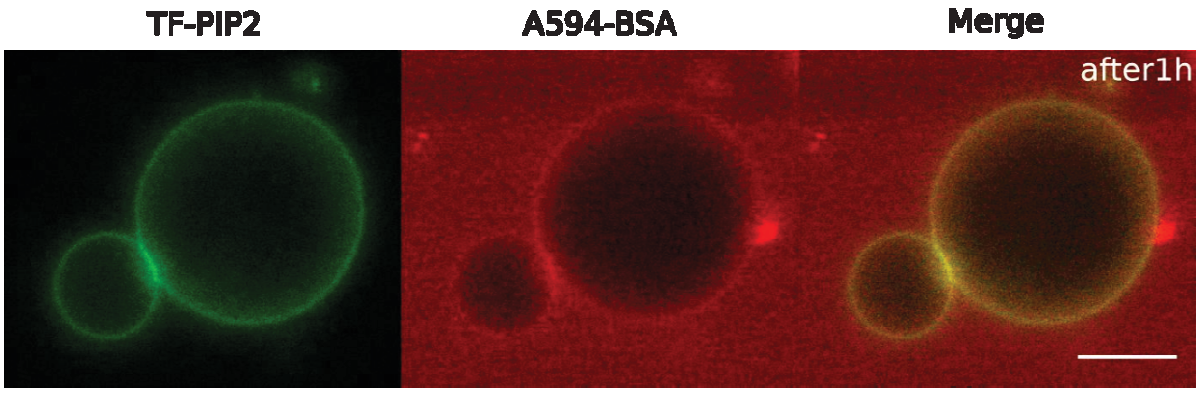

Figure 4.18: GUV incubation in Alexafluor-594 labelled BSA. Scale bar corresponds to 10 μm.

The authors reasoned the abnormal size of the membrane invagination (2-3 μm) when compared to that of the actual viral particle (200 nm) by suggesting the possible role of cellular or viral factors in regulating the size of the newly formed viral particle in cells. Indeed, very recently it has been shown that RNA can act as a key determinant in the size control of the newly formed VLPs in HIV-1 virus (Faivre-Moskalenko et al. 2014). Thus, in our study, lack of genomic RNA could be one of the reasons for high polydispersity in the size of membrane invaginations. Finally, to ascertain that the membrane invaginations are not due to mere aggregation of proteins on the model membrane, BSA was incubated with the TF-PI(4,5)P_2 labelled GUVs. We found that BSA did not induce any membrane vesiculation. (figure 4.18). The self-association property of HIV-1 Gag in conjunction with its specific lipid interaction seems to be responsible of the membrane reshaping up to vesicle release as it is the case for other viruses like the Vesicular Stomatitis Virus (Solon et al. 2005).

4.3.6 Gag as a minimal system can induce vesiculation of membranes

Multiple factors can induce membrane curvature (Reinhard Lipowsky 2013; McMahon and Gallop 2005; Simunovic et al. 2016). A detailed note on the various scenarios that can induce membrane curvature is illustrated in the figure 1.14 under Chapter-1. Multimerization of proteins along the surface of the membrane can exert sufficient pressure, when exceeds membrane rigidity, which can initiate membrane bending (Reinhard Lipowsky 2013). Proteins like COPI-I, COPI-II, and Clathrin gather as scaffolds to curve membranes that in turn can recruit curvature

inducing proteins like epsin and BAR domain proteins (Kirchhausen 2012). Many retroviral proteins assemble along the inner leaflet of the plasma membrane were known to alter the membrane curvature and bud out of the host cell (Bush and Vogt 2014). Viral proteins of retroviruses like New Castle disease virus (Shnyrova et al. 2007) and Vesicular Stomatitis Virus (Solon et al. 2005) were shown to induce membrane invaginations and vesiculation. While referring to the energy required in inducing a 100 nm radius vesicle from a flat membrane as high, Shnyrova et al., proposed that protein condensation on the surface of the membrane can be powerful enough to induce membrane curvature by surpassing the barrier of membrane rigidity and even regulate membrane topology (Shnyrova et al. 2007). In the same work, the researchers have shown that the protein is inducing vesiculation on both SLBs and GUVs.

In our study, the Gag protein tends to induce negative curvature to PI(4,5)P_2 containing SLBs, similar to the data shown for M protein of New Castle disease virus (Shnyrova et al. 2007).Many peptides/polymers induce negative curvature on SLBs (Arouri et al. 2010). Some compounds does this by insertion of hydrophobic helixes into the bilayer (Arouri et al. 2010), others (protein scaffolds) tend to curve the lipid membrane along the interaction point (Rossetti et al. 2004; Shnyrova et al. 2007). For the later, the curvature can be generated by repulsive interactions between the charged domains of adjacent adsorbed molecules (Adams et al. 2014; Rossetti et al. 2004) or decrease in entropy of those domains (Reinhard Lipowsky 2013).It could be possible that the repulsion between the charged domains (NC and P6) of the closely packed Gag molecules in a multimer can impart the necessary curvature to the surface of the lipid - like it is the case for Adams et al. 2014 and Rossetti et al. 2004. This will, indeed, induce the bound lipid bilayer to bend – lifting off from the sensing surface of QCM-D. Nevertheless, such a mechanism can't be applied to P39 that lacks both the charged NC and P6 domains. However, for a successful detachment of the SLB from the solid support, it is necessary to have sufficient number of protein molecules per cluster (Reinhard Lipowsky 2013).The change in the membrane shape observed during self-assembly of Gag can also be lipid domain driven. As mentioned earlier, Gag protein is able to induce lipid clusters enriched in PI(4,5)P_2 and also Cholesterol. These domains when exceeds specific linear size will acquire high free energy associated with boundary line that propel to acquire a curvature at the expense of little bending energy(Lipowsky 1993; Lipowsky and Dimova 2002). Interestingly, the energy required to detach these

enriched regions will be higher for small protein clusters than for large multimers (Lipowsky et al. 2013).

In our study, HIV-1 MA protein has never been shown to induce such vesicle creation. Even a multimerizable derivative of the protein with or without myristate has not revealed any signs of inducing vesiculation on GUVs (Keller, Kräusslich, and Schwille 2013). In that respect, and with regards to the data obtained in this study using QCM-D and fluorescence microscopy, it is evident that multimerization of a capsid domain containing protein is the main contribution to the protein's ability to bend lipid bilayer.

4.4 Conclusion

Our work demonstrated the role of multimerization in the ability of protein to induce morphological changes to the lipid bilayer. Different proteins used in this study are comparable: for they have similar affinity towards $PI(4,5)P_2$ containing lipid bilayers, except for MA protein. To compensate, higher concentrations of MA protein were tried so to attain better binding ratios and multimerizing ability. In spite of this, MA protein tends to behave similarily to that of EFA6-PH. Both these proteins bound to the membrane without affecting any morphological changes to the lipid bilayer as revealed from the fluorescence microscopic experiments. Moreover, a single slope ΔD-ΔF plot for both these proteins suggested the same conclusion. Contrary to the above proteins, FL-Gag and its two multimerizing mutants, P39 and WM shown a completely different profile for their interaction on SLBs. QCM-D results clearly suggested a conformational change in the protein structure followed by destabilization of the membrane. For both FL-Gag and WM, the change is very evident from the multiple slopes observed in the ΔD-ΔF plot. Lacking NC and P6 domain, P39 is more linear and doesn't need a conformational change to form multimers. This is clearly evident from the slopes of the frequency shift compared for all the three proteins in the figure 4.12(D). The slopes are proportional to the rate of multimerization and the ΔD-ΔF plot is more linear for P39 than for FL-Gag or WM. Further, correlating the results from QCM and fluorescence microscopy revealed that multimerization of the proteins is responsible for destabilization of the lipid bilayer. Except for EFA6-PH, MA and MARCKS peptide, FL-Gag and its mutants that are able to multimerize has shown to bend the membrane. While these proteins were also found to cluster $PI(4,5)P_2$, their ability to bend membranes has not been reported before, in the absence of RNA or in a physiologically relevant medium. From previous literature, the QCM-D results obtained for these proteins are found to be in supportive to the assumption – "multimerizing Gag protein can induce membrane bending". In addition, our fluorescence microscopy data reassures the membrane bending property of the proteins and it is dependent on the clustering of the proteins that can help detach the lipid bilayer from the solid support. Many parameters could affect the process of membrane bending and equal number of mechanisms has been proposed in the literature (Kirchhausen 2012; Reinhard Lipowsky 2013). Ability of protein to cluster lipids and thereby creating a phase separation could be one way. Followed by, the repulsion of charged domains in a tightly packed protein cluster could impart a

curvature to the lipid interacting end of the cluster. In either scenario, sufficient energy is required to overcome the bending rigidity and adhesive nature of lipid bilayer towards the solid support. Like it was mentioned by Shnyrova et al. 2007 and Reinhard Lipowsky 2013, the amount of energy required to bend membranes on SLBs is very high and this energy required is inversely proportional to the area to be bent (Reinhard Lipowsky 2013). In support to our findings, very recently, it was found that HIV-1 matrix protein alone is able to reduce the bending moduli of PI(4,5)P_2 containing membranes and thus lowering the free energy required for membrane structuring (O'Neil et al. 2016).

Chapter-5

Conclusions and Future perspectives

5.1 Conclusions

Lack of a prevention method and advancements in antiretroviral drug therapy made AIDS a chronic and manageable disease. From the first HIV-1 specific antiretroviral drug therapy in 1990s to the current and more advanced combinational therapy (highly active antiretroviral therapy, (HAART)), molecular mechanisms related to one or the other stages in the HIV-1 replication are being targeted (for a detailed review (Arts and Hazuda 2012)). Given the turnover of HIV-1 replication, mathematical modeling suggested that targeting at least two mechanisms through combinational therapy could provide a durable inhibition (Stengel 2008). But, the efficiency of the therapy depends on multiple factors such as drug tolerance, drug-drug interactions and optimal drug levels. Each of these can lead to virologic failure and the evolution of drug resistance. While the pursuit for a prevention strategy is ongoing, current drug resistance levels call for an immediate review of the existing antiretroviral drugs potency in improving the longevity of the HIV-1 infected patients (Iyidogan and Anderson 2014; Siliciano and Siliciano 2013). At this stage, a lot of effort has to be put in for finding new drugs by exploiting novel druggable viral targets (Shafer 2016; Waheed and Tachedjian 2016). Recently, the late stage of HIV-1 replication ie., HIV-1 assembly and maturation, is being considered as a potential target for the development of new class of drugs (Prevelige 2011a; D. Wang, Lu, and Li 2015). HIV-1 Gag protein is the prime orchestrator of new particle assembly. Gag interaction with $PI(4,5)P_2$ lipid present in the inner leaflet of the plasma membrane is the initial step of this process, followed by multimerization of the protein. Targeting these steps could potentially cripple the formation of new viral particles and thus, decrease the number of new infective viral particles produced(Prevelige 2011b; Spearman 2016). To develop a new class of drugs – mechanisms occurring at the molecular-level has to be understood in-depth. Starting from what is already known – so far, through this dissertation – we strived to answer specific questions relevant to the early steps of the HIV-1 Gag assembly ie., the protein ability to interact with specific lipids and the role of protein's multimerization capacity in the assembly process. Using model membranes and purified Gag proteins, we tried to replicate the assembly process *in vitro*. The results of these studies are described in detail in the previous chapters, and the conclusions arising from those results are briefly described below.

5.1.1 Gag can bind to P(4,5)P_2 containing basic composition lipid membranes

Co-sedimentation assay and QCM measurements confirmed that, despite lacking the myristate, the proteins can still be able to interact with PI(4,5)P_2 containing lipid bilayers. Although the MA domain is primarily responsible for HIV-1 Gag binding to the PM, the ten times higher apparent affinity for membrane models observed for FL-Gag, P39 and WM confirms that the NC domains and CA-CA multimerization of Gag are involved in membrane binding efficiency. Indeed, the NC domain of Gag alone has recently been described to bind PI(4,5)P_2 containing lipid membranes with an apparent K*p* as high as 7 μM (Kempf et al. 2015a). It has already been shown that the driving force for membrane association stems largely from ionic interactions between multimerized Gag and negatively charged phospholipids (Dalton et al. 2007). With nearly similar affinity towards PI(4,5)P_2 containing membranes as that of Gag protein and its mutants, EFA6-PH and MARCKS peptide interaction with the lipid bilayers are comparable.

5.1.2 Fluorescence quenching studies revealed the difference in the interaction of protein with PI(4,5)P_2present in lipid bilayers with opposing curvature

Even though the affinity towards PI(4,5)P_2 present in either LUVs or SLBs produced a similar result, fluorescence quenching studies revealed the differential binding of Gag protein to lipid bilayers with opposing curvature. Opposite change in the fluorescence intensity of labelled PI(4,5)P_2 present in the LUV (increasing effect) or SLB (decreasing affect) has been observed upon Gag addition. However, in both cases the change in fluorescence is proportional to the concentration of the protein added – suggesting a concentration dependent nature of the interaction. While there observed no effect of probe type or probe concentration on this opposing result of fluorescence change either in LUVs or in SLBs, FLIM studies presented an interesting explanation. Gag being a multimerizing protein can affect a local curvature by flattening of LUVs and curving of SLBs during the interaction. Thus, this resulted in an opposite change in the fluorescence intensity as the overall quenching of the TF-labelled PI(4,5)P_2 differed with the lipid bilayer curvature. Supporting this hypothesis, MARCKS peptide which is not inducing any curvature is leading to the same overall quenching of TF-PI(4,5)P_2 on flat and curved membranes.

5.1.3 Gag multimerization on lipid bilayers induced the formation of PI(4,5)P_2 nanodomains

In our studies, we found that the multimerization capacity of the protein is enhanced in the presence of lipid membrane when compared to that of in solution. The multimerization property of the mutant, WM, has found here to be only ~2 folds lower to that of FL-Gag on membrane while it was found to be ~ 100 folds in solution. This is important because, Gag protein multimerization not only enhanced the capacity to bind membranes, but also, most importantly, in generating PI(4,5)P_2 enriched lipid nanodomains in the membrane. Another proof regarding the role of multimerization in affecting the clustering of PI(4,5)P_2 on SLBs has been presented with two other proteins. While EFA6-PH being a non-multimerizing protein has not induced any change in the fluorescence intensity of TF-PI(4,5)P_2 containing LUVs or SLBs, MLV Gag protein that has very low multimerization capacity yielded only a very little decrease in the fluorescence intensity on SLBs. All these results proves that multimerization of protein is responsible for clustering of lipids. Further, FRAP experiments on SLBs confirmed the clustering of PI(4,5)P_2 by Gag as the fractional recovery does not reached to 1 after the addition of the protein. Moreover, linescan FCS has also suggested this clustering property of Gag as the diffusion of the lipids varied after the addition of Gag. However, an attempt to visualize the clusters on GUVs produced a uniform binding all over the membrane. But, a fast decorrelation obtained for TF-PI(4,5)P_2 and A594-FL-Gag suggested the presence of PI(4,5)P_2 clusters that are less than 200 nm in size. However, as a general mechanism, it can be concluded that proteins with basic interfaces can recruit acidic lipids that, in turn, can facilitate recruitment and clustering of these proteins into nanodomains (van den Bogaart et al. 2011). A similar cooperative mechanism could also happen when HIV-1 Gag binds to PI(4,5)P_2 during viral assembly at the plasma membrane. Cytoplasmic proteins such as ezrin(Al-Momany et al. 2014; X. Chen et al. 2015), syntaxin-1 (Honigmann et al. 2013) have also been described to induce or interact with PI(4,5)P_2 nanoclusters. Interestingly, the matrix domain of Gag is not able to quench TF-PI(4,5)P_2. This could be that the formed trimers of MA proteins have their PI(4,5)P_2 interacting regions far apart from each other (greater than the affective quenching distance, 50Å) to induce quenching of the clustered PI(4,5)P_2. Although it can be argued that the affinity of the

MA protein is low compared to the FL-Gag, a comparable high concentration has never yielded any change in the fluorescent intensity (either on LUVs or on SLBs).

5.1.4 Gag induces co-clustering of lipids, but excludes Sphingomyelin

It has been shown that cholesterol may facilitate Gag membrane binding and that Gag could sense cholesterol (Barros et al. 2016; Dick et al. 2012). Moreover, cholesterol has also been shown to be crucial for virus infectivity (Shahan Campbell et al. 2004; Hawkes et al. 2015). Although there are still remaining critical issues about the $PI(4,5)P_2$ role in the formation of cholesterol-dependent lipid domains, $PI(4,5)P_2$ could form clusters in the presence of cholesterol alone (Jiang et al. 2014). Our results also show that cholesterol is laterally redistributed during Gag assembly and participate to the formation of cholesterol/$PI(4,5)P_2$/Gag enriched domains. Further, this clustering of lipids is concentration dependent and interestingly is independent of the surrounding lipid chemical nature. In contrast, sphingomyelin is not at all sorted during HIV-1 Gag multimerization – both in simple and complex lipid mixtures. From this result, it can be hypothesized that sphingomyelin as such is not involved directly in the HIV-1 assembly, but it can be trapped later on, like it was proposed earlier (Kerviel et al. 2013b).

5.1.5 Gag assembly occurs in the Liquid disordered phase of the membranes

Experiments on phase separated GUVs revealed the preferred partitioning of Gag ie., in L*d* region where TF-P(4,5)P2 is present. Further, the results of temperature induced phase separation of Gag bound GUVs (phase-separating composition) proved that the protein partitions preferentially into L*d* region. Thus, it can be concluded that Gag multimerization and the associated $PI(4,5)P_2$ enriched nanoclustering mainly occur or, at least, initiate in L*d* phases, i.e., more likely outside of lipid raft domains. The lack of myristate in the different Gag variants tested here could explain the Gag L*d* phase localization (O. Wolf Lindwasser and Resh 2002). Nevertheless, our results are consistent with the L*d* phase GUV localization of multimerizable myristoylated MA protein observed by Keller et al. (Keller, Kräusslich, and Schwille 2013). Since HIV-1 Gag has been often found into detergent resistant membranes (DRM) (Ono and Freed 2001), Gag multimers could partition into rafts after assembly, or rafts could be trapped by

these nascent PI(4,5)P_2-Gag nanodomains through transbilayer lipid interaction, as already proposed (Kerviel et al. 2013b) or as it has been recently shown for GPi anchored proteins (Raghupathy et al. 2015).

5.1.6 QCM-D studies revealed a difference between non-multimerizing and multimerizing proteins

Non-multimerizing proteins like EFA6-PH and MARCKS peptide produced a gradual decrease in the frequency shift (mass adsorption) followed by a plateau. ΔD-ΔF plots of the QCM-D results gave a linear curve for all the different concentrations used. This has shown that the adlayer formed didn't affect the morphology of the protein/lipid bilayer. Low affinity of MA towards PI(4,5)P_2 remained the same even on SLBs. To compensate, higher concentrations of MA protein were tried to attain better binding ratios and multimerizing ability. In spite of this, MA protein tends to behave similar to that of EFA6-PH by producing linear ΔD-ΔF plots. While this result certainly doesn't confirm the formation of multimers of MA, but definitely suggests that MA protein doesn't affect the morphology of the lipid bilayer. QCM-D plot for multimerizing proteins, FL-Gag, P39 and WM resulted in completely different sensorgram profiles from that of the non-multimerizing proteins. This protein binding resulted in decreased frequency shift followed by a sharp increase and ended in a plateau, a three step process. Further, the ΔD-ΔF plots have multiple slopes for these multimerizing proteins. But, at a lower concentration of these multimerizing proteins there observed no such multiple slopes in ΔD-ΔF plots and the frequency shifts is similar to that of non-multimerizing proteins. Thus, concluding that this multimerization property is concentration dependent. Moreover, the bent conformation of the protein also has an effect on the rate of multimerization. Lacking NC and P6 domain, P39 is more linear and doesn't need a conformational change to form multimers. This is clearly evident from the slopes of the frequency shift compared to all the three proteins. This concludes that rate of multimerization is in the order of P39>FL-Gag>WM.

5.1.7 Gag as a minimal system can induce membrane vesiculation and multimerization is responsible for this lipid bilayer deformation.

Fluorescence microscopy of SLBs and GUVs revealed the vesiculation of lipid membranes upon Gag interaction. Except for EFA6-PH, MA and MARCKS peptide, FL-Gag and its mutants that are able to multimerize has shown to bend the membrane. While the Gag proteins are found to cluster $PI(4,5)P_2$, their ability to induce membrane has not been reported before – vesiculation despite lacking myristate and RNA. Both QCM-D and fluorescence microscopic data revealed the role of multimerization on the ability of Gag protein to bend membranes. From the obtained results, it can be concluded that membrane deformation upon Gag interaction is multimerization dependent which is in turn dependent on the concentration of the protein. A linear decrease in the size of the GUVs treated with Gag and the presence of membrane invaginations suggests that membrane vesiculation is also observed on GUVs treated with Gag protein. Additionally, previous literature on membrane vesicle-inducing proteins and polymers presented a similar QCM-D profile. Finally, data from QCM-D and fluorescence microscopy resulted in the conclusion that multimerizing Gag protein can induce membrane vesiculation.

5.2 Future Perspectives

This dissertation work presented the affinity of Gag protein towards $PI(4,5)P_2$ containing lipid bilayers and emphasized the role of Gag multimerization in lipid clustering and membrane deformation for the first time. For the questions asked in section 1.5 and results obtained here supports that the "alternate hypothesis" (as defined in section 1.5) is the mechanism of gag/lipid clustering as proposed by our team earlier (Kerviel et al. 2013b).

This "alternative hypothesis" suggests that the protein is able to bind acidic lipids present in the membrane and induce the formation of lipid clusters. Further, this lipid enrichment could alter the diffusion of lipids present in the membrane and eventually, trap raft components of the outer layer. Figure 5.1 illustrates the possible mechanism that can occur during the HIV-1 Gag assembly process derived from the results obtained in this study. While this work has been

successful in presenting the initial steps of HIV-1 Gag assembly process, whether the lipid enrichment on one side of the lipid bilayer can trap raft components has not been proved, yet. Below are the possible experiments that can provide a definite answer to the question: how sphingomyelin enrichment observed in viral membranes? And what are the possible regulars involved in the size controlling of new viral particles?

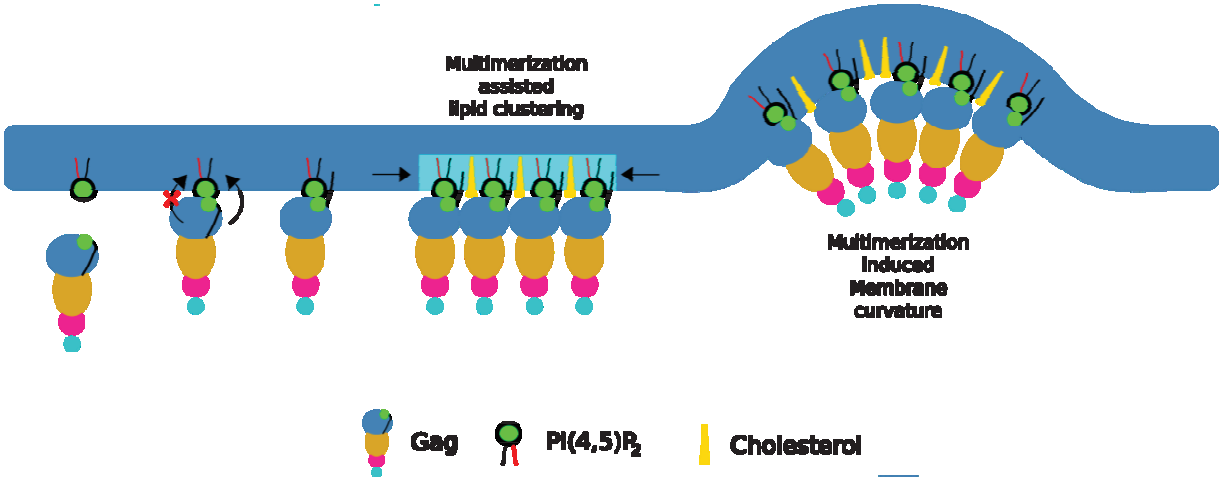

Figure 5.1: Schematic representation of possible assembly mechanism of HIV-1 Gag.

5.2.1 Development of asymmetric lipid bilayers and actin reconstituted lipid bilayers

Asymmetric membranes are the hallmark of plasma membranes. The highly complex lipid compositions of both the monolayers have specific functions. Earlier, lipidomic results of cholesterol and sphingomyelin enrichment in viral membranes has been addressed. Through alternate hypothesis, our team proposed the trapping of these raft components by protein induced lipid domains. To observe this phenomenon, it is important to use asymmetric bilayers similar to that of cellular plasma membrane. Once developed, these bilayers can be used to study multiple different proteins that are known to interact with plasma membrane. Further, to be biologically relevant, reconstitution of actin network could affectively present the complete setting similar to that of the plasma membrane to study the protein-lipid interactions. A possible role of actin in regulating the size of the assembly platform of HIV Gag can be studied. For that it was proposed that actin gets nucleated near $PI(4,5)P_2$ domains and can act as a potential diffusion barrier for $PI(4,5)P_2$pools and nanodomains, thus effectively hindering the fusion of adjacent pools and domains (Arumugam and Bassereau 2015; Trimble and Grinstein 2015).

5.2.2To study the formation of lipid domains and assembly platforms generated by HIV-1 Gag

In-depth knowledge on how the protein forms lipids domains and assembly platforms in the process of developing into a new viral particle could help spot new target regions for antiviral drug development.

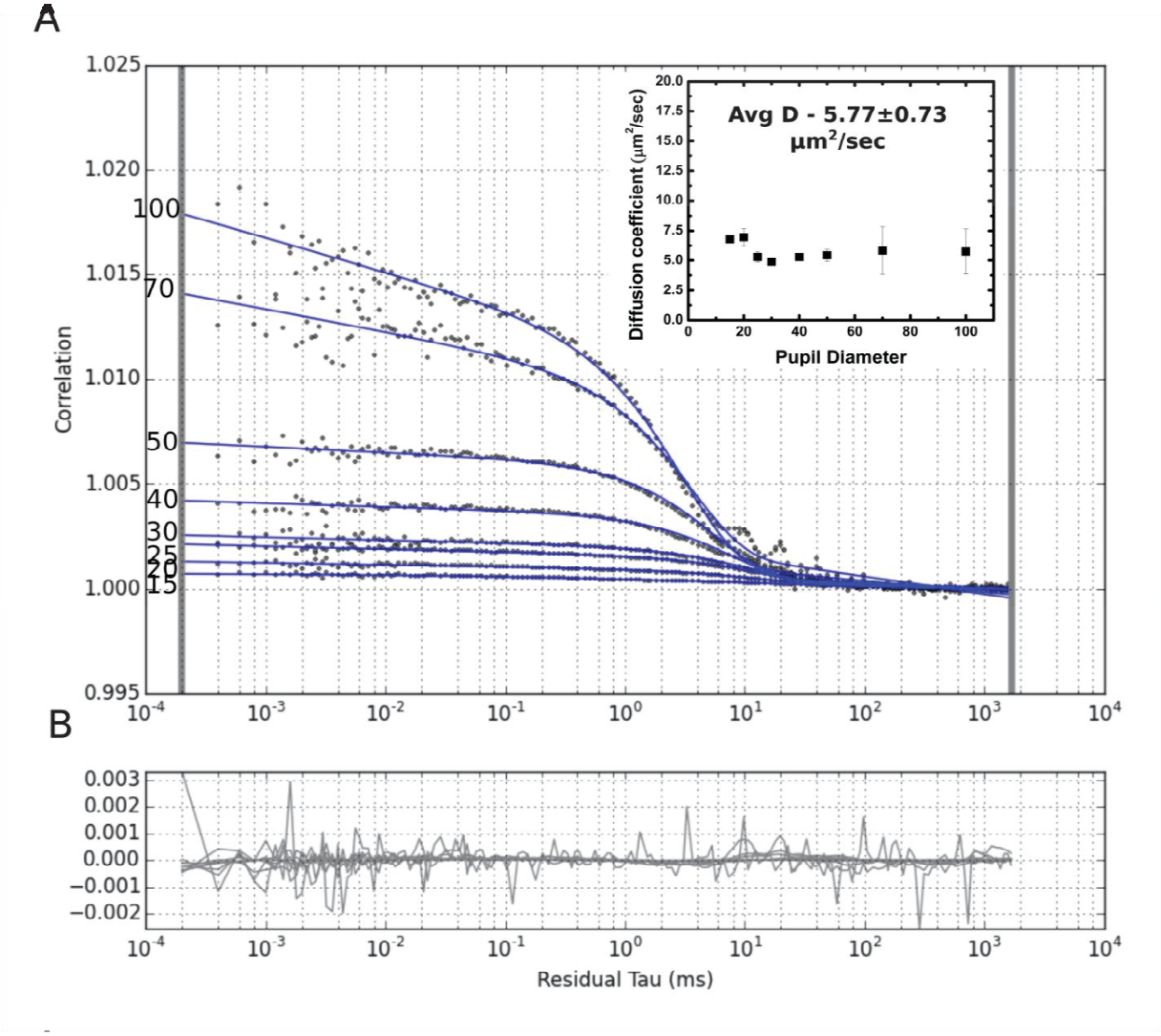

Figure 5.2: svFCScorrelograms obtained for the TF-PIP$_2$ present in basic SLBs. (A) Average autocorrelation curves obtained at different waist lengths. Each autocorrelation curve is obtained from a minimum of 10-20 acquisitions. The obtained diffusion coefficient values are presented in the inset with an average D of 5.77±0.73 µm^2/sec. (B) Near perfect fitting of the autocorrelation curves. svFCS data was processed using the pycorr fit software.

Using techniques such as spot-variation FCS ((Favard et al. 2011; Wawrezinieck et al. 2005)and single molecule methods can dramatically help us understand this process, for they have a resolution as high as 40 nm. Very recently, researchers have employed these super resolution techniques to understand various events in viral replication cycle such as viral disassembly on entry (Yingxin Ma et al. 2016) and viral maturation process in the late phases (Janina Hanne et al. 2016).

We performed spot-variation FCS measurements on TF-PIP_2 labelled basic supported lipid bilayers. It is an interesting method to understand the lipid lateral diffusion as it can provide good resolutions to probe nanoscale domains. As a preliminary study, TF-PIP_2 lateral diffusion in simple basic membranes is studied. After calibrating the system with rhodamine B solution, the ω^2 was determined for all the various pupil widths, 100, 70, 50, 40, 30, 25, 20 and 15. Using this control, the lateral diffusion coefficient for the TF-PIP_2 in supported lipid bilayers was determined. In figure 5.3, a similar plot resulted in a linear curve that deviates slightly from the origin – suggesting the diffusion of the lipid is very much homogenous.

Figure 5.2(A) presents the autocorrelation curves obtained at various pupil radii for the TF labelled $PI(4,5)P_2$. From which lateral diffusion coefficient of the labelled lipid was extracted. Using svFCS, we found that in a simple lipid bilayer with 68% egg PC, 30% brain PS, 1% and brain $PI(4,5)P_2$, the diffusion of the lipid labelled 1% TF-$PI(4,5)P_2$ lipid is 5.77±0.737 μm^2/sec (figure 5.2). Using this preliminary data, the diffusion coefficient of the $PI(4,5)P_2$ in the presence of Gag will be calculated. By gradually increasing the concentration of the Gag protein, it is possible to study the proportion of freely diffusing TF-PIP2 and trapped lipids which extent of lipid trapping property of the protein.

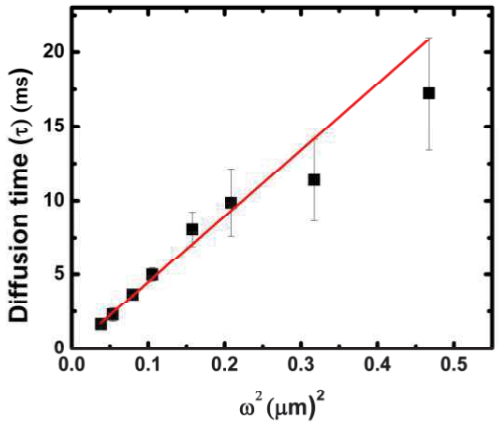

Figure 5.3: svFCS diffusion time of TF-PIP_2 in basic composition SLBs with respect to varying waist radii.

Further, by varying the pupil radii, it is even possible to understand the domain formation induced by Gag protein.

5.2.3 Role of RNA in multimerization and thus, in the formation of lipid domains

Genomic RNA has been shown to be a part of the initial events in HIV-1 assembly (Kutluay and Bieniasz 2010; Roldan et al. 2004). Another study suggested the role of RNA in preventing the Gag from binding to lipids other than PI(4,5)P_2(Chukkapalli, Oh, and Ono 2010). Very recently, two different studies were performed to understand the role of viral RNA enrichment in new particle formation (Carlson et al. 2016) and RNA requirement in Gag-mediated budding (Gui et al. 2015) using *in vitro* models. While the earlier study hasn't reported the formation of membrane deformations, the later suggested that RNA is necessary for the formation of membrane budding and non-myristoylated Gag/Gag CA protein alone doesn't induce any membrane invaginations. While our observations are opposite to that of Gui et al. 2015(Gui et al. 2015), the authors of that study has not shown whether the non-myristate Gag is able to bind the lipid bilayers either in the presence of RNA or in its absence. Further, it is well known that urea is a chaotropic agent and using the reaction buffer could potentially denaturate the protein (Bennion and Daggett 2003; Yamaguchi and Miyazaki 2014). This questions the results obtained in the presence of urea for both myristate Gag and non-myristate Gag shown in this study. Nevertheless, the results of myristate Gag induced budding in the presence of RNA further emphasize the role of RNA in the HIV-1 assembly process. But, it is yet to be established for its role in multimerization and even viral size regulation, if any. Thus, studying the role of genomic RNA in HIV-1 assembly could also present a potential target for antiviral drug development.

5.2.4 Cell based studies with labelled lipids and Gag protein

In vitro studies, using biomimetic membranes is often used to understand specific interactions between molecules of relevance. These *in vitro* studies can act as stepping stones in understanding a complex process that is occurring in cells. While deciphering the pieces in a puzzle using model membranes, ultimately, *in cellulo* studies will provide a holistic picture and substantial proof for the results obtained on minimalistic model membranes. Especially,

dynamics of lipids *in cellulo* is completely different from that of the model membranes due to the high complex nature of the plasma membrane. So, studying the lipid domain formation by assembly platforms in relevant cell lines is still a challenge to overcome.

References

Accola, M A, B Strack, and H G Göttlinger. 2000. "Efficient Particle Production by Minimal Gag Constructs Which Retain the Carboxy-Terminal Domain of Human Immunodeficiency Virus Type 1 Capsid-p2 and a Late Assembly Domain." *Journal of virology* 74(12): 5395–5402.

Adams, Peter G. et al. 2014. "Lipopolysaccharide-Induced Dynamic Lipid Membrane Reorganization: Tubules, Perforations, and Stacks." *Biophysical Journal* 106(11): 2395–2407.

Alajlouni, Ruba, Karen E. Drahos, Carla V. Finkielstein, and Daniel G S Capelluto. 2011. "Lipid-Mediated Membrane Binding Properties of Disabled-2." *Biochimica et Biophysica Acta - Biomembranes* 1808(11): 2734–44.

Alfadhli, Ayna et al. 2007. "Human Immunodeficiency Virus Type 1 Matrix Protein Assembles on Membranes as a Hexamer." *Journal of virology* 81(3): 1472–78.

Alfadhli, Ayna, Robin Lid Barklis, and Eric Barklis. 2009. "HIV-1 Matrix Organizes as a Hexamer of Trimers on Membranes Containing Phosphatidylinositol-(4,5)-Bisphosphate." *Virology* 387(2): 466–72. http://linkinghub.elsevier.com/retrieve/pii/S0042682209001524 (March 9, 2016).

Allender, D W, and M Schick. 2006. "Phase Separation in Bilayer Lipid Membranes: Effects on the Inner Leaf due to Coupling to the Outer Leaf." *Biophysical journal* 91(8): 2928–35.

Al-Momany, a., L. Li, R. T. Alexander, and B. J. Ballermann. 2014. "Clustered PI(4,5)P2 Accumulation and Ezrin Phosphorylation in Response to CLIC5A." *Journal of Cell Science* 127(24): 5164–78. http://jcs.biologists.org/cgi/doi/10.1242/jcs.147744.

Aloia, R. C., Curtain, C. C. & Jensen, F. C. 1992. "Advances in Membrane Fluidity." In ed. C. C. Aloia, R. C. & Curtain. NewYork: Wiley-Liss, 283–304.

Aloia, R C et al. 1988. "Lipid Composition and Fluidity of the Human Immunodeficiency Virus." *Proceedings of the National Academy of Sciences of the United States of America* 85(3): 900–904. http://www.ncbi.nlm.nih.gov/pubmed/2829209 (June 1, 2016).

Aloia, R C, H Tian, and F C Jensen. 1993. "Lipid Composition and Fluidity of the Human Immunodeficiency Virus Envelope and Host Cell Plasma Membranes." *Proceedings of the National Academy of Sciences of the United States of America* 90(11): 5181–85. http://www.ncbi.nlm.nih.gov/pubmed/8389472 (June 1, 2016).

Alves, Natália M, Catherine Picart, and João F Mano. 2009. "Self Assembling and Crosslinking of Polyelectrolyte Multilayer Films of Chitosan and Alginate Studied by QCM and IR Spectroscopy." *Macromolecular Bioscience* 9: 776–85. http://www.ncbi.nlm.nih.gov/pubmed/19340816.

Anraku, Kensaku et al. 2010. "Highly Sensitive Analysis of the Interaction between HIV-1 Gag and Phosphoinositide Derivatives Based on Surface Plasmon Resonance." *Biochemistry* 49(25): 5109–16. http://www.ncbi.nlm.nih.gov/pubmed/20496925 (October 1, 2014).

Arouri, Ahmad et al. 2010. "Morphological Changes Induced by the Action of Antimicrobial Peptides on Supported Lipid Bilayers." *J. Phys. Chem. B* 115(1): 158–67. http://dx.doi.org/10.1021/jp107577k.

Arts, Eric J., and Daria J. Hazuda. 2012. "HIV-1 Antiretroviral Drug Therapy." *Cold Spring Harbor Perspectives in Medicine* 2(4).

Arumugam, Senthil, and Patricia Bassereau. 2015. "Membrane Nanodomains: Contribution of Curvature and Interaction with Proteins and Cytoskeleton." *Essays in biochemistry* 57: 109–19. http://essays.biochemistry.org/content/57/109.abstract.

Bacia, Kirsten, Dag Scherfeld, Nicoletta Kahya, and Petra Schwille. 2004. "Fluorescence

Correlation Spectroscopy Relates Rafts in Model and Native Membranes." *Biophysical journal* 87(2): 1034–43. http://dx.doi.org/10.1529/biophysj.104.040519.

Bailey, Christina M et al. 2015. "Size Dependence of Gold Nanoparticle Interactions with a Supported Lipid Bilayer: A QCM-D Study." *Biophysical chemistry* 203–204: 51–61. http://www.sciencedirect.com/science/article/pii/S0301462215001052.

Barrera, F N, E Hurtado-Gomez, M C Lidon-Moya, and J L Neira. 2006. "Binding of the C-Terminal Domain of the HIV-1 Capsid Protein to Lipid Membranes: A Biophysical Characterization." *Biochemical Journal* 394: 345–53. ISI:000235476700038.

Barros, Marilia et al. 2016. "Membrane Binding of HIV-1 Matrix Protein: Dependence on Bilayer Composition and Protein Lipidation." *Biophysical Journal* 110(3): 577a. http://www.sciencedirect.com/science/article/pii/S0006349515042678.

Bastiaanse, E M, K M Höld, and A Van der Laarse. 1997. "The Effect of Membrane Cholesterol Content on Ion Transport Processes in Plasma Membranes." *Cardiovascular research* 33(2): 272–83.

Baumann, Martina K., Marcus J. Swann, Marcus Textor, and Erik Reimhult. 2011. "Pleckstrin Homology-Phospholipase C-δ 1 Interaction with Phosphatidylinositol 4,5-Bisphosphate Containing Supported Lipid Bilayers Monitored in Situ with Dual Polarization Interferometry." *Analytical Chemistry* 83(16): 6267–74.

Bennion, Brian J, and Valerie Daggett. 2003. "The Molecular Basis for the Chemical Denaturation of Proteins by Urea." *Proceedings of the National Academy of Sciences of the United States of America* 100(9): 5142–47. http://www.pnas.org/content/100/9/5142.full.

Ben-Tal, N, B Honig, C Miller, and S McLaughlin. 1997. "Electrostatic Binding of Proteins to Membranes. Theoretical Predictions and Experimental Results with Charybdotoxin and Phospholipid Vesicles." *Biophysical journal* 73(4): 1717–27. http://www.ncbi.nlm.nih.gov/pubmed/9336168 (June 1, 2016).

Bharat, Tanmay a M et al. 2014. "Cryo-Electron Microscopy of Tubular Arrays of HIV-1 Gag Resolves Structures Essential for Immature Virus Assembly." *Proceedings of the National Academy of Sciences of the United States of America* 111(22): 8233–38. http://www.pubmedcentral.nih.gov/articlerender.fcgi?artid=4050629&tool=pmcentrez&rendertype=abstract.

Bhattacharya, Jayanta, Alexander Repik, and Paul R Clapham. 2006. "Gag Regulates Association of Human Immunodeficiency Virus Type 1 Envelope with Detergent-Resistant Membranes." *Journal of virology* 80(11): 5292–5300. http://www.ncbi.nlm.nih.gov/pubmed/16699009 (June 1, 2016).

Blin, Guillaume et al. 2008. "Quantitative Analysis of the Binding of Ezrin to Large Unilamellar Vesicles Containing Phosphatidylinositol 4,5 Bisphosphate." *Biophysical journal* 94(3): 1021–33. http://www.pubmedcentral.nih.gov/articlerender.fcgi?artid=2186265&tool=pmcentrez&rendertype=abstract (October 1, 2014).

Blom, T. S. et al. 2001. "Mass Spectrometric Analysis Reveals an Increase in Plasma Membrane Polyunsaturated Phospholipid Species upon Cellular Cholesterol Loading." *Biochemistry* 40(48): 14635–44.

Bocanegra, Rebeca et al. 2013. "Association Equilibrium of the HIV-1 Capsid Protein in a Crowded Medium Reveals That Hexamerization during Capsid Assembly Requires a Functional C-Domain Dimerization Interface." *Biophysical journal* 104(4): 884–93. http://www.ncbi.nlm.nih.gov/pubmed/23442967 (September 2, 2016).

van den Bogaart, Geert et al. 2011. "Membrane Protein Sequestering by Ionic Protein–lipid Interactions." *Nature* 479(7374): 552–55.

Boldyrev, I A et al. 2007. "New BODIPY Lipid Probes for Fluorescence Studies of Membranes." *J Lipid Res* 48(7): 1518–32. http://www.ncbi.nlm.nih.gov/pubmed/17416929.

Bowzard, J Bradford et al. 1998. "Importance of Basic Residues in the Nucleocapsid Sequence for Retrovirus Gag Assembly and Complementation Rescue." *Journal of virology* 72(11): 9034–44. http://www.pubmedcentral.nih.gov/articlerender.fcgi?artid=110320&tool=pmcentrez&rendertype=abstract.

Brown, Deborah A., and John K. Rose. 1992. "Sorting of GPI-Anchored Proteins to Glycolipid-Enriched Membrane Subdomains during Transport to the Apical Cell Surface." *Cell* 68(3): 533–44.

Brügger, Britta et al. 2006. "The HIV Lipidome: A Raft with an Unusual Composition." *Proceedings of the National Academy of Sciences of the United States of America* 103(8): 2641–46. http://www.ncbi.nlm.nih.gov/pubmed/16481622 (June 1, 2016).

Bryant, Martin, and L Ratner. 1990. "Myristoylation-Dependent Replication and Assembly of Human Immunodeficiency Virus 1." *... of the National Academy of Sciences* 87(January): 523–27. http://www.pnas.org/content/87/2/523.short (November 5, 2014).

Burniston, M T et al. 1999. "Human Immunodeficiency Virus Type 1 Gag Polyprotein Multimerization Requires the Nucleocapsid Domain and RNA and Is Promoted by the Capsid-Dimer Interface and the Basic Region of Matrix Protein." *Journal of virology* 73(10): 8527–40. http://www.pubmedcentral.nih.gov/articlerender.fcgi?artid=112873&tool=pmcentrez&rendertype=abstract.

Bush, Di L., and Volker M. Vogt. 2014. "In Vitro Assembly of Retroviruses." *Annual Review of Virology* 1(1): 561–80. http://www.jbc.org/content/early/2014/08/22/jbc.M114.596148.abstract\nhttp://www.annualreviews.org/doi/abs/10.1146/annurev-virology-031413-085427.

Callahan, E M, and J W Wills. 2000. "Repositioning Basic Residues in the M Domain of the Rous Sarcoma Virus Gag Protein." *J.Virol.* 74(23): 11222–29.

Campbell, S et al. 2001a. "Modulation of HIV-like Particle Assembly in Vitro by Inositol Phosphates." *Proceedings of the National Academy of Sciences* 98(19): 10875–79.

———. 2001b. "Modulation of HIV-like Particle Assembly in Vitro by Inositol Phosphates." *Proceedings of the National Academy of Sciences* 98(19): 10875–79. http://www.pnas.org/cgi/doi/10.1073/pnas.191224698.

Campbell, S, and A Rein. 1999. "In Vitro Assembly Properties of Human Immunodeficiency Virus Type 1 Gag Protein Lacking the p6 Domain." *Journal of virology* 73(3): 2270–79. http://www.pubmedcentral.nih.gov/articlerender.fcgi?artid=104472&tool=pmcentrez&rendertype=abstract.

Campbell, Shahan et al. 2004. "The Raft-Promoting Property of Virion-Associated Cholesterol, but Not the Presence of Virion-Associated Brij 98 Rafts, Is a Determinant of Human Immunodeficiency Virus Type 1 Infectivity." *Journal of virology* 78(19): 10556–65.

Cantor, Robert S. 1997. "Lateral Pressures in Cell Membranes: A Mechanism for Modulation of Protein Function." *The Journal of Physical Chemistry B* 101(10): 1723–25. http://pubs.acs.org/doi/abs/10.1021/jp963911x (June 1, 2016).

Carlson, Lars-Anders et al. 2016. "Reconstitution of Selective HIV-1 RNA Packaging in Vitro

by Membrane-Bound Gag Assemblies." *eLife* 5. http://elifesciences.org/lookup/doi/10.7554/eLife.14663.

Catimel, Bruno et al. 2008. "The PI(3,5)P2 and PI(4,5)P2 Interactomes." *Journal of Proteome Research* 7(12): 5295–5313.

Centers for Disease Control (CDC). 1981. "Kaposi's Sarcoma and Pneumocystis Pneumonia among Homosexual Men - New York and California." *Morbidity and Mortality Weekly Report (MMWR)* 30(25): 305–8.

Chan, Robin et al. 2008a. "Retroviruses Human Immunodeficiency Virus and Murine Leukemia Virus Are Enriched in Phosphoinositides." *Journal of virology* 82(22): 11228–38. http://www.ncbi.nlm.nih.gov/pubmed/18799574 (June 2, 2016).

———. 2008b. "Retroviruses Human Immunodeficiency Virus and Murine Leukemia Virus Are Enriched in Phosphoinositides." *Journal of virology* 82(22): 11228–38. http://www.ncbi.nlm.nih.gov/pubmed/18799574 (June 1, 2016).

Charlier, Landry et al. 2014. "Coarse-Grained Simulations of the HIV-1 Matrix Protein Anchoring: Revisiting Its Assembly on Membrane Domains." *Biophysical journal* 106(3): 577–85. http://www.ncbi.nlm.nih.gov/pubmed/24507598 (June 2, 2016).

Chen, Kang et al. 2008. "Solution NMR Characterizations of Oligomerization and Dynamics of Equine Infectious Anemia Virus Matrix Protein and Its Interaction with PIP2." *Biochemistry* 47(7): 1928–37.

Chen, Xiaodong et al. 2015. "Phosphatidylinositol 4,5-Bisphosphate Clusters the Cell Adhesion Molecule CD44 and Assembles a Specific CD44-Ezrin Heterocomplex, as Revealed by Small Angle Neutron Scattering." *The Journal of biological chemistry* 290(10): 6639–52. http://www.ncbi.nlm.nih.gov/pubmed/25572402 (July 21, 2016).

Chen, Yong et al. 2012. "Genome-Wide Functional Annotation of Dual-Specificity Protein- and Lipid-Binding Modules That Regulate Protein Interactions." *Molecular Cell* 46(2): 226–37.

Cheng, Cathy I, Yi-Pin Chang, and Yen-Ho Chu. 2012. "Biomolecular Interactions and Tools for Their Recognition: Focus on the Quartz Crystal Microbalance and Its Diverse Surface Chemistries and Applications." *Chemical Society reviews* 41(5): 1947–71. http://www.ncbi.nlm.nih.gov/pubmed/22158962.

Cho, Nam-Joon et al. 2007. "Binding Dynamics of Hepatitis C Virus' NS5A Amphipathic Peptide to Cell and Model Membranes." *Journal of virology* 81(12): 6682–89. http://www.pubmedcentral.nih.gov/articlerender.fcgi?artid=1900085&tool=pmcentrez&rendertype=abstract.

Cho, Nam-Joon, Curtis W Frank, Bengt Kasemo, and Fredrik Höök. 2010. "Quartz Crystal Microbalance with Dissipation Monitoring of Supported Lipid Bilayers on Various Substrates." *Nat. Protoc.* 5(6): 1096–1106. http://www.ncbi.nlm.nih.gov/pubmed/20539285.

Cho, Wonhwa, and Robert V Stahelin. 2005. "Membrane-Protein Interactions in Cell Signaling and Membrane Trafficking." *Annual review of biophysics and biomolecular structure* 34: 119–51. http://www.ncbi.nlm.nih.gov/pubmed/15869386 (June 1, 2016).

Chukkapalli, Vineela et al. 2008. "Interaction between the Human Immunodeficiency Virus Type 1 Gag Matrix Domain and Phosphatidylinositol-(4,5)-Bisphosphate Is Essential for Efficient Gag Membrane Binding." *Journal of virology* 82(5): 2405–17. http://www.ncbi.nlm.nih.gov/pubmed/18094158 (June 2, 2016).

Chukkapalli, Vineela, Seung J Oh, and Akira Ono. 2010. "Opposing Mechanisms Involving RNA and Lipids Regulate HIV-1 Gag Membrane Binding through the Highly Basic Region

of the Matrix Domain." *Proceedings of the National Academy of Sciences of the United States of America* 107(4): 1600–1605.
Chukkapalli, Vineela, and Akira Ono. 2011. "Molecular Determinants That Regulate Plasma Membrane Association of HIV-1 Gag." *Journal of Molecular Biology* 410(4): 512–24.
Cockcroft, Shamshad. 2007. "Trafficking of Phosphatidylinositol by Phosphatidylinositol Transfer Proteins." *Biochemical Society symposium* (74): 259–71. http://www.ncbi.nlm.nih.gov/pubmed/17233595.
Cooper, Matthew A., and Victoria T. Singleton. 2007. "A Survey of the 2001 to 2005 Quartz Crystal Microbalance Biosensor Literature: Applications of Acoustic Physics to the Analysis of Biomolecular Interactions." *Journal of Molecular Recognition* 20(3): 154–84.
Corbalan-Garcia, Senena, and Juan C. Gómez-Fernández. 2014. "Signaling through C2 Domains: More than One Lipid Target." *Biochimica et Biophysica Acta - Biomembranes* 1838(6): 1536–47.
Crane, Jonathan M, and Lukas K Tamm. 2004. "Role of Cholesterol in the Formation and Nature of Lipid Rafts in Planar and Spherical Model Membranes." *Biophysical journal* 86(5): 2965–79. http://www.sciencedirect.com/science/article/pii/S0006349504743477.
Dalton, Amanda K et al. 2007. "Electrostatic Interactions Drive Membrane Association of the Human Immunodeficiency Virus Type 1 Gag MA Domain." *Journal of virology* 81(12): 6434–45.
Dalton, Amanda K, P. S. Murray, Diana Murray, and Volker M Vogt. 2005. "Biochemical Characterization of Rous Sarcoma Virus MA Protein Interaction with Membranes." *Journal of Virology* 79(10): 6227–38. http://www.ncbi.nlm.nih.gov/pubmed/15858007\nhttp://www.pubmedcentral.nih.gov/articlerender.fcgi?artid=PMC1091718\nhttp://jvi.asm.org/cgi/doi/10.1128/JVI.79.10.6227-6238.2005.
Datta, Siddhartha A.K., Joseph E. Curtis, et al. 2007a. "Conformation of the HIV-1 Gag Protein in Solution." *Journal of Molecular Biology* 365(3): 812–24. http://linkinghub.elsevier.com/retrieve/pii/S0022283606014537 (March 17, 2016).
Datta, Siddhartha A.K., Zhuojun Zhao, et al. 2007. "Interactions between HIV-1 Gag Molecules in Solution: An Inositol Phosphate-Mediated Switch." *Journal of Molecular Biology* 365(3): 799–811.
Datta, Siddhartha A K, Joseph E. Curtis, et al. 2007b. "Conformation of the HIV-1 Gag Protein in Solution." *Journal of Molecular Biology* 365(3): 812–24.
Datta, Siddhartha A K et al. 2011. "Solution Properties of Murine Leukemia Virus Gag Protein: Differences from HIV-1 Gag." *Journal of virology* 85(23): 12733–41. http://www.pubmedcentral.nih.gov/articlerender.fcgi?artid=3209342&tool=pmcentrez&rendertype=abstract.
Daum, Bertram et al. 2016. "Supramolecular Organization of the Human N-BAR Domain in Shaping the Sarcolemma Membrane." *Journal of Structural Biology* 194(3): 375–82.
Deshmukh, Lalit, Rodolfo Ghirlando, and G Marius Clore. 2015. "Conformation and Dynamics of the Gag Polyprotein of the Human Immunodeficiency Virus 1 Studied by NMR Spectroscopy." *Proceedings of the National Academy of Sciences of the United States of America* 112(11): 3374–79. http://www.ncbi.nlm.nih.gov/pubmed/25713345 (March 17, 2016).
Diaz-Griffero, Felipe et al. 2007. "Comparative Requirements for the Restriction of Retrovirus Infection by TRIM5?? And TRIMCyp." *Virology* 369(2): 400–410.

Dick, Robert a, Shih Lin Goh, Gerald W Feigenson, and Volker M Vogt. 2012. "HIV-1 Gag Protein Can Sense the Cholesterol and Acyl Chain Environment in Model Membranes." *Proceedings of the National Academy of Sciences of the United States of America* 109(46): 18761–66. http://www.pubmedcentral.nih.gov/articlerender.fcgi?artid=3503231&tool=pmcentrez&rendertype=abstract (October 1, 2014).

Dippold, Holly C. et al. 2009. "GOLPH3 Bridges Phosphatidylinositol-4- Phosphate and Actomyosin to Stretch and Shape the Golgi to Promote Budding." *Cell* 139(2): 337–51.

Dixon, Matthew C. 2008. "Quartz Crystal Microbalance with Dissipation Monitoring: Enabling Real-Time Characterization of Biological Materials and Their Interactions." *Journal of Biomolecular Techniques* 19(3): 151–58.

Döbereiner, H G et al. 1993. "Budding and Fission of Vesicles." *Biophysical journal* 65(4): 1396–1403. http://www.pubmedcentral.nih.gov/articlerender.fcgi?artid=1225866&tool=pmcentrez&rendertype=abstract.

Drücker, Patrick, Milena Pejic, Hans-Joachim Galla, and Volker Gerke. 2013. "Lipid Segregation and Membrane Budding Induced by the Peripheral Membrane Binding Protein Annexin A2." *The Journal of biological chemistry* 288(34): 24764–76. http://www.pubmedcentral.nih.gov/articlerender.fcgi?artid=3750172&tool=pmcentrez&rendertype=abstract (October 30, 2014).

Edition, Third. *Principles of Fluorescence Spectroscopy*.

Ellenbroek, Wouter G et al. 2011. "Divalent Cation-Dependent Formation of Electrostatic PIP2 Clusters in Lipid Monolayers." *Biophysical journal* 101(9): 2178–84. http://www.ncbi.nlm.nih.gov/pubmed/22067156 (June 2, 2016).

Faini, Marco, Rainer Beck, Felix T. Wieland, and John A G Briggs. 2013. "Vesicle Coats: Structure, Function, and General Principles of Assembly." *Trends in Cell Biology* 23(6): 279–88.

Faivre-Moskalenko, Cendrine et al. 2014. "RNA Control of HIV-1 Particle Size Polydispersity." *PLoS ONE* 9(1).

Falkenburger, Björn H, Jill B Jensen, and Bertil Hille. 2010. "Kinetics of M1 Muscarinic Receptor and G Protein Signaling to Phospholipase C in Living Cells." *The Journal of general physiology* 135(2): 99–114. http://www.pubmedcentral.nih.gov/articlerender.fcgi?artid=2812502&tool=pmcentrez&rendertype=abstract.

Faria, N. R. et al. 2014. "The Early Spread and Epidemic Ignition of HIV-1 in Human Populations." *Science* 346(6205): 56–61.

Favard, Cyril, J??r??me Wenger, Pierre Fran??ois Lenne, and Herv?? Rigneault. 2011. "FCS Diffusion Laws in Two-Phase Lipid Membranes: Determination of Domain Mean Size by Experiments and Monte Carlo Simulations." *Biophysical Journal* 100(5): 1242–51.

Feigenson, Gerald W. 2007. "Phase Boundaries and Biological Membranes." *Annual review of biophysics and biomolecular structure* 36: 63–77. http://www.pubmedcentral.nih.gov/articlerender.fcgi?artid=2642956&tool=pmcentrez&rendertype=abstract.

Feigenson, Gerald W. 2009. "Phase Diagrams and Lipid Domains in Multicomponent Lipid Bilayer Mixtures." *Biochimica et Biophysica Acta - Biomembranes* 1788(1): 47–52.

Ferguson, Shawn M, and Pietro De Camilli. 2012. "Dynamin, a Membrane-Remodelling

GTPase." *Nature reviews. Molecular cell biology* 13(2): 75–88. http://www.pubmedcentral.nih.gov/articlerender.fcgi?artid=3674567&tool=pmcentrez&rendertype=abstract\nhttp://www.ncbi.nlm.nih.gov/pubmed/22233676\nhttp://www.pubmedcentral.nih.gov/articlerender.fcgi?artid=PMC3519936.

Forshey, Brett M, Uta von Schwedler, Wesley I Sundquist, and Christopher Aiken. 2002. "Formation of a Human Immunodeficiency Virus Type 1 Core of Optimal Stability Is Crucial for Viral Replication." *Journal of virology* 76(11): 5667–77. http://www.pubmedcentral.nih.gov/articlerender.fcgi?artid=137032&tool=pmcentrez&rendertype=abstract.

Freed, Eric O. 2015. "HIV-1 Assembly, Release and Maturation." *Nature reviews. Microbiology* 13(8): 484–96. http://www.ncbi.nlm.nih.gov/pubmed/26119571 (June 1, 2016).

Fujii, Ken, James H Hurley, and Eric O Freed. 2007. "Beyond Tsg101: The Role of Alix in 'ESCRTing' HIV-1." *Nature reviews. Microbiology* 5(12): 912–16.

Fung, Bernard Kwok-Keung, and Lubert Stryer. 1978. "Surface Density Determination in Membranes by Fluorescence Energy Transfer." *Biochemistry* 17(24): 5241–48. http://www.ncbi.nlm.nih.gov/pubmed/728398\nhttp://pubs.acs.org/doi/abs/10.1021/bi00617a025.

Gambhir, Alok, Gyöngyi Hangyás-Mihályné, Irina Zaitseva, David S Cafiso, Jiyao Wang, Diana Murray, Srinivas N Pentyala, Steven O Smith, Stuart McLaughlin, et al. 2004. "Electrostatic Sequestration of PIP2 on Phospholipid Membranes by Basic/Aromatic Regions of Proteins." *Biophysical journal* 86(4): 2188–2207. http://linkinghub.elsevier.com/retrieve/pii/S0006349504742782.

———. 2004. "Electrostatic Sequestration of PIP2 on Phospholipid Membranes by Basic/aromatic Regions of Proteins." *Biophysical journal* 86(4): 2188–2207. http://www.ncbi.nlm.nih.gov/pubmed/15041659 (March 18, 2016).

Gamble, Theresa R. et al. 1997. "Structure of the Carboxyl-Terminal Dimerization Domain of the HIV-1 Capsid Protein." *Science (New York, N.Y.)* 278(5339): 849–53.

Gamper, Nikita, and Mark S. Shapiro. 2007. "Target-Specific PIP 2 Signalling: How Might It Work?" *The Journal of Physiology* 582(3): 967–75. http://www.pubmedcentral.nih.gov/articlerender.fcgi?artid=2075238&tool=pmcentrez&rendertype=abstract.

Ganser-Pornillos, Barbie K et al. 2004. "Assembly Properties of the Human Immunodeficiency Virus Type 1 CA Protein." *Journal of virology* 78(5): 2545–52. http://www.pubmedcentral.nih.gov/articlerender.fcgi?artid=369201&tool=pmcentrez&rendertype=abstract.

Gay, B et al. 1998. "Morphopoietic Determinants of HIV-1 Gag Particles Assembled in Baculovirus-Infected Cells." *Virology* 247(2): 160–69. http://www.ncbi.nlm.nih.gov/pubmed/9705909.

Gentile, M et al. 1994. "Determination of the Size of HIV Using Adenovirus Type 2 as an Internal Length Marker." *Journal of virological methods* 48(1): 43–52. http://www.ncbi.nlm.nih.gov/pubmed/7962259.

Gericke, Arne, Nicholas R. Leslie, Mathias Lösche, and Alonzo H. Ross. 2013. "PtdIns(4,5)P2-Mediated Cell Signaling: Emerging Principles and PTEN as a Paradigm for Regulatory Mechanism." *Advances in Experimental Medicine and Biology* 991: 85–104.

Gil, T et al. 1998. "Theoretical Analysis of Protein Organization in Lipid Membranes." *Biochimica et biophysica acta* 1376(3): 245–66.

http://www.ncbi.nlm.nih.gov/pubmed/9804966 (June 1, 2016).
Gokhale, Nikhil a et al. 2005. "Phosphoinositide Specificity of and Mechanism of Lipid Domain Formation by Annexin A2-p11 Heterotetramer." *The Journal of biological chemistry* 280(52): 42831–40. http://www.ncbi.nlm.nih.gov/pubmed/16230353 (October 1, 2014).
Gonen, T et al. 2005. "Lipid-Protein Interactions in Double-Layered Two-Dimensional AQPO Crystals." *Nature* 438(December): 633–38. <Go to ISI>://000233593100042.
Göttlinger, H G, T Dorfman, J G Sodroski, and W a Haseltine. 1991. "Effect of Mutations Affecting the p6 Gag Protein on Human Immunodeficiency Virus Particle Release." *Proceedings of the National Academy of Sciences of the United States of America* 88(8): 3195–99.
Grigorov, Boyan et al. 2009. "A Role for CD81 on the Late Steps of HIV-1 Replication in a Chronically Infected T Cell Line." *Retrovirology* 6: 28. http://www.ncbi.nlm.nih.gov/pubmed/19284574 (June 2, 2016).
Gross, I et al. 2000. "A Conformational Switch Controlling HIV-1 Morphogenesis." *The EMBO journal* 19(1): 103–13. http://www.pubmedcentral.nih.gov/articlerender.fcgi?artid=1171782&tool=pmcentrez&rendertype=abstract.
Grover, Jonathan R et al. 2013. "Roles Played by Capsid-Dependent Induction of Membrane Curvature and Gag-ESCRT Interactions in Tetherin Recruitment to HIV-1 Assembly Sites." *Journal of Virology* 87(8): 4650–64. http://jvi.asm.org/content/87/8/4650.abstract.
Gui, Dong et al. 2015. "A Novel Minimal in Vitro System for Analyzing HIV-1 Gag-Mediated Budding." *Journal of Biological Physics* 41(2): 135–49. http://link.springer.com/10.1007/s10867-014-9370-z.
Hamard-Peron, E et al. 2010a. "Targeting of Murine Leukemia Virus Gag to the Plasma Membrane Is Mediated by PI(4,5)P2/PS and a Polybasic Region in the Matrix." *Journal of Virology* 84(1): 503–15. http://jvi.asm.org/cgi/doi/10.1128/JVI.01134-09.
———. 2010b. "Targeting of Murine Leukemia Virus Gag to the Plasma Membrane Is Mediated by PI(4,5)P2/PS and a Polybasic Region in the Matrix." *Journal of virology* 84(1): 503–15. http://www.ncbi.nlm.nih.gov/pubmed/19828619 (June 2, 2016).
Hamard-Peron, Elise, and Delphine Muriaux. 2011. "Retroviral Matrix and Lipids, the Intimate Interaction." *Retrovirology* 8(1): 15. http://www.pubmedcentral.nih.gov/articlerender.fcgi?artid=3059298&tool=pmcentrez&rendertype=abstract (October 13, 2014).
Hanada, K., M. Nishijima, Y. Akamatsu, and R. E. Pagano. 1995. "Both Sphingolipids and Cholesterol Participate in the Detergent Insolubility of Alkaline Phosphatase, a Glycosylphosphatidylinositol-Anchored Protein, in Mammalian Membranes." *Journal of Biological Chemistry* 270(11): 6254–60.
Harrist, Alexia V., Elena V. Ryzhova, Thomas Harvey, and Francisco Gonz??lez-Scarano. 2009. "Anx2 Interacts with HIV-1 Gag at Phosphatidylinositol (4,5) Bisphosphate-Containing Lipid Rafts and Increases Viral Production in 293T Cells." *PLoS ONE* 4(3).
Hawkes, David et al. 2015. "Properties of HIV-1 Associated Cholesterol in Addition to Raft Formation Are Important for Virus Infection." *Virus Research* 210: 18–21.
Heimburg, T, B Angerstein, and D Marsh. 1999. "Binding of Peripheral Proteins to Mixed Lipid Membranes: Effect of Lipid Demixing upon Binding." *Biophysical journal* 76(5): 2575–86. http://www.ncbi.nlm.nih.gov/pubmed/10233072 (June 1, 2016).
Helfrich, W. 1986. "Size Distributions of Vesicles : The Role of the Effective Rigidity of

Membranes." *Journal de Physique* 47(2): 321–29.
Hendrix, Jelle et al. 2015. "Live-Cell Observation of Cytosolic HIV-1 Assembly Onset Reveals RNA-Interacting Gag Oligomers." *The Journal of cell biology* 210(4): 629–46.
Henne, William Mike et al. 2010. "FCHo Proteins Are Nucleators of Clathrin-Mediated Endocytosis." *Science (New York, N.Y.)* 328(5983): 1281–84.
Hill, C P et al. 1996. "Crystal Structures of the Trimeric Human Immunodeficiency Virus Type 1 Matrix Protein: Implications for Membrane Association and Assembly." *Proc. Natl. Acad. Sci. USA* 93(7): 3099–30104. http://www.ncbi.nlm.nih.gov/entrez/query.fcgi?cmd=Retrieve&db=PubMed&dopt=Citation&list_uids=8610175.
Hjort Ipsen, J. et al. 1987. "Phase Equilibria in the Phosphatidylcholine-Cholesterol System." *BBA - Biomembranes* 905(1): 162–72.
Hogue, Ian B et al. 2011. "Gag Induces the Coalescence of Clustered Lipid Rafts and Tetraspanin-Enriched Microdomains at HIV-1 Assembly Sites on the Plasma Membrane." *Journal of virology* 85(19): 9749–66. http://www.pubmedcentral.nih.gov/articlerender.fcgi?artid=3196429&tool=pmcentrez&rendertype=abstract (October 13, 2014).
Hogue, Ian B, G Nicholas Llewellyn, and Akira Ono. 2012. "Dynamic Association between HIV-1 Gag and Membrane Domains." *Molecular biology international* 2012: 979765. http://www.pubmedcentral.nih.gov/articlerender.fcgi?artid=3399408&tool=pmcentrez&rendertype=abstract (October 13, 2014).
Holm, K, K Weclewicz, R Hewson, and M Suomalainen. 2003. "Human Immunodeficiency Virus Type 1 Assembly and Lipid Rafts: Pr55(gag) Associates with Membrane Domains That Are Largely Resistant to Brij98 but Sensitive to Triton X-100." *J Virol* 77(8): 4805–17.
Holm, Kirsi, Katarzyna Weclewicz, Roger Hewson, and Maarit Suomalainen. 2003. "Human Immunodeficiency Virus Type 1 Assembly and Lipid Rafts: Pr55(gag) Associates with Membrane Domains That Are Largely Resistant to Brij98 but Sensitive to Triton X-100." *Journal of virology* 77(8): 4805–17. http://www.ncbi.nlm.nih.gov/pubmed/12663787 (June 2, 2016).
Honigmann, Alf et al. 2013. "Phosphatidylinositol 4,5-Bisphosphate Clusters Act as Molecular Beacons for Vesicle Recruitment." *Nature structural & molecular biology* 20(6): 679–86. http://dx.doi.org/10.1038/nsmb.2570.
Höök, F, M Rodahl, B Kasemo, and P Brzezinski. 1998. "Structural Changes in Hemoglobin during Adsorption to Solid Surfaces: Effects of pH, Ionic Strength, and Ligand Binding." *Proceedings of the National Academy of Sciences of the United States of America* 95(21): 12271–76.
Höök, Fredrik et al. 2001. "Variations in Coupled Water, Viscoelastic Properties, and Film Thickness of a Mefp-1 Protein Film during Adsorption and Cross-Linking: A Quartz Crystal Microbalance with Dissipation Monitoring, Ellipsometry, and Surface Plasmon Resonance Study." *Analytical Chemistry* 73(24): 5796–5804. http://pubs.acs.org/doi/abs/10.1021/ac0106501 (August 4, 2016).
Horvath, Caroline A J et al. 2007. "Epsin: Inducing Membrane Curvature." *International Journal of Biochemistry and Cell Biology* 39(10): 1765–70.
Huang, M, J M Orenstein, M A Martin, and E O Freed. 1995. "p6Gag Is Required for Particle Production from Full-Length Human Immunodeficiency Virus Type 1 Molecular Clones

Expressing Protease." *Journal of virology* 69(11): 6810–18. http://www.pubmedcentral.nih.gov/articlerender.fcgi?artid=189593&tool=pmcentrez&rendertype=abstract.
Hurley, James H., Evzen Boura, Lars Anders Carlson, and Bartosz R??ycki. 2010. "Membrane Budding." *Cell* 143(6): 875–87.
Huvent, Isabelle et al. 1998. "Interaction and Co-Encapsidation of Human Immunodeficiency Virus Type 1 Gag and Vif Recombinant Proteins." *Journal of General Virology* 79(5): 1069–81.
Hymes, KennethB. et al. 1981. "Kaposi'S Sarcoma in Homosexual Men—a Report of Eight Cases." *The Lancet* 318(8247): 598–600. http://www.sciencedirect.com/science/article/pii/S0140673681927409.
Ing??lfsson, Helgi I. et al. 2014. "Lipid Organization of the Plasma Membrane." *Journal of the American Chemical Society* 136(41): 14554–59.
Ingólfsson, Helgi I et al. 2014. "Lipid Organization of the Plasma Membrane." *Journal of the American Chemical Society*. http://pubs.acs.org/doi/abs/10.1021/ja507832e (October 1, 2014).
Inlora, Jingga et al. 2014. "Membrane Binding and Subcellular Localization of Retroviral Gag Proteins Are Differentially Regulated by MA Interactions with Phosphatidylinositol-(4,5)-Bisphosphate and RNA." *mBio* 5(6).
Israelachvili, Jacob N. 1977. "Refinement of the Fluid-Mosaic Model of Membrane Structure." *BBA - Biomembranes* 469(2): 221–25.
Itoh, Toshiki, and Pietro De Camilli. 2006. "BAR, F-BAR (EFC) and ENTH/ANTH Domains in the Regulation of Membrane-Cytosol Interfaces and Membrane Curvature." *Biochimica et Biophysica Acta - Molecular and Cell Biology of Lipids* 1761(8): 897–912.
Iyidogan, Pinar, and Karen S. Anderson. 2014. "Current Perspectives on HIV-1 Antiretroviral Drug Resistance." *Viruses* 6(10): 4095–4139.
Janina Hanne, Fabian Göttfert, Jiří Schimer, Maria Anders-Össwein, Jan Konvalinka, Johann Engelhardt, Barbara Müller, Stefan W. Hell, and Hans-Georg Kräusslic. 2016. "Stimulated Emission Depletion Nanoscopy Reveals Time-Course of Human Immunodeficiency Virus Proteolytic Maturation." *ACS nano* 10(8).
Janosch, Sascha et al. 2004. "Partitioning of Dual-Lipidated Peptides into Membrane Microdomains: Lipid Sorting vs Peptide Aggregation." *Journal of the American Chemical Society* 126(24): 7496–7503.
Jiang, Zhiping et al. 2014. "Cholesterol Stabilizes Fluid Phosphoinositide Domains." *Chemistry and Physics of Lipids* 182: 52–61.
Johnson, Corey M, Gurunadh R Chichili, and William Rodgers. 2008. "Compartmentalization of Phosphatidylinositol 4,5-Bisphosphate Signaling Evidenced Using Targeted Phosphatases." *The Journal of biological chemistry* 283(44): 29920–28. http://www.ncbi.nlm.nih.gov/pubmed/18723502 (June 2, 2016).
Johnson, Kristen A, Geoffrey J F Taghon, Jordan L Scott, and Robert V Stahelin. 2016. "The Ebola Virus Matrix Protein, VP40, Requires Phosphatidylinositol 4,5-Bisphosphate (PI(4,5)P2) for Extensive Oligomerization at the Plasma Membrane and Viral Egress." *Scientific reports* 6: 19125. http://www.nature.com/srep/2016/160112/srep19125/full/srep19125.html.
Jolly, Clare, and Quentin J Sattentau. 2007. "Human Immunodeficiency Virus Type 1 Assembly, Budding, and Cell-Cell Spread in T Cells Take Place in Tetraspanin-Enriched Plasma

Membrane Domains." *Journal of virology* 81(15): 7873–84. http://www.ncbi.nlm.nih.gov/pubmed/17522207 (June 2, 2016).

Jones, L J et al. 1997. "Quenched BODIPY Dye-Labelled Casein Substrates for the Assay of Protease Activity by Direct Fluorescence Measurement." *Analytical biochemistry* 251(2): 144–52. http://www.ncbi.nlm.nih.gov/pubmed/9299009 (June 2, 2016).

Kalvodova, Lucie et al. 2009. "The Lipidomes of Vesicular Stomatitis Virus, Semliki Forest Virus, and the Host Plasma Membrane Analyzed by Quantitative Shotgun Mass Spectrometry." *Journal of virology* 83(16): 7996–8003.

Karolin, J, L B a Johansson, L Strandberg, and T Ny. 1994. "Fluorescence And Absorption Spectroscopic Properties Of Dipyrrometheneboron Difluoride (Bodipy) Derivatives In Liquids, Lipid-Membranes, And Proteins." *Journal Of The American Chemical Society* 116(17): 7801–6. <Go to ISI>://A1994PD69700042.

Keller, Heiko, Hans-Georg Kräusslich, and Petra Schwille. 2013. "Multimerizable HIV Gag Derivative Binds to the Liquid-Disordered Phase in Model Membranes." *Cellular microbiology* 15(2): 237–47. http://www.ncbi.nlm.nih.gov/pubmed/23121220 (October 1, 2014).

Kempf, Noémie et al. 2015a. "The HIV-1 Nucleocapsid Protein Recruits Negatively Charged Lipids To Ensure Its Optimal Binding to Lipid Membranes." *Journal of Virology* 89(3): 1756–67. http://www.pubmedcentral.nih.gov/articlerender.fcgi?artid=4300737&tool=pmcentrez&rendertype=abstract.

———. 2015b. "The HIV-1 Nucleocapsid Protein Recruits Negatively Charged Lipids to Ensure Its Optimal Binding to Lipid Membranes." *Journal of virology* 89(3): 1756–67. http://www.ncbi.nlm.nih.gov/pubmed/25410868 (June 1, 2016).

Kerviel, a et al. 2013a. "Virus Assembly and Plasma Membrane Domains: Which Came First?" *Virus research* 171(2): 332–40. http://www.ncbi.nlm.nih.gov/pubmed/22989508.

———. 2013b. "Virus Assembly and Plasma Membrane Domains: Which Came First?" *Virus research* 171: 332–40. http://www.sciencedirect.com/science/article/pii/S0168170212003103.

Kiessling, Volker, Chen Wan, and Lukas K. Tamm. 2009. "Domain Coupling in Asymmetric Lipid Bilayers." *Biochimica et Biophysica Acta - Biomembranes* 1788(1): 64–71.

Kim, Yeun Ju, Maria Luisa Guzman-Hernandez, and Tamas Balla. 2011. "A Highly Dynamic ER-Derived Phosphatidylinositol-Synthesizing Organelle Supplies Phosphoinositides to Cellular Membranes." *Developmental Cell* 21(5): 813–24.

Kinnunen, P K et al. 1994. "Lipid Dynamics and Peripheral Interactions of Proteins with Membrane Surfaces." *Chemistry and physics of lipids* 73(1–2): 181–207. http://www.ncbi.nlm.nih.gov/pubmed/8001181 (June 1, 2016).

Kirchhausen, Tom. 2012. "Bending Membranes." *Nature Cell Biology* 14(9): 906–8. http://dx.doi.org/10.1038/ncb2570.

Klemm, Robin W. et al. 2009. "Segregation of Sphingolipids and Sterols during Formation of Secretory Vesicles at the Trans-Golgi Network." *Journal of Cell Biology* 185(4): 601–12.

Kolay, Sourav, Urbashi Basu, and Padinjat Raghu. 2016. "Control of Diverse Subcellular Processes by a Single Multi-Functional Lipid Phosphatidylinositol 4,5-Bisphosphate [PI(4,5)P2]." *The Biochemical journal* 473(12): 1681–92. http://www.ncbi.nlm.nih.gov/pubmed/27288030.

Kozlov, Michael M. et al. 2014. "Mechanisms Shaping Cell Membranes." *Current Opinion in*

Cell Biology 29(1): 53–60.
Kräusslich, H G et al. 1995. "The Spacer Peptide between Human Immunodeficiency Virus Capsid and Nucleocapsid Proteins Is Essential for Ordered Assembly and Viral Infectivity." *Journal of virology* 69(6): 3407–19. http://www.ncbi.nlm.nih.gov/pubmed/7745687 (June 1, 2016).
Krementsov, Dimitry N et al. 2010. "HIV-1 Assembly Differentially Alters Dynamics and Partitioning of Tetraspanins and Raft Components." *Traffic (Copenhagen, Denmark)* 11(11): 1401–14. http://www.ncbi.nlm.nih.gov/pubmed/20727121 (June 2, 2016).
Krishnan, Kannan et al. 2009. "Profilin Interaction with Phosphatidylinositol (4,5)-Bisphosphate Destabilizes the Membrane of Giant Unilamellar Vesicles." *Biophysical journal* 96(12): 5112–21. http://www.pubmedcentral.nih.gov/articlerender.fcgi?artid=2712054&tool=pmcentrez&rendertype=abstract (October 1, 2014).
Kull, F. Jon, and Sharyn A. Endow. 2013. "Force Generation by Kinesin and Myosin Cytoskeletal Motor Proteins." *Journal of cell science* 126(Pt 1): 9–19. http://www.pubmedcentral.nih.gov/articlerender.fcgi?artid=3603507&tool=pmcentrez&rendertype=abstract.
Kutateladze, Tatiana G. 2010. "Translation of the Phosphoinositide Code by PI Effectors." *Nature chemical biology* 6(7): 507–13. http://www.pubmedcentral.nih.gov/articlerender.fcgi?artid=3182472&tool=pmcentrez&rendertype=abstract.
Kutluay, Sebla B., and Paul D. Bieniasz. 2010. "Analysis of the Initiating Events in HIV-1 Particle Assembly and Genome Packaging." *PLoS Pathogens* 6(11).
Kuzmin, Peter I. et al. 2005. "Line Tension and Interaction Energies of Membrane Rafts Calculated from Lipid Splay and Tilt." *Biophysical Journal* 88(2): 1120–33. http://www.pubmedcentral.nih.gov/articlerender.fcgi?artid=1305117&tool=pmcentrez&rendertype=abstract.
Kwong, Peter D et al. 1998. "Structure of an HIV gp120 Envelope Glycoprotein in Complex with the CD4 Receptor and a Neutralizing Human Antibody." *Nature* 393(June): 648–59.
Lee, Anthony G. 2011. "Biological Membranes: The Importance of Molecular Detail." *Trends in Biochemical Sciences* 36(9): 493–500.
Legendre-Guillemin, Valerie et al. 2004. "ENTH/ANTH Proteins and Clathrin-Mediated Membrane Budding." *Journal of cell science* 117(Pt 1): 9–18.
Van Lehn, Reid C et al. 2014. "Lipid Tail Protrusions Mediate the Insertion of Nanoparticles into Model Cell Membranes." *Nature communications* 5: 4482. http://www.ncbi.nlm.nih.gov/pubmed/25042518.
Lemmon, Mark A. 2010. "Pleckstrin Homology (PH) Domains." In *Handbook of Cell Signaling, 2/e*, , 1093–1101.
Levental, Ilya, Andrejs C???bers, and Paul A. Janmey. 2008. "Combined Electrostatics and Hydrogen Bonding Determine Intermolecular Interactions between Polyphosphoinositides." *Journal of the American Chemical Society* 130(28): 9025–30.
Levin, Judith G., Jianhui Guo, Ioulia Rouzina, and Karin Musier-Forsyth. 2005. "Nucleic Acid Chaperone Activity of HIV-1 Nucleocapsid Protein: Critical Role in Reverse Transcription and Molecular Mechanism." *Progress in Nucleic Acid Research and Molecular Biology* 80: 217–86.
Lichtenberg, Dov, Félix M. Goñi, and Heiko Heerklotz. 2005. "Detergent-Resistant Membranes

Should Not Be Identified with Membrane Rafts." *Trends in Biochemical Sciences* 30(8): 430–36.

Lindwasser, O. Wolf, and Marilyn D. Resh. 2002. "Myristoylation as a Target for Inhibiting HIV Assembly: Unsaturated Fatty Acids Block Viral Budding." *Proceedings of the National Academy of Sciences* 99(20): 13037–42. http://www.pnas.org/content/99/20/13037\nhttp://www.ncbi.nlm.nih.gov/pubmed/12244217\nhttp://www.pnas.org/content/99/20/13037.full.pdf\nhttp://www.pnas.org/content/99/20/13037.short.

Lindwasser, O W, and M D Resh. 2001. "Multimerization of Human Immunodeficiency Virus Type 1 Gag Promotes Its Localization to Barges, Raft-like Membrane Microdomains." *Journal of virology* 75(17): 7913–24. http://www.ncbi.nlm.nih.gov/pubmed/11483736 (June 1, 2016).

Lingappa, Jaisri R et al. 2014. "How HIV-1 Gag Assembles in Cells: Putting Together Pieces of the Puzzle." *Virus research*: 1–19. http://www.ncbi.nlm.nih.gov/pubmed/25066606 (October 1, 2014).

Lingwood, Daniel, and Kai Simons. 2007. "Detergent Resistance as a Tool in Membrane Research." *Nature protocols* 2(9): 2159–65.

Lipowsky, R. 1993. "Domain-Induced Budding of Fluid Membranes." *Biophysical journal* 64(4): 1133–38. http://dx.doi.org/10.1016/S0006-3495(93)81479-6.

Lipowsky, Reinhard. 2013. "Spontaneous Tubulation of Membranes and Vesicles Reveals Membrane Tension Generated by Spontaneous Curvature." *Faraday Discuss* 161: 305–31.

Lipowsky, Reinhard, and Rumiana Dimova. 2002. "Domains in Membranes and Vesicles." *Journal of Physics: Condensed Matter* 15: S31–45.

Lorizate, Maier et al. 2009. "Probing HIV-1 Membrane Liquid Order by Laurdan Staining Reveals Producer Cell-Dependent Differences." *The Journal of biological chemistry* 284(33): 22238–47. http://www.pubmedcentral.nih.gov/articlerender.fcgi?artid=2755948&tool=pmcentrez&rendertype=abstract (October 13, 2014).

———. 2013. "Comparative Lipidomics Analysis of HIV-1 Particles and Their Producer Cell Membrane in Different Cell Lines." *Cellular microbiology* 15(2): 292–304. http://www.ncbi.nlm.nih.gov/pubmed/23279151 (June 1, 2016).

Macia, Eric et al. 2008a. "The Pleckstrin Homology Domain of the Arf6-Specific Exchange Factor EFA6 Localizes to the Plasma Membrane by Interacting with Phosphatidylinositol 4,5-Bisphosphate and F-Actin." *Journal of Biological Chemistry* 283(28): 19836–44.

———. 2008b. "The Pleckstrin Homology Domain of the Arf6-Specific Exchange Factor EFA6 Localizes to the Plasma Membrane by Interacting with Phosphatidylinositol 4,5-Bisphosphate and F-Actin." *The Journal of biological chemistry* 283(28): 19836–44. http://www.ncbi.nlm.nih.gov/pubmed/18490450 (June 1, 2016).

Madsen, K. L., V. K. Bhatia, U. Gether, and D. Stamou. 2010. "BAR Domains, Amphipathic Helices and Membrane-Anchored Proteins Use the Same Mechanism to Sense Membrane Curvature." *FEBS Letters* 584(9): 1848–55.

Mani, Timmy et al. 2011. "FERM Domain Phosphoinositide Binding Targets Merlin to the Membrane and Is Essential for Its Growth-Suppressive Function." *Molecular and cellular biology* 31(10): 1983–96. http://www.pubmedcentral.nih.gov/articlerender.fcgi?artid=3133355&tool=pmcentrez&rendertype=abstract.

Marsh, Derek. 2006. "Elastic Curvature Constants of Lipid Monolayers and Bilayers." *Chemistry and Physics of Lipids* 144(2): 146–59.
Mateu, Mauricio G. 2009. "The Capsid Protein of Human Immunodeficiency Virus: Intersubunit Interactions during Virus Assembly." *The FEBS journal* 276(21): 6098–6109. http://www.ncbi.nlm.nih.gov/pubmed/19825044 (September 2, 2016).
McLaughlin, Stuart, Jiyao Wang, Alok Gambhir, and Diana Murray. 2002. "PIP(2) and Proteins: Interactions, Organization, and Information Flow." *Annual review of biophysics and biomolecular structure* 31: 151–75.
McMahon, Harvey T, and Jennifer L Gallop. 2005. "Membrane Curvature and Mechanisms of Dynamic Cell Membrane Remodelling." *Nature* 438(7068): 590–96. http://www.ncbi.nlm.nih.gov/pubmed/16319878.
van Meer, Gerrit. 2005. "Cellular Lipidomics." *The EMBO journal* 24(18): 3159–65.
Mercredi, Peter Y. et al. 2016. "Structural and Molecular Determinants of Membrane Binding by the HIV-1 Matrix Protein." *Journal of Molecular Biology* 428(8): 1637–55.
Mironov, Alexander et al. 2003. "ER-to-Golgi Carriers Arise through Direct En Bloc Protrusion and Multistage Maturation of Specialized ER Exit Domains." *Developmental Cell* 5(4): 583–94.
Mogilner, Alex. 2006. "On the Edge: Modeling Protrusion." *Current Opinion in Cell Biology* 18(1): 32–39.
Mouritsen, O.G. 2005. Interfaces *Life–as a Matter of Fat: The Emerging Science of Lipidomics.*
Müller, Barbara, Tilo Patschinsky, and Hans-Georg Kräusslich. 2002. "The Late-Domain-Containing Protein p6 Is the Predominant Phosphoprotein of Human Immunodeficiency Virus Type 1 Particles." *Journal of virology* 76(3): 1015–24. http://www.pubmedcentral.nih.gov/articlerender.fcgi?artid=135845&tool=pmcentrez&rendertype=abstract.
Munro, James B et al. 2014. "A Conformational Transition Observed in Single HIV-1 Gag Molecules during in Vitro Assembly of Virus-like Particles." *Journal of virology* 88(6): 3577–85. http://www.pubmedcentral.nih.gov/articlerender.fcgi?artid=3957938&tool=pmcentrez&rendertype=abstract.
Murakami, Tsutomu. 2012. "Retroviral Env Glycoprotein Trafficking and Incorporation into Virions." *Molecular biology international* 2012: 682850. http://www.pubmedcentral.nih.gov/articlerender.fcgi?artid=3395148&tool=pmcentrez&rendertype=abstract.
Murate, Motohide, and Toshihide Kobayashi. 2016. "Revisiting Transbilayer Distribution of Lipids in the Plasma Membrane." *Chemistry and Physics of Lipids* 194: 58–71.
Murray, Diana, Anna Arbuzova, Barry Honig, and Stuart McLaughlint. 2002. "The Role of Electrostatic and Nonpolar Interactions in the Association of Peripheral Proteins with Membranes." *Current Topics in Membranes* 52: 277–307.
Nam-Joon Cho, Edward A. Pham, Rachel J. Hagey, Vincent J. Lévêque, Han Ma, Klaus Klumpp, and Jeffrey S. Glenn. 2016. "Reconstitution and Functional Analysis of a Full-Length Hepatitis C Virus NS5B Polymerase on a Supported Lipid Bilayer." *ACS Cent. Sci.,* 2(7): 456–66.
Nguyen, D H, and J E Hildreth. 2000. "Evidence for Budding of Human Immunodeficiency Virus Type 1 Selectively from Glycolipid-Enriched Membrane Lipid Rafts." *Journal of virology* 74(7): 3264–72. http://www.ncbi.nlm.nih.gov/pubmed/10708443 (June 1, 2016).

O'Neil, Lauren et al. 2016. "HIV-1 Matrix-31 Membrane Binding Peptide Interacts Differently with Membranes Containing PS vs. PI(4,5)P2." *Biochimica et Biophysica Acta (BBA) - Biomembranes*. http://linkinghub.elsevier.com/retrieve/pii/S0005273616302991.

Ohvo-Rekilä, Henna, Bodil Ramstedt, Petra Leppimäki, and J. Peter Slotte. 2002. "Cholesterol Interactions with Phospholipids in Membranes." *Progress in Lipid Research* 41: 66–97.

Olety, Balaji, Sarah L Veatch, and Akira Ono. 2015. "Phosphatidylinositol-(4,5)-Bisphosphate Acyl Chains Differentiate Membrane Binding of HIV-1 Gag from That of the Phospholipase Cδ1 Pleckstrin Homology Domain." *Journal of virology* 89(15): 7861–73. http://www.ncbi.nlm.nih.gov/pubmed/25995263 (June 2, 2016).

Ono, A., J. M. Orenstein, and E. O. Freed. 2000. "Role of the Gag Matrix Domain in Targeting Human Immunodeficiency Virus Type 1 Assembly." *Journal of Virology* 74(6): 2855–66. http://jvi.asm.org/cgi/doi/10.1128/JVI.74.6.2855-2866.2000 (June 2, 2016).

Ono, A, and E O Freed. 2001a. "Plasma Membrane Rafts Play a Critical Role in HIV-1 Assembly and Release." *Proceedings of the National Academy of Sciences of the United States of America* 98(24): 13925–30. http://www.ncbi.nlm.nih.gov/pubmed/11717449 (June 1, 2016).

———. 2001b. "Plasma Membrane Rafts Play a Critical Role in HIV-1 Assembly and Release." *Proceedings of the National Academy of Sciences of the United States of America* 98(24): 13925–30. http://www.ncbi.nlm.nih.gov/pubmed/11717449 (June 2, 2016).

Ono, a, and E O Freed. 2001. "Plasma Membrane Rafts Play a Critical Role in HIV-1 Assembly and Release." *Proceedings of the National Academy of Sciences of the United States of America* 98(24): 13925–30.

Ono, A, and E O Freed. 2004. "Cell-Type-Dependent Targeting of Human Immunodeficiency Virus Type 1 Assembly to the Plasma Membrane and the Multivesicular Body." *Journal of Virology* 78(3): 1552–63. <Go to ISI>://000188205900049.

Ono, Akira et al. 2004. "Phosphatidylinositol (4,5) Bisphosphate Regulates HIV-1 Gag Targeting to the Plasma Membrane." *Proceedings of the National Academy of Sciences of the United States of America* 101(41): 14889–94.

———. 2011. "Relationships between Plasma Membrane Microdomains and HIV-1 Assembly." 102(6): 335–50.

Ono, Akira, Abdul A Waheed, and Eric O Freed. 2007. "Depletion of Cellular Cholesterol Inhibits Membrane Binding and Higher-Order Multimerization of Human Immunodeficiency Virus Type 1 Gag." *Virology* 360(1): 27–35. http://www.ncbi.nlm.nih.gov/pubmed/17095032 (June 2, 2016).

Ono, Akira, Abdul A Waheed, Anjali Joshi, and Eric O Freed. 2005. "Association of Human Immunodeficiency Virus Type 1 Gag with Membrane Does Not Require Highly Basic Sequences in the Nucleocapsid: Use of a Novel Gag Multimerization Assay." *Journal of virology* 79(22): 14131–40. http://www.ncbi.nlm.nih.gov/pubmed/16254348 (June 2, 2016).

PALADE, G. E. 1953. "AN ELECTRON MICROSCOPE STUDY OF THE MITOCHONDRIAL STRUCTURE." *Journal of Histochemistry & Cytochemistry* 1(4): 188–211. http://jhc.sagepub.com/content/1/4/188.abstract.

Palsdottir, Hildur, and Carola Hunte. 2004. "Lipids in Membrane Protein Structures." *Biochimica et Biophysica Acta - Biomembranes* 1666(1–2): 2–18.

Pike, L J. 2006a. "Rafts Defined: A Report on the Keystone Symposium on Lipid Rafts and Cell Function." *J Lipid Res* 47(7): 1597–98.

———. 2006b. "Rafts Defined: A Report on the Keystone Symposium on Lipid Rafts and Cell

Function." *J Lipid Res* 47(7): 1597–98. http://www.ncbi.nlm.nih.gov/pubmed/16645198\nhttp://www.jlr.org/content/47/7/1597.full.pdf.

Pike, Linda J, Xianlin Han, Koong-Nah Chung, and Richard W Gross. 2002. "Lipid Rafts Are Enriched in Arachidonic Acid and Plasmenylethanolamine and Their Composition Is Independent of Caveolin-1 Expression: A Quantitative Electrospray Ionization/mass Spectrometric Analysis." *Biochemistry* 41(6): 2075–88. http://www.ncbi.nlm.nih.gov/pubmed/11827555 (June 1, 2016).

Pornillos, Owen et al. 2009. "X-Ray Structures of the Hexameric Building Block of the HIV Capsid." *Cell* 137(7): 1282–92.

Prevelige, Peter E. 2011a. "New Approaches for Antiviral Targeting of HIV Assembly." *Journal of Molecular Biology* 410(4): 634–40. http://linkinghub.elsevier.com/retrieve/pii/S0022283611003779.

———. 2011b. "New Approaches for Antiviral Targeting of HIV Assembly." *Journal of Molecular Biology* 410(4): 634–40.

Provitera, P. et al. 2001. "Role of the Major Homology Region in Assembly of HIV-1 Gag." *Biochemistry* 40(18): 5565–72.

Raghupathy, Riya et al. 2015. "Transbilayer Lipid Interactions Mediate Nanoclustering of Lipid-Anchored Proteins." *Cell* 161(3): 581–94.

Rebaud, Samuel, Anne Simon, et al. 2014. "Comparison of VILIP-1 and VILIP-3 Binding to Phospholipid Monolayers." *PLoS ONE* 9(4).

Rebaud, Samuel, Conan K. Wang, et al. 2014. "Specific Interaction to PIP2 Increases the Kinetic Rate of Membrane Binding of VILIPs, a Subfamily of Neuronal Calcium Sensors (NCS) Proteins." *Biochimica et Biophysica Acta - Biomembranes* 1838(10): 2698–2707.

Rebecchi, M, a Peterson, and S McLaughlin. 1992. "Phosphoinositide-Specific Phospholipase C-Delta 1 Binds with High Affinity to Phospholipid Vesicles Containing Phosphatidylinositol 4,5-Bisphosphate." *Biochemistry* 31(51): 12742–47.

van Rheenen, J et al. 2005. "PIP2 Signaling in Lipid Domains: A Critical Re-Evaluation." *EMBO Journal* 24(9): 1664–73. http://embojnl.embopress.org/content/embojnl/24/9/1664.full.pdf.

Roger H. Miller, and Nava Sarver. 1995. "Therapeutic Targets." *Molecular Medicine* 1(July): 479–85.

Roldan, Ariel et al. 2004. "In Vitro Identification and Characterization of an Early Complex Linking HIV-1 Genomic RNA Recognition and Pr55Gag Multimerization." *Journal of Biological Chemistry* 279(38): 39886–94.

Rossetti, Fernanda F et al. 2004. "Interaction of poly(L-Lysine)-G-Poly(ethylene Glycol) with Supported Phospholipid Bilayers." *Biophysical journal* 87(September): 1711–21.

Roux, Aurélien et al. 2010. "Membrane Curvature Controls Dynamin Polymerization." *Proceedings of the National Academy of Sciences of the United States of America* 107(9): 4141–46.

Roy, Ambrish, Alper Kucukural, and Yang Zhang. 2010. "I-TASSER: A Unified Platform for Automated Protein Structure and Function Prediction." *Nature protocols* 5(4): 725–38.

Saad, Jamil S et al. 2006. "Structural Basis for Targeting HIV-1 Gag Proteins to the Plasma Membrane for Virus Assembly." *Proceedings of the National Academy of Sciences of the United States of America* 103(30): 11364–69. http://www.pnas.org/content/103/30/11364.abstract.

Saarikangas, Juha et al. 2009. "Molecular Mechanisms of Membrane Deformation by I-BAR Domain Proteins." *Current Biology* 19(2): 95–107.
Saarikangas, Juha, Hongxia Zhao, and Pekka Lappalainen. 2010. "Regulation of the Actin Cytoskeleton-Plasma Membrane Interplay by Phosphoinositides." *Physiological reviews* 90: 259–89.
Sackmann, Erich. 1984. *Physical Basis for Trigger Processes and Membrane Structures*. D. Chapman. London: Academic Press.
Sakaguchi, Takemasa et al. 2005. "AIP1/Alix Is a Binding Partner of Sendai Virus C Protein and Facilitates Virus Budding." *Journal of virology* 79(14): 8933–41. http://www.pubmedcentral.nih.gov/articlerender.fcgi?artid=1168738&tool=pmcentrez&rendertype=abstract.
Salvemini, Iyrri L et al. 2014. "Low PIP(2) Molar Fractions Induce Nanometer Size Clustering in Giant Unilamellar Vesicles." *Chemistry and physics of lipids* 177: 51–63. http://www.ncbi.nlm.nih.gov/pubmed/24269375 (June 2, 2016).
Sarmento, Maria J. et al. 2014. "Ca2 + Induces PI(4,5)P2 Clusters on Lipid Bilayers at Physiological PI(4,5)P2 and Ca2 + Concentrations." *Biochimica et Biophysica Acta - Biomembranes* 1838(3): 822–30.
Schur, F. K. M. et al. 2016. "An Atomic Model of HIV-1 Capsid-SP1 Reveals Structures Regulating Assembly and Maturation." *Science* 353(6298): 506–8. http://www.sciencemag.org/cgi/doi/10.1126/science.aaf9620.
von Schwedler, Uta K, Kirsten M Stray, Jennifer E Garrus, and Wesley I Sundquist. 2003. "Functional Surfaces of the Human Immunodeficiency Virus Type 1 Capsid Protein." *Journal of virology* 77(9): 5439–50. http://www.pubmedcentral.nih.gov/articlerender.fcgi?artid=153941&tool=pmcentrez&rendertype=abstract.
Sezgin, Erdinc, and Petra Schwille. 2011. "Fluorescence Techniques to Study Lipid Dynamics." *Cold Spring Harbor perspectives in biology* 3(11): a009803. http://www.ncbi.nlm.nih.gov/pubmed/21669985 (June 1, 2016).
Shafer, Robert W. 2016. "The Future of HIV-1 Therapeutics. Resistance Is Futile?" ed. Gary P. Wormser. *Clinical Infectious Diseases* 62(1): 136–37. http://cid.oxfordjournals.org/lookup/doi/10.1093/cid/civ806.
Shaikh, Saame Raza, and Michael A. Edidin. 2006. "Membranes Are Not Just Rafts." *Chemistry and Physics of Lipids* 144(1): 1–3.
Shibata, Yoko, Gia K. Voeltz, and Tom A. Rapoport. 2006. "Rough Sheets and Smooth Tubules." *Cell* 126(3): 435–39.
Shnyrova, Anna V. et al. 2007. "Vesicle Formation by Self-Assembly of Membrane-Bound Matrix Proteins into a Fluidlike Budding Domain." *Journal of Cell Biology* 179(4): 627–33.
Shnyrova, Anna V., Vadim A. Frolov, and Joshua Zimmerberg. 2009. "Domain-Driven Morphogenesis of Cellular Membranes." *Current Biology* 19(17).
Shogomori, H, and D A Brown. 2003. "Use of Detergents to Study Membrane Rafts: The Good, the Bad, and the Ugly." *Biol Chem* 384(9): 1259–63. http://www.ncbi.nlm.nih.gov/entrez/query.fcgi?cmd=Retrieve&db=PubMed&dopt=Citation&list_uids=14515986.
Siliciano, Janet D., and Robert F. Siliciano. 2013. "Recent Trends in HIV-1 Drug Resistance." *Current Opinion in Virology* 3(5): 487–94.
Silvius, J.R. 2002. "Lipidated Peptides as Tools for Understanding the Membrane Interactions of

Lipid-Modified Proteins." In *Peptide–lipid Interactions*, ed. S.A. Simon and T.J. McIntosh. Elsevier, 371–95.
Silvius, John R. 2003. "Role of Cholesterol in Lipid Raft Formation: Lessons from Lipid Model Systems." *Biochimica et Biophysica Acta - Biomembranes* 1610(2): 174–83.
Simons, Kai, and Mathias J Gerl. 2010. "Revitalizing Membrane Rafts: New Tools and Insights." *Nature reviews. Molecular cell biology* 11(10): 688–99. http://www.ncbi.nlm.nih.gov/pubmed/20861879 (July 15, 2014).
Simons, K, and E Ikonen. 1997. "Functional Rafts in Cell Membranes." *Nature* 387(6633): 569–72. http://www.ncbi.nlm.nih.gov/pubmed/9177342.
Simons, K, and D Toomre. 2000. "Lipid Rafts and Signal Transduction." *Nature reviews. Molecular cell biology* 1(1): 31–39. http://www.ncbi.nlm.nih.gov/pubmed/11413487 (June 2, 2016).
Simunovic, Mijo, Coline Prévost, Andrew Callan-Jones, and Patricia Bassereau. 2016. "Physical Basis of Some Membrane Shaping Mechanisms." *Philosophical Transactions of the Royal Society A: Mathematical, Physical and Engineering Sciences* 374(2072): 20160034. http://rsta.royalsocietypublishing.org/lookup/doi/10.1098/rsta.2016.0034.
Singer, S J, and G L Nicolson. 1972. "The Fluid Mosaic Model of the Structure of Cell Membranes." *Science (New York, N.Y.)* 175(4023): 720–31. http://www.ncbi.nlm.nih.gov/pubmed/4333397 (June 1, 2016).
Solon, Jérôme, Olivier Gareil, Patricia Bassereau, and Yves Gaudin. 2005. "Membrane Deformations Induced by the Matrix Protein of Vesicular Stomatitis Virus in a Minimal System." *Journal of General Virology* 86(12): 3357–63.
Spearman, Paul. 2016. "HIV-1 Gag as an Antiviral Target: Development of Assembly and Maturation Inhibitors." *Current topics in medicinal chemistry* 16(10): 1154–66. http://www.ncbi.nlm.nih.gov/pubmed/26329615.
Spencer, Herbert. 1864. I The London, Edinburgh, and Dublin Philosophical Magazine and Journal of Science *The Principles of Biology*.
Stachowiak, Jeanne C et al. 2012. "Membrane Bending by Protein-Protein Crowding." *Nature cell biology* 14(9): 944–49. http://www.ncbi.nlm.nih.gov/pubmed/22902598 (July 17, 2014).
Staneva, Galya, Miglena I. Angelova, and Kamen Koumanov. 2004. "Phospholipase A2 Promotes Raft Budding and Fission from Giant Liposomes." *Chemistry and Physics of Lipids* 129(1): 53–62.
Stengel, Robert F. 2008. "Mutation and Control of the Human Immunodeficiency Virus." *Mathematical Biosciences* 213(2): 93–102.
Thomas, James A. et al. 2006. "Human Immunodeficiency Virus Type 1 Nucleocapsid Zinc-Finger Mutations Cause Defects in Reverse Transcription and Integration." *Virology* 353(1): 41–51.
Toner, M, G Vaio, a McLaughlin, and S McLaughlin. 1988. "Adsorption of Cations to Phosphatidylinositol 4,5-Bisphosphate." *Biochemistry* 27(19): 7435–43.
Trimble, William S., and Sergio Grinstein. 2015. "Barriers to the Free Diffusion of Proteins and Lipids in the Plasma Membrane." *Journal of Cell Biology* 208(3): 259–71.
Trkola, Alexandra et al. 1996. "CD4-Dependent, Antibody-Sensitive Interactions between HIV-1 and Its Co-Receptor CCR-5." *Nature* 384(6605): 184–87.
Usami, Yoshiko et al. 2009. "The ESCRT Pathway and HIV-1 Budding." *Biochemical Society transactions* 37(Pt 1): 181–84.

Valentine, Kathleen G et al. 2010. "Reverse Micelle Encapsulation of Membrane-Anchored Proteins for Solution NMR Studies." *Structure (London, England : 1993)* 18(1): 9–16. http://www.ncbi.nlm.nih.gov/pubmed/20152148 (June 2, 2016).

Vaz, W.L., E.C. Melo, and T.E. Thompson. 1989. "Translational Diffusion and Fluid Domain Connectivity in a Two-Component, Two-Phase Phospholipid Bilayer." *Biophysical Journal* 56(5): 869–76. http://linkinghub.elsevier.com/retrieve/pii/S000634958982733X.

Veatch, Sarah L., and Sarah L. Keller. 2005. "Seeing Spots: Complex Phase Behavior in Simple Membranes." *Biochimica et Biophysica Acta - Molecular Cell Research* 1746(3): 172–85.

VerPlank, L et al. 2001. "Tsg101, a Homologue of Ubiquitin-Conjugating (E2) Enzymes, Binds the L Domain in HIV Type 1 Pr55(Gag)." *Proceedings of the National Academy of Sciences of the United States of America* 98(14): 7724–29. http://www.pubmedcentral.nih.gov/articlerender.fcgi?artid=35409&tool=pmcentrez&rendertype=abstract.

Vlach, Jiri, and Jamil S Saad. 2013. "Trio Engagement via Plasma Membrane Phospholipids and the Myristoyl Moiety Governs HIV-1 Matrix Binding to Bilayers." *Proceedings of the National Academy of Sciences of the United States of America* 110(9): 3525–30. http://www.ncbi.nlm.nih.gov/pubmed/23401539 (June 2, 2016).

Voinova, M. V., M. Rodahl, M. Jonson, and B. Kasemo. 1999. "Viscoelastic Acoustic Response of Layered Polymer Films at Fluid-Solid Interfaces: Continuum Mechanics Approach." *Physica Scripta* 59(5): 391–96. http://arxiv.org/abs/cond-mat/9805266\nhttp://stacks.iop.org/1402-4896/59/i=5/a=011?key=crossref.30a2d3565410847580964c95084fe001.

Votteler, J??rg, and Wesley I. Sundquist. 2013. "Virus Budding and the ESCRT Pathway." *Cell Host and Microbe* 14(3): 232–41.

Waheed, Abdul A, and Gilda Tachedjian. 2016. "Why Do We Need New Drug Classes for HIV Treatment and Prevention?" *Current topics in medicinal chemistry* 16(12): 1343–49. http://www.ncbi.nlm.nih.gov/pubmed/26459806.

Wan, Chen, Volker Kiessling, and Lukas K. Tamm. 2008. "Coupling of Cholesterol-Rich Lipid Phases in Asymmetric Bilayers." *Biochemistry* 47(7): 2190–98.

Wang, Dan, Wuxun Lu, and Feng Li. 2015. "Pharmacological Intervention of HIV-1 Maturation." *Acta Pharmaceutica Sinica B* 5(6): 493–99. http://linkinghub.elsevier.com/retrieve/pii/S2211383515000787.

Wang, Jiyao et al. 2002. "Lateral Sequestration of Phosphatidylinositol 4,5-Bisphosphate by the Basic Effector Domain of Myristoylated Alanine-Rich C Kinase Substrate Is due to Nonspecific Electrostatic Interactions." *Journal of Biological Chemistry* 277(37): 34401–12.

Wang, Kathleen F., Ramanathan Nagarajan, and Terri A. Camesano. 2015. "Differentiating Antimicrobial Peptides Interacting with Lipid Bilayer: Molecular Signatures Derived from Quartz Crystal Microbalance with Dissipation Monitoring." *Biophysical Chemistry* 196: 53–57.

Wang, Yu Hsiu, David R. Slochower, and Paul A. Janmey. 2014. "Counterion-Mediated Cluster Formation by Polyphosphoinositides." *Chemistry and Physics of Lipids* 182: 38–51.

Wang YH, Bucki R, Janmey PA. 2016. "Cholesterol-Dependent Phase-Demixing in Lipid Bilayers as a Switch for the Activity of the Phosphoinositide-Binding Cytoskeletal Protein Gelsolin." *Biochemistry* 55(24): 3361–69.

Wawrezinieck, Laure, Hervé Rigneault, Didier Marguet, and Pierre-François Lenne. 2005.

"Fluorescence Correlation Spectroscopy Diffusion Laws to Probe the Submicron Cell Membrane Organization." *Biophysical journal* 89(6): 4029–42. http://www.pubmedcentral.nih.gov/articlerender.fcgi?artid=1366968&tool=pmcentrez&rendertype=abstract.

Wawrzyniak, Anna Maria, Rudra Kashyap, and Pascale Zimmermann. 2013. "Phosphoinositides and PDZ Domain Scaffolds." *Advances in Experimental Medicine and Biology* 991: 41–57.

Weinstein J N, Ralston E, Leserman L D, Klausner R D, Dragsten P, Henkart P, Blumenthal R. 1984. *Liposome Technology*. ed. Gregoriadis G. Boca Raton, Florida: CRC.

Wendt, H et al. 1995. "Kinetics of Folding of Leucine Zipper Domains." *Biochemistry* 34(12): 4097–4107. http://www.ncbi.nlm.nih.gov/pubmed/7696274 (June 2, 2016).

Wiegers, K et al. 1998. "Sequential Steps in Human Immunodeficiency Virus Particle Maturation Revealed by Alterations of Individual Gag Polyprotein Cleavage Sites." *Journal of virology* 72(4): 2846–54.

Wills, J W, and R C Craven. 1991. "Form, Function, and Use of Retroviral Gag Proteins." *AIDS (London, England)* 5(6): 639–54. http://www.ncbi.nlm.nih.gov/pubmed/1883539 (June 1, 2016).

Wu, Lijun et al. 1996. "CD4-Induced Interaction of Primary HIV-1 gp120 Glycoproteins with the Chemokine Receptor CCR-5." *Nature* 384(6605): 179–83.

Wu, Yuntao. 2004. "HIV-1 Gene Expression: Lessons from Provirus and Non-Integrated DNA." *Retrovirology* 1: 13. http://www.pubmedcentral.nih.gov/articlerender.fcgi?artid=449739&tool=pmcentrez&rendertype=abstract.

Yamaguchi, Hiroshi, and Masaya Miyazaki. 2014. "Refolding Techniques for Recovering Biologically Active Recombinant Proteins from Inclusion Bodies." *Biomolecules* 4(1): 235–51. http://www.mdpi.com/2218-273X/4/1/235/.

Yingxin Ma, Zhike He, Tianwei Tan, Wei Li, Zhiping Zhang, Shuang Song, Xiaowei Zhang, Qinxue Hu, Peng Zhou§, Yuntao Wu, Xian-En Zhang, and Zongqiang Cui. 2016. "Real-Time Imaging of Single HIV-1 Disassembly with Multicolor Viral Particles." *ACS nano* 10(6): 6273–82.

Yu, Naiyin, and Michael F. Hagan. 2012. "Simulations of HIV Capsid Protein Dimerization Reveal the Effect of Chemistry and Topography on the Mechanism of Hydrophobic Protein Association." *Biophysical Journal* 103(6): 1363–69.

Zech, Tobias et al. 2009. "Accumulation of Raft Lipids in T-Cell Plasma Membrane Domains Engaged in TCR Signalling." *The EMBO journal* 28(5): 466–76. http://www.ncbi.nlm.nih.gov/pubmed/19177148 (June 1, 2016).

Zhao, Gongpu et al. 2013. "Mature HIV-1 Capsid Structure by Cryo-Electron Microscopy and All-Atom Molecular Dynamics." *Nature* 497(7451): 643–46. http://www.pubmedcentral.nih.gov/articlerender.fcgi?artid=3729984&tool=pmcentrez&rendertype=abstract\nhttp://www.nature.com/doifinder/10.1038/nature12162.

Zhou, Cheng-jing, Rashid A Akhtar, and Ata A Abdel-latif. 1993. "Purification and Characterization of Phosphoinositide-Specific Phospholipase C from Bovine Iris Sphincter Smooth Muscle." *Biochemical Journal* 289(2): 401–9.

Zhou, W, L J Parent, J W Wills, and M D Resh. 1994. "Identification of a Membrane-Binding Domain within the Amino-Terminal Region of Human Immunodeficiency Virus Type 1 Gag Protein Which Interacts with Acidic Phospholipids." *Journal of virology* 68(4): 2556–69. http://www.ncbi.nlm.nih.gov/pubmed/8139035 (June 2, 2016).

Zhou, W, and M D Resh. 1996. "Differential Membrane Binding of the Human Immunodeficiency Virus Type 1 Matrix Protein." *Journal of virology* 70(12): 8540–48. http://www.ncbi.nlm.nih.gov/pubmed/8970978 (June 2, 2016).

Zimmerberg, Joshua, and Michael M Kozlov. 2006. "How Proteins Produce Cellular Membrane Curvature." *Nature reviews. Molecular cell biology* 7(1): 9–19. http://www.ncbi.nlm.nih.gov/pubmed/16365634.

Abstract

Gag polyprotein of HIV-1 is made of four main domains Matrix (MA), Capsid (CA), Nucleocapsid (NC), and P6 and is the prime orchestrator of virus assembly that occurs during the late phase of replication. It is well known that Gag interacts with host cell lipids while self-assembling along the inner-leaflet of the plasma membrane in order to generate virus-like particles (VLPs). Budding of these VLPs out of the living cell is described to be ESCRT dependent. Structural, functional and simulation-based studies have shown that Gag membrane binding is mediated by a bipartite interaction. One specific electrostatic interaction, between the highly basic region (HBR) of its MA domain and the host cell acidic lipid phosphatidylinositol bisphophate ($PI(4,5)P_2$), plus a hydrophobic interaction through Gag's myristate insertion in the plasma membrane. It is still an opened question whether Gag would specifically recognise pre-existing lipid domains such as rafts to optimise its multimerization or, on the contrary, would reorganise lipids during its multimerization. During my Ph.D., I explored the second hypothesis using purified myr(-) Gag protein and model membranes containing fluorescently labelled $PI(4,5)P_2$.

Binding experiments have shown strong affinities of these purified proteins towards $PI(4,5)P_2$ containing lipid bilayers. Using $PI(4,5)P_2$ fluorescence self-quenching properties, I found that the multimerizing Gag generates $PI(4,5)P_2$/Cholesterol enriched nanoclusters. On the opposite, sphingomyelin was excluded from these nanoclusters. In addition to this, using a fluorescently labelled myr(-) Gag, I have observed its preferable partitioning into lipid disordered (L*d*) phases of the giant unilamellar vesicles (GUVs). Further, a possibility of whether HIV-1 Gag alone, as a minimal system, can induce the formation of vesicles on $PI(4,5)P_2$/PS containing supported lipid bilayers (SLBs) & GUVs was tested. Using quartz crystal microbalance (QCM-D) and fluorescence microscopy techniques, I monitored the self-assembly of HIV-1 Gag with time and found that Gag is sufficient to generate membrane curvature and vesicle release. Moreover, using mutants of this protein, I found that having MA and CA domain is enough for Gag to produce vesicle-like structures. Taken together, these results suggest that binding and multimerization of Gag protein does not occur in pre-existing lipid domains (such as "rafts") and this multimerization is more likely to induce $PI(4,5)P_2$/Cholesterol nanoclusters. This nanophase separation could locally play a role in the membrane curvature needed for the budding of the virus.